Queen Mary
University of London

Post-Impact Compression Behaviour of Continuous Fibre Composite Materials

Prichard, Jonathan Clive

The copyright of this thesis rests with the author and no quotation from it or information derived from it may be published without the prior written consent of the author

For additional information about this publication click this link.
http://qmro.qmul.ac.uk/jspui/handle/123456789/1874

Information about this research object was correct at the time of download; we occasionally make corrections to records, please therefore check the published record when citing. For more information contact scholarlycommunications@qmul.ac.uk

Post-Impact Compression Behaviour of Continuous Fibre Composite Materials

Jonathan Clive Prichard

This thesis is submitted for the degree of
Doctor of Philosophy

Queen Mary and Westfield College

B L
LO
UNIV

ABSTRACT

Compression-after-impact testing is widely used to assist in the development and selection of materials for aircraft applications. Presently, there are no standard test methods in existence. The most widely used industrial tests require large specimens which are expensive to manufacture and test.

The results of an experimental study of the compression-after-impact test are reported. A miniaturised testing arrangement was used to investigate the effects of specimen width, thickness and lay-up on the measured compression strength of undamaged and impact damaged specimens. A toughened carbon / epoxy was used for the above work. In addition three other materials were tested (a carbon / polyetheretherketone (APC), a glass / epoxy (GRP) and another carbon / epoxy).

The in-plane extent of delamination damage after impact was measured using an ultrasonic C-scanning method. The carbon and glass reinforced epoxy materials had similar resistance to the initiation and propagation of impact damage. The APC was much more resistant to the formation of impact damage.

The measured strength of undamaged specimens was dependent upon specimen geometry, decreasing with width increase and increasing with thickness increase. The strength of impact damaged specimens was independent of width. Increasing the thickness increased the incident impact energy required to initiate damage and, therefore, delayed the onset of residual strength reductions.

The strength of undamaged quasi-isotropic and 0/90 laminates was very similar and higher than for ±45 laminates. After impact the 0/90 material was strongest. The residual strength of the quasi-isotropic and ±45 materials were very similar.

The APC retained the highest proportion of its initial strength over a range of incident impact energies. This was attributed to its resistance to the formation of impact damage. The GRP was the most damage tolerant material.

Contents

List of Figures 8

List of Tables 16

Introduction 17

Chapter 1 Background and Literature Review

1.1 Introduction 20
1.2 Impact Testing 20
1.2.1 Test Methods 20
1.2.2 Effect of Testing Geometry on the Initiation and Propagation of Impact Damage 21
1.2.2.1 Flexed Beam Testing 21
1.2.2.2 Flexed Plate Testing 25
1.2.2.3 Thermoplastic Matrix Composites 26
1.2.3 Detection of Impact Damage 26
1.2.4 Instrumentation 28
1.2.5 Effect of Material 30
1.3 Buckling 31
1.3.1 Introduction 31
1.3.2 Instability Buckling 31
1.3.3 Buckling of Columns 32
1.3.4 Buckling of Plates 32
1.4 Compression Testing 34
1.4.1 Introduction 34
1.4.2 Types of Compression Test 34
1.4.3 Failure Modes 36
1.4.4 Uses of Compression Test Data 36
1.5 Post-Impact Compression Testing 37
1.5.1 The Test and its Uses 37
1.5.2 Failure Process 39
1.5.3 Effect of Material 41
1.5.4 Current understanding of the effect of Material Properties on the Post-Impact Compression Strength 44
1.5.5 Combined Compression and Impact Testing 45

Chapter 2 Experimental Plan and Aims of Project

2.1 Experimental Plan 54
2.2 Aims of Project 55

Chapter 3 Materials and Experimental Methods

3.1 Materials 57
3.1.1 Material Suppliers and Identification Codes 57
3.1.2 Processing 58
3.1.2.1 Fibre Lay-up 58
3.1.2.2 Toughened Carbon / Epoxy 58
3.1.2.3 Carbon / Epoxy 59
3.1.2.4 Glass / Epoxy 59
3.1.2.5 APC 60
3.1.2.6 Laminate Sizes 60
3.1.3 Material Quality Control 60
3.2 Test Methods 62
3.2.1 Impact Testing 62
3.2.1.1 Impact Machine 62
3.2.1.2 Calculation of the Constant n' used in Equation 1.3 and Plate Stiffness (K_p) 63
3.2.2 Production of Compression Test Specimens 64
3.2.3 Compression Testing 64
3.2.3.1 Anti-Buckling Guide 64
3.2.3.2 Details of Compression Test 65
3.2.3.3 Testing of Initially Undamaged Specimens 65
3.2.4 Non-Destructive Testing 66
3.2.5 Microscopy 67

Chapter 4 Material Quality

4.1 Introduction 81
4.2 Results of Ultrasonic C-Scanning 81
4.3 Results of Interlaminar Shear Strength Tests 82
4.3.1 Results for TCE Material 82
4.3.2 Results for APC, CE and GRP Materials 84
4.4 Results of Void and Volume Fraction Measurements 85
4.5 Discussion 85
4.5.1 TCE Material 85
4.5.2 Other Materials 88

Chapter 5 Impact Testing and Assessment of Damage

5.1 Introduction 95
5.2 Instrumented Impact Testing 95
5.2.1 Interpretation of Instrumented Impact Tests 95
5.2.2 Effect of Specimen Width 97
5.2.3 Effect of Clamping 98
5.2.4 Effect of Lay-up 98
5.2.5 Effect of Thickness 99
5.2.6 Effect of Material 99
5.2.7 Calculation of the Constant n' used in Equation 1.3 and Plate Stiffness (Kp) 100
5.3 Detection and Assessment of Impact Damage 101
5.3.1 Non-Destructive Techniques 101
5.3.1.1 Damage Detection and Presentation of Results 101
5.3.1.2 Effect of Specimen Width 101
5.3.1.3 Effect of Clamping 102
5.3.1.4 Effect of Lay-up 102
5.3.1.5 Effect of Thickness 102
5.3.1.6 Effect of Material 103
5.3.2 Microscopy 104
5.3.2.1 Specimens Examined 104
5.3.2.2 Presentation of Results and General Comments 104
5.3.2.3 Effect of Lay-up 105
5.3.2.4 Effect of Thickness 106
5.3.2.5 Effect of Material 106
5.4 Discussion 107
5.4.1 Introduction 107
5.4.2 Accuracy of Instrumented Impact Test Data 107
5.4.3 Choice of Impact Tests Conditions 108
5.4.4 Damage Initiation 109
5.4.5 Final Damage State 116
5.4.5.1 Introduction 116
5.4.5.2 Accuracy of Measurements 117
5.4.5.3 General Observations Relating to the Damage State After Impact 117
5.4.5.4 Effect of Specimen Width 119
5.4.5.5 Effect of Thickness 119
5.4.5.6 Effect of Lay-up 119
5.4.5.7 Effect of Material 120

5.4.5.8 The use of Instrumented Impact Data to Assess the Total Amount of Damage 120

Chapter 6 Compression Testing of Initially Undamaged Specimens

6.1 Introduction 163
6.2 Compression Strength and Modulus 163
6.2.1 Results 163
6.2.2 Effect of Specimen Width and Lay-up 164
6.2.3 Effect of Thickness 165
6.2.4 Effect of Material 165
6.3 Buckling Behaviour 165
6.3.1 Results for GRP-QI-16-55 165
6.3.2 Effect of Lay-up 166
6.3.3 Effect of Material 167
6.4 Discussion 167
6.4.1 Introduction 167
6.4.2 Buckling Behaviour 167
6.4.3 Strength Measurements 169
6.4.3.1 Failure Modes 169
6.4.3.2 Effect of Specimen Geometry 170
6.4.3.3 Effect of Material 172
6.4.4 Final Comments 173

Chapter 7 Post-Impact Compression Testing

7.1 Introduction 193
7.2 Results 193
7.2.1 Results for TCE-QI-16-55 193
7.2.1.1 Post-Impact Compression Strength 193
7.2.1.2 Assessment of Scatter in PICS Test Results 194
7.2.1.3 Specimen Dimensions 195
7.2.1.4 Effect of Clamping During Impact Test 195
7.2.1.5 Effect of Loading Rate During Compression Testing 196
7.2.2 Effect of Specimen Width 196
7.2.3 Effect of Lay-up 196
7.2.4 Effect of Thickness 197
7.2.5 Effect of Material 197
7.2.5.1 Comparison of TCE and APC Materials 197
7.2.5.2 Comparison of TCE and CE Materials 200

7.2.5.3 Comparison of TCE and GRP Materials 200
7.3 Discussion 202
7.3.1 Introduction 202
7.3.2 Accuracy of Results 202
7.3.3 Effect of Specimen Geometry 203
7.3.3.1 Specimen Width 204
7.3.3.2 Specimen Thickness 207
7.3.3.3 Effect of Clamping During Impact 208
7.3.3.4 Effect of Loading Rate 209
7.3.4 Effect of Material 209
7.3.4.1 Fibre Lay-up 209
7.3.4.2 Effect of Material 211
7.3.5 Utility of the Post-Impact Compression Test 213
7.3.6 Assessment of the Miniaturised Post-Impact Compression Test 214

Chapter 8 Concluding Discussion
8.1 Introduction 240
8.2 Impact 240
8.3 Compression Testing of Previously Undamaged Specimens 241
8.4 Post-Impact Compression Testing 242

Chapter 9 Conclusions
9.1 Compression Testing of Previously Undamaged Specimens 244
9.2 Post-Impact Compression Testing 244
9.3 Materials 245

Suggestions For Further Work 247

Acknowledgements 249

References 250

Appendix 261

List of Figures

Chapter 1

1.1 (a) Effect of beam length on damage initiation energy for low and high velocity impacts.....47
(b) Effect of target thickness on damage initiation energy for low and high velocity impacts.....47

1.2 Schematics to show damage progression due to (a) contact induced stresses and (b) flexure induced stresses.....48

1.3 Load versus (a) edge displacement and (b) lateral displacement to show the difference between the buckling behaviour of perfect and imperfect plates.....48

1.4 Schematic to show effect of specimen width on the predicted buckling load.....49

1.5 Schematic to show the post-impact compression test. (a) Impact and (b) Compression.....50

1.6 Examples of anti-buckling guides. (a) End loaded. (b) Shear loaded.....51

1.7 Schematics to show the buckling modes of delaminated composites.....52

1.8 (a) Schematic to show Whitcomb model. (b) Failure load versus delamination half- length.....52

1.9 Typical results of post-impact compression tests.....53

1.10 Schematic showing results of combined compression and impact test.....53

Chapter 3

3.1 Schematic to show details of the pressclave (a) Lay-up of materials. (b) Assembly in press.....71

3.2 Temperature versus time record for TCE processing. (a) Curing. (b) Curing and cooling.....72

3.3 Impact support and clamping conditions.....73

3.4 Diagram to show position of measurement points and fibre directions for compression specimens.....74

3.5 Schematic drawing of the anti-buckling guide.....75

3.6 Diagram to show compression specimen support conditions.....76

3.7 Set-up procedure for the anti-buckling guide.....77

3.8 Photograph of anti-buckling guide and specimen during a compression test.....78

3.9 Positions for the mesurement of lateral deflection.....79

3.10 Schematic to show operation of the ultrasonic C-scan.....80

Chapter 4

4.1 (a) Average ILSS for TCE-±45-16 material..... 91
(b) Average ILSS for TCE-0/90-16 material..... 91
(c) Average ILSS for TCE-QI-16, 24 and 32 material..... 91
4.2 (a) Frequency distribution for ILSS tests on TCE-±45-16 material..... 92
(b) Frequency distribution for ILSS tests on TCE-0/90-16 material..... 92
(c) Frequency distribution for ILSS tests on TCE-QI-16 material..... 92
4.3 Cumulative frequency plot on normal probability scale for the TCE-QI-16 material ILSS results..... 93
4.4 Frequency distribution for tests on TCE-0-16 material..... 94

Chapter 5

5.1 Instrumented impact data for TCE-0/90-16 material.
(a) Force, (b) Velocity, (c) Displacement and (d) Absorbed Energy plotted as a function of time. Spec No 14/5, Incident Impact Energy 4.73 J..... 123
Force versus time curves for:
(e) Spec No 11/3, Incident Impact Energy 1.25 J..... 124
(f) Spec No 12/2, Incident Impact Energy 1.94 J..... 124
(g) Spec No 14/2, Incident Impact Energy 11.34 J..... 124
5.2 (a) Impact force versus incident impact energy.
Material, TCE-QI-16-55..... 125
(b) Absobed energy versus incident impact energy.
Material, TCE-QI-16-55..... 125
(c) Total absorbed energy versus incident impact energy
Material, TCE-QI-16-55..... 126
(d) Normalised total absorbed energy versus incident impact energy.
Material, TCE-QI-16-55..... 126
5.3 (a) Effect of specimen width on force F1. Material TCE-QI-16..... 127
(b) Effect of specimen width on absorbed energy at F1.
Material TCE-QI-16..... 127
(c) Effect of specimen width on force F2. Material TCE-QI-16..... 128
(d) Effect of specimen width on absorbed energy at F2.
Material TCE-QI-16..... 128
(e) Effect of specimen width on normalised total absorbed energy.
Material, TCE-QI-16..... 129

5.4 Comparison of absorbed energies at damage initiation for different specimen widths and lay-ups for TCE 16 ply material..... 129
5.5 (a) Effect of clamping during impact on force F1. Material, TCE-QI-16-55..... 130
(b) Effect of clamping during impact on absorbed energy at force F1. Material, TCE-QI-16-55..... 130
(c) Effect of clamping during impact on normalised total absorbed energy. Material, TCE-QI-16-55..... 131
5.6 (a) Effect of lay-up on total absorbed energy. Material, TCE-QI, 0/90 and ±45-16-45, 55 and 75..... 132
(b) Normalised total absorbed energy versus incident impact energy. Material, TCE-0/90-16-45, 55 and 75..... 132
(c) Normalised total absorbed energy versus incident impact energy. Material, TCE-±-16- 55..... 133
(d) Effect of lay-up on the normalised total absorbed energy. Material, TCE-QI, 0/90 and ±45-16-45, 55 and 75..... 133
5.7 (a) Effect of fibre stacking sequence on force F1. Material, TCE-QI and QI*-16-55..... 134
(b) Effect of fibre stacking sequence on absorbed energy at F1. Material, TCE-QI and QI*-16-55..... 134
(c) Effect of fibre stacking sequence on normalised total absorbed energy. Material, TCE-QI and QI*-16-55..... 135
5.8 (a) Effect of material thickness on force F1. Material TCE-QI-16, 24 and 32-55..... 136
(b) Effect of material thickness on absorbed energy at F1. Material, TCE-QI-16, 24 and 32-55..... 136
5.9 (a) Effect of material thickness on the average force at damage initiation. Material, TCE-QI-16, 24 and 32-55..... 137
(b) Effect of material thickness on the average absorbed energy at damage initiation. Material TCE-QI-16, 24 and 32-55..... 137
5.10 (a) Total absorbed energy versus incident impact energy. Material, TCE-QI-24-55..... 138
(b) Total absorbed energy versus incident impact energy. Material, TCE-QI-32-55..... 138
(c) Effect of thickness on the total absorbed energy. Material, TCE-QI-16, 24 and 32-55..... 139

5.11 (a) Effect of material on force F1.
Material, TCE, CE, GRP, APC-QI-16-55. 140
(b) Effect of material on the absorbed energy at F1.
Material, TCE, CE, GRP, APC-QI-16-55. 140
5.12 Effect of material on the average absorbed energies at F1. 141
5.13 (a) Normalised total absorbed energy versus incident impact energy.
Material, TCE-QI-16-55. 142
(b) Normalised total absorbed energy versus incident impact energy.
Material, CE-QI-16-55 142
(c) Normalised total absorbed energy versus incident impact energy.
Material, GRP-QI-16-55. 143
(d) Effect of material on normalised total absorbed energy.
Material, TCE, CE, GRP, APC-QI-16-55. 143
5.14 Results of ultrasonic C-scans showing damaged areas in
GRP-0/90-16-55 specimens. 144
5.15 Photographs showing impact damage in GRP-0/90-16-55 specimens. 145
5.16 (a) Damage area versus incident impact energy. Material, GRP-QI-16-55. 146
(b) Total absorbed energy versus incident impact energy.
Material, GRP-QI-16-55. 146
5.17 Impact damaged areas for TCE-QI-16 specimens of different widths. 147
5.18 (a) Effect of specimen width on damage width.
Material, TCE-QI-16-45, 55 and 75. 148
(b) Effect of specimen width on damage width.
Material, TCE-0/90-16-45, 55 and 75. 148
(c) Effect of specimen width on damage width.
Material, TCE-±45-16-45, 55 and 75 149
5.19 Effect of clamping during impact test on damage width.
Material, TCE-QI-16-55. 149
5.20 (a) Effect of lay-up on damage width.
Material, TCE-QI, 0/90 and ±45-16-55 150
(b) Effect of stacking sequence on damage width.
Material, TCE-QI and QI*-16-55 150
5.21 Effect of material thickness on damage width.
Material, TCE-QI-16, 24 and 32-55. 151
5.22 Effect of material on damage width.
Material, TCE, CE, GRP, APC-QI-16-55. 151

5.23 Montage of 35 mm contact prints showing general view of impact damage in a sectioned TCE-QI-16-55 specimen..... 152
5.24 Detail of impact damage in TCE-0/90-16 material. Spec No 49/3. Incident Impact Energy 1.78 J..... 153
5.25 Schematic diagrams showing the through thickness distribution of damage in TCE specimens.
(a) TCE-0/90-16. Spec No 49/3. Incident Impact Energy 1.78 J..... 154
(b) TCE-0/90-16. Spec No 49/5. Incident Impact Energy 5.01 J..... 154
(c) TCE-0/90-16. Spec No 49/7. Incident Impact Energy 11.89 J..... 154
(d) TCE-QI-16. Spec No 48/2. Incident Impact Energy 1.50 J..... 155
(e) TCE-QI-16. Spec No 48/4. Incident Impact Energy 3.99J..... 155
(f) TCE-QI-16. Spec No 48/7. Incident Impact Energy 10.01 J..... 155
(g) TCE-QI-24. Spec No 50/6. Incident Impact Energy 2.98 J..... 156
(h) TCE-QI-24. Spec No 50/7. Incident Impact Energy 5.06 J..... 156
(i) TCE-QI-24. Spec No 50/9. Incident Impact Energy 11.96 J..... 156
(j) TCE-QI-32. Spec No 51/7. Incident Impact Energy 5.97 J..... 157
(k) TCE-QI-32. Spec No 51/8. Incident Impact Energy 11.96 J..... 157
5.26 (a) Positions of Delaminations for TCE-0/90-16 material..... 158
(b) Positions of Delaminations for TCE-QI-16 material..... 159
(c) Numbers of delaminated interfaces in sectioned specimens..... 160
5.27 Photograph of sectioned APC specimen showing permenant plastic deformation after impact testing.
Spec No 53/4. Incident Impact Energy 15.14 J..... 161
5.28 Data from fig 5.9 (a) replotted..... 162

Chapter 6

6.1 (a) Stress - strain curves for compression tests on previously undamaged specimens. Material, TCE-QI-16-55..... 175
(b) Stress - strain curves for compression tests on previously undamaged specimens. Material, GRP-QI-16-55..... 176
(c) Comparison of stress-strain curves for compression tests on TCE and GRP-QI-16-55 specimens..... 177
6.2 Typical compression failure in unsupported region of specimens.
(a) Spec No 21/5. (b) Spec No 22/5..... 178
6.3 Photograph of an end crushing failure. Spec No 39/2. TCE-QI-24-55..... 179

6.4 Effect of specimen width on measured plate modulus.
Material, TCE-QI, 0/90 and ±45-16-45, 55 and 75..... 180
6.5 Calculated and measured moduli.
Material, TCE-QI, 0/90 and ±45-16-45, 55 and 75..... 180
6.6 Effect of specimen width on compression strength.
Material, TCE-QI-16-45, 55 and 75. 180
6.7 (a) Effect of specimen thickness on plate modulus.
Material, TCE-QI-16, 24 and 32-55. 181
(b) Effect of specimen thickness on compression strength.
Material, TCE-QI-16, 24 and 32-55. 181
6.8 (a) Effect of material on plate modulus.
Material, TCE, CE, APC, GRP-QI-16-55. 182
(b) Effect of material on compression strength.
Material, TCE, CE, APC and GRP-QI-16-55..... 182
6.9 Deformed profiles of compression specimens for GRP-QI-16-55.
(a) Spec 25/2 (b) Spec 26/12 (c) Spec 25/11..... 183/4
6.10 Load versus lateral deflection curves for tests at low loads.
Material, GRP-QI-16-55. 185
6.11 Load versus lateral deflection to failure. Material, GRP-QI-16-55..... 185
6.12 (a) Comparison of load versus deflection curves for 'low' and 'high' load tests on specimen 25/11. Material, GRP-QI-16-55. 186
(b) Comparison of load versus deflection curves for 'low' and 'high' load tests on Specimen 26/12. Material, GRP-QI-16-55..... 186
(c) Comparison of load versus deflection curves for 'low' and 'high' load tests on specimen 25/2. Material, GRP-QI-16-55..... 186
6.13 Deformed profiles of compression specimens.
(a) TCE-0/90-16-75, Spec 11/6. (b) TCE-0/90-16-75, Spec 11/5..... 187
(c) TCE-QI-16-75, Spec 33/1. (d) TCE-QI-16-75, Spec 32/2..... 188
(e) TCE-0/90-16-75, Spec 11/2. 189
6.14 Effect of lay-up on load versus lateral deflection curves for 75 mm wide specimens. Material, TCE-QI and 0/90-16-75..... 190
6.15 Deformed profiles of compression specimens for TCE-QI-16-55.
(a) Spec 34/3 (b) Spec 34/6..... 191
6.16 Effect of material on load versus lateral deflection curves.
Materials, TCE, APC, GRP-QI-16-55. 192

Chapter 7

7.1 Compression strength versus incident impact energy for TCE-QI-16-55. 218

7.2 Shear type failure at edge of specimen after impact and compression testing. Spec No 41/2. Incident Impact Energy 0.96 J. TCE-QI-16-55. 219

7.3 Typical stress-strain curves for PICS tests on TCE-QI-16-55 material..... 220

7.4 Plate modulus versus incident impact energy for TCE-QI-16-55..... 221

7.5 (a) Photographs showing impact damage in GRP-QI-16-55 specimens..... 222
(b) Photographs showing damage state after compression testing of the specimens shown in fig 7.5 (a). 223

7.6 Drawing to show an example of a specimen shape where all of the angles at the corners are less than 90 degrees. 224

7.7 Effect of clamping during impact on compression strength. Material, TCE-QI-16-55..... 225

7.8 Effect of loading rate on compression strength. Material, TCE-QI-16-55..... 225

7.9 (a) Effect of specimen width on compression strength. Material, TCE-QI-16-45, 55 and 75. 226
(b) Effect of specimen width on compression strength. Material, TCE-0/90-16-45, 55 and 75. 226
(c) Effect of specimen width on compression strength. Material, TCE-±-16-45, 55 and 75..... 227

7.10 (a) Effect of lay-up on PICS for TCE-0/90, QI and ±45-16-45, 55 and 75 materials. 228
(b) Stress-strain curves for PICS tests on TCE-±45-16-55..... 229

7.11 Effect of stacking sequence on PICS for TCE-QI and QI*-16 materials. 230

7.12 Effect of specimen thickness on compression strength for TCE-QI-16, 24 and 32-55 material..... 231

7.13 Compression strength versus incident imapct energy for TCE and APC-QI-16-55..... 231

7.14 Compression strength versus damage width for TCE and APC-QI-16-55 material..... 231

7.15 Compression strength plotted as a function of damage width with 95% confidence and prediction intervals. Material, TCE-QI-16-55. 232

7.16 Compression strength plotted as a function of damage width with 95% confidence and prediction intervals. Material, APC-QI-16-55..... 232

7.17 Compression strength versus damage width. Comparison of 95% prediction intervals for TCE and APC-QI-16-55. 233

7.18 Normalised compression strength versus damage width. Comparison of 95% prediction intervals for TCE and APC-QI-16-55..... 233

7.19 Compression strength versus incident impact energy for TCE and CE-QI*-16-55 materials..... 234
7.20 Compression strength versus damage width for TCE and CE-QI*-16-55 materials..... 234
7.21 Compression strength versus incident impact energy for TCE and GRP-QI-16-55 materials..... 235
7.22 Normalised compression strength versus incident impact energy for TCE and GRP-QI-16-55 materials..... 235
7.23 Compression strength versus damage width with 95% confidence and prediction intervals for GRP-QI-16-55 materials..... 236
7.24 Normalised compression strength versus damage width for TCE and GRP-QI-16-55 materials..... 236
7.25 Normalised compression strength versus damage width. Comparison of 95% prediction intervals for TCE and GRP-QI-16-55..... 237
7.26 Stress-strain graphs for residual compression tests on GRP-QI-16-55 material..... 238
7.27 (a) Comparison of data for TCE-QI-32-55 and results from Ilcewicz et al (1989)..... 239
7.27 (b) Comparison of data for TCE-QI-24-55 and results from Ilcewicz et al (1989)..... 239

List of Tables

Chapter 2

2.1 Combinations of materials, lay-ups, thicknesses and specimen widths tested..... 56

Chapter 3

3.1 Details of materials and suppliers..... 69
3.2 Laminate sizes..... 70

Chapter 4

4.1 Frequency distribution data for ILSS tests on TCE, 16 ply material..... 89
4.2 Average ILSS results for TCE-0-16 material..... 90
4.3 Results of volume fraction measurements..... 90

Chapter 5

5.1 Results of impact tests: forces and absorbed energies at damage initiation..... 122

Chapter 6

6.1 Average compression moduli and strengths for compression tests on previously undamaged material..... 174

Chapter 7

7.1 Dimensions of TCE-QI-16-55 compression specimens..... 216
7.2 Dimensions and calculated angles of TCE-QI-16-55 compression specimens..... 217

Introduction

Advanced composite materials have several properties which make them suitable for aircraft structural applications. They have high specific stiffness and strength, good fatigue properties (at least in tension), good corrosion resistance and are highly formable (Baker et al, 1985). According to Dorey (1984) weight savings of between 10-30% can be achieved for direct material replacement and up to 50% for complete structural designs.

The origins of these materials can be traced back to the late 1930's when flax thread was impregnated with phenolic resin to produce what was probably the first example of a "high performance" composite. A number of fibres were investigated during the next two decades but none were found that had the specific stiffness and strength properties required for structural aircraft applications (McMullen, 1984). In 1961 Shindo developed a process for making carbon fibres from polyacrylonitrile (PAN) precursor. The fibres did not have outstanding properties but were stiffer than the glass fibres available at that time (McMullen, 1984). By the mid-1960's a process had been developed at the Royal Aircraft Establishment to produce high modulus, high strength carbon fibres from PAN (Hull, 1981). When combined with thermosetting resins which had already been developed for glass reinforced composites a material was produced which had excellent specific stiffness and strength values (Stubbington, 1988). These properties made composite materials viable for use in aircraft structural applications and during the late 1960's and early 1970's the first investigative programmes aimed at quantifying the potential of the new materials were undertaken (Anderson (1987), Anglin (1987)).

Composite materials are now widely used both in military (Sharples (1980), Anderson (1987), Stubbington (1988), Anglin (1987)) and commercial (Dexter (1980), Anglin (1987)) aircraft structures. One example of a military aircraft where composites have been extensively used is the U.S. Navy's Harrier AV-8B has carbon/epoxy material in the forward fuselage, horizontal stabiliser, elevators, rudder, overwing fairings, wingbox skin and structure, ailerons and flaps. In total CFRP accounts for 26% of the airframe mass (Stubbington (1988), Anglin (1987)). In general the adoption of composite components for commercial aircraft has been more cautious. For example the Boeing 737-300 employs composite materials for control surfaces, fairings and nacelle components, which account for approximately 3% of the airframe mass. (Anglin, 1987). However civil projects have been undertaken which made greater use of composites than military projects of the same era. One example is the Lear Fan (a small passenger aircraft designed to carry two pilots and six to eight passengers) was the first aircraft constructed entirely from advanced composites. Development of the aircraft began in 1977 and a prototype

flew in 1981, however technical and financial problems eventually forced the project to be abandoned in 1985 (Hart-Smith, 1989). Another example is the Beach Starship, a turboprop business plane, which was the first all-composite pressurised aircraft to be certified. Fuel savings of more than one third have been claimed over jets with comparable performance (Advanced Composites Engineering, 1988).

The introduction of composite materials into aircraft has been hindered to some extent by the complexities of designing with anisotropic, inhomogeneous materials. Currently a methodology exists for designs based on a stiffness requirement, however problems are encountered when a strength criteria is to be satisfied. Design data for strength are difficult to measure since the test results are often sensitive to the test geometry. Apart from this composites are prone to a fairly wide range of defects and damage arising during both manufacture and service. This damage can seriously affect the residual strength of the material and this needs to be accounted for at the design stage. The damage tolerance problem is dealt with in metallic aircraft by using a fracture mechanics approach (Baker et al 1985). However a design methodology has not yet been developed for composite materials. Part of the problem is that fracture toughness measurements are influenced by the test method but more importantly the applicability of fracture mechanics to composite materials is questionable (Harris et al, 1988). The consequence of this is that designs cannot be optimised.

Baker et al (1985) identified delaminations as possibly the most important type of defect because they can cause large reductions in residual compressive strength and can be difficult to detect. Delaminations can develop during service due to: (a) through thickness stresses developed at free edges, holes, ply terminations or ply drops, bonded or co-cured joints and bolted joints. (b) Effects of moisture and temperature, for example residual thermal stresses from processing and moisture gradients through the thickness of the laminate. (c) Low energy impact damage caused by runway stones, hail stones, tyre disintegration and dropped tools for example (Baker et al (1985), Garg (1988), Kupczyk (1988)). Of these low energy impact has been identified as the most insidious (Baker et al, 1985) because: (a) the probability of occurrence is high (for example operators of the Dornier 328 find that the majority of damage occurs during service work between flights or during maintenance, with an average of one damage per month (Kupczyk, 1988)), (b) the damage is likely to remain undetected (since routine non-destructive testing (NDT) is almost always confined to potential hot-spots as full scale NDT is both costly and time consuming) and (c) large reductions in residual compressive strength can occur (Baker et al, 1985).

The problem of these large reductions in residual compressive strength has led to materials development programmes aimed at improving the relevant properties. The post-impact compression strength (PICS) test has been widely adopted to assess the effectiveness of materials developments and to help in materials selection for aircraft applications. It is one of a series of tests which are commonly used to assess the toughness and damage tolerance of a material. For example NASA use edge-delamination, double cantilever beam (to measure interlaminar fracture toughness, G_{Ic}), open hole tension and compression and PICS tests to evaluate laminated composites (Anon, 1982).

1 Background and Literature Review

1.1 Introduction

This chapter is divided into four sections:
(1.2) Impact Testing
(1.3) Buckling
(1.4) Compression Testing
(1.5) Post-Impact Compression Testing

Impact testing and post-impact compression testing are covered in most detail while the sections on buckling and compression testing have been included to provide background information.

1.2 Impact Testing

1.2.1 Test Methods

Tests originally developed for assessing the impact behaviour of homogeneous, isotropic materials (for example Charpy and Izod type tests) have been found to be of limited use when applied to composite materials because of the complexity of the failure processes. Instead tests designed to simulate in-service conditions have been widely adopted. Dropweight tests (simulating dropped tools) and ballistic tests (simulating runway stones) are commonly used. These tests have the advantage that the effect of the impact damage on some other mechanical property can be measured (Dorey, 1987). Both flexed beam and flexed plate configurations have been used, although the flexed plate type is more popular with either circular or square / rectangular supports commonly in use. The advantage of the beam type specimen is that measured properties can be related to the overall anisotropy of the material from which the beams have been cut (Hogg et al, 1988). However edge effects resulting from the lay-up of the material (Bowles, 1988) or the quality of the specimen preparation may affect the results (Hogg et al, 1988). This is not a problem for the flexed plate method where edge effects are unlikely to affect the result. The flexed plate method corresponds more closely with the in-service conditions (Hogg et al (1988), Bowles (1988)).

1.2.2 Effect of Testing Geometry on the Initiation and Propagation of Impact Damage

The importance of specimen geometry on the results of impact tests was realised at an early stage. Workers in the early 1970's began to investigate the problem (see for example Bradshaw et al, 1972). It is therefore somewhat surprising that few systematic studies on the influence of geometric effects on the impact response of composite structures have been undertaken (Cantwell et al, 1989 (b)). However the important parameters have been identified and investigated and will be dealt with in the following sections.

1.2.2.1 Flexed Beam Testing

For flexed beam testing the specimen span, thickness, width and lay-up were identified as variables which could affect the results of impact tests. The effect of these variables has been investigated under "low" and "high" velocity impact conditions. "Low" velocity impacts generally refer to dropweight tests while "high" velocity refers to gas gun tests. There does not appear to be a universally accepted definition of the difference between "low" and "high" velocity impacts. Sjoblom et al (1988) define "low" velocity as a velocity low enough to cause the same structural response as a static load. In other words dynamic behaviour and stress wave effects are negligible. The effect of these variables on damage initiation and propagation for composites with thermosetting matrix materials will be considered in the following two sections. Differences in behaviour observed for thermoplastic matrix materials will be presented in section 1.2.2.3.

(a) Damage Initiation

Cantwell (1985) identified two damage initiation mechanisms. The first is matrix cracking between lower surface fibres caused by bending-induced tensile stress. This initiation mechanism is most likely to occur for beams which are flexible. Specimen flexibility is a function of the span of the beam and the thickness and lay-up of the material. Large spans or thin specimens lead to more flexible specimen response. The energy required to initiate damage by this mechanism for a simply supported beam specimen can be estimated from the following equation (Dorey, 1987):

$$\text{Energy} = (1 / 18)\,(\sigma^2 / E)\,w\,t\,L \qquad \text{Eq 1.1}$$

where: σ is the flexural strength, E is the flexural modulus, w is the specimen width, t is the specimen thickness and L is the unsupported length.

The second initiation mechanism identified by Cantwell (1985) was matrix cracking on the contact surface. These cracks are initiated by large tensile stresses generated at the periphery of the contact area (See Greszczuk, 1982 for more detail). This initiation mechanism is most likely to occur for stiff, inflexible beams since higher contact stresses are developed when the target is stiff.

Another initiation mechanism which was not discussed by Cantwell is that of delamination at (or close to) the neutral axis caused by bending induced shear stresses. The energy required to initiate damage by this mechanism for a simply supported beam specimen can be estimated from the following equation (Dorey, 1987):

$$\text{Energy} = (2 / 9)\,(\tau^2 / E)\,(w\,L^3 / t) \qquad \text{Eq 1.2}$$

where: τ is the interlaminar shear strength.

Less energy is required to initiate damage for materials with low interlaminar shear strength, short spans or large thicknesses. In common with the short beam shear test the span-to-depth ratio of 5 is usually required to initiate this type of damage before tensile flexural failure occurs.

The equations (1.1 and 1.2) given above do not include a term to account for energy absorbed by contact deformations. This was accounted for by Greszczuk (1982) in the following equation:

$$\text{Energy} = (1 / 2)\,(F^2 / K_p) + (2 / 5)\,(F^{5/3} / n'^{2/3}) \qquad \text{Eq 1.3}$$

where: F is the force at damage initiation, K_p is the stiffness of the specimen and n' is a constant linking contact forces and deflections ($P = n'\,\alpha^{3/2}$, where: α is the contact deflection).

Equations allowing both K_p and n' to be calculated are given by Greszczuk (1982). Alternatively they can measured experimentally. For a simply supported beam specimen the theoretical stiffness is:

$$Kp = (4\,E\,b\,t^3) / L^3 \qquad \text{Eq 1.4}$$

and

$$P = (2 / 3)\,(b\,t^2 / L)\,\sigma \qquad \text{Eq 1.5}$$

If equations 1.4 and 1.5 are substituted into the first term of equation 1.3 the result is the same as that given by Dorey (1987) in equation 1.1.

The effect of specimen span and thickness on the damage initiation energy has been investigated in some detail by Cantwell (1989 (a)) for both low and high energy impacts. The trends found for variations in span are shown in fig 1.1(a). For low velocity impacts, the energy required to initiate damage rises as the span is increased. The specimen becomes more flexible as the span is increased and more energy is absorbed by the specimen in bending before damage initiates. For short spans, damage is initiated by contact induced stresses. As the specimen becomes more flexible a change in failure mode occurs and lower surface matrix cracking is initiated. The situation is different for high velocity impacts. The initiation energy remains constant with beam length and damage initiates on the contact surface for the beam lengths studied by Cantwell (1989 (a)). The reason given for this behaviour is that at high velocities the beam does not have time to respond in flexure before damage initiates and hence less energy is absorbed. This observation was also made by Dorey (1987).

The effect of thickness on the damage initiation energy for low and high velocity impacts found experimentally by Cantwell (1989 (a)) is shown in fig 1.1 (b). For low velocity impacts and thin specimens damage initiated on the lower surface. The energy required to initiate damage increased as the thickness (and therefore the stiffness) of the specimen increased. In thicker specimens the damage initiated on the upper surface due to contact induced stresses. Increases in thickness caused the initiation energy to fall as the specimen became thicker and higher contact forces were generated. The same trends were observed for high velocity tests. However the initiation energies were lower showing that high velocity impact is a more severe loading condition.

Damage initiation energy was not affected by specimen width for high velocity impacts (Cantwell, 1988). Again the effect of specimen geometry is reduced for high velocity impact because the specimen does not have time to respond in flexure.

Soulezelle (1987) also identified specimen flexibility as an important parameter for tests on flexed beams. The energy required to initiate damage decreased as specimen flexibility was increased. Changes in specimen flexibility were achieved by varying both the lay-up and ply stacking sequence (Soulezelle, 1987).

(b) Damage Development

Once damage has been initiated, in the form of a tensile matrix crack, on the contact surface of the specimen the crack is found to propagate through the first ply where it is deflected into the interlaminar region, forming a delamination (Cantwell, 1985). This type of behaviour is often observed for fibre reinforced materials because of the low ratio of interfacial shear strength to the tensile strength of the fibre (Hull, 1981). Takeda et al (1982) and Boll et al (1986) noted that delamination cracks usually propagate near or at fibre - resin interfaces. Boll et al suggest that residual stresses in the resin near to the fibres provide a low energy path for crack propagation.The delamination grows away from the point of impact until it is deflected into the next ply by a matrix shear crack. These shear cracks are caused by contact induced shear stresses which radiate out from the contact periphery. As the contact area changes so does the position of the maximum shear stresses. This generates shear cracks at different locations in the material (Cantwell, 1985). The resulting damage pattern is shown schematically in fig 1.2 (a). Similar mechanisms cause the bending-induced tensile cracks on the lower side of the specimen to propagate, giving the damage pattern shown in fig 1.2 (b) (Cantwell, 1985). Superimposed upon the contact-induced stresses are bending-induced tensile, compressive and shear stresses. Again, the span and thickness dimensions are important, short spans or thick specimens causing high shear stresses close to the neutral axis and promoting delamination (Dorey, 1987).

Fibre lay-up has some effect on the damage state. Wu et al (1988) found that delaminations only form when a change in ply orientation occurs. In addition Guynn et al (1985) found that lemniscate (or "peanut") shaped delaminations formed with their major axis oriented parallel to the fibres in the ply furthest away from the impact point.

As the impact energy is increased a point is reached where the striker will penetrate the material. Cantwell (1985) reported that a fustrum-shaped shear plug is often ejected. The effect of specimen span was the same as that observed for damage initiation. For low velocity impacts, the energy required to penetrate the material increased and for high velocity impacts the energy was constant. The effects can again be explained in terms of specimen stiffness. Increases in specimen thickness were found to increase the energy required to penetrate the specimens. However little difference was found between the penetration energies for high and low velocity impacts. The reason given for this is that a large part of the incident energy is dissipated by a shear out process and only a small amount of energy was absorbed in bending because the specimens were small (50 x 25

mm). The suggestion is that penetration energies would be different if larger structures were to be tested (Cantwell, 1989 (a)).

As would be expected the total area of damage (measured using ultrasonic C-scan) was found by Cantwell (1989 (a)) to increase rapidly with increasing incident energy. In addition the damage area was found to be greater for the high velocity impacts. This occurs because the impact energy is not absorbed by elastic deformation of the specimen and is therefore available for damage creation (Cantwell, 1989 (a)). Akoi et al (1980) also found that the extent of in-plane damage initially increased with increasing velocity (impact energy). However at sufficiently high velocities, the extent of in-plane damage was found to be only slightly larger than the cross section of the projectile because a shear-out mechanism operated. In addition stress waves in the material have been found to initiate damage under high velocity loading conditions. The impact causes a compressive stress wave to travel through the material until it is reflected from the back surface as a tensile stress wave causing failure at the first weak interface and fibre spalling on the back face (Dorey, 1982). This could further explain the differences between the damage areas for the high and low velocity impacts. There is also the possibility that these stress waves could promote delamination within the material.

Verpoest at al (1987) and Sjoblom et al (1988) consider that the total amount of energy absorbed during the impact event should be a more direct measure of the amount of damage formed than the incident impact energy. This is a perfectly logical statement and the total absorbed energy (measured using instrumented impact machines) is often quoted for this reason. However Reed et al (1988) found a poor correlation between the amount of energy absorbed and the extent of damage.

1.2.2.2 Flexed Plate Testing

The damage initiation and propagation mechanisms for plate type specimens are the same as those described in the previous section. Again target flexibility is an important parameter (Cantwell, 1989 (a)). Either circular or square / rectangular supports are most commonly used and so the flexibility depends upon the support ring diameter or the length / width of the rectangular support. Cantwell (1989 (b)) states that "... the impact performance [of plate type coupons] is not significantly different from that of beam like coupons". Verpoest et al (1987) investigated the effect of support diameter on the impact of glass / epoxy laminates. The response of material supported on 40 mm and 80 mm diameter ring supports was compared. As would be expected (based on the previous comments about specimen flexibility) higher forces, lower deflections, higher absorbed

energies and damage areas were observed for the 40 mm diameter support conditions. The authors also compared the impact response of specimens supported on a 40 mm diameter and 40 mm square supports. Only small differences were found for the peak forces measured. The total amount of energy absorbed was slightly higher and the damage area slightly lower for the specimen tested on the square support.

1.2.2.3 Thermoplastic Matrix Composites

The effect of geometry and the types of damage found in thermoplastic matrix composites are generally very similar to those described above for thermosetting matrix materials. However there is one important difference in the behaviour of thermoplastic matrix materials which stems from their ability to deform plastically. Morton et al (1989) compared the damage found in carbon fibre reinforced toughened epoxy and APC-2 (a thermoplastic matrix material). They found that the amount of delamination and matrix cracking was smaller in the APC-2 and attributed this to the ability of the thermoplastic to absorb energy in local permanent deformation. Similar results have been reported by other workers (Dorey et al (1985), Bishop (1985), Brandt et al (1986)).

1.2.3 Detection of Impact Damage

There are a large number of methods for detecting damage in composite materials. These can be conveniently divided into destructive and non-destructive methods. Stone et al (1987) reviewed the non-destructive techniques which have been applied to composite materials. They discuss a number of techniques (ultrasonics, radiography, thermography, eddy currents, mechanical impedance, acoustic emission and fibre optics) but point out that ultrasonic techniques and x-radiography have been most widely used. There are really only two commonly used destructive methods. The first is sectioning followed by polishing and microscopy and the second is the "deply" technique. The sectioning / polishing technique is well know and does not require further description here. The deply technique was developed especially for use with laminated composite materials and is described by Freeman (1982). Briefly, it involves marking the damage by using a dye penetrant and then thermally degrading the matrix material so that the material can be separated into individual plies while the integrity of each ply is maintained. The areas of delamination can then be identified by locating the stained areas. Fibre failure can also be seen to a lesser extent although matrix cracks cannot be seen because most of the matrix material has been removed (Freeman, 1982).

Cantwell (1985) compared the results of ultrasonic C-scanning, optical microscopy, X-radiography and the deply technique when used to locate impact damage. The ultrasonic C-scan was found to be most useful for detecting delamination damage. Fibre failures and other matrix cracks generally being too small to be resolved. The disadvantage of the C-scanning technique is that it only gives the in-plane extent of damage and does not identify the through thickness distribution (Cantwell, 1985). However ultrasonic techniques are available which do allow an indication of the through thickness distribution of damage to be obtained. These techniques and some of the problems involved are described by Stone et al (1987). Preuss et al (1988) used a time-of-flight C-scanning system to monitor the in-plane extent of delamination to approximately ± 1 mm and the through thickness position of damage in a 56 ply laminate to better than ± 1 mm. More sophisticated machines are being developed to allow three dimensional images of delamination damage to be obtained (Stone et al, 1987).

Cantwell (1985) found that the damage could be studied in more detail by using penetrant enhanced X-radiography. An X-ray opaque fluid is introduced into the material to highlight the damage. The maximum extent of delamination and matrix cracks (where they frequently extended 10 mm or more) were detected. Fibre fractures were more difficult to detect because the damage only extended a few millimetres and is often obscured by delamination damage, both above and below the fibre fractures.

The thermal deply technique was found to be much better for locating fibre fractures. It was also possible to locate the position (both in-plane and through thickness) and extent of delamination damage. However matrix cracks could not be seen because most of the matrix is removed during the de-plying stage (Cantwell, 1985).

Cantwell (1985) and Guynn et al (1985) found that the in-plane extent of delamination damage measured using both the X-ray and deply techniques was smaller than that measured using the ultrasonic C-scanning technique. The reason for this is that unless the damage is well formed there may be a problem in getting the dye or x-ray opaque fluid to penetrate completely. Guynn et al (1985) suggest that more complete penetration can be achieved either by flexing the specimen to open up the cracks while the penetrant is introduced or applying a vacuum to assist penetration. For thick specimens (or specimens without surface damage) they suggest that a hole (0.04 inches in diameter) can be drilled through the impact centre to provide a path for the penetrant.

Cantwell (1985) found that sectioning followed by optical microscopy was capable of revealing delamination, fibre breaks and matrix cracking and although destructive considered it to be a powerful technique.

1.2.4 Instrumentation

The widespread use of instrumentation has led to a much greater understanding of impact testing in recent years (Reed, 1989). In this section a brief account of the methods used and some of the problems associated with each will be presented.

The most commonly used method employs a transducer to measure the variation of force during the impact event. Strain gauges or piezo-electric devices are commonly used (Sjoblom et al, 1988). The force acting on the striker is measured and it is assumed that the same force is sustained by the specimen. This primary data can then be processed (by applying classical Newtonian mechanics and integrating) to provide information about the velocity, displacement and energy variations with time throughout the test (Reed, 1989). The analysis gives the following equations (Reed et al, 1988):

$$V_t = V_0 + gt - \frac{1}{m}\int_0^t F\,dt \qquad \text{Eq 1.6}$$

$$x_t = V_0 t + gt^2 - \frac{1}{m}\iint_0^t\int_0^t F\,dt\,dt \qquad \text{Eq 1.7}$$

$$E_t = V_0\int_0^t F\,dt + g\int_0^t t\,F\,dt - \frac{1}{2m}\left(\int_0^t F\,dt\right)^2 \qquad \text{Eq 1.8}$$

where: V_t = Velocity of the impactor at time t
x_t = Displacment at time t
E_t = Absorbed energy at time t
F = Force
m = Mass of the impactor
V_0 = Impact velocity

The force and energy at damage initiation, the peak force and absorbed energy at the peak force and the total amount of absorbed energy are often used to compare the differences between materials (Cheresh et al, 1987).

The force transducers are usually calibrated statically although techniques are available which allow dynamic calibrations to be performed. It can be argued that the absolute values of force and other measured parameters are not necessarily required if the tests is being used for comparative purposes.

Other techniques are available for monitoring impact tests. For example accelerometers (Daniel, 1986) or velocity measuring devices (for example laser doppler (Gibson et al, 1988)) can be employed. Again classical Newtonian mechanics can be used to derive data which has not been measured directly. There is some debate about which system provides the most accurate data. However, these discussions are perhaps relatively unimportant when the current level of understanding of the data obtained is considered (Reed, 1989).

Ireland (1973) states that the signal obtained is made up from four components:

(a) The true response of the specimen
(b) Inertial loading of the tup
(c) Low frequency vibrations of the specimen and tests machine
(d) High frequency noise in the electronics of the measuring equipment

The aim is to measure the true response of the system. However isolating this response from the others is a problem. Electronic filtering of the signal before data storage can distort the force - time signal (causing both reductions in size and movement in time of the force peaks) when applied in the 2 - 10 KHz range. There is a growing reluctance to electronically filter the raw data because oscillations on the force - time curve can be associated with the progression of damage and are part of the specimen response. Post-processing of the stored data is becoming more popular and has the advantage that the original data can always be retrieved (Reed, 1989).

Discussion about the accuracy of the measuring equipment is put into context when the inherent scatter in data associated with composite materials is considered. In an experimental assessment of several impact test methods applied to composite materials Kakarala et al (1987) found that data scatter was greater than 20% for most impact test methods.

1.2.5 Effect of Material

Problems with composite materials under impact loading conditions were identified at an early stage in the development of these materials and a requirement for improved composite toughness was identified (Bucknall, 1989). A number of different approaches have been used to improve the toughness of composites. These include:

(a) toughening of thermosetting matrix materials by reducing crosslink density or adding a toughening agent such as rubber or thermoplastic (Bucknall (1989), Recker et al (1989))
(b) the use of inherently tough thermoplastics as matrix materials (Davies et al (1985), Leach (1989), Ghaseminejhad et al (1990))
(c) fibre coatings to toughen the fibre / matrix interface (Bucknall, 1989)
(d) interleafing (Hirschbuehler (1985), Masters (1987 (a) and (b)), Sun et al (1988))
(e) hybridisation (using glass / kevlar fibres) (Curtis, 1989)
(f) use of carbon fibres with higher strains to failure (Cantwell et al, 1986)
(g) woven fibre forms (Brandt et al, 1989)

Varying degrees of improvement in composite toughness have been achieved using these methods. However it is very difficult to find quantitative evidence to support a statement that one method is better than another. Part of the problem is that it is difficult to define exactly what is meant by "toughness" when dealing with composite materials (Bucknall, 1989). This is one reason why the dropweight test has been adopted to simulate in-service conditions. However, the lack of standardisation of these testing methods has been a major drawback. We have already seen that the results of impact tests are generally highly dependant upon the exact testing geometry. Reed et al (1988) state that "The overall consequence [of this lack of standardisation] is that comparison between materials, judgements about their relative merits and the establishment of a consensus are elusive".

In spite of these problems it is inevitable that the materials with superior properties will emerge. At the present time, the general consensus appears to be that thermoplastic matrices offer the best resistance to impact damage. The results of impact tests have been supported by fracture mechanics testing which show these materials to be considerably tougher than composites with epoxy matrices (Williams, 1990). At least nine different thermoplastic materials have been used as matrix materials for composites (Leach, 1989). Of these Poly(ether ether ketone) (PEEK) has received a large amount of attention in the literature. The impact performance of carbon reinforced PEEK has been shown to be far superior to epoxy based composites (see for examples: Bishop (1985), Dorey et al (1985), Morton et al (1989)).

1.3 Buckling

1.3.1 Introduction

Any investigation of compression testing inevitably turns its attention to the problem of buckling at some stage. In this section information relating to the buckling is presented as an aid to understanding later discussion.

1.3.2 Instability Buckling

Theoretical studies tend to concentrate on instability buckling. In this analysis it is assumed that initial compression loading will not result in any out-of-plane deformation of the compression member in question. At some critical load large out-of-plane deformations occur for small increases in load, the compression member is said to have buckled. This is illustrated in fig 1.3. In practice out-of-plane deformations invariably occur as soon as the load is applied because of the problem of applying a perfectly aligned compression force and because of imperfections in the material or structure itself. Equations have been developed to account for initial curvature in nominally flat plates although instability type buckling loads are still predicted. The type of force - deflection behaviour found experimentally is compared with the theoretical prediction in fig 1.3. The experimental and predicted force - deflection curves approach each other for higher loads, when the effect of initial imperfections is negligible (Buskell et al, 1985). When lateral deflections occur as soon as load is applied the concept of instability buckling is no longer applicable, in fact it is difficult to define a single buckling load.

In the following two sections the instability buckling behaviour of columns and plates will be discussed.

1.3.3 Buckling of Columns

The well known Euler equation is used to calculate the instability buckling loads for columns. The buckling load P_{crit} is calculated from the following formula:

$$P_{crit} = k \pi^2 E I / L^2 \qquad \text{(Eq 1.9)}$$

where: k is an end constraint factor varying between 1 for simply supported ends to 4 for clamped ends; E is the compressive Youngs modulus; I is the second moment of area and L is the free length of the column.

It is assumed that the column is straight and that concentric and axial end loads are applied. The formula calculates the load at which elastic instability occurs. When applied to composite materials a correction factor is employed to account for the relatively low ratio of shear to axial modulus (approximately 0.04 compared to approximately 0.31 for metals) (Lee, 1987). The corrected critical load is calculated from:

$$P \text{ (corrected)} = P_{crit} / (1 + n P_{crit} / A G) \qquad \text{(Eq 1.10)}$$

where: n is 1.2 for rectangular columns; A is the cross sectional area and G is the composite shear modulus.

In practice the value of k, the end constraint factor, must be determined experimentally since true simple or clamped support conditions cannot be achieved in practice (Port, 1982).

1.3.4 Buckling of Plates

Timoshenko (1935) gives a good account of the techniques used to predict the instability buckling behaviour of plates made from homogeneous isotropic materials. An account of the methods used to extend the theory to laminated composite materials is given by Leissa (1985 (a)). The analysis is more complicated when dealing with laminated composite materials because additional calculations have to be made to account for fibre and matrix properties, fibre orientations and stacking sequences. The complexity is further increased when plies are not stacked symmetrically because of coupling between bending and midplane stretching as transverse deflections occur (Leissa, 1985 (b)).

There are three types of edge constraint (free, simply supported and clamped) giving 21 possible combinations of edge constraints. In addition there are a large number of possible loading configurations (Leissa, 1987(b)). There are very few exact solutions to the equations and approximate methods must be used in most cases (Leissa, 1987(b)). Based on 'a reasonably comprehensive' literature search, Leissa (1985 (b)) revealed 300 references dealing with the buckling behaviour of rectangular composite unstiffened plates. For these reasons no attempt has been made here to present solutions to buckling problems. The reader is referred to Leissa (1985 (a) and (b)).

Unfortunately, very few reliable experimental results have been gathered against which the theory can be checked. Experimental difficulties common to buckling studies on all types of material such as obtaining the desired boundary conditions and inplane loading conditions are encountered as well as problems associated with composite materials. For example exposed fibres at the edges of the plate make the desired loading and boundary conditions more difficult to achieve and internal discontinuities can affect the reliability and reproducibility of the results (Leissa, 1985 (b)).

The predictive equations are useful for assessing the likely effect of dimensional changes (for example specimen height, width and thickness) on the buckling load. For example fig 1.4 shows the buckling load plotted as a function of specimen width (specimen height and thickness assumed to be constant). For columns, the Euler type analysis predicts a linear increase in buckling load as the specimen width increases. Analysis using equations derived for plates shows that the buckling load decreases as the specimen width increases. The maximum buckling load is achieved when the transition from column to plate type behaviour occurs. This type of behaviour has been confirmed experimentally for L section struts made from aluminium alloy (Timoshenko, 1935). The equations used for this example are applicable to isotropic materials. The same trends are predicted by equations derived for plates with anisotropic properties (see for example Brunelle et al, 1983). In fact the isotropic plate solution can be recovered from the equations derived for anisotropic materials (see Brunelle et al, 1983). The equations could also be used to predict the effect of length and thickness on the buckling load.

1.4 Compression Testing

1.4.1 Introduction

Post-impact compression strength test methods have been influenced to some degree by the techniques previously developed for measuring the compression strength of undamaged material. In this section the techniques used to measure compressive strength are presented and the problems highlighted.

Compression strength is widely acknowledged as being one of the most difficult of the intrinsic materials properties to measure for composites (Clark et al (1981), Whitney et al (1982), Leonard (1989)). A large number of testing methods have been developed over the years. Leonard (1989) lists 15 different methods, and there are probably many more than this in existence. A major problem is that the measured strength is highly dependent upon the test method used. For example Woolstencroft et al (1981) used five different methods to measure the compression strength of a unidirectional carbon / epoxy material. The measured strengths varied between 1016 and 1840 MPa (with coefficients of variation of 8.5 and 6.0 % respectively). Tests methods are designed with two (sometimes conflicting) requirements to satisfy, the first is that a uniform state of stress is achieved in the test section and the second is that the material fails in compression before geometric instability occurs (Leonard, 1989). In the next section the different types of test will be described and the advantages and disadvantages of each will be presented.

1.4.2 Types of Compression Test

Different authors have used different criteria for grouping compression test methods. Two methods have been used. Whitney et al (1982) grouped test methods by specimen type and Port (1982) used the method of load transfer into the specimen to categorise the different techniques:

(a) Specimen Type

Whitney et al (1982) identified three generic test methods:

Type I tests utilise relatively short, unsupported test sections to inhibit geometric instability. Test specimens are usually loaded through friction using wedge-action friction grips. Test fixtures are designed to insure that the load is applied along the specimen centreline. Both the Celanese (Anon, 1987) and ITTRI (Whitney et al, 1982) test methods

employ this method. The Celanese fixture uses truncated conical cones contained in matching cylindrical end fittings. These cylindrical end fittings are contained within a tube to ensure axial loading of the specimen (Whitney et al, 1982). The problem with this type of specimen is that it is difficult to achieve perfect cone-to-cone contact. The ITTRI method overcomes this problem by using linear bearings and hardened shafts to ensure linear loading. Serrated wedges contained in solid steel bases are used to transfer the load into the specimen. Both types of specimen require end tabs (Whitney et al, 1982). Clark et al (1981) found that the flatness and parallelism of the end tabs was important and variations in these parameters produced significant strain variations in the specimens and consequently lower strength values. The Celanese method requires very precise alignment of the specimen in the fixture while the ITTRI method requires long soak periods for high temperature testing. Another type I test method is the Northrop method (Whitney et al, 1982). This uses off-set unsupported lengths to provide some support along the whole length of the specimen. This test has the advantage that the test fixture is simpler than those required for the Celanese or ITTRI test method (Whitney et al, 1982).

Type II tests utilise a relatively long test section which is fully supported to inhibit geometric buckling. The ASTM D695 (Anon, 1985 (b)), SWRI (Whitney et al, 1982), and Lockheed (Ryder et al, 1977) methods are all examples of type II tests. The Lockheed test is discussed in some detail by Ryder et al (1977). They found that the test provided a relatively simple method for measuring the compression properties of large gauge length coupons. Whitney et al (1982) state that the type II methods give strength data which is consistently lower than the values obtained using the type I tests for unidirectional materials (loaded in the fibre direction). However, for laminates with multiple fibre directions the results are comparable to those obtained using type I tests.

Type III utilises a honeycomb core to inhibit buckling of the test specimen. Two loading methods are used to cause failure: (a) edgewise loading of the sandwich through self-aligning bearing blocks; (b) four point bending. In the four point bending method a steel face plate is used on the tension side of the beam. The steel and the core material and the dimensions of the sandwich and support conditions are chosen so that failure occurs in the composite test specimen on the compression face of the beam. These test methods have been found to measure higher strengths than any of the other test methods (Whitney et al, 1982).

(b) Method of Load Transfer

Port (1982) categorised test methods by the method used to transfer load into the specimens. Three categories were defined: (a) shear loading, (b) direct loading and (c) combination of shear and direct loading. The Celanese and ITTRI test methods described above use the shear loading method. End loading methods are described by (Port (1982) and Clark et al (1981)). The problem with end loading is that end buckling, brooming or splitting of the material can occur (Ryder et al, 1977). A combination of end and shear loading was used by Port (1982) and was found to measure a high compressive strength with low variability (in conjunction with a wasted specimen). The specimen is bonded to an accurately machined aluminium end block. A closely controlled adhesive thickness is required. Approximately half the load is transferred by shear and half by end loading. Barker et al (1987) used a steel end block with hardened steel inserts and adjustable side face clamps to transfer approximately 20 % of the load by shear and 80 % of the load through the end of the specimens. They found that failures within the gripped portion of the specimen were avoided for both waisted and unwaisted specimens. Four point bending of sandwich type specimens cannot be classified under any of the above headings and were not considered by Port (1982).

1.4.3 Failure Modes

Port (1982) cites the results of previous workers (Ewins et al, 1973) who found that shear failures were found for tests on unidirectional material tested in compression at room temperature. For elevated temperature tests (above 100 °C) a microbuckling failure mode was observed. Changes in the properties of matrix materials have occurred since and microbuckling failures are normally observed for thermosetting (Port, 1982) and thermoplastic (Purslow, 1988) unidirectional composites. Port (1982) attributes this change in behaviour to the reduction in matrix stiffness which have been introduced to produce less brittle materials. The consequence of this is that the matrix offers less support to the fibres during compression loading and microbuckling occurs before shear failure.

1.4.4 Uses of Compression Test Data

Clearly a large amount of work has been directed towards the design of test methods designed to measure the compressive strength of composite materials. In reality the results are of somewhat limited use. Lee (1987) summarised the situation stating that "The general applicability of unidirectional compression strength data for design purposes may

be of limited value, partly because many designs are controlled by geometric instability rather than material strength. It is not clear how samples under test, which are small in comparison with real structures, represent the behaviour of bulk materials. Such measurements do, however, give a valuable indication of developments in materials and potential design values". Another limiting factor is that delamination damage (formed during impact) can severely reduce compression strength. This has lead to the widespread use of post-impact compression strength tests which will be covered in the next section.

1.5 Post-Impact Compression Testing

1.5.1 The Test and its Uses

As the name suggests the post-impact compression strength test is divided into two parts. The first part is a low energy impact designed to induce a low level of impact damage in the material. In the second part of the test the residual compression strength (or strain to failure) is measured in a direction perpendicular to the impact direction. This is shown schematically in fig 1.5. Ideally tests over a range of impact energies should be carried out. When this is done the strength (or strain) at failure is usually plotted against impact energy or impact energy normalised with respect to specimen thickness. It is common for materials to be tested and compared at only one impact energy.

It is important to distinguish between resistance to damage and damage tolerance. The impact test can be used to assess the resistance of a material to the initiation and propagation of damage and is therefore not a damage tolerance test. The post-impact compression part of the test is a damage tolerance test because it measures the effect of impact damage on the compression strength of the material. This may seem an obvious comment to make but there is some confusion in the literature with several different and sometimes erroneous definitions of exactly what is meant by the term damage tolerance.

The test was designed to provide a method of screening materials, both for development and selection purposes. It is important to note that the test does not generate design data. This is because it is difficult to relate the results of tests on small coupons to the response of larger structures (Sjoblom et al, 1989). We have already seen in section 1.2 that the extent of impact damage is highly dependent upon the testing geometry. Specimen and loading geometry also plays an important role during the compression test. The global buckling load must be higher than the load required to cause local buckling and subsequent failure in the impacted region (Sjoblom et al, 1989).

In order to overcome the global buckling problem some authors have chosen to use a specimen with a short gauge length similar to the specimens used to measure the strength of undamaged material (see section 1.4). Verpoest et al (1987) used an ITTRI type fixture with a free length of 20 mm to measure the residual compression strength of glass / epoxy laminates. A similar approach was used by Ishai et al (1990) who chose a 25 mm free specimen length. A more common approach to the global buckling problem has been to use a fixture to support the specimen during the compression test. These fixtures are usually called 'anti-buckling guides' (ABG's). Quite a large number of different designs for ABG's have appeared in the literature over the years. Three examples will be given to demonstrate the range of approaches adopted. Fig 1.6 (a) shows the ABG used for the Boeing test. The specimen is end loaded and supported along the vertical edges to prevent buckling. The specimen is prevented from expanding laterally when the load is applied. Fig 1.6 (b) shows the ABG design suggested by CRAG (Curtis, 1988). Load is now introduced through shear and the specimen is free to deform laterally.

Another type of ABG (which has been less widely used) is the holehedral design. The specimen is clamped between two plates. An opening (usually circular or square) is cut in each plate so that the specimen an deform out-of-the plane in the damaged region. This type of ABG was used by Sjoblom et al (1989). They used a shear loading method, employing standard hydraulic wedge grips with grip inserts to minimise the unsupported length.

Studies of the effect of ABG designs on PICS do not appear to have been performed. The reason for this is that there are so may variables that it would be a very large task indeed. However the results of an investigation into ABG design for fatigue testing was reported by Matondang et al (1984). They maintain that holehedral type ABG's can produce misleading results if the support restricts local buckling which delays the spread of delamination. In the case of the holehedral ABG designed by Sjoblom et al (1989) the specimen is supported on a 50 mm diameter ring and impacted with a 12.7 mm diameter spherical impacter. The holes in the holehedral ABG were only 31.75 mm (1.25 inches) in diameter. This means that some of the impact damage could be prevented from deforming out-of-plane during the compression test.

In addition a large range of specimen sizes have also been used. The NASA test (Anon, 1985 (a)) calls for a specimen of 254 in length, 125 mm in width and 48 plies (6 mm thick assuming a ply thickness of 0.125 mm). At the other end of the scale Ishai (1990) used a specimen 70 mm in length, 8 mm in width and 6.4 mm in thickness. These two examples probably represent the smallest and largest specimens which have been used. Traditionally

larger specimens have been specified, possibly because they went some way to simulating service conditions. However the use of large specimens meant that the tests were very expensive to perform. Sjoblom et al (1989) estimated that the cost for one data point (average of five tests) was $ 5,000 when the NASA (Anon, 1985 (a)) test was used. In addition to the cost of the material, expensive machining of the specimens and high capacity test machines are required (Sjoblom et al, 1989). Recently researchers have begun to investigate the feasibility of using smaller test specimens in an attempt to reduce the cost of the test (Sjoblom et al (1989), Ishai et al (1990), Davies et al (1990)). The utility of these miniaturised tests has not been fully assessed. Davies et al (1990) compared results from a miniaturised test with those obtained using what they describe as "the full" test. The miniaturised test used 50 x 50 mm, 32 ply specimens impacted on a 40 mm diameter ring. After impact a 3 mm thick PMMA sheet was bonded to the faces of the specimen and the block tested in compression. The authors found little difference between the two materials tested based on the results of the miniaturised test. Large differences were revealed by "the full" test. The conclusion was that the miniaturised test was not successful. The reason given was that the small size of the specimen restricted the input of impact energy. However it could be argued that the use of the PMMA plates to stabilise the specimen inhibits the out-of-plane deformation around the impact damage. Therefore, although the failure occurs through the impact damage in each test, different failure mechanisms may be responsible for the failures.

It is clear that a standardised test method is required. At the present time a SACMA (Anon, 1988 (b)) PICS test is being assessed for possible adoption as an ASTM standard. The SACMA test is essentially the same as the Boeing test (Anon, 1982). It uses the same specimen size and impact conditions although the ABG has been slightly redesigned and the text rewritten incorporating some other minor changes. Adoption of this test method would have the advantage that the considerable data base already in existence would still be valid (Sjoblom et al, 1989). However the SACMA test is still expensive and standardisation of this test at the present time could result in unnecessarily expensive testing being performed in the future.

1.5.2 Failure Process

In order to understand the results of a mechanical test such as the post-impact compression test it is usually desirable to identify and understand the failure processes. In the case of the PICS test the failure process is complex and according to Kutlu et al (1990) "....the effect of delamination on the residual stiffness and strength of the structure is not

well understood". In this section the current understanding of the failure processes will be described by combining information from several sources.

Kardomateas et al (1988) identified three possible buckling modes for delaminated laminates loaded in compression. The first was global buckling of the laminate. This occurs when the delamination is short (fig 1.7 (a)). The second was local buckling which occurs for relatively large delamination lengths (fig 1.7 (b)). For intermediate delamination lengths, a mixed mode buckle occurs (fig 1.7 (c)). If global buckling occurs then it is likely that the small amount of damage will not affect the strength of the laminate. Therefore we are most interested in the local and mixed buckling modes.

Jones et al (1984) made the observation that the concept of instability buckling is totally inapplicable to this problem. They argue that delaminations cause the laminate to become asymmetric and therefore applied in-plane loads automatically leads to out-of-plane deformation, removing the possibility for instability buckling to occur. The laminate theory supporting this argument is given by Baker et al (1985).

Once delamination buckling has occurred both peel and shear stresses at the delamination front cause the delamination to grow (Baker et al, 1985) Several authors have reported that the damage grows in a direction perpendicular to the applied load (Bishop et al (1983), Mousley (1984), Stuart et al (1989), Pavier et al (1990)) with little growth in the loading direction.

Hoskin et al (1986) stated that the final cause of failure of the bulk material is not fully understood. They believe that the final failure is caused by a combination of out-of-plane bending resulting from loss of symmetry and reduction in the net cross section. Greenhalgh (1989) tested an impact damaged foam filled stringer panel and found that "the final collapse involved both unstable delamination growth and compressive fracture initiated at the impacted area". It was not possible to ascertain the exact failure sequence. One of the problems involved in identifying the final failure mode in compression tests is that the evidence may be destroyed by damage processes occurring later on in the failure sequence (Hogg et al, 1988).

The effect of delamination size on the initial buckling mode was discussed earlier. It should be no surprise that the initial delamination size has also been found to affect the ultimate strength. Baker et al (1985) reported that both numerical and experimental results have shown that once a certain size of delamination is reached further significant increases in size only result in a small decrease in compressive strength. Apart from the size of the

delamination another important factor controlling the strength is its through thickness position. Donaldson (1987) used a 1-D delamination model originally developed by Whitcomb to investigate the effect of damage position. The model is shown schematically in fig 1.8 (a). It assumes that the damage grows in the loading direction and so does not model the situation which is known to exist during a post-impact compression test. However the author states that it should be adequate for predicting trends. Fig 1.8 (b) shows the failure load plotted as a function of the delamination half length for a 64 ply (±45, 0 90) laminate with the ply sequence shown on the graph and delaminations inserted at different depths. The position of the delamination is indicated in the ply lay-up by the arrows. As the number of plies (t) in the buckled region increases (i.e. the depth of delamination increases) the curves shift vertically (to give lower critical loads) and horizontally (to higher crack lengths). Except at low crack lengths the deeper delaminations cause the largest reductions in residual strength. It is also apparent from these curves that increasing the crack length does not cause further decreases in strength, as was mentioned above.

1.5.3 Effect of Material

The post-impact compression test has been in fairly widespread use for approximately ten years. The test was specifically designed to compare the performance of different materials, and as one may have expected, some understanding of the effect of different material parameters has emerged. However the effect of the wide range of material parameters does not appear to have been investigated and reported in a systematic manner. The situation is similar to that described earlier for impact testing, the lack of a standard testing method means that the current understanding has been reached by consensus of opinion rather than by direct comparison of results. In the first part of this section the effect of the most important material parameters will be presented. In the second part some explanation of the reasons for these effects, based on the literature, will be presented.

Improvements in the toughness of composite materials have traditionally been sought in order to improve the damage resistance and tolerance of composite materials (Masters, 1987 (a)). In section 1.2 some of the methods used to improve the impact properties of composite materials were presented. In general these toughening methods have also been found to improve the residual compression strength of these materials. Composites with epoxy matrix materials are often taken as base-line materials against which improvements are measured. Brandt (1986) et al found considerable improvements in residual strength when a toughened epoxy was compared to a 'standard' epoxy. Fig 1.9 shows the compression strengths of the two materials plotted as a function of impact energy.

Improvements in residual compression strength for toughened epoxy matrix materials have been reported by several other authors (See for examples: Manders et al (1986), Griffin (1987), Lee et al (1988), Recker et al (1989), Morton et al (1989)). Improvements in the residual compression strength of epoxy materials have also been achieved by using thermoplastic materials as a toughening agent. See for example work by Recker et al (1989 and 1990). After an impact (energy of 6.7 J / mm) the material toughened with the thermoplastic had a compression strength of 310 MPa while the 'second generation' epoxy matrix, which they used for comparison had a residual compression strength of 200 MPa after an identical impact (Recker et al, 1989). Other workers have found that the use of thermoplastics as matrix materials produces superior compression properties after impact. Referring again to the results of Brandt et al (1986) shown in fig 1.9, the material with the thermoplastic matrix shows the least degradation in compression strength when compared to its original strength. This result was also found by other authors (see for example: Bishop (1985), Dorey et al (1985) and Morton et al (1989). Apart from the superior residual strength other differences between the behaviour of thermosetting and thermoplastic matrix materials have been observed. Bishop (1985) reported that a linear decrease in compression strength with impact energy was observed for a composite with a thermoplastic matrix material (APC-1). In comparison, the strength of the materials with thermosetting matrix materials tends to fall quickly at low impact energies and than level out (see for example the results of Brandt et al (1986) shown in fig 1.9. or the results of Dorey et al (1985) and Morton et al (1989).

Interleafing carbon / epoxy composites with thermoplastics has also led to large improvements in residual compression strength. Masters (1987 (a)) studied the effect of interleafing on 6 different materials. In each case the residual compression strength was improved when the results of tests on materials with interleafs was compared with tests on the same materials without interleafing. In one case the compression strength was 410 MPa for an interleafed material compared to 220 MPa for the same material without interleafing. The reason for the large increase in residual compression strength is that the interleafs dramatically reduce the extent of delamination formed during the impact event. In the process however, tensile matrix cracks tend to penetrate more deeply into the material (Sun et al, 1988). This may adversely affect the residual tensile strength of the material. Two additional disadvantages of the method are that fabrication of parts with complex shapes is difficult and high fibre volume fractions cannot be attained (Aldstadt et al, 1990).

Significant improvements in residual compression strength were reported by Brandt et al (1989) when woven fibre forms were used for carbon fibre composites. Three

dimensional fabrics were found to have higher residual compression strengths than two dimensional fabrics. While the reinforcement in the through thickness dimension improves the resistance to damage and damage tolerance this must be balanced against the corresponding loss in the in-plane properties (Brandt et al, 1989). Improvements in residual compression strength were not found to be significant when the results of tests on 2-D and 3-D reinforced glass fibre composites were compared. The authors state that glass fibre reinforced composites already have good damage tolerance and the effect of reinforcement in the through thickness direction is therefore limited (Brandt et al, 1989). Hybrid materials make use of glass (and kevlar) fibres to improve the resistance to impact damage. However the superior resistance in impact does not translate to give superior residual compression strength (Curtis, 1989).

Fibre coatings were also mentioned in section 1.2 as a method of improving toughness, however the method does not appear to have been widely investigated. Stuart et al (1989) state that "Little effort has been put forth on characterisation of the resin - fibre interface for potential improvements in composite damage tolerance performance". They investigated the effect of fibre - matrix interface properties on the toughness and residual compression strength of Toray T-800H carbon fibres. Different degrees of adhesion between the matrix and fibres was achieved by using different surface treatments. They report a significant (20 %) increase in residual compression strength, for a bismaleimide based resin, resulting from an increase in the fibre surface treatment. Manders et al (1986) also drew attention to the importance of the fibre - matrix interface for damage tolerance.

The strain to failure of carbon fibres has also been identified as an important parameter affecting the residual compression strength. Cantwell et al (1986) compared the residual compression strength of a carbon fibre reinforced epoxy. One was reinforced with 'high strain' (1.53% strain at failure) and the other with 'high strength' fibres (1.14 % strain at failure). The residual compression strength of the material reinforced with the 'high strain' fibres was 30 % greater than the material with the 'high strength fibres. Manders et al (1986) reported that fibre tensile strength had relatively little influence on residual compression strength.

The use of tough matrix materials and fibres with high failure strains as routes to improve the residual compression strength of composite materials appears to have been successful. However, simply choosing fibres with high strains to failure and tough matrix materials does not necessarily translate into a tough composite (Curtis, 1987). The effect of the interface, in particular fibre surface treatment and sizing, was identified by Curtis as an important area for future study.

1.5.4 Current understanding of the effect of Material Properties on the Post - Impact Compression Strength

There has been some discussion in the literature relating to the relative importance of mode I and mode II strain energy release rates on residual compression strength. Odagiri (1986), Masters (1987) and Recker et al (1990) found experimentally that a linear correlation between residual compression strength and G_{IIc} appears to exist. Stuart et al (1989) also found a correlation between residual compression strength and G_{IIc}. The reason for the link between G_{IIc} and improved residual compression strength was then investigated. Modelling of the compression test by Donaldson (1987) predicted significant increases in compression strength for increases in G_{IIc}. Conversely modelling by Wedgewood et al (1988) predicted a linear relationship between residual compression strength and G_{Ic}. The situation appears to have been clarified by Ilcewicz et al (1989) who tested two materials with similar moduli and undamaged strength, but with different interlaminar fracture toughness. They plotted residual compression strength against the damage diameter, measured after the impact test. The results were found to lie on the same curve. Their results indicate that G_{IIc} has little effect on the compression test. Previously the same authors (Dost et al, 1988) had found that the tough material required much higher impact energies to obtain the same damage size as the material with lower toughness. It appears that high mode II fracture toughness is required to minimise the extent of delamination damage during the impact event, while specimen stability and mode I fracture toughness are important during the compression test.

However the ability of a material to resist impact damage is not only controlled by fracture toughness. For example Morton et al (1989) attributed the superior damage tolerance of a thermoplastic matrix composite (when compared to a carbon epoxy) to its ability to absorb energy by plastic deformation during the impact test. Cantwell et al (1986) found that a composite utilising high strain fibres was able to absorb energy by elastic deformation during the impact test, resulting in less damage being incurred in comparison with a material with standard high strength fibres. Large improvements in the residual compression strength were found for the material reinforced with high strain fibres (see above).

1.5.5 Combined Compression and Impact Testing

Another test which has received some attention and is closely related to the post-impact compression test is the combined compression and impact test. In this test the specimen is preloaded in compression and then subjected to an impact test, usually by firing a projectile from a gas gun. The preload is increased until catastrophic failure occurs at a given incident impact energy. Fig 1.10 shows the method used to plot the results. The pre-load (or pre-strain) is plotted against the incident impact energy. If catastrophic failure does not occur an open circle is plotted, and if catastrophic failure does occur then a filled circle is plotted. After testing over a range of impact energies a line is faired between the open and closed points to give a failure threshold line, which indicates the combination of preload and impact energy to just cause catastrophic failure. Specimens which do not fail catastrophically are often loaded in compression to measure their residual strength and the results are plotted on the same graph (see for example Avva, 1983). This test has not been widely used and most of the work appears to have been carried out by, or on behalf of, NASA.

The combined compression and impact test is performed because it is perceived to be a more rigorous loading condition than compression following after an impact test. Rhodes et al (1979) suggest that the results of the combined test can be used to predict lower bound values of the compression after impact tests.

Some work has been done to investigate the effect of specimen geometry on the results of the combined test (see Rhodes et al (1979) and Avva (1983)). Rhodes et al (1979) studied the effect of specimen width, using specimens 125 and 381 mm wide and 254 mm in height. Specimen thicknesses ranged from 5.6 to 7.5 mm. Two different anti-buckling guides were used. The wider specimen was supported at intermediate points across its width (at 1/3 points). The authors state that the interior supports used for the wide specimen did not affect the strain at failure and did not find any effect of specimen width on the failure threshold curves. Avva (1983) kept the specimen width constant (76.2 mm) and varied the specimen length. Specimens with lengths of 88.9, 120.7 and 152.4 mm were tested. The tentative conclusion based on the results was that the behaviour of the laminates appeared to be independent of specimen size (width - to - length ratio) for the combined impact / compression test. However he stated that extensive testing was necessary before "any positive and useful conclusions can be drawn".

Avva (1983) also compared the results for different thickness specimens. Failure strain (or normalised failure strain) were plotted against impact energy per ply (or unit

thickness). However the use of the impact energy per ply as a method of comparing size effects is questioned and the author considers the method to be "of dubious value". The use of the absolute impact energy was considered to be a more reliable approach.

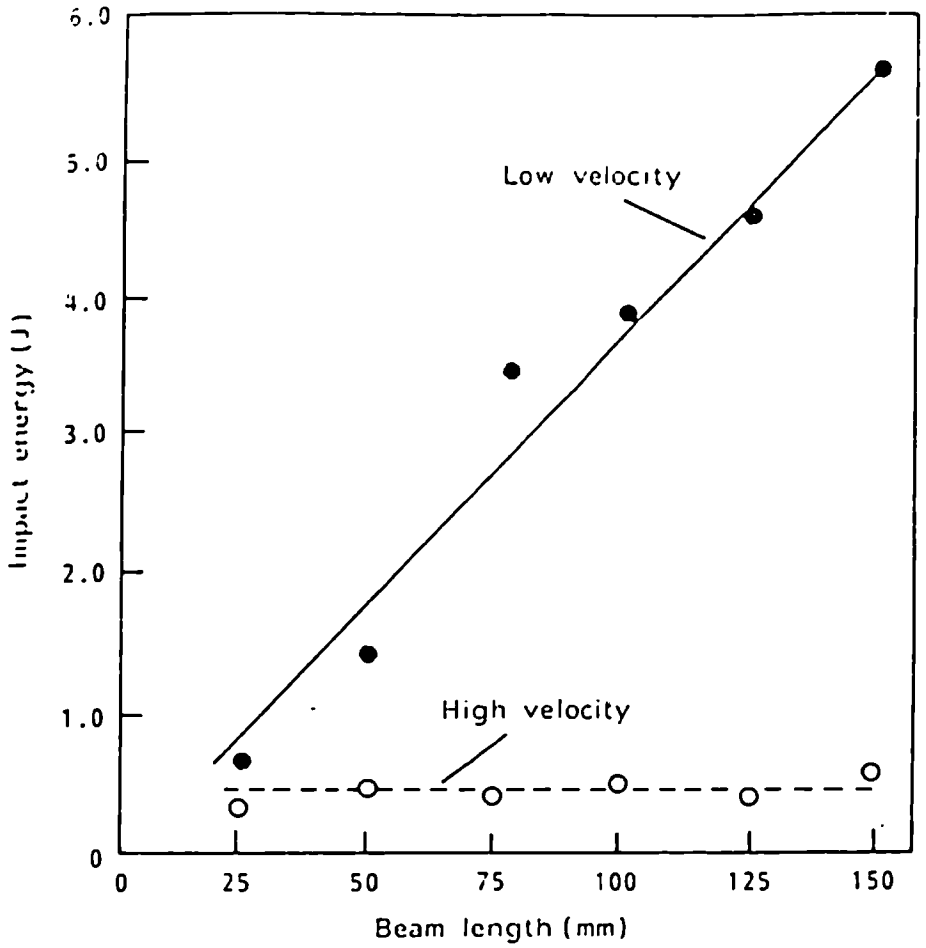

Fig 1.1 (a) Effect of beam length on damage initiation energy for low and high velocity impacts. (Reproduced from Cantwell et al, 1990)

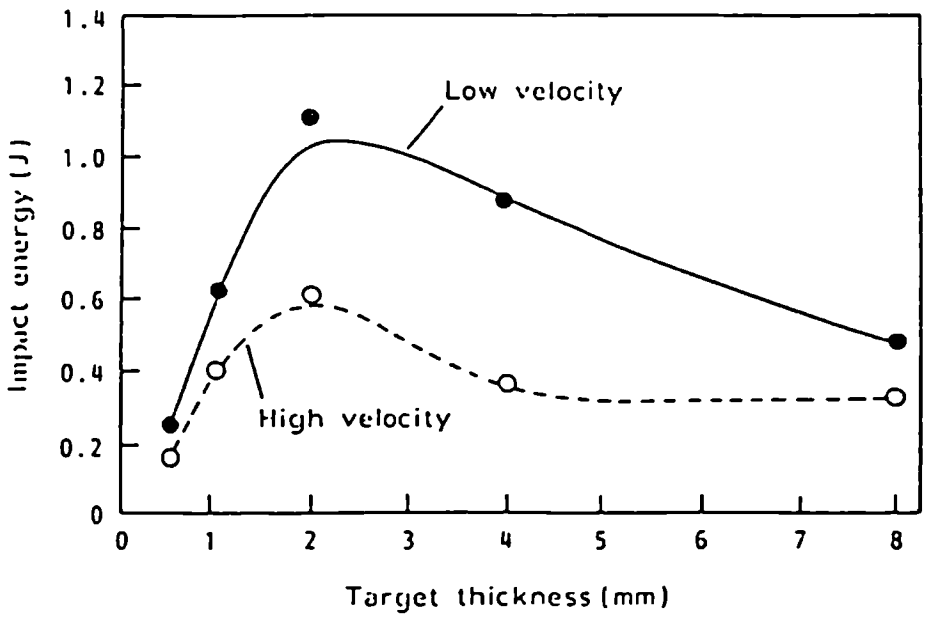

Fig 1.1 (b) Effect of target thickness on damage initiation energy for low and high velocity impacts. (Reproduced from Cantwell et al, 1990)

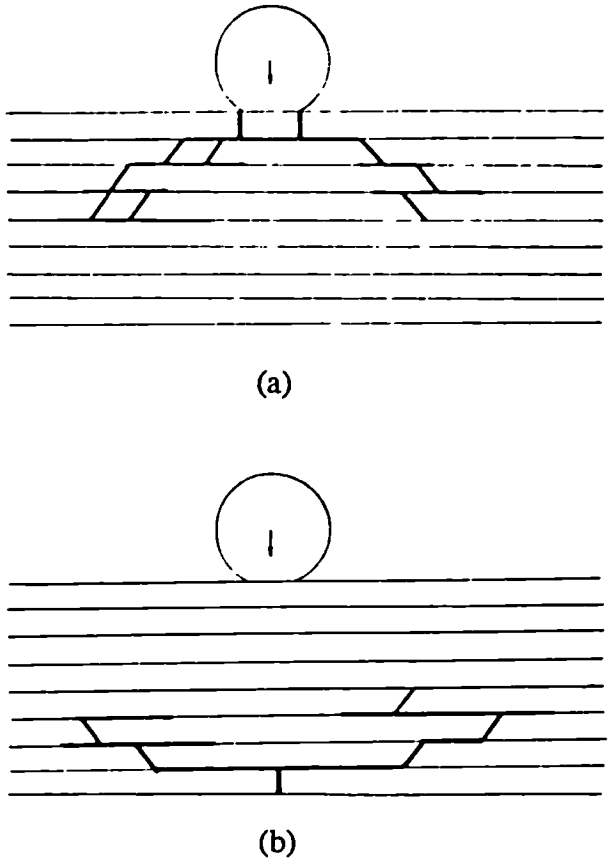

Fig 1.2 Schematics to show damage progression due to (a) contact induced stresses and (b) flexure induced stresses. (Reproduced from Cantwell et al, 1985)

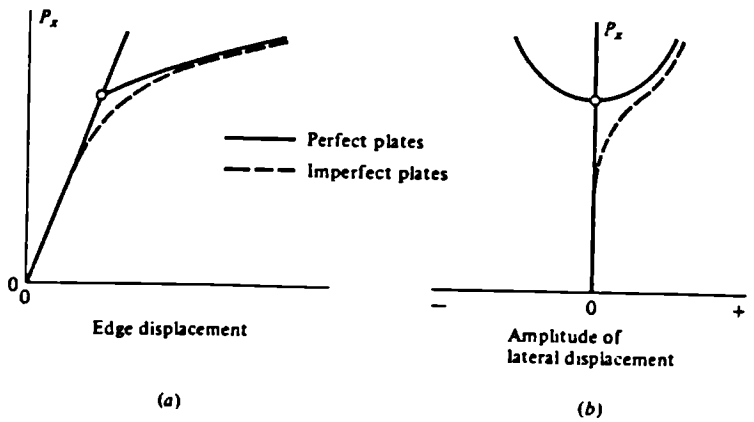

Fig 1.3 Load versus (a) edge displacement and (b) lateral displacement to show the difference between the buckling behaviour of perfect and imperfect plates. (Reproduced from Brush et al, 1975)

Buckling Force (F)

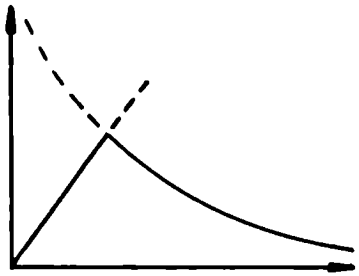

Specimen Width (w)

Buckling Stress (σ)

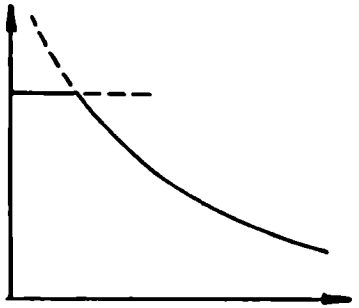

Specimen Width (w)

Euler Column

$$F = \pi^2 E t^3 w / 12 L^2$$

Plate

$$F = \pi^2 E t^3 K / 12 w (1 - \nu^2)$$

where: F is the critical buckling force
σ is the critical buckling stress
E is the Youngs Modulus
t is the specimen thickness
w is the specimen width
L is the specimen length
ν is the Poissons ratio
K is a function of L / w:

Euler Column

$$\sigma = \pi^2 E t^2 / 12 L^2$$

Plate

$$\sigma = \pi^2 E t^2 K / 12 w^2 (1 - \nu^2)$$

Note: The Euler analysis is for a column with simply supported ends. Since it is a one dimensional analysis the sides are considered to be 'free'. In this example the equations for the plate are given for simple supports on each edge because there is no exact solution for a plate simply supported ends and 'free' sides. The same trend would be expected for a plate with 'free' sides.

Fig 1.4 Schematic to show effect of specimen width on the predicted buckling load.

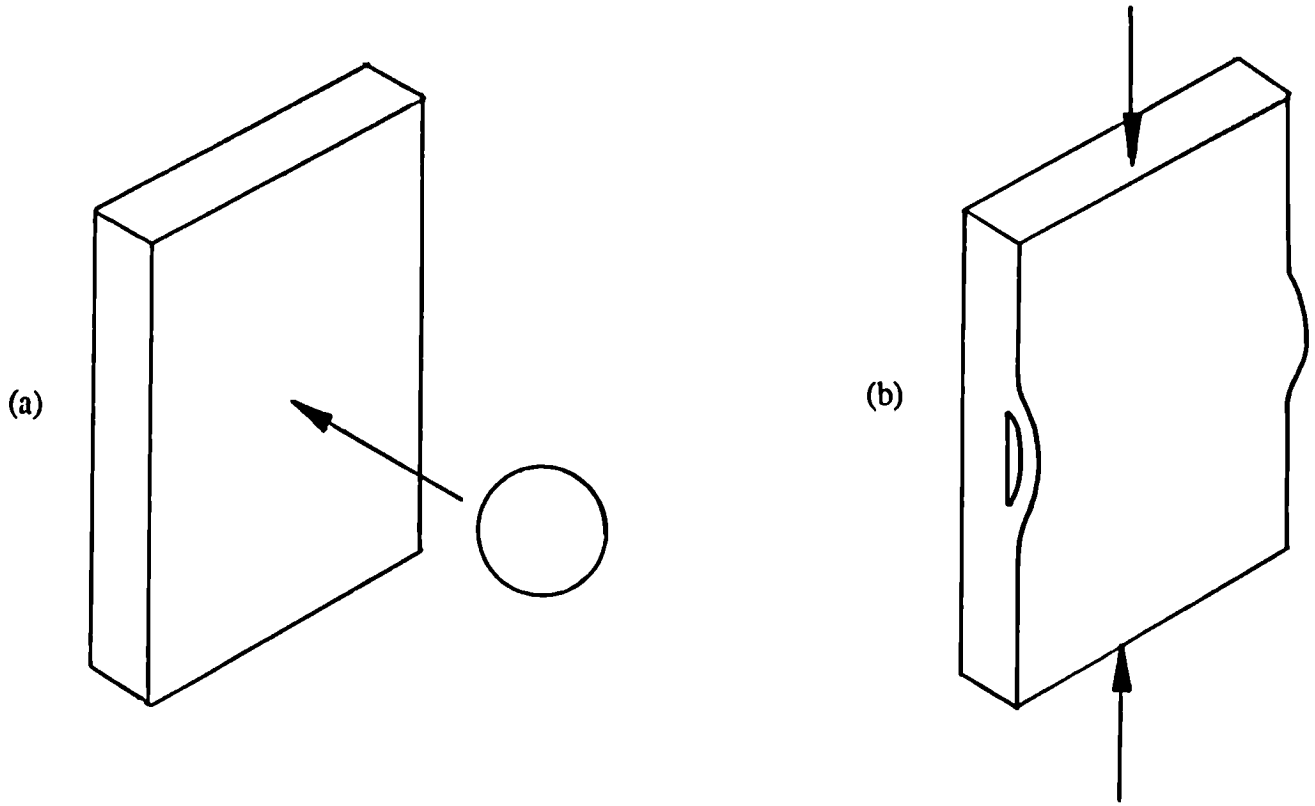

Fig 1.5 Schematic to show the post-impact compression test. (a) Impact and (b) Compression.

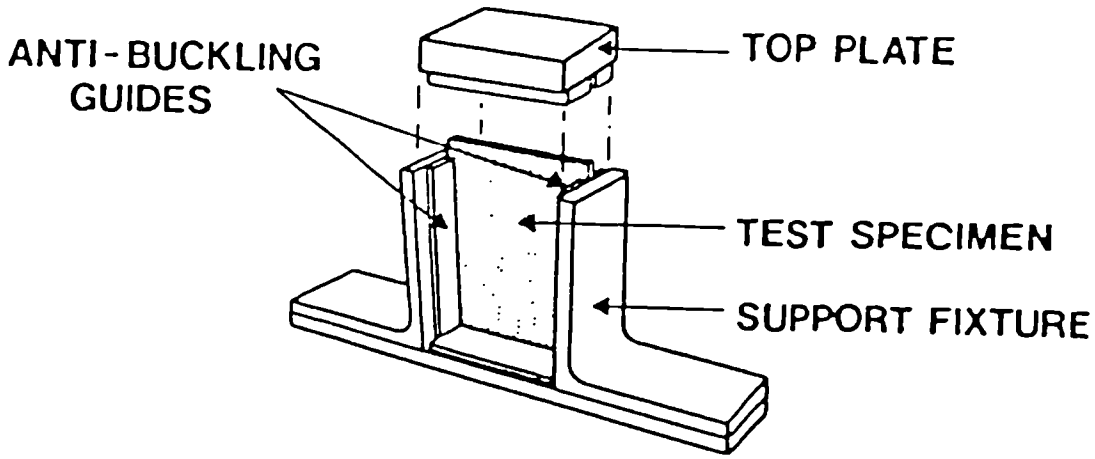

(a)

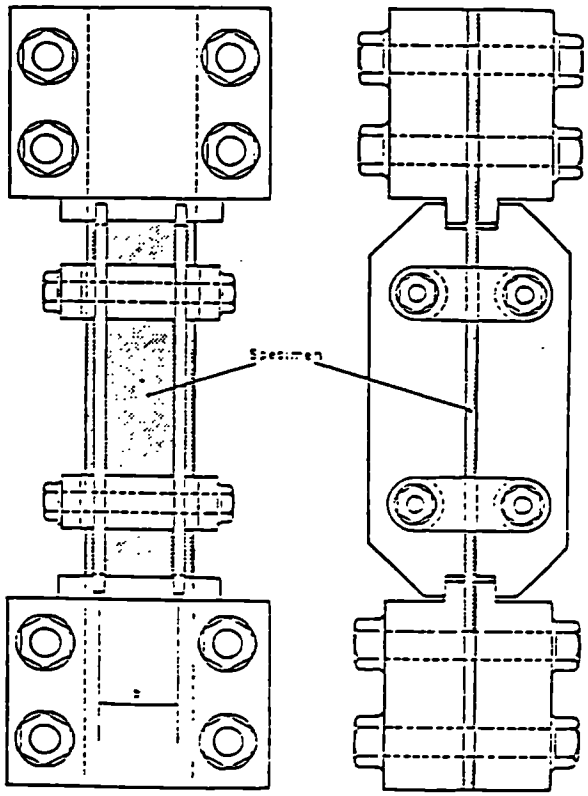

(b)

Fig 1.6 Examples of anti-buckling guides. (a) End loaded (Reproduced from Anon, 1982 (a)). (b) Shear loaded (Reproduced from Curtis, 1988).

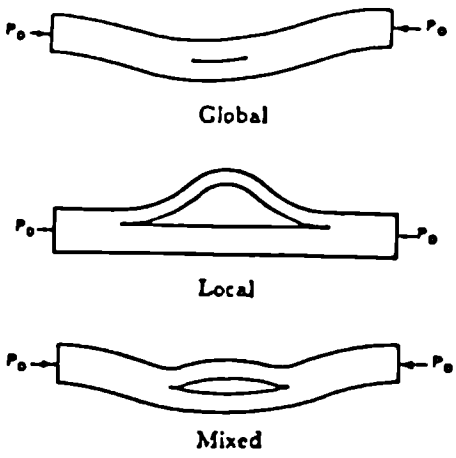

Fig 1.7 Schematics to show the buckling modes of delaminated composites. (Reproduced from Kardomateas et al, 1988).

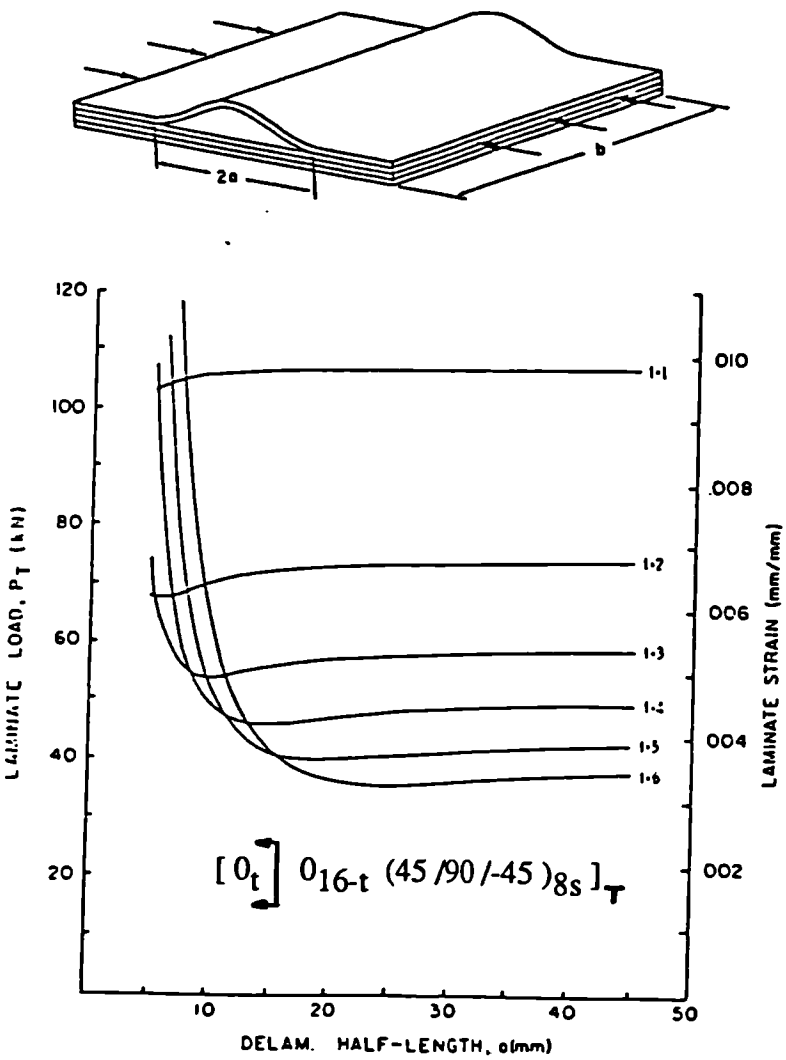

Fig 1.8 (a) Schematic to show Whitcomb model. (b) Failure load versus delamination half-length. (Reproduced from Donaldson, 1987).

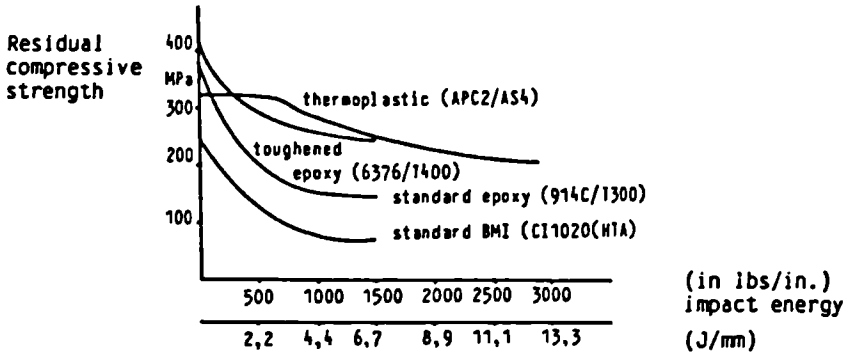

Fig 1.9 Typical results of post-impact compression tests. (Reproduced from Brandt et al, 1986).

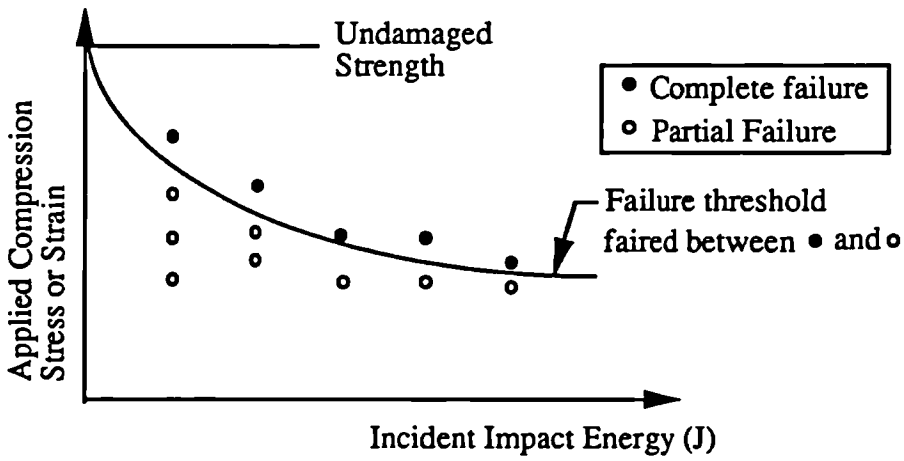

Fig 1. 10 Schematic showing results of combined compression and impact test.

2 Experimental Plan and Aims of Project

2.1 Experimental Plan

Initial investigations revealed that there are a large number of variables associated with the PICS test, both for the impact and subsequent compression test. In order to reduce the number of variables a decision was made to standardise the impact conditions for this work. The impact test conditions were chosen to initiate and propagate delamination damage as the major type of damage in the material.

This left testing variables related to the compression part of the test. An analysis of these variables revealed that they could be divided conveniently into three groups:

(1) Specimen variables:	Height	
	Width	
	Thickness	
	Lay-up	
(2) ABG design variables:	Type of support:	holehedral (size/ shape of opening)
		edge (flat, knife, curved)
	Type of load transfer:	end
		shear
		combination
(3) Testing variables:	Loading rate	
	Test temperature	

The number of possible designs and variations on designs of ABG's is large (and the list above is not exhaustive) and a comprehensive investigation of the effect of ABG design on the results of PICS testing was considered to be beyond the time and financial constraints of this work. Consequently, a more limited, but self contained, testing programme was devised to assess the effect of some specimen variables, namely: specimen width, thickness and lay-up.

The results of the investigations would probably have been most useful to the testing community as a whole if the experimental programme were carried out using specimens and jigs of the same size and design as the Boeing test, which is probably the most widely used PICS test . However, this was not practical because of the size and thickness of the

specimens. The supply of material (both in terms of the quantity required and the time needed to process it) and the availability of a high capacity compression testing machine were the limiting factors. To overcome these problems it was decided that a 'miniaturised' test specimen and ABG would be used for the work. In order to make some assessment of the 'miniaturised' test the intention was to test a range of materials and compare the ranking with results available in the literature.

A range of materials were chosen: a glass / epoxy (GRP), a carbon / epoxy (CE), a carbon / toughened epoxy (TCE) and a carbon / thermoplastic (Aromatic Polymer Composite (APC)). These were chosen because they covered a range of materials used in aircraft applications. The carbon based materials are all suitable for primary structural applications and glass based materials have been used in helicopter rotor blade construction (Dorey, 1984).

A testing programme was designed to assess the effect of the variables mentioned above. Table 2.1 shows the combinations of materials, lay-ups, thicknesses and specimen widths tested. During the course of the work some assessment of the effect of specimen clamping during the impact test, loading rate during the compression test and changes in the stacking sequence of QI laminates on PICS was also undertaken.

2.2 Aims of Project

In summary the aims of the project were:

(a) To assess the effect of specimen aspect ratio, thickness and lay-up on the results of PICS tests.

(b) To assess the utility of a 'miniaturised' PICS test.

(c) To assess in more general terms the fitness of the PICS test for its stated purpose.

Material	Lay-up	Thickness (Ply)	Specimen Width (mm)
TCE	0/90	16	45 55 75
	±45	16	45 55 75
	QI	16	45 55 75
	QI	24	55
	QI	32	55
CE	QI	16	55
GRP	QI	16	55
APC	QI	16	55

Table 2.1 Combinations of materials, lay-ups, thicknesses and specimen widths tested.

3 Materials and Experimental Methods

3.1 Materials

3.1.1 Material Suppliers and Identification Codes

Four commercially available materials were chosen, one from each of the types specified in chapter 2. Table 3.1 gives some details of these materials.

Fibredux 924C and APC-2 are current state-of-the-art materials suitable for use in aircraft structural applications. Fibredux 914C has been widely used for aircraft structural applications and has been described as 'the standard' high temperature epoxy system in western Europe (Partridge, 1989).

To avoid confusion the following abbreviations will be used to identify the materials throughout this thesis:

Material	Description	Abbreviation
Fibredux 924C	Toughened Carbon / Epoxy	TCE
Fibredux 914C	Carbon / Epoxy	CE
Fibredux 913G	Glass Reinforced Epoxy (Plastic)	GRP
APC-2	Aromatic Polymer Composite	APC

The following format will be used to identify the type of specimen tested: TCE-QI-16-55 where:
Suffix 1 = Material (TCE, CE, GRP or APC)
Suffix 2 = Lay-up (QI, ±45 or 0/90)
Suffix 3 = No of ply (16, 24 or 32)
Suffix 4 = Specimen width (45, 55 or 75 mm)

3.1.2 Processing

3.1.2.1 Fibre Lay-up

Three symmetric fibre lay-up's were used for this work. Unless otherwise stated the following fibre sequences and thicknesses were used:

Lay-up	Fibre Sequence	No of Ply	Nominal Thickness (mm)	*Abbreviation
Crossply	$[0, 90]_{4s}$	16	2	0/90
Angle-ply	$[-45, +45]_{4s}$	16	2	±45
Quasi-isotropic	$[-45, 0, +45, 90]_{2s}$	16	2	QI (16)
	$[-45, 0, +45, 90]_{3s}$	24	3	QI (24)
	$[-45, 0, +45, 90]_{4s}$	32	4	QI (32)

* Note : Based on cured ply thickness of 0.125 mm.

In addition a number of unidirectional 16 ply laminates were manufactured in order to compare the interlaminar shear strength of material manufactured in-house with the suppliers data.

The zero and 90 degree directions relate to the axis of the compression specimens. These are shown in fig 3.4

3.1.2.2 Toughened Carbon / Epoxy

The pre-preg was delivered in two batches; batch 1 (83.5 roll metres) in August 1988 and batch 2 (198.5 roll metres) in October 1989. The material was stored and processed in accordance with the manufacturer's recommendations (Anon, 1988 (a)).

A pressclave was used to process the material. The constituent parts and operating principle are shown schematically in fig 3.1. Fig 3.1(a) shows the two halves of the pressclave and the relative positions of the various materials required for processing. The peel ply on either side of the laminate provides a path for the vacuum to act over the entire upper and lower surfaces of the laminate. The cork dam prevents resin flowing away from the fibres at the edge of the laminate during processing. Bagging film prevents the laminate sticking to the base plate and the silicon rubber mat. Fig 3.1 (b) shows the pressclave in the closed position between the platens of the press. The press provides the heat required and holds the two halves of the pressclave together. The silicon rubber mat

acts as a seal between the upper and lower chambers of the pressclave. The lower chamber is evacuated using a vacuum pump and holes around the edge of the base plate allow the vacuum to reach the material. Laminate consolidation pressure is provided by the introduction of nitrogen gas into the upper chamber; the nitrogen is supplied from a gas cylinder via a regulator. A thermocouple, positioned approximately 5 mm into the laminate at its mid-plane, halfway along one edge, enables the temperature to be monitored during the curing cycle.

The following cure cycle was used for this material: under a vacuum (measured as 29 inches of mercury in the lower chamber) the material was heated to 120 ^{o}C at a heating rate of 8 ^{o}C/min (manufacturer's recommend between 2 and 8 ^{o}C/min). At 120 ^{o}C the vacuum was vented and a pressure of 700 KPa (approximately 100 psi) was applied to the laminate by introducing nitrogen gas at this pressure into the upper chamber. The same rate of heating was continued until 180 ^{o}C was reached. This temperature was then held (± 5 ^{o}C) for 2 hours. The laminate was allowed to cool slowly under pressure until 60 ^{o}C was reached. A typical temperature / time plot is shown in fig 3.2.

The above method was used to process all of the TCE material except for laminates 1 - 5 inclusive. For these laminates the upper layer of peel ply was followed by a layer of breather material. This was included to provide a path for the vacuum to reach the material being processed. In addition a steel caul plate was placed on top of the breather in an attempt to provide an even pressure over the surface of the material. This was followed by a layer of pressure bagging and the silicone rubber mat as before.

3.1.2.3 Carbon / Epoxy

This material (1 laminate) was processed at Ciba-Geigy (Duxford). The material was processed in an autoclave to the manufacturer's own recommendations (Anon, 1984).

3.1.2.4 Glass / Epoxy

This material was processed in-house using a simple compression moulding route. The cycle followed was that recommended by the manufacturer's (Anon, 1983). The laminate was heated to 150 ^{o}C at a rate of 9 ^{o}C/min (manufacturer's recommend less than 15 ^{o}C/min) under a pressure of 2000 KPa (approximately 290 psi) and cured for 20 minutes at this temperature. The finished laminate was then removed from the press and allowed to cool.

3.1.2.5 APC

This material was also processed in-house using the following procedure: the laminate was built up by spot welding the individual plies together around the edges, using a high temperature soldering iron. The unconsolidated laminate was placed in a simple matched mould and the whole assembly was then placed in a press, with platens pre-heated to 380 ^{o}C. After a 20 minute dwell at a pressure of 480 KPa (approximately 70 psi) the pressure was increased to 1400 KPa (approximately 200 psi) for 5 minutes. The matched mould was then transferred into platens pre-heated to 210 ^{o}C and a pressure of 2000 KPa (approximately 290 psi) was applied for 5 minutes. Finally, the matched mould was removed from the press and the laminate was removed from the mould immediately and allowed to cool.

3.1.2.6 Laminate Sizes

Table 3.2 shows the sizes of each type of laminate produced. All of the material processed in-house was supplied in 300 mm wide rolls. In the case of the APC-2 it was necessary to make 300 mm square laminates because this was the size required for the matched mould. In order to do this the ±45 degree layers had to be made from two pieces of material, one large piece and a small patch in one corner. The joint between the two pieces of material was parallel to the fibre direction. The GRP material was processed in the same way for convenience. It is assumed that the CE material processed at Ciba-Geigy was also made in this way from 300 mm wide stock. All of the TCE laminates with ±45 degree fibres were made without patching and are therefore smaller. For laminates with ±45 degree fibres the largest laminate which can be made from 300 mm wide stock is 212 mm square. The 0/90 laminates were reduced to 275 mm square because this was the maximum size which would fit in the pressclave.

3.1.3 Material Quality Control

Two methods were used to check the quality of the material. As a general check on overall laminate quality an ultrasonic C-scanning technique was used. This technique is described in detail in section 3.2.4. A quantitative check on material quality was obtained by measuring the interlaminar shear strength (ILSS) of material cut from each laminate after C-scanning. The short-beam shear test method was used, and was carried out using the method specified by the Composites Research Advisory Group (Curtis, 1988). The ILSS test was chosen for two reasons, firstly because it requires only a small amount of

material and secondly it measures a matrix dependant property and is therefore a good indicator of the quality of the cured resin.

In addition the fibre volume fraction and void content were measured for a few of the TCE laminates. The following procedure was used:

Specimens weighing approximately 1 gramme were dried in a vacuum oven at a temperature of 70 ^{o}C until a constant weight was achieved. The density of the specimens was then measured using a displacement method. The specimen was first weighed in air and then immersed in water using a balance capable of measuring to 0.0001 g. The density of the specimen was calculated from the following equation:

$$\rho_c = M_a \rho_w / (M_a - M_b) \qquad \text{Eq 3.1}$$

where: M_a is the weight of the specimen in air
M_b is the weight of the specimen in water
ρ_w is the density of water
ρ_c is the density of the specimen

The specimen was then boiled in a flask containing 10 ml of nitric acid for 1$^{1/2}$ hours. When cool the acid was diluted with distilled water and filtered through a paper filter (which had previously been weighed (M_c) using a Buchner filtration flask and pump. The flask was washed, first with distilled water and then with acetone, to ensure that all of the fibres were recovered. The acetone also dissolves the residue left from the matrix material on the filter and fibres. After removing as much of the liquid as possible the filter and fibres were dried in an oven at 120-150 ^{o}C for 45 minutes. The filter and fibres were then weighed (M_d). The weight of fibres (M_f) was then calculated by subtracting the original weight of the filter (M_c) from the weight of the filter and fibres (M_d). The volume fraction of fibres was then calculated:

$$V_f (\%) = (100\ M_f \rho_c) / (M_a\ \rho_f) \qquad \text{Eq 3.2}$$

where: V_f is the fibre volume fraction
M_f is the weight of fibres
ρ_c is the original density of the specimen
M_a is the original weight of the specimen
ρ_f is the density of the fibres

The theoretical density of void free material (ρ_t) can now be calculated from:

$$\rho_t = V_f \rho_f + (100 - V_f) \rho_r \qquad \text{Eq 3.3}$$

where: ρ_r is the density of the resin
$(100 - V_f)$ is the matrix volume fraction

The void content (V_v) can now be calculated:

$$V_v = 100 (\rho_t - \rho_c) / \rho_t \qquad \text{Eq 3.4}$$

Finally, the resin volume fraction (V_r) can be calculated:

$$V_r = 100 - V_t - V_v \qquad \text{Eq 3.5}$$

3.2 Test Methods

3.2.1 Impact Testing

3.2.1.1 Impact Machine

A low energy dropweight impact machine was used for this work. This machine had previously been designed and built in-house. A 20 mm diameter tup weighing 3.96 Kg can be dropped from a maximum height of 0.4 metres giving a maximum incident impact energy of 15.5 Joules (J). A device was used to prevent multiple strikes of the specimen. The specimen was supported on a 40 mm diameter ring and clamped in position by a plate, also with a 40 mm diameter hole (fig 3.3). The two screws on either side of the top plate were initially fastened finger tight before being tightened by a further half turn with a hexagonal key. These impact conditions were used because previous experience had shown that delamination damage would result from low energy impact. The clamping arrangement was chosen to avoid different impact responses when testing specimens of different widths.

The machine has a velocity recorder to measure the speed of the striker just before it makes contact with the specimen. The velocity is calculated by measuring the time taken for a 2 mm diameter pin to fall through a photodiode sensing device. The position of the sensor can be adjusted so that the velocity is recorded just before the impacter makes contact with the specimen. The velocity is used to calculate the incident impact energy

(kinetic energy) of the striker and is also required for use in some other calculations (see below).

The tup is instrumented and can measure forces up to 10 KN. The load sensor utilises strain gauges (semi-conductor type) bonded on to flats cut into the shaft of the impacter and arranged into a half-bridge so that bending stresses are eliminated. The load cell is calibrated statically. During an impact test the force variation with time is stored by a transient recorder (CEAST Advanced Fractoscope System MK3). This force / time data is down-loaded to a computer where the velocity and displacement of the tup and the energy absorbed by the specimen at any time (t) can be derived using the equations given in chapter 1 (Eq's 1.6, 1.7 and 1.8).

3.2.1.2 Calculation of the Constant n' used in Equation 1.3 and Plate Stiffness (K_p)

In order to use equation 1.3 the values of K_p and n' need to be obtained.

(a) Estimation of K_p

An estimate of the value of the specimen stiffness (K_p) was made by dividing the measured force (F1) by the measured deflection (d1) at damage initiation for each specimen and then finding the average for a number of specimens. However this calculation underestimates the stiffness because the measured deflection is a combination of bending (d_b) and contact deformations (d_c). The calculated stiffness can be corrected by estimating the value of the contact deformation from $d_c = (F1 / n')^{2/3}$ (from the definition linking force deflection and n' given after eq 1.3). The deflection due to bending can than be calculated ($d_b = d1 - d_c$) and used to calculate a corrected value of K_p ($K_p = F1 / d_b$).

(b) Measurement of n'

The value of n' was measured by performing an indentation test using the same loading nose as was used for the impact tests. The material was supported on a flat surface and the force-deflection curve measured. A loading rate of 0.5 mm/min was used. A graph of force against (deflection)$^{3/2}$ was then drawn and the value of n' was found from the slope of the curve ($n' = P / \alpha^{3/2}$).

3.2.2 Production of Compression Test Specimens

Specimens were cut from the laminates using a diamond impregnated slitting wheel. A 10 mm wide strip around the edge of each laminate was discarded simply to ensure that specimens were manufactured from sound material. In the case of laminates produced in the pressclave this was necessary in any case because they tended to be substantially thinner in this region. The specimen edges were cut to coincide with the 0 and 90 degree fibre directions, with the specimen height being parallel to the 0 degree direction. This was achieved by using one of the laminate edges as a reference, the same edge having been used to align the fibres during the manufacture of the laminate.

After cutting the specimen squareness was checked by using a 3 inch engineer's square. The specimen dimensions were measured at the points shown in fig 3.4. The height, width and diagonal dimensions were measured using a pair of vernier calipers (0 to 12 inches with 0.001 inch divisions). These dimensions were then converted to mm. The thicknesses were measured using a 0 - 25 mm micrometer with 0.01 mm divisions. The average thickness, width and height were calculated for each specimen. By combining the width and length measurements with the corner to corner measurements the angles at each corner can be calculated (using the cosine rule) to check the squareness of the specimen.

3.2.3 Compression Testing

3.2.3.1 Anti-Buckling Guide

An anti-buckling guide (ABG) was designed to support the specimens during compression loading. This is shown in fig 3.5. One of the brackets can be moved so that the different specimen widths can be accommodated. The specimen support conditions are shown in fig 3.6. The same amount of support is offered to each specimen, independent of specimen width; i.e. 10 mm at each end and 5 mm at each side are supported.

The following procedure was adopted for clamping a specimen into the ABG:

(a) One of the side supports was set so that it was perpendicular to the base using an engineer's square (fig 3.7 (a))

(b) The base support and second side support were then positioned so that they were in line with the first support (fig 3.7 (b)) forming a vertical plane in line with A-A.

(c)-(d) The other side and end supports were then fitted, but not tightened. Each new specimen was fitted by tightening the side supports in turn, with the specimen positioned next to the support bracket (fig 3.7 (c) - (d)).

(e) The end support was then tightened with the specimen positioned centrally between the brackets (fig 3.7 (e)). At this stage the specimen was free to slide, both laterally and vertically.

(f) The specimen was then lifted vertically out of the ABG and the loading plate was fitted. Finally, the specimen was slid back into the ABG with the loading plate fitted and the whole assembly was positioned centrally in the compression testing machine (fig 3.8).

3.2.3.2 Details of Compression Test

Unless otherwise stated the compression tests were carried out at a loading rate of 0.3 mm/min. The tests were all carried out on a Schenk Treble tension / compression testing machine using a 100 KN load cell. The load was recorded as a function of time during the test (a pen sweeprate of 25 sec / cm was used). The maximum load was also stored and presented on a digital readout at the end of the test.

Nominal stresses were calculated by dividing the force by the average thickness times the average width measured for each specimen (see section 3.2.2). Nominal specimen strains were calculated by multiplying the feedrate by the time (measured from the force versus time plot) and dividing by the original length of the specimen. Finally, a nominal plate modulus was found by taking the slope of the appropriate part of the stress versus nominal strain curve.

3.2.3.3 Testing of Initially Undamaged Specimens

The following procedure was used to measure the out-of-plane deformations of undamaged compression specimens:

The specimen was positioned in the ABG using the procedure described in section 3.2.3.1. A dial-test-indicator (DTI) was then positioned to read the out-of-plane displacement at one of five positions on the specimen (see fig 3.9). A 0 - 25 mm DTI with 0.01 mm divisions was used. The specimen was then loaded at 0.3 mm/min and the lateral deflection was read from the DTI at appropriate load intervals. At this loading rate it was possible to read the DTI and the load simultaneously without stopping the machine.

Initially the deflections were only measured at low loads (compared with the failure load of the specimen). The same procedure was repeated for each of the five measuring points, the specimen being completely unloaded between measurements. Finally, the specimen was tested to failure. For some specimens the lateral deflection was measured up to failure for the position previously found to give the maximum deflection. The problem with this however was that the failure of the specimen often produced very high lateral accelerations, which caused damage to the DTI's by bending the small internal gear teeth.

The data was plotted in two ways, firstly the deflected profiles of the specimens were plotted for different loads, giving a series of profiles on the same diagram. Secondly the maximum lateral deflection was plotted as a function of load. This data can be used to assess the buckled profile and the nature of the buckling process.

3.2.4 Non-Destructive Testing

An ultrasonic C-scanning machine was used to assess the quality of laminates after manufacture and the extent of damage after impact testing. The principle of operation of this type of machine has been described elsewhere (Stone et al, 1986) and therefore will not be repeated here.

A Meccasonics C-scanning machine was used for this work (courtesy of the Department of Aeronautics, Imperial College of Science Technology and Medicine). A double through transmission technique, using a 10 MHz probe (transmitter / receiver) focussed on a glass reflector was employed. The specimens were supported at the edges on metal rods 10 mm above the glass. The transducer was scanned back-and-forth across the specimen, indexing in 1 mm steps after each pass over the material. The data was stored on a computer which processes the data from the scanned direction at 1 mm intervals, the 'scan' is therefore broken down into a series of points on a 1 mm gridiron.

When using a double through transmission technique it is the amplitude of the signal reflected back from the glass which is of interest. The amplitude of the glass echo received when scanning a material (A_m) is compared with the amplitude of the glass echo received when there is no material between the transducer and the glass (A_g). The attenuation level is calculated from the following formula:

$$\text{Attenuation level} = 10 \log \left(A_g / A_m\right)$$

This is usually expressed in decibels (dB). Zero dB corresponds to zero attenuation.

The glass echo is separated out from the other echos by using an electronic gate (see fig 3.10). The machine is calibrated by positioning the transducer over the glass and artificially attenuating the echo signal using a resistance box. A calibration file is built up in the computer which records the voltage (i.e. the amplitude of the glass reflection echo) for different attenuation levels, from 0 dB up to approximately 50 dB in 1 dB steps. When scanning a material the amplitude of the glass reflection is modified by the material and the attenuation level is found by referring to the calibration file. Finally the attenuation levels are plotted (either on a monitor or a colour jet printer) as a function of position, to produce an 'attenuation map' for the material scanned. Different ranges of attenuation are represented by different colours. These ranges can be modified to highlight areas of interest.

In the case of the GRP specimens it was not necessary to use the ultrasonic C-scan because the impact damage was clearly visible. However, some specimens were C-scanned so that an estimate of the accuracy of the ultrasonic C-scanning machine could be made. The GRP specimens were photographed after impact testing and again after compression testing. The specimens were back-lit and photographed on black and white 35 mm film.

3.2.5 Microscopy

A sectioning and polishing technique was used to determine the through thickness distribution of impact damage. The specimens were 60 mm square and were impact tested in the same fixture as the PICS test specimens (see section 3.2.1). After ultrasonic C-scanning the specimens were sectioned through the impact centre parallel to the 90 degree fibres using a diamond impregnated slitting wheel. They were then set in an acrylic potting resin. After the resin had cured the specimens were polished using silicone carbide paper, starting with 220 grade followed by 800 and then 1000. The final polish was with "Brasso" metal polish.

The specimens were then photographed using a low power microscope on 35 mm black and white film. The magnification of the microscope was adjusted so that the image filled the frame of the camera in the thickness direction. A series of photographs were then taken to cover the entire length (60 mm) of the specimen. The film was contact printed and a montage was made to show the whole of the specimen. The final magnification of the montage depended on the thickness of the specimen being photographed:

Thickness	Final Magnification
16 ply (2 mm)	X 8
24 ply (3 mm)	X 6
32 ply (4 mm)	X 4

Individual frames of interest were magnified further by printing using an enlarger when printing the negatives .

Matrix			Fibre			Pre-preg	
Material	Manfu's Name	Manuf's Code	Type	Manuf's Name	Manuf's Code	Manuf's Name	Manuf's Code
Rubber Toughened Epoxy	Ciba-Geigy	Fibredux 924	Carbon	Torayca	T800H	Ciba-Geigy	F924C
Epoxy	Ciba-Geigy	Fibredux 914	Carbon	Grafil	XAS	Ciba-Geigy	F914C
Epoxy	Ciba-Geigy	Fibredux 913	E Glass	---	---	Ciba-Geigy	F913G
Poly-etheretherketone	ICI / Fiberite	---	Carbon	Hercules	AS4	ICI/Fiberite	APC-2

Table 3.1 Details of materials and suppliers

Material	Layup	Thickness	Size (mm)
TCE	0	16	212 x 88
	0/90	16	275 x 275
	±45	16	212 x 212
	QI	16	212 x 212
	QI	24	212 x 212
	QI	32	212 x 212
CE	QI	16	300 x 300
GRP	QI	16	300 x 300
APC	QI	16	300 x 300

Table 3.2 Laminate sizes

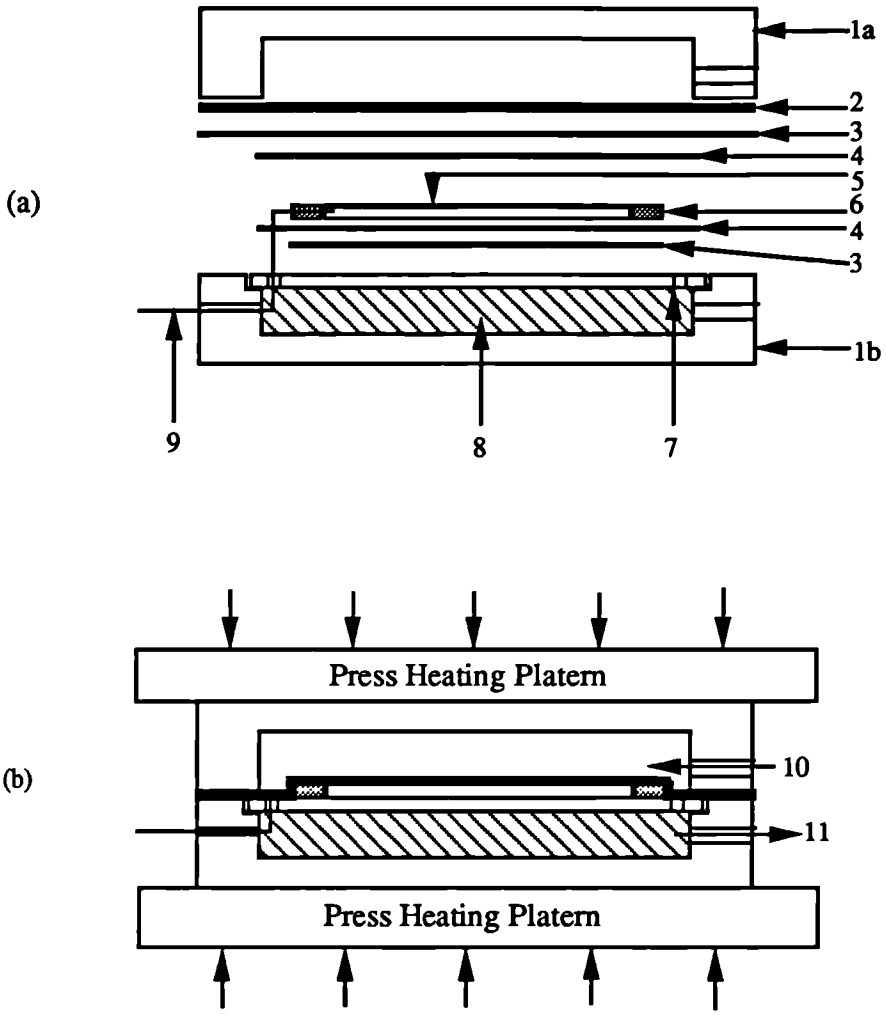

KEY

1 (a) and (b) - 2 halves of pressclave
2 Silicone Rubber mat
3 Pressure Bag
4 Peel Ply
5 Laminate
6 Cork Dam
7 Baseplate
8 Nomex Honeycomb (to support baseplate)
9 Thermocouple
10 Nitrogen gas inlet
11 Vacuum outlet

Fig 3.1 Schematic to show details of the Pressclave

(a) Lay-up of materials
(b) Assembly in press

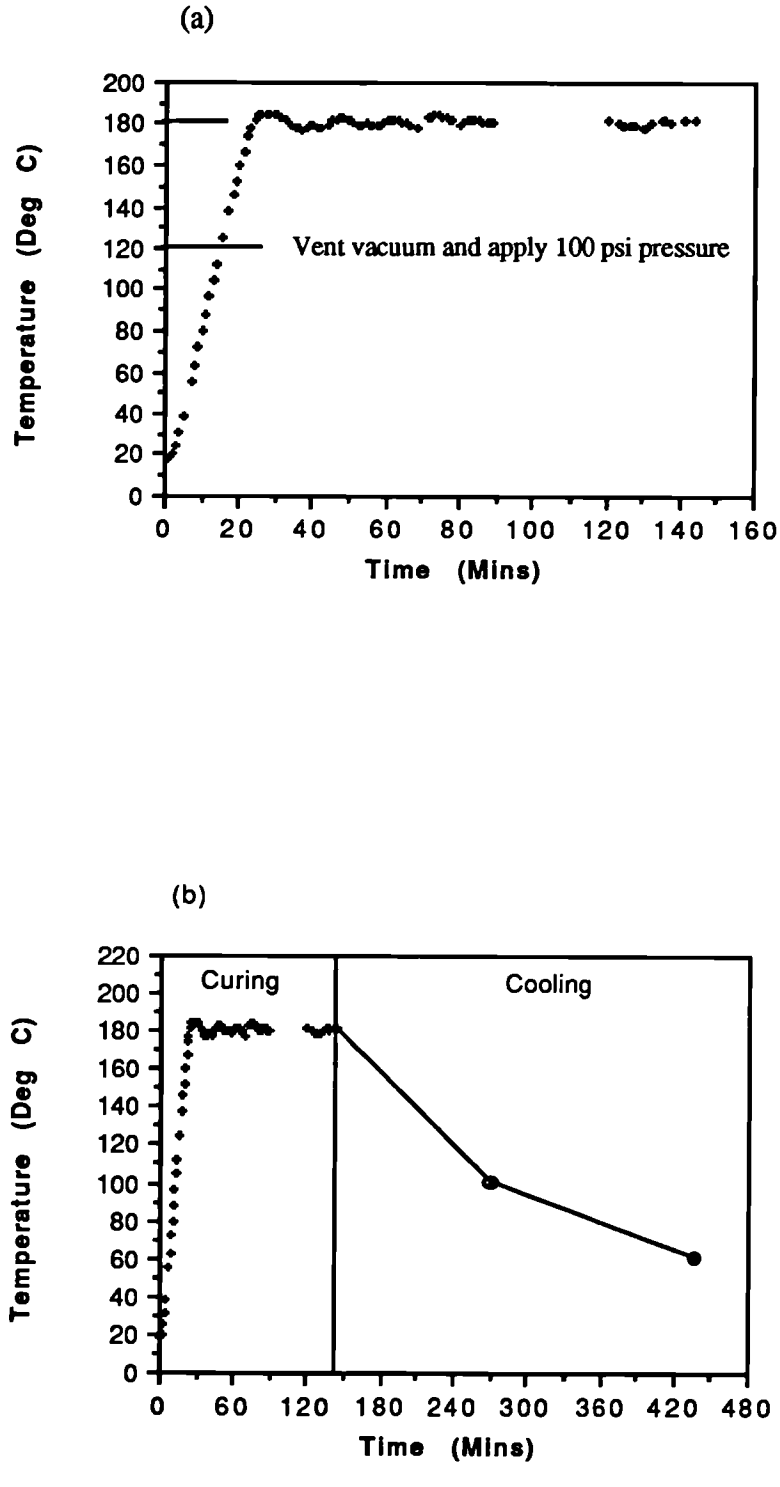

Fig 3.2 Temperature versus time record for TCE processing.
(a) Curing. (b) Curing and Cooling.

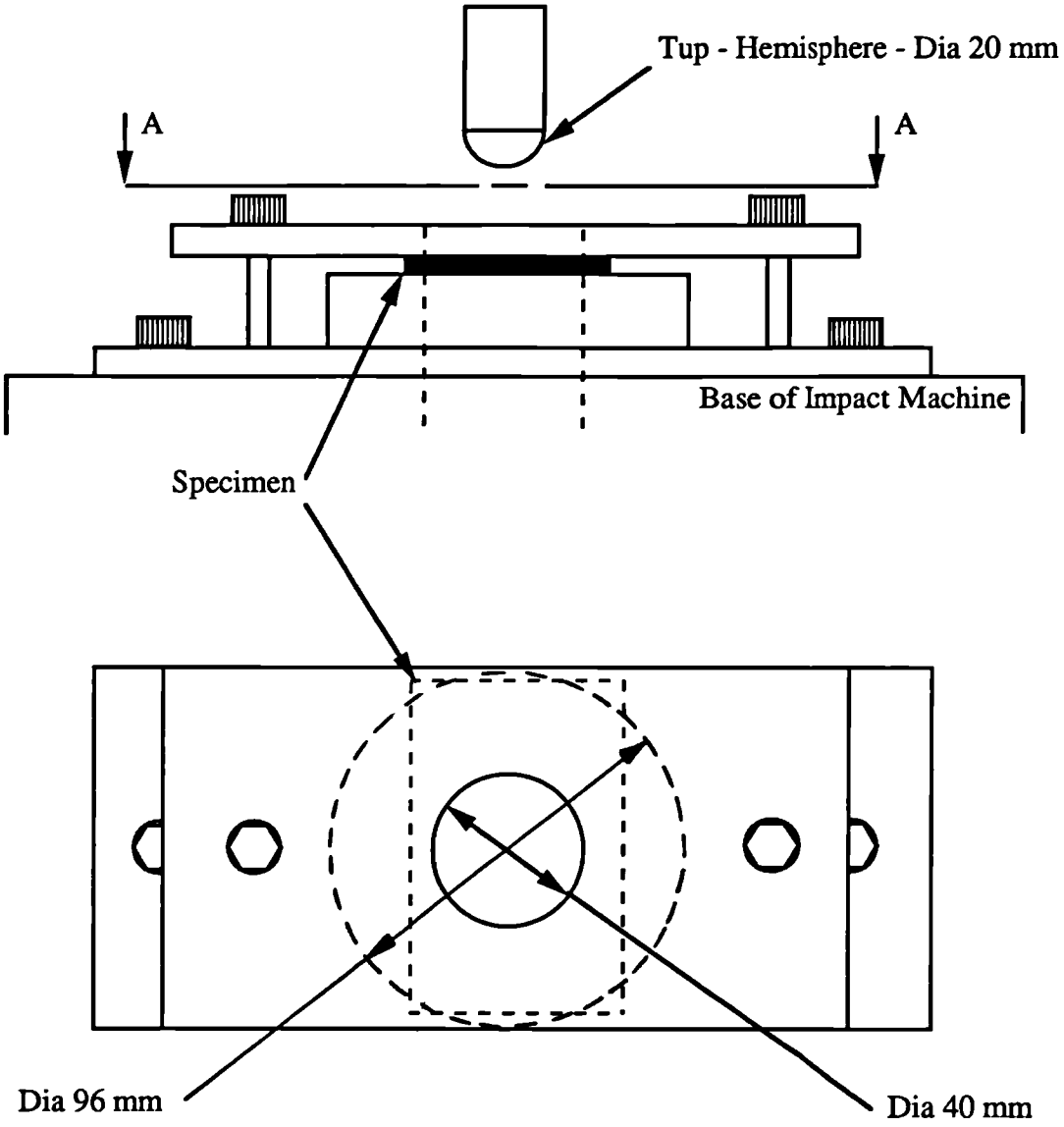

Fig 3.3 Impact support and clamping conditions.

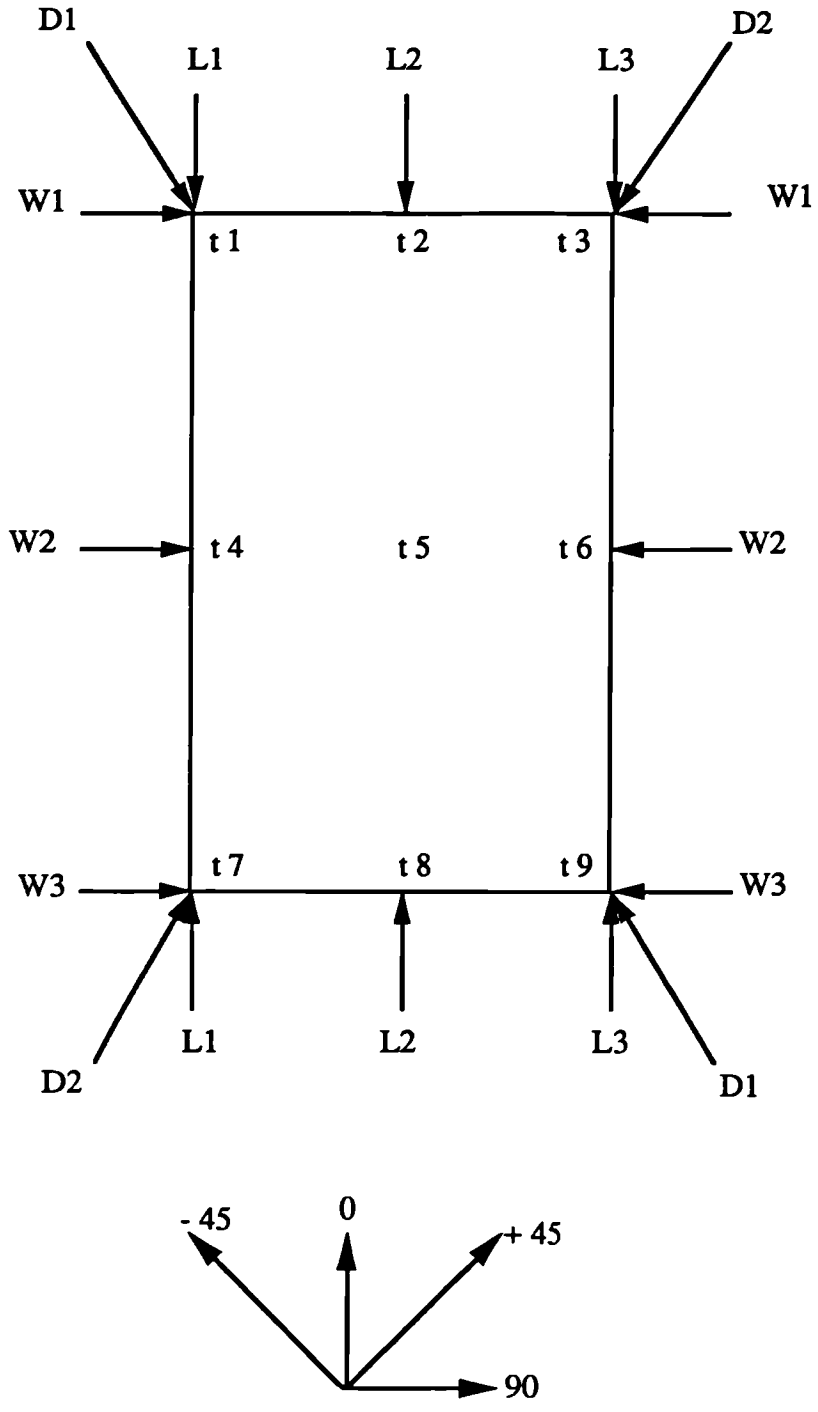

Fig 3.4 Diagram to show position of measurement points and fibre directions for compression specimens.

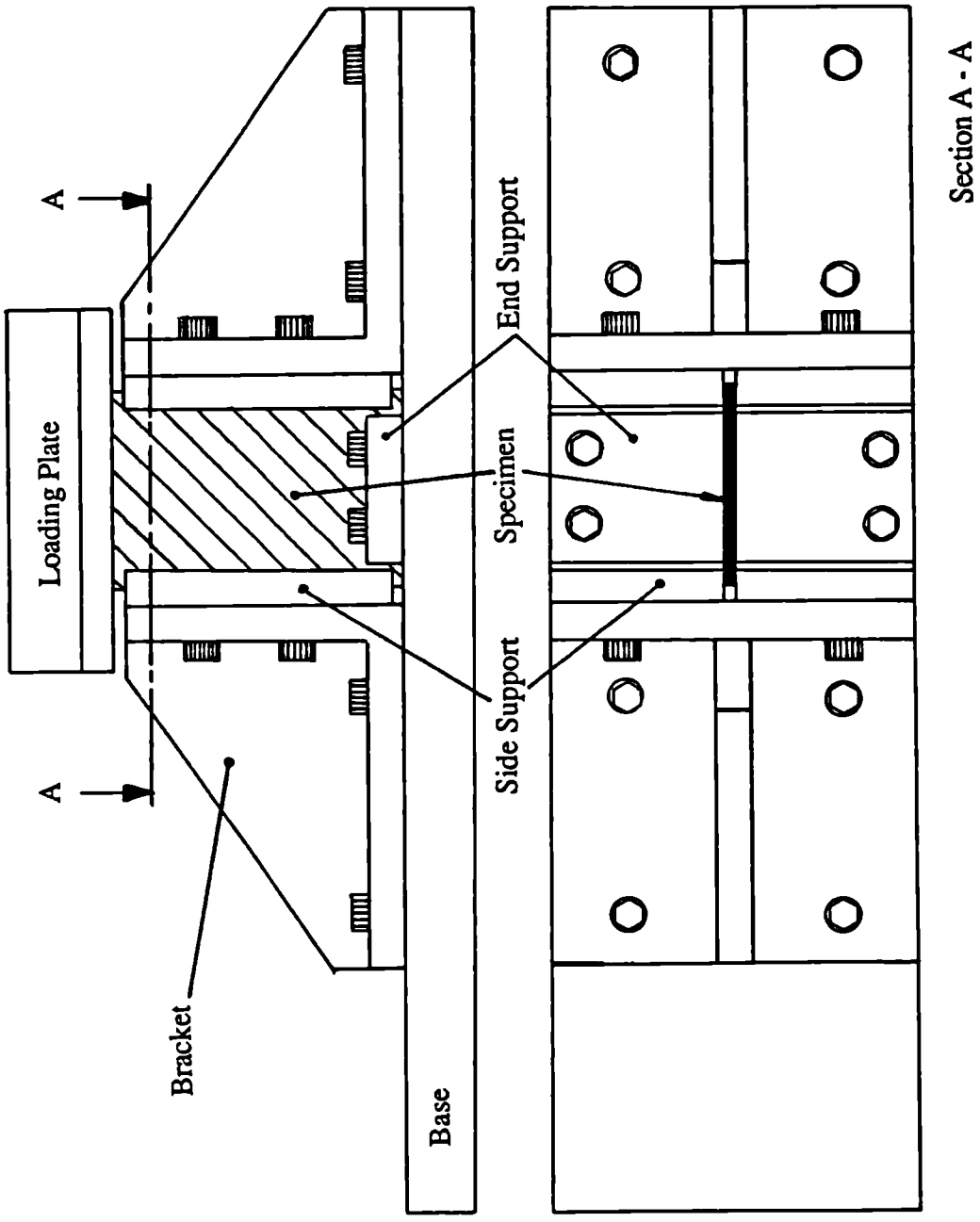

Fig 3.5 Schematic drawing of the anti-buckling guide.

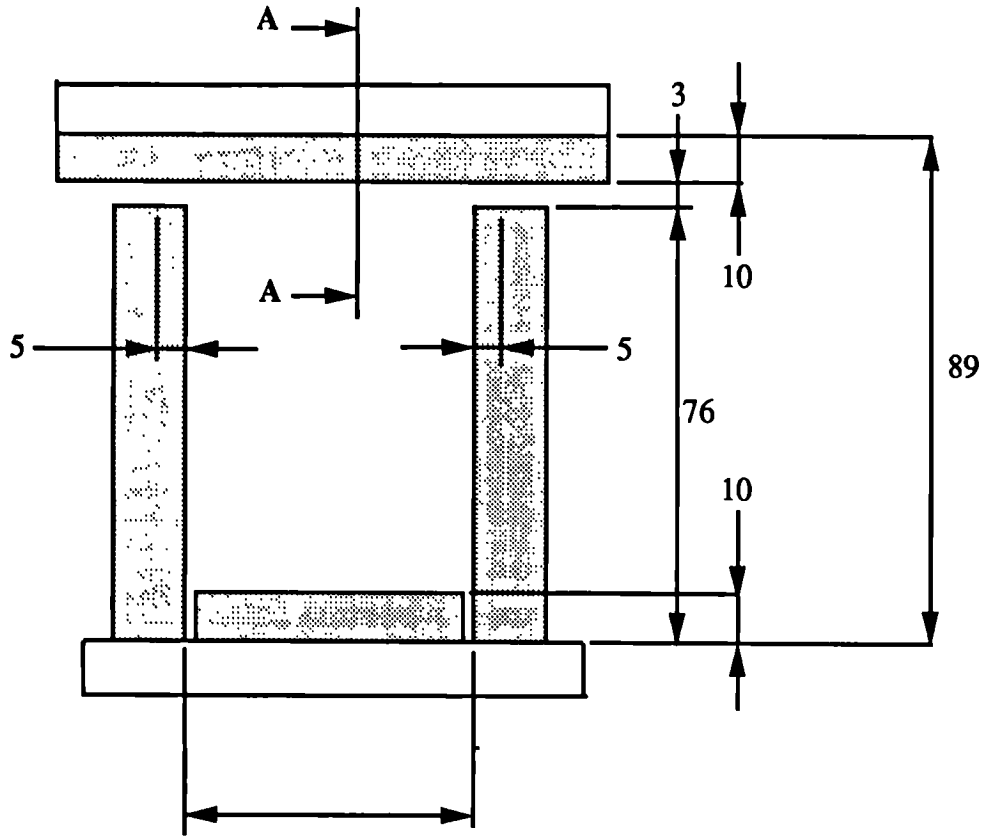

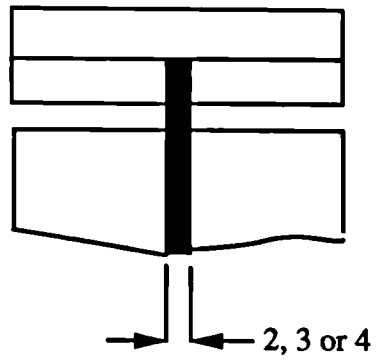

Part Section A-A

Figure 3.6 Diagram to show compression specimen support conditions.

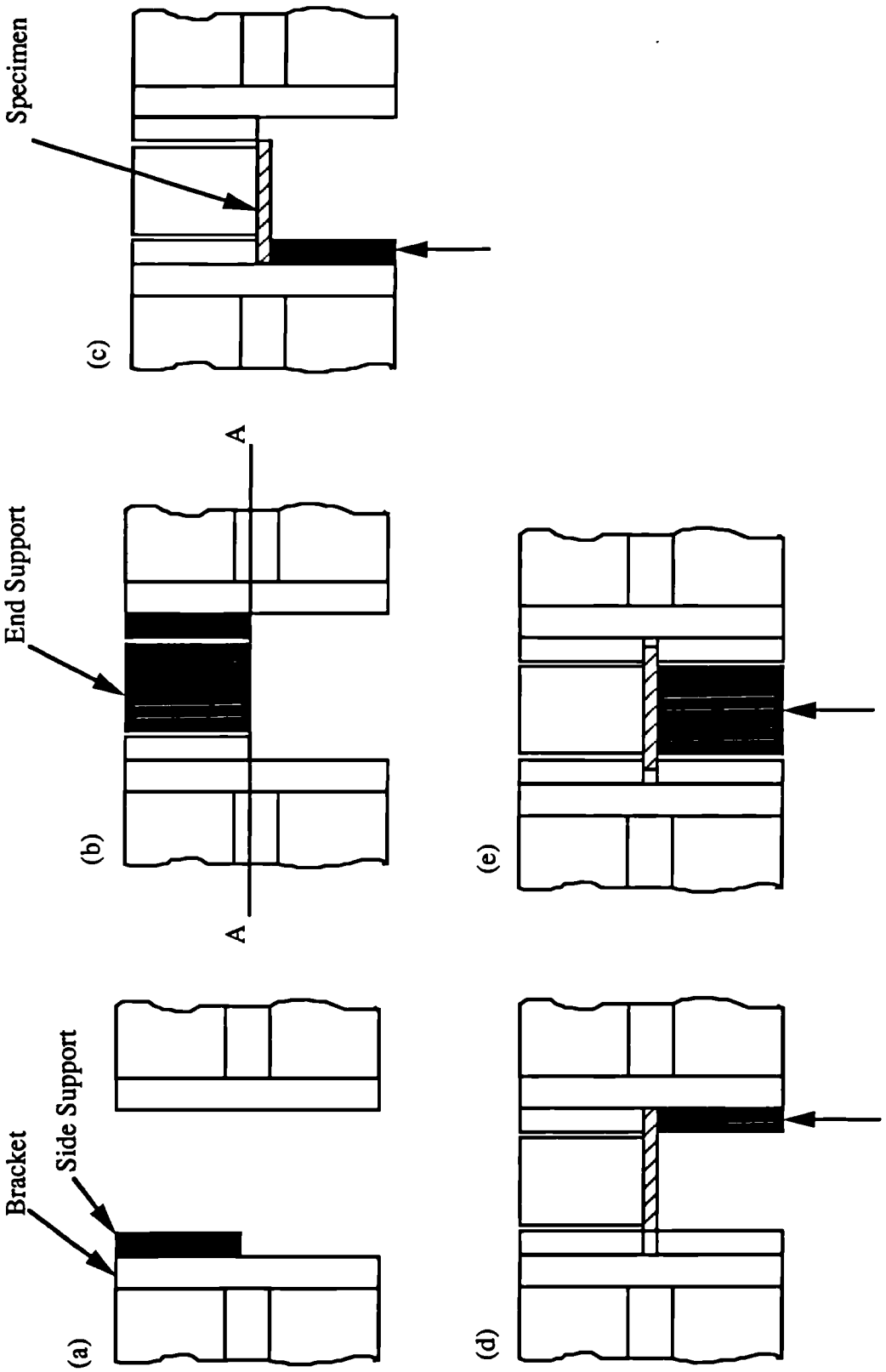

Fig 3.7 Set-up procedure for the anti-buckling guide.

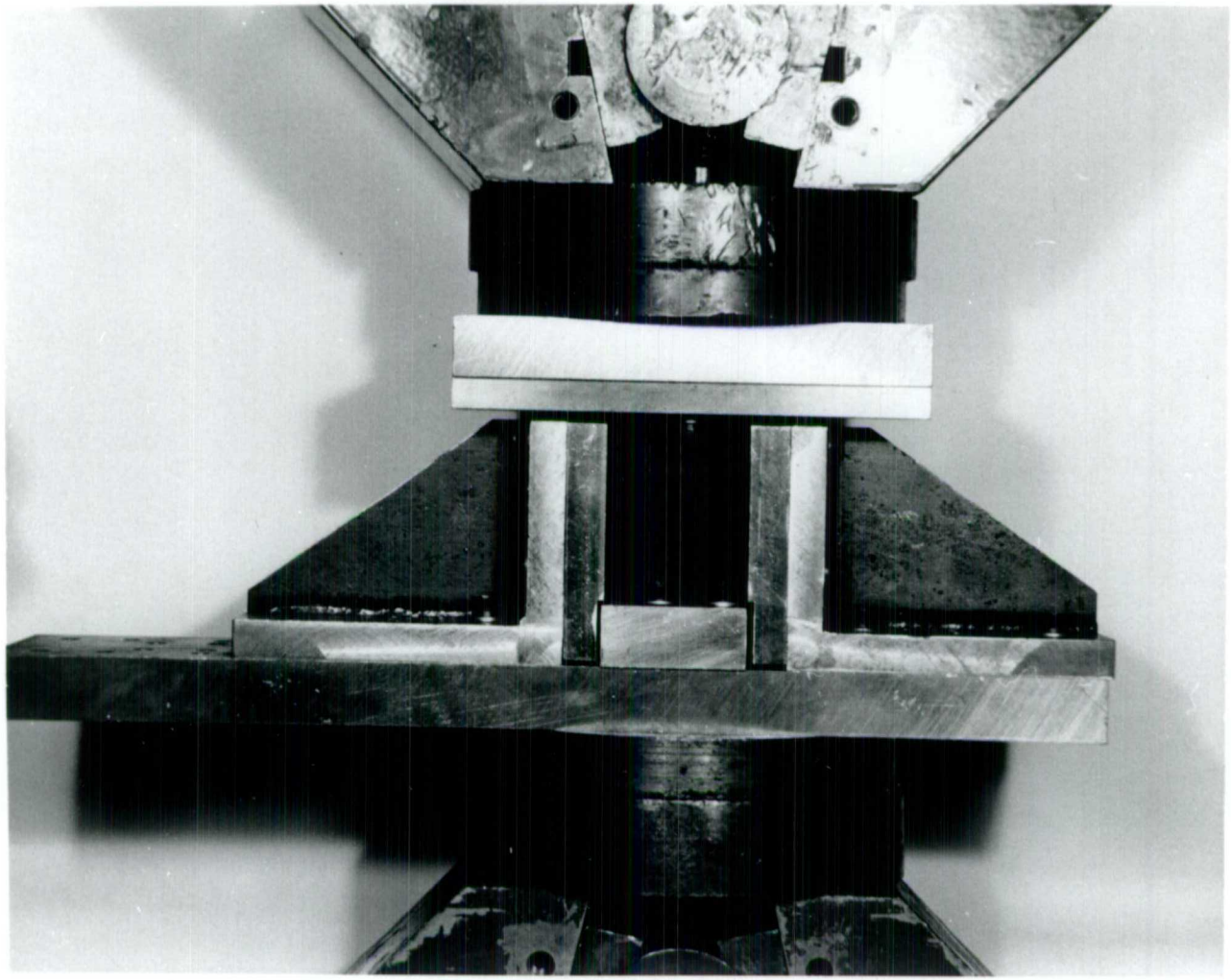

Fig 3.8 Photograph of anti-buckling guide and specimen during a compression test.

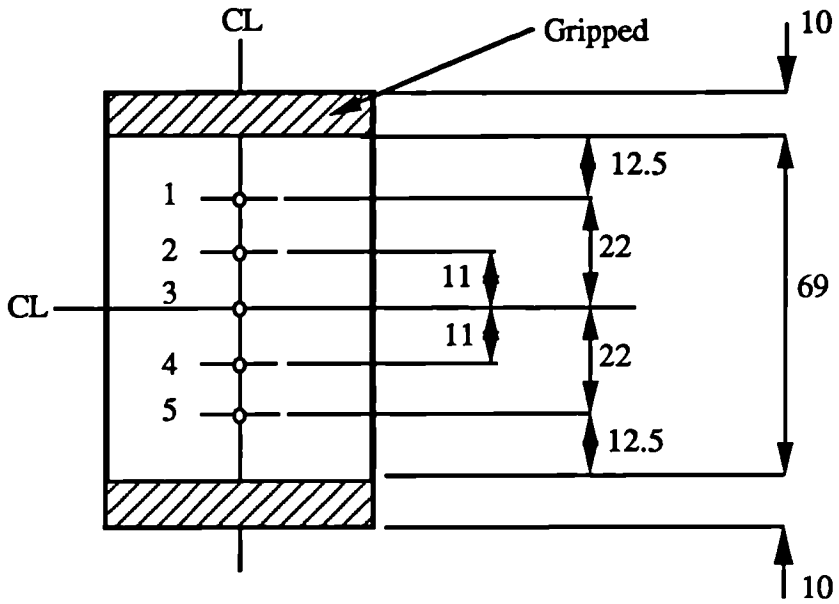

Fig 3.9 Positions for the measurement of lateral deflection.

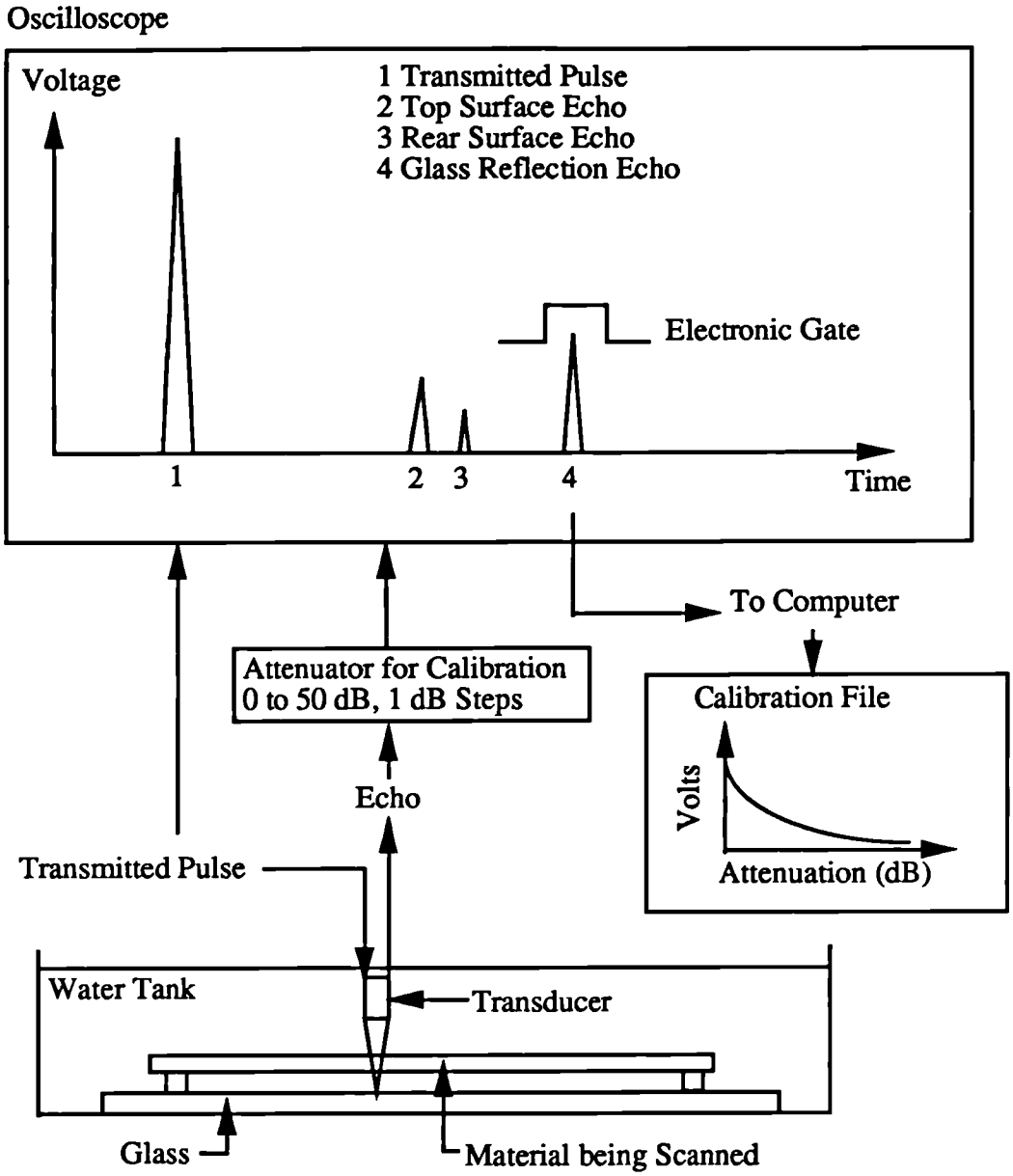

Fig 3.10. Schematic to show operation of the ultrasonic C-Scan.

4 Material Quality

4.1 Introduction

In this chapter the results of tests designed to assess the quality of the materials used for the main testing programme will be presented and discussed. An ultrasonic C-scanning machine was used to assess the general quality of the material while the interlaminar shear strength was measured to assess the mechanical properties of the material. Measurements of the fibre volume fraction and void content were made on a small number of specimens.

4.2 Results of Ultrasonic C-Scanning

The ultrasonic C-scan was used as a method of screening the material to reveal any major defects resulting from processing. Initially three laminates made from Fibredux 914C and processed by Ciba-Geigy were scanned to provide a reference against which the material processed for this work could be compared. The following results were obtained:

Thickness	Attenuation Level (dB)
16	9
24	12 (Patches at 11)
32	15 (Patches at 16)

Over this range of thicknesses a linear relationship between attenuation level and thickness (a change of approximately 3 dB / mm) was observed. Compared to the range over which the equipment is calibrated (0 to approximately 50 dB) the effect of material thickness was small.

Having established the attenuation levels which could be expected for correctly processed material, some specimens were scanned which contained delamination damage resulting from low energy impact. Attenuation levels of greater than 48 dB were obtained (Note: the machine was only calibrated up to approximately 50 dB). This gave an indication of the attenuation levels which would be expected if there were a 'major' defect resulting from processing.

These two experiments provided bounds within which the quality of the material manufactured for the experimental programme could be assessed. No strict 'pass' or 'fail' criterion was used, each laminate being assessed within the guide lines. Because of the subjective nature of the pass - fail criterion the individual colour prints showing the

attenuation levels over each plate have not been reproduced here. In the event only one laminate (the first one to be manufactured) was discarded. There was a very clear cut case for rejection with attenuation levels ranging from 12 dB to greater than 50 dB being measured. The rest of the laminates were accepted, in most cases the attenuation levels were in line with those found for the 'standard' Fibredux 914C material. The maximum attenuation level which was found to extend over a large area was 25 dB (for a 32 ply laminate) and this laminate was also accepted. Laminates with small spots of higher attenuation were also accepted since these are often caused by air bubbles on the surface of the material. In a small number of cases higher levels of attenuation were found at a corner, and although the laminate was accepted the material from the corner was not used to manufacture specimens.

The use of the ultrasonic C-scanning technique was judged to be successful as a screen to assess the general quality of the whole plate, before mechanical tests on small samples of material were performed. The interlaminar shear strength test was chosen to give a more objective assessment of the material quality. The results of these tests are reported in the following section.

4.3 Results of Interlaminar Shear Strength Tests

The results of ILSS tests on specimens cut from the laminates have been used to assess the variation in quality of the material used for the main testing programme. In addition some material was also manufactured with a unidirectional (0) lay-up so that the ILSS could be compared with the manufacturer's data.

4.3.1 Results for TCE Material

(a) 0/90, ±45 and QI Lay-ups

In general five tests were performed on material cut from each laminate. The individual results for each laminate are listed in appendix A along with the average and standard deviation. These results have been plotted as bar charts in fig 4.1. Three graphs have been plotted, one for each lay-up. If the material were of even quality we would expect to find that the average ILSS was similar for all of the laminates. For the ±45 and 0/90 laminates this appears to be a reasonable assumption. For the 0/90 material the low ILSS of laminate number 1 confirmed the results of the ultrasonic C-scan and justified the decision to discard the material. (Note: the data for this laminate will be ignored in all further calculations). However in the case of the QI(16) laminates there are four (2, 3, 4 and 35)

which have ILSS's noticeably lower than the rest. In order to assess whether these are due to genuine differences in material quality or whether they can be attributed to scatter in the results caused by the test method, it is appropriate to perform a statistical analysis of the results. This will also be done for the other lay-ups to give confidence in the observations made above.

The first step is to find out whether the data is normally distributed. A simple initial check on the normality of the data can be achieved by plotting the frequency distribution. The results are shown in table 4.1 and fig 4.2. For each lay-up the data does not appear to follow a normal distribution because the requirement of symmetry is not fulfilled. A more conclusive method of establishing the normality of a set of data is to plot the cumulative frequency (expressed as a percentage) on normal probability paper (Bajpai et al, 1978). If the data is normal then it will lie on a straight line. This type of curve is shown in fig 4.3 for the QI data. Similar results were obtained for the other two lay-ups. There is some doubt as to the normality of the data and consequently an analysis using statistics based on the normal distribution may not be appropriate.

Instead a statistical analysis using a non-parametric method (also known as distribution free method) will be used. As the name suggests the method does not require the data to conform to any particular distribution. The appropriate non-parametric is the Kruskal-Wallis test (Sokal et al, 1969). This is a test for differences of location in ranked data grouped by a single classification. The method is described in appendix D. The null hypothesis is that there is no difference in the location of the ILSS data for the different laminates of a particular lay-up. The analysis gives the following results:

Lay-up	Total No of Tests	Number of Groups (a)	Statistic H	Correction Factor for Ties (D)	Adjusted H (H/D)	$\chi^2_{0.05,\,(a-1)}$
0/90	35	7	6.90	0.9999	6.90	12.59
±45	48	9	13.71	0.9995	13.72	15.51
QI	56	12	28.90	0.9995	28.91	19.68

The last column of the table above gives the value of χ^2 for $\alpha = 0.05$ and a-1 degrees of freedom. In this case the null hypothesis is accepted for the 0/90 and ±45 lay-ups since H is less than $\chi^2_{0.05,\,(a-1)}$ while the null hypothesis is rejected for the QI lay-up because H is greater than $\chi^2_{0.05,\,(a-1)}$. The statistical analysis confirms the earlier observation that the quality of the ±45 and 0/90 laminates appears to be consistent while there appears to be differences between the ILSS's of some of the QI laminates.

It is interesting to note (fig 4.1(c)) that there does not appear to be any effect of thickness on the measured ILSS values for the QI material over the range of thicknesses tested (2, 3 and 4 mm). A span-to-depth-ratio of 5 was used in each case and the shear strength calculated from 0.75 F / w t (where F is the failure force, w is the specimen width and t the specimen thickness).

(b) ILSS of Uni-directional Material

Ciba-Geigy quote an ILSS of 120 MPa for this material (Anon, 1988 (a)) at a fibre volume fraction of 60%. Several laminates were manufactured and tested to validate the processing method used. Although the material used for the main testing programme was not post-cured, several different post-cure cycles (Anon, 1988 (a)) were used on this material in an attempt to match the value of ILSS quoted by Ciba-Geigy. The results are shown in table 4.2 (Note: averages of five tests are quoted and the full set of data can be found in appendix A). The ILSS is between 10% and 14.1% lower (for the highest and lowest average values respectively) than the value quoted by Ciba-Geigy.

A statistical analysis was also carried out on the data for the unidirectional material. All of the results were considered as a single data set (because differing post-cure cycles did not appear to affect the result very much). Again the data did not follow a normal distribution (fig 4.4) and the Kruskal-Wallis test was therefore used. The results are shown in the following table:

Lay-up	Total No of Tests	Number of Groups (a)	Statistic H	Correction Factor for Ties (D)	Adjusted H (H/D)	$\chi^2_{0.05,(a-1)}$
0	34	7	6.31	0.9995	6.31	12.59

Again the null hypothesis is accepted since H is smaller than $\chi^2_{0.05,(a-1)}$. This supports the observation made earlier that the strengths were not affected very much by the different post-curing cycles.

4.3.2 Results for APC, CE and GRP Materials

ILSS measurements were made on specimens taken from the three APC laminates and the CE laminate. No tests were carried out on material from the two GRP laminates, however tests on a uni-directional laminate manufactured using the same material and method gave ILSS's identical to those quoted by the manufacturer. The results for the APC and CE material can be found in appendix A.

The results for these two materials are of less use than those obtained for the TCE material because there is less data, and the results could not be compared with manufacturer's data because it was not available for these lay-ups. In any case the value of the results for the APC material is questionable because of the problem of plastic deformation which makes it difficult to obtain a valid shear failure. The following results were obtained for the three APC laminates:

Laminate No	ILSS (MPa)	SD	Cv (%)
21	83.8	1.5	1.8
22	89.4	4.6	5.1
53	91.2	4.2	4.6

The coefficients of variation indicate reasonable quality within each laminate. When the average values are compared laminate 21 is slightly lower than was measured for the other two laminates. However the difference was not large enough to warrant rejecting the material.

The average ILSS value for the CE material was 66.4 MPa (SD = 4.7) (Note: the lay-up was $[-45,90,+45,0]_{4S}$. Again the C_V of 7.1 % shows that the material was apparently of even quality within the laminate. Without strengths from other laminates to compare it with, the result is of little use.

4.4 Results of Void and Volume Fraction Measurements

The void content and volume fractions of fibre and matrix was measured for five samples taken from five different laminates. A resin density of 1.31 g/cc (Anon, 1988 (a)) and fibre density of 1.83 g/cc (Galiotis, 1990) were used in the calculations. The results are shown in table 4.3.

4.5 Discussion

4.5.1 TCE Material

The ultrasonic C-scan was used to monitor the general quality of laminates by comparing the attenuation level with that of reference laminates and impact damaged laminates. All other things being equal the variation in the attenuation level is caused by variations in the void content of the material. In fact the Composites Research Advisory Group (CRAG)

(Curtis, 1988) suggest that the ultrasonic C-scanning technique can be used to measure the void content of composite laminates. In order to do this a calibration must be performed to find the relationship between the specific attenuation level (dB / mm) and void content. Specimens of different thickness and void content must be scanned, after which the void content is measured using some other method (for example the density measurement / resin removal technique). The method relies on the fact that ultrasound is attenuated by air, so the higher the void content the higher the attenuation should be. However, Judd et al (1978) state that the level of attenuation will also be influenced by: (a) the state of cure of the resin, (b) the fibre volume fraction, (c) the condition of the fibre matrix interface, (d) delaminations and (e) foreign inclusions. It must be assumed that the effects due to (a) - (c) above are negligible compared to the effect of the voids, and that areas of delamination and foreign inclusions can be differentiated from variations in void content.

The reason that the ultrasonic C-scan is useful as a quality screening method is that reductions in (a) interlaminar shear strength, (b) shear strength, (c) longitudinal and transverse flexural strength, (d) longitudinal and transverse tensile strength and modulus, (e) compression strength and modulus, (f) fatigue resistance and (g) high temperature properties occur as the void content (and hence attenuation level) increases (Judd et al, 1978). For example, a decrease in interlaminar shear strength of 7% for every 1% of voids (up to a total void content of 4%) was reported by Judd et al (1978). However an increase in resistance to impact damage has been reported as the void content increases (Judd et al, 1978).

Only one laminate (laminate number 1) was identified by the C-scan results as being defective (attenuation levels of 12 to greater than 50 dB being recorded, compared to 9 dB for the reference material). The decision to reject the laminate was subsequently supported by the low interlaminar shear strength (approximately 50% of the value achieved for other laminates of the same lay-up and thickness). Other laminates had slightly higher attenuation levels than were recorded for the reference material, but were not high enough to warrant rejection based on the results of the ultrasonic C-scans alone. The results suggested that in general the void content was slightly higher in the material processed for this work than in the reference laminates.

Separate measurements of the void content of samples from five laminates were made. The void content of the laminates tested lay between 2 and 3% (see table 4.3). Judd et al (1978) suggest that the accuracy of the density measurement method, which was used for these measurements, is ±0.5%. This level of voids is slightly higher than the level of 1%

which is usually aimed for. From the same experiments the volume fraction of fibre and matrix was also determined. The values of between 62.2 and 62.8% for the fibres in the ±45, 0/90 and QI materials are reasonable, since the nominal fibre volume fraction of the prepreg was 60% and some matrix is inevitably lost during processing. The fibre volume fraction of 64.8% for the unidirectional material is somewhat higher, suggesting that more flow took place during processing for this lay-up. This would perhaps be expected since the fibres all lie in a single direction and could channel the matrix to the edges of the material.

In order to check the processing method, ILSS tests on unidirectional material were undertaken to allow comparison with the material manufacturer's data. The ILSS was found to be between 10 and 14% lower than the value of 120 MPa quoted by the manufacturer for this material (Anon, 1988 (a)). Based on the results reported by Judd et al (1978) a difference in void content of 2% between the material tested by Ciba-Geigy and the material tested for this work would explain this difference in ILSS. If it is assumed that the void content of the material processed by Ciba-Geigy was 1%, then a void content of 3% would explain the difference completely. Since the void content of the material used for this work was between 2 and 3% it would appear unlikely that differences in void content are entirely to blame. Another contributing factor could be that the ILSS value quoted by Ciba-Geigy relates to a material with a fibre volume fraction of 60% (Anon, 1988 (a)). Decreases in the matrix volume fraction would be expected to lead to decreases in ILSS. The matrix volume fraction of the unidirectional material processed in this work was 33.2%, compared to an assumed value of 39% for the Ciba-Geigy material (assuming volume fractions of 60% fibres, 39% matrix and 1% voids). It seems probable that both higher void content and a lower matrix volume fraction contributed to the differences in ILSS. For the multidirectional material, used for the main testing programme, the matrix volume fractions are slightly higher. Loss of strength due to lack of matrix should therefore be lower but the effect of slightly higher void content may still affect the ILSS.

It would appear that the processing method used in this work was adequate even though the void contents were slightly higher than the ideal. The use of ILSS tests to assess the quality of the processed material are considered to be useful because they are sensitive to variations in void content which is a good indicator of the adequacy of the processing method.

The ILSS tests on the unidirectional material were performed to assess the quality of the material in comparison with the manufacturer's data. ILSS tests on the rest of the material

were performed to assess the consistency of the processing method. For the ±45 and 0/90 materials the differences between the measured ILSS's were small. The statistical test showed that the differences were not significant. However in the case of the QI laminates the statistical test showed that the differences were significant. Several laminates (2, 3, 4 and 35) had noticeably lower ILSS's than the rest. The low ILSS of laminates 2, 3 and 4 is almost certainly caused by a low matrix volume fraction. As was reported in chapter 3 a slightly different lay-up was used in the pressclave for laminates 1 to 5 inclusive. The breather material is thought to have bled resin out of the laminate during processing. This would leave the material slightly 'dry' leading to a reduction in ILSS. At the time this was not identified as a problem and the processing method was changed because of the poor surface finish which was being obtained. The texture of the breather material was responsible for this. The reason for the slightly lower ILSS of laminate number 35 is not known.

The results of the ILSS testing have indicated that the material from laminates 2, 3, 4 and 35 may be of slightly inferior quality. The analysis of the impact and compression tests will be analysed with this in mind.

4.5.2 Other Materials

ILSS's were measured for the three APC laminates and the CE laminate. The results for the APC material indicated that the processing method was consistent. However no data was available against which the absolute value could be checked.

It is tempting to compare the different materials by looking at their ILSS's, however this can be misleading. For example Leach (1989) quotes an ILSS of 110 MPa for a 'typical current carbon / epoxy system' and value of 105 MPa for APC-2. In the same table an interlaminar fracture toughness of 0.22 KJ / m^2 is given for the epoxy system compared to 2.1 - 2.7 KJ / m^2 given for the APC-2. The problem is that true interlaminar failure is hard to achieve during the ILSS test, particularly for the thermoplastic material which tends to deform plastically.

±45

Group Mid-Point (MPa)	Range (MPa)	Frequency
40.40	38.19 - 42.61	1
44.82	42.61 - 47.03	3
49.24	47.03 - 51.45	10
53.66	51.45 - 55.87	16
58.08	55.87 - 60.29	14
62.50	60.29 - 64.71	4

0/90

Group Mid-Point (MPa)	Range (MPa)	Frequency
79.00	76.88 - 81.12	1
83.23	81.12 - 85.35	0
87.47	85.35 - 89.58	4
91.70	89.58 - 93.81	6
95.95	93.81 - 98.04	16
100.17	98.04 - 102.27	7
104.40	102.27 - 106.50	1

QI

Group Mid-Point (MPa)	Range (MPa)	Frequency
55.00	52.41 - 57.59	1
60.19	57.59 - 62.78	1
65.37	62.78 - 69.97	3
70.56	69.97 - 73.15	7
75.74	73.15 - 78.34	14
80.93	78.34 - 83.52	14
86.12	83.52 - 88.71	13
91.30	88.71 - 93.90	3

Uni-directional

Group Mid-Point (MPa)	Range (MPa)	Frequency
98.00	96.69 - 99.31	1
100.62	99.31 - 101.92	5
103.23	101.92 - 104.54	9
105.85	104.54 - 107.16	8
108.46	107.16 - 109.77	5
111.08	109.77 - 112.39	4
113.70	112.39 - 115.00	2

Table 4.1 Frequency distribution data for ILSS tests on TCE, 16 ply material.

		Post-Cure		
Laminate No		None	180 °C x 2 Hours	210 °C x 4 Hours
17	Av	103.7 MPa	105.2 MPa	-
	SD	2.3 MPa	5.1 MPa	-
	Cv	2.2%	4.9%	-
18	Av	105.9 MPa	108.0 MPa	103.1 MPa
	SD	5.2 MPa	3.7 MPa	4.4 MPa
	Cv	4.9%	3.4%	4.2%
19	Av	-	-	107.7 MPa
	SD	-	-	3.3 MPa
	Cv	-	-	3.1%
36	Av	106.5 MPa	-	-
	SD	2.2 MPa	-	-
	Cv	2.1%	-	-

Table 4.2 Average ILSS results for TCE-0-16 material.

Laminate Number	Layup	V_f (%)	V_v (%)	V_m (%)
7	±45	62.2	2.8	35.0
15	0/90	61.5	2.5	36.0
18	0	64.8	2.0	33.2
32	QI	62.5	2.4	35.1
35	QI	62.8	3.0	34.2

V_f = volume fraction of fibres
V_v = volume fraction of voids
V_m = volume fraction of matrix

Table 4.3 Results of volume fraction measurements

Fig 4.1 (a) Average ILSS for TCE-±45-16 material.

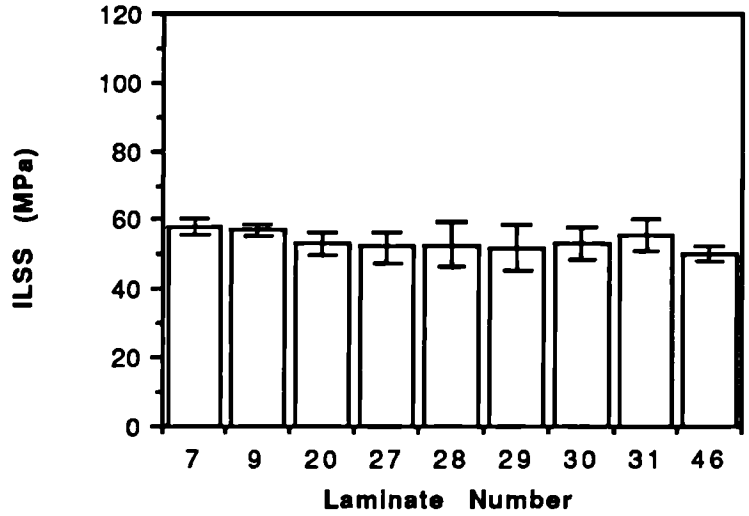

Fig 4.1 (b) Average ILSS for TCE-0/90-16 material.

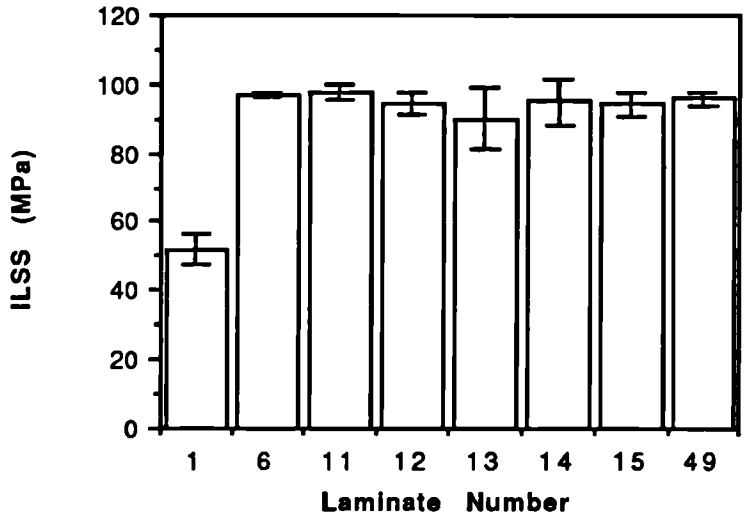

Fig 4.1 (c) Average ILSS for TCE-QI-16, 24 and 32 material.

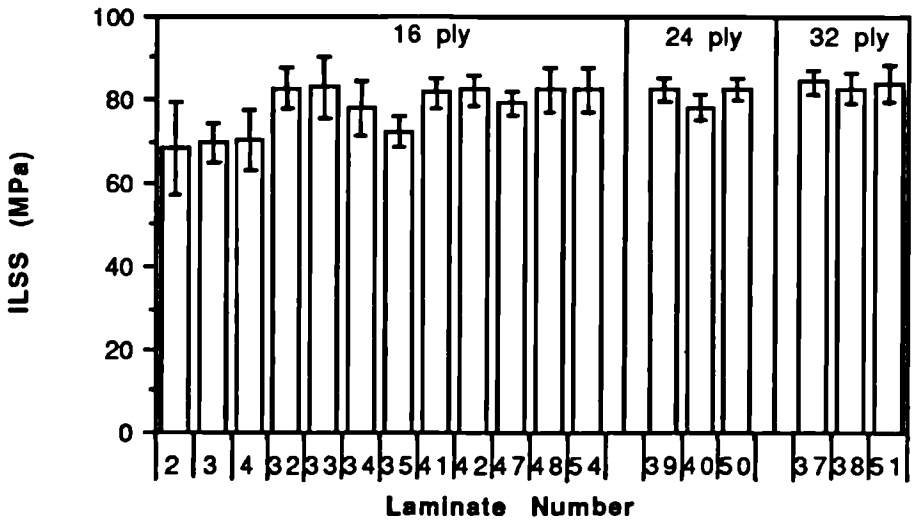

Fig 4.2(a) Frequency distribution for ILSS tests on TCE-±45-16 material.

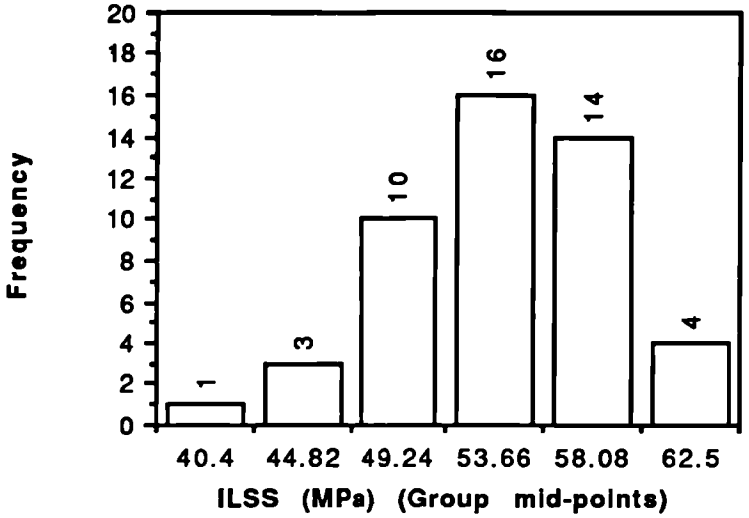

Fig 4.2(b) Frequency distribution for ILSS tests on TCE-0/90-16 material.

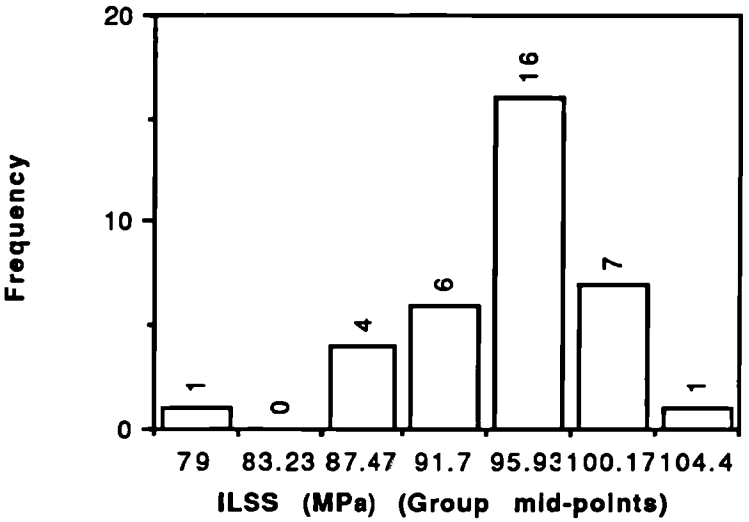

Fig 4.2(c) Frequency distribution for ILSS tests on TCE-QI-16 material.

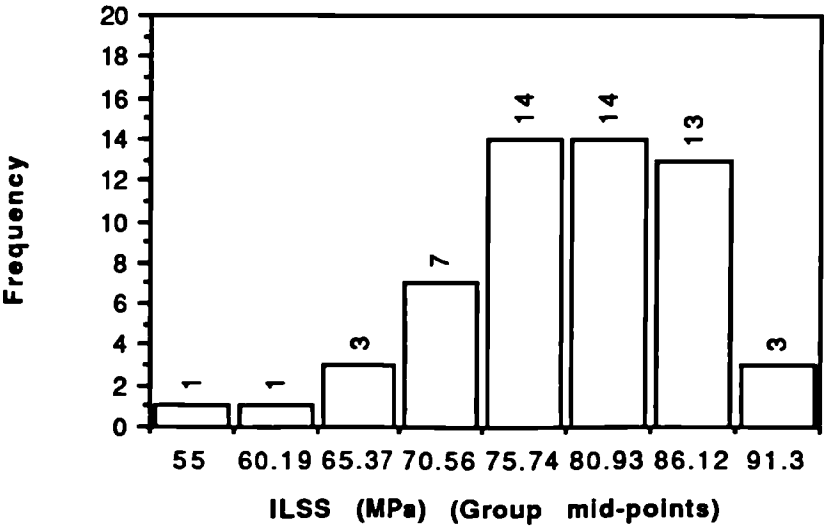

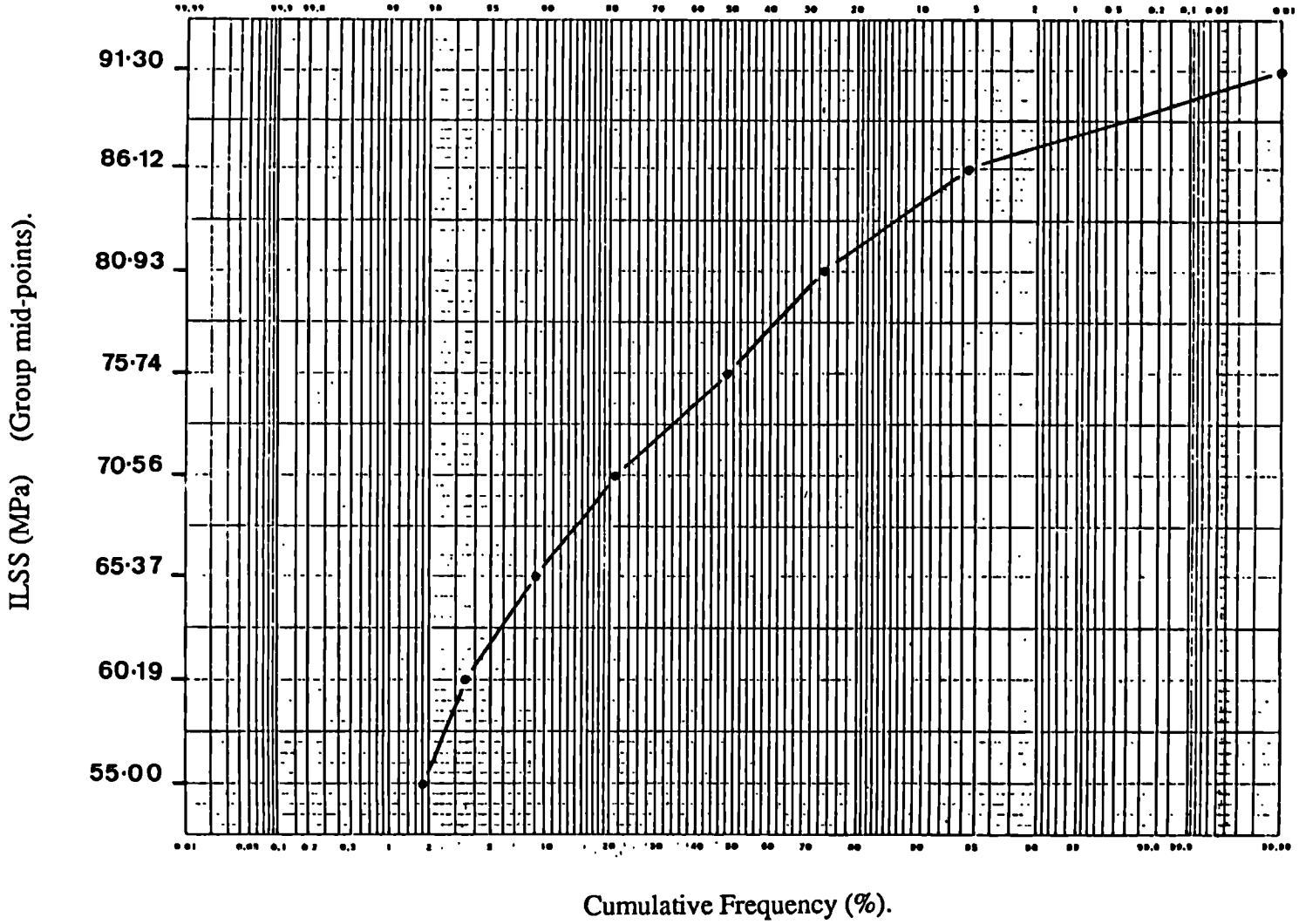

Fig 4.3 Cumulative frequency plot on normal probability scale for the TCE-QI-16 material ILSS results.

Fig 4.4 Frequency distribution for ILSS tests on TCE-0-16 material.

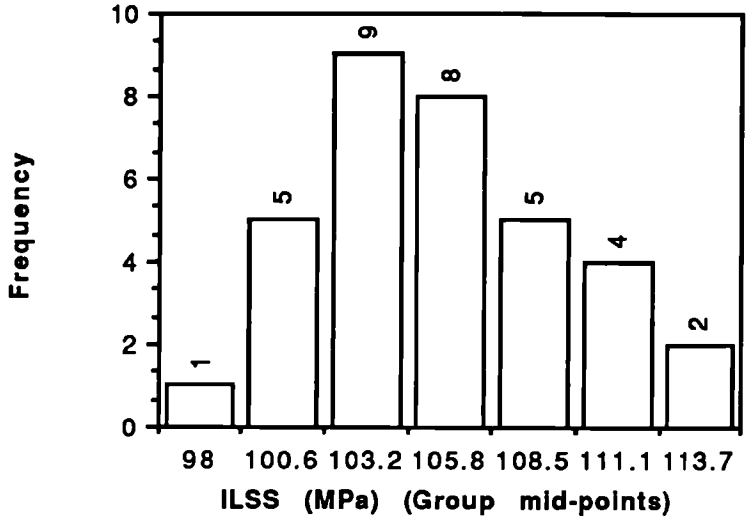

5 Impact Testing and Assessment of Damage

5.1 Introduction

In this chapter the results of impact tests and subsequent assessment of damage will be presented and discussed. Except for those which were sectioned for microscopy the results relate to specimens which were subsequently tested in compression. The results of all of the impact tests are tabulated in appendix B.

5.2 Instrumented Impact Testing

5.2.1 Interpretation of Instrumented Impact Tests

In this section examples of the results of individual impact tests will be shown for the TCE-0/90-16 material. The data for the TCE-QI-16 material will then be presented to show how the results of a number of individual tests are combined.

Figs 5.1 (a) - (d) show the results from an impact test on the TCE-0/90-16 material. The load drop at F1 indicates that damage was initiated in the material. Ultrasonic C-scans of carbon reinforced material and optical inspection of glass reinforced material, revealed that delamination damage was associated with this load peak for all of the materials tested. The other curves reveal that the impacter rebounded from the specimen. Between times t_0 and t_3 the striker velocity is decreasing while the displacement and absorbed energy are increasing. The kinetic energy of the striker is being dissipated, some of the energy is stored by elastic bending of the specimen, while the remainder is consumed by the initiation and propagation of damage, or by friction between the specimen and the support / clamping device. At t_2 the maximum force (F2) is reached. The force has already decreased before the velocity is zero and the displacement and absorbed energy are at a maximum (t_3). Between t_3 and t_4 the stored elastic energy in the specimen is returned to the striker causing it to rebound. At t_4 the force has fallen to zero and the striker is no longer in contact with the specimen. Further calculation of velocity, displacement and time are therefore meaningless and the curves have not been continued beyond t_4. Fig 5.1 (c) shows that there was still a small displacement when contact between the the striker and the specimen was broken. At the incident impact energies used in this work the impacter always rebounded from the specimen and the shape of the curves in figs 5.1 (b) - (d) are similar to those for all the other tests.

Several variations of the force-time curves were observed over the range of incident impact energies used. These are shown in figs 5.1 (e) - (g). In fig 5.1 (e) the smooth curve indicates that no damage was initiated in the material and the tup simply rebounded from the specimen. In this case the first force peak (F1) and the maximum force (F2) coincide. In fig 5.1 (f) the load drop at F1 again corresponds to the initiation of delamination damage, but now damage has initiated at the maximum force. In this case the velocity of the striker is not close to zero at the maximum force. Instead the velocity is zero and the displacement and absorbed energy reach a maximum close to the load peak marked A. Most of the energy has been dissipated during the damage initiation process, consequently the force only increases again slightly. As the incident energy is increased the size of the load peak A increases as there is more energy available to drive the striker into the material. The curve shown in fig 5.1 (g) is essentially the same as 5.1 (a), except the additional load peak marked B indicates the initiation of secondary damage in the form of fibre spalling on the back face of the specimen (the side opposite to the contact surface).

While the results of individual tests provide information about the impact event, the results of a number of tests over a range of incident impact energies are more useful for assessing the performance of a material. The results are usually plotted as a function of incident impact energy. Of particular interest in this work are the forces and absorbed energies at the force peaks (F1 and F2) and the total amount of energy absorbed during the test (at t_3).

Fig 5.2 shows these parameters plotted as a function of incident impact energy. Figs 5.2 (a) and (b) show that the first peak force (F1) and absorbed energy (AE1) initially increase with increasing incident impact energy and then become relatively constant, this occurs when the incident impact energy is high enough to initiate damage. The graphs show that the force and energy required to initiate damage appear to be independent of incident impact energy. An estimate of the 'damage initiation energy' can be obtained if the absorbed energies at damage initiation are averaged over a number of tests. The assumption is that damage would just be initiated if the incident impact energy was just equal to the 'damage initiation energy'. This damage initiation energy is a useful parameter for assessing the effect of materials variations. The average forces and absorbed energies at damage initiation for all of the materials tested are shown in table 5.1. These values have been calculated from the data tabulated in appendix B by taking the average value of F1 and AE1 for all specimens where damage was initiated.

Fig 5.2 (a) shows that the force F2 increases with increasing incident impact energy. A change of slope in the curve is observed when damage initiation occurs. The stiffness of the specimen is reduced (due to damage in the material) resulting in lower peak forces than would have otherwise occurred. Fig 5.2 (b) shows that in general at F2 the absorbed energy is equal to the incident energy (the diagonal line indicates complete energy absorption). This occurs because the striker has almost been bought to rest when the maximum force has been reached. The exception to this is when the force - time curve is of the type shown in fig 5. 1 (f). The trend for the peak force and associated absorbed energy to increase will continue until full penetration of the specimen occurs; the maximum force and absorbed energy should then become constant.

The total absorbed energy is usually plotted against incident impact energy in the same way as was done for AE1 and AE2 above. Fig 5.2 (c) shows that the amount of absorbed energy increases with incident impact energy. This trend should continue until full penetration occurs, when the total absorbed energy should become constant. Another way of plotting this data is to normalise the total absorbed energy with respect to the incident impact energy. The data from fig 5.2 (c) is plotted in this way in fig 5.2 (d). This type of plot has been found to show the differences between the performance of different materials more clearly.

For reasons which will be discussed later the absorbed energy at damage initiation and the total absorbed energy will be used to assess the effect of different variables, although other parameters will be used where appropriate.

5.2.2 Effect of Specimen Width

One of the objectives of the impact test arrangement was to induce the same type and extent of damage into specimens of different width prior to compression testing. One way of checking that this was achieved is to compare the results of instrumented tests. Figs 5.3 (a) - (e) show all of the impact data for different specimen widths from tests on TCE-QI-16 material. These results suggest that variations in specimen width did not have a large effect on the measured parameters. Similar results were obtained for the ±45 and 0/90 lay-ups. On closer inspection it is evident that the force at damage initiation for the TCE-QI-16-45 specimens is lower than for the 55 and 75 mm wide specimens (see table 5.1). However the absorbed energy is the same for all three specimen widths. Fig 5.4 shows the average absorbed energies at damage initiation for each lay-up and width. Small differences between the absorbed energies at damage initiation for different specimen

widths are evident. However there does not appear to be a systematic effect of width and the small differences are attributed to scatter, inherent in these materials.

5.2.3 Effect of Clamping

A small number of tests were performed to investigate the effect of clamping the specimens during impact. Fig 5.5 shows the force and absorbed energy at damage initiation, and total absorbed energy plotted against incident impact energy. A small difference in the absorbed energy at damage initiation was apparent (fig 5.5 (b)), the unclamped specimens absorbing slightly more energy. This had no effect on the force at damage initiation (fig 5.5 (a)) or the total absorbed energy (fig 5.5 (c)). Large differences in the results were not observed for the other measured parameters.

5.2.4 Effect of Lay-up

The results showing the effect of lay-up on the average absorbed energy at damage initiation have already been plotted in fig 5.4. The results show that the absorbed energies at damage initiation are similar for the ±45 and 0/90 materials. This was expected because the impact support conditions are essentially symmetric and testing a ±45 laminate should be equivalent to testing a 0/90 laminate which has been rotated through 45 degrees. In comparison the QI material absorbs approximately half as much energy at damage initiation.

The situation is slightly different when the total absorbed energies are compared. As before a general increase in the total absorbed energy with incident impact energy is evident for all three lay-ups (fig 5.6 (a)). When the normalised total absorbed energies are compared there is a clear difference between the response of the 0/90 and ±45 laminates (figs 5.6 (b) and (c)). The data for all three lay-ups has been plotted in fig 5.5 (d). The ±45 and QI materials are seen to perform in a similar manner. This difference between the performance of the ±45 and 0/90 laminates was not expected for the reason given above. These results demonstrate the value of normalising the absorbed energy data. Differences in the behaviour are immediately apparent in fig 5.6 (d) where they were not in fig 5.6 (a).

In addition tests were also carried out on two QI materials with slightly different lay-ups, only the fibre sequence was changed. One material had a $[-45, 0, +45, 90]_{2s}$ lay-up (QI) while the other had a $[-45, 90, +45, 0]_{2s}$ lay-up (QI*). The change in fibre sequence is equivalent to an in-plane rotation through 90 degrees in this case and, again because of the symmetry of the impact test conditions, the stacking sequence should not make any

difference. This is confirmed by the results shown in fig 5.7 (a) - (c). The average force and absorbed energy at damage initiation for the QI and QI* materials were very similar (see table 5.1).

5.2.5 Effect of Thickness

Fig 5.8 shows the forces and absorbed energies at F1 plotted as a function of incident impact energy for each thickness. The horizontal lines represent the average forces and energies at damage initiation. These average values are plotted as a function of thickness in fig 5.9. The results show that a linear relationship appears to exist between both force and absorbed energy, at damage initiation and thickness, over the range of thicknesses tested.

The effect of thickness on the total absorbed energy is shown in figs 5.10 (a) and (b) for the QI(24) and QI(32) materials (the results for the 16 ply material have already been plotted in fig 5.3 (e)). The trends for the three thicknesses are shown together in fig 5.10 (c). (The individual data points have not been plotted for clarity). The trend appears to be similar for each thickness. An initial peak is followed by a fall in the proportion of the incident energy which is absorbed. In the case of the 16 ply material this increases again at approximately 9 J.

5.2.6 Effect of Material

Figs 5.11 (a) and (b) show the forces and absorbed energies at damage initiation, plotted against incident impact energy for the four materials tested. Again the horizontal lines correspond to the average values of force and absorbed energy at damage initiation for each material. In fig 5.12 the average absorbed energies at damage initiation are plotted. It is apparent from these graphs that the forces and absorbed energies at damage initiation are very similar for all the materials with epoxy matrices, irrespective of fibre type, and that the average initiation energy for APC is considerably higher than for the epoxy based materials. It is also apparent that the scatter in the data is much greater for APC. This increase in scatter may be attributed to the fact that the load drop at damage initiation is less well defined on the force-time curves for APC than for the epoxy based materials; the thermoplastic matrix of the APC being less brittle than the thermosetting epoxy materials. For the APC material there is some indication that the absorbed energy at damage initiation is decreasing as the incident impact energy increases (although the same trend is not observed for the force). If this was the case the calculation of an average absorbed energy at damage initiation, over a range of incident impact energies, would obviously cease to be

meaningful. In the absence of more conclusive results the apparent trend has been attributed to scatter in the data.

The normalised total absorbed energies are plotted against incident impact energy for APC, CE and GRP materials in figs 5.13 (a), (b) and (c) respectively. The results for the TCE material have already been shown in fig 5.3 (e). Similar trends are shown by the APC, CE and GRP materials - an initial increase in absorbed energy followed by a second linear portion of lower slope. There are two points on the GRP curve lying well away from the main trend. A dotted line has been drawn through these points to indicate that there are possibly two different lines corresponding to two different failure processes: the shape of the curve with the dotted line bearing a close resemblance to the curve for the TCE material (fig 5.3 (e)).

Fig 5.13 (d) shows the curves for the four materials plotted together. The difference between the two curves for APC and GRP is clear - at any given incident energy the GRP absorbs more energy up to approximately 14 J where the two curves are converging. The GRP, TCE and CE materials behave in a similar manner at very low incident energies (up to approximately 1 J) and appear to be converging at approximately 14 J. The behaviour between 1 and 14 J is different.

5.2.7 Calculation of the Constant n' used in Equation 1.3 and Plate Stiffness (K_p)

Static indentation tests were carried out on all of the materials. The table below shows the results obtained. The average of three tests was taken for each material.

Material	n' ($N/m^{3/2}$)
TCE-0/90 and ±45-16	0.75×10^9
TCE-QI-16	0.63×10^9
TCE-QI-24	0.64×10^9
TCE-QI-32	0.61×10^9
GRP-QI-16	0.71×10^9
CE-QI-16	0.86×10^9
APC-QI-16	0.74×10^9

The values of K_p are shown in table 5.2. The calculations to find the corrected value of K_p are also summarised in the table.

5.3 Detection and Assessment of Impact Damage

5.3.1 Non-Destructive Techniques

5.3.1.1 Damage Detection and Presentation of Results

Some examples of ultrasonic C-scan results for the GRP-0/90-16-55 material are shown in fig 5.14. The in-plane extent of delamination damage is clearly shown by the area of higher attenuation (shown in blue). Fig 5.15 shows photographs of the same specimens - the same areas of delamination are revealed, except that now it is clear that there is a through thickness distribution of damage which was not detected by the C-scan.

It is common practice to plot the in-plane damage area as a function of incident impact energy. This has been done for the GRP-QI-16-55 material and the results are shown in fig 5.16 (a). The arrow on the energy axis represents the damage initiation energy previously measured from the instrumented impact tests (see table 5.1). After damage initiation the damage area increases rapidly before becoming relatively constant. The constant value is equivalent to that of a 40 mm diameter circle. This area (approximately 1256 mm^2) is indicated by a horizontal line on the graph. The damage area does not increase further with increasing incident impact energy. However the total absorbed energy does increase (fig 5.16 (b)) indicating that the total amount of damage in the material is increasing. Since the damage is not extending laterally it is assumed that damage is being initiated at more interfaces within the material.

The usefulness of measuring the damage area was questioned during the course of this work and instead the maximum damage width (measured parallel to the specimen ends) was chosen as the damage parameter. This is simpler to measure and, as will be seen later, the choice can be justified when addressing the problem of post-impact compression strength. The damage width, measured from the ultrasonic C-scan for carbon reinforced materials and photographs for the glass reinforced material, will be used in the rest of this section to investigate the effect of the various parameters changed during the impact tests.

5.3.1.2 Effect of Specimen Width

The results of instrumented impact tests suggested that there was no effect of specimen width on the amount of damage induced. Fig 5.17 shows the damaged areas traced from ultrasonic C-scan plots for the TCE-QI-16 45, 55 and 75 mm wide specimens. Analysis of the original C-scans showed that the damage was contained within the area of the 40

mm diameter support ring for the 55 and 75 mm wide specimens. However for the 45 mm specimens the damage spread to the edge of the specimens for incident impact energies above 5.68 J. However the damage did not spread far outside the 40 mm diameter area for the 0/90 and ±45 specimens of all widths.

Fig 5.18 (a) shows damage width plotted against incident impact energy for each specimen width for the TCE-QI-16 material. Apart from the 45 mm specimens already mentioned the extent of damage appears to be independent of specimen width. The results for the 0/90 and ±45 specimens are shown in figs 5.18 (b) and (c) respectively. For these two lay-ups there does not appear to be any effect of specimen width on the extent of damage observed.

5.3.1.3 Effect of Clamping

A small difference between the lateral extent of damage was observed when impact tests were carried out on clamped and unclamped specimens. Fig 5.19 shows that for low incident energies the damage width was slightly less for the un-clamped specimens. This was the expected result, the clamped specimens are subjected to more severe stresses than the unclamped specimens.

5.3.1.4 Effect of Lay-up

Large differences in damage width were not observed for the different lay-ups tested. Fig 5.20 (a) shows the results for the TCE-QI, 0/90 and ±45-16-55 materials. As expected changes in the stacking sequence of the QI material were also found to have little effect (fig 5.20 (b)).

5.3.1.5 Effect of Thickness

The effect of specimen thickness on damage width is shown in fig 5.21. Again the trend is the same for all three thicknesses. The damage width increases to approximately 40 mm where it becomes constant. The effect of specimen thickness is to shift the curves to the right in fig 5.21 because damage initiates at higher energies for thicker specimens.

5.3.1.6 Effect of Material

The results of instrumented impact tests have already shown that the damage initiation energy is similar for the three epoxy based materials, irrespective of the specific resin, or the type of fibre used. The similarity between the response of these materials is again apparent when the damage widths are compared (fig 5.22). A clear difference between the behaviour of the epoxy based materials and the APC was observed. For a given incident impact energy the damage width is smaller for the APC than for the epoxy based materials. However, if the incident impact energy were to be further increased the damage width would be expected to reach 40 mm and the curves for all of the materials would join.

The results in fig 5.22 show that the scatter in the APC data is greater than for the epoxy based materials. This was also seen in the results of the instrumented impact tests and is apparent in the results of other workers. See for example Bishop (1985) where damage area was plotted against incident impact energy.

5.3.2 Microscopy

5.3.2.1 Specimens Examined

Fourteen 60 mm square specimens were sectioned, polished and examined under an optical microscope. The following table gives details of the materials and impact energies used:

Specimen Number	Material	Lay-up	Thickness(Ply)	Incident Impact Energy (J)
49/3	TCE	0/90	16	1.78
49/5	TCE	0/90	16	5.01
49/7	TCE	0/90	16	11.99
48/2	TCE	QI	16	1.50
48/4	TCE	QI	16	3.99
48/7	TCE	QI	16	10.01
50/6	TCE	QI	24	2.98
50/7	TCE	QI	24	5.06
50/9	TCE	QI	24	11.96
51/7	TCE	QI	32	5.97
51/8	TCE	QI	32	11.96
53/2	APC	QI	16	4.00
53/3	APC	QI	16	8.97
53/4	APC	QI	16	15.14

The incident impact energies were chosen to reveal the through thickness distribution when:

(a) Damage had just been initiated

(b) The damage width first reached approximately 40 mm

(c) The maximum incident energy for that material was used

5.3.2.2 Presentation of Results and General Comments

The specimens were photographed in small sections and a montage was made to show the whole specimen. An example of one of the montages (which has been re-photographed and reduced in size) is shown in fig 5.23. The position and extent of damage was scaled from the photographs and transferred onto a schematic drawing of the specimen (see fig 5.25). Delaminations and shear cracks are shown on the drawings. Small amounts of

local deformation on the impacted surface and fibre spalling (on the 'back face' of the specimens) has not been shown.

A further diagram (see fig 5.26) was constructed to show the through thickness position of delamination damage. Lines with arrow heads have been used to represent 'major' delaminations ('major' being defined as any delamination further than 5 mm from the impact centre) while lines without arrows represent 'minor' delaminations (within 5 mm of the impact centre). In addition the lines have been joined at their bases to indicate where shear cracks join delaminations in different interfaces.

The polishing technique was found to be satisfactory for the material with the epoxy matrix. Delaminations and shear cracks showed up clearly. A good correlation between the extent of damage measured from the sectioned material and the ultrasonic C-scan was found. In contrast the damage was much more difficult to see in the APC material. The delaminations did not open up in the more ductile thermoplastic matrix material. Even simple correlation between the lateral extent of delamination, seen in the sectioned specimens and the ultrasonic C-scan results, was not possible. Consequently it was not possible to construct the diagrams showing the extent and through thickness distribution of the damage.

5.3.2.3 Effect of Lay-up

Only QI and 0/90 specimens were sectioned (it had been assumed that the damage for a ±45 specimen would be identical to that for the 0/90 material, since a square specimen and symmetrical support / impacter were used). The results for these two lay-ups are shown in figs 5.25 (a) - (c) and 5.25 (d) - (f) for the 0/90 and QI materials respectively. Looking first at the schematic diagrams of the damage, similar trends can be seen for both lay-ups; the lateral extent of damage is increasing as the incident impact energy increases, confirming the trends observed from the ultrasonic C-scans. Looking at the numbers of the delaminated interfaces (fig 5.26 (c)) it can be seen that the total number of delaminated interfaces is lowest for the intermediate impact energy for each lay-up. The number of 'major' delaminations remains surprisingly constant, apparently unaffected by the energy level. In each lay-up (fig 5.25) a higher density of 'minor' delamination damage and shear cracks are observed in the area close to the impact centre for the highest energy levels.

If the positions of delaminations and shear cracks are compared for different energy levels some patterns emerge for both materials. In both cases delaminations do not appear at the neutral axis where the highest shear stresses may have been expected. One of the reasons

for this is simply that the two plies either side of the neutral axis are oriented in the same direction and have effectively combined to form one homogeneous ply as is shown in fig 5.24. Further patterns can be seen in the damage distribution, particularly for the 0/90 material where pairs of delaminations joined by shear cracks appear in the same positions at different impact energies (fig 5.25 (a) - (c)).

5.3.2.4 Effect of Thickness

The results for the 24 ply material are shown in figs 5.25 (g) - (i) and 5.26 (c) and for the 32 ply material in figs 5.25 (j) - (k) and 5.26 (d). Looking first at the results for the 24 ply material it can be seen that the number of delaminated interfaces again falls as incident impact energy is increased from 2.98 to 5.06 J and again the number of 'major' delaminations remains fairly constant. The effect cannot be assessed for the 32 ply material because only two specimens were tested.

There is some indication that for the 24 and 32 ply materials the 'major' delaminations appear to be associated with the interfaces between +45 degree and 0 or 90 plies in the top half of the laminate and with -45 degree plies in the bottom half of the laminate.

Although only a few specimens have been tested, the general indications are that patterns of damage appear to be similar for the three thicknesses of material investigated.

5.3.2.5 Effect of Material

For the reason stated above it is not possible to assess the extent and distribution of damage for the APC material. However differences between the damage state of the APC and TCE materials were apparent. The APC material showed evidence of plastic deformation in the form of local denting on the impact surface and the formation of a dome visible on the un-impacted surface. This can be clearly seen in fig 5.27 which shows the specimen impacted at 14.62 J. This type of damage was not seen for the TCE material where the damage would be best described as barely visible, except for at the highest energy levels where fibre spalling occurred on the back-face.

5.4 Discussion

5.4.1 Introduction

This section has been divided into four parts. In section 5.4.2 the accuracy of the instrumented impact data is assessed. Some points relating to the choice of impact test conditions suitable for PICS tests are examined in section 5.4.3. In the final two sections the effect of specimen variables on the initiation (section 5.4.4) and final damage state (section 5.4.5) are discussed.

5.4.2 Accuracy of Instrumented Impact Test Data

The loadcell of the impact machine used for this work was calibrated statically. This means that the forces measured during an impact test are not absolute because dynamic effects have not be accounted for. These dynamic effects occur because components in the load measuring system (for example the adhesive used to bond the strain gauges onto the loadcell or the response of the transient recorder) may be sensitive to the rate at which load is applied. The effect of loading rate is generally assumed to be constant (but not necessarily small) and therefore the data can be used to compare the response of different materials.

Accepting that the measured forces are not absolute, the next problem is to assess how repeatable the measurements are. In practice this is difficult because measuring errors and scatter in the data due to specimen / material variability are difficult (if not impossible) to separate. The total scatter for the materials tested can be assessed by looking at the coefficient of variation (C_V) for the measured forces at damage initiation. The C_V varies between 0.8 and 8.4% over the whole range of materials tested (see table 5.1). Since coefficients of variation of up to 10% are not unusual for these types of material for quasi-static tests it would seem probable that most of the scatter can probably be attributed to inherent material variability (particularly since a failure point is being measured) and that the contribution from measuring errors is small.

Once the force has been measured equations 1.6, 1.7 and 1.8 can be used to estimate the velocity, displacement and absorbed energy respectively, provided that the velocity of the striker at the moment of impact is known. Since there are now two measured parameters (force and the velocity at the time of impact) the errors would be expected to be higher for the derived data than they were for the raw data. This can be seen in the data shown in table 5.1. For the absorbed energy the coefficient of variation varies between 8.0 and

18.5% (where five or more results were available). However the measurement of the force and velocity are not the only sources of error. In order for the velocity, displacement and absorbed energy to be calculated the force-time data must be integrated. The raw data is usually down loaded to a computer and the integration performed numerically (for example by using Simpsons rule). The accuracy of the integration will depend upon the step size used. Inspection of the results shown in appendix B shows that the errors in measurement and data processing can add up and the situation can occur where at (F2) more energy has been absorbed than was initially supplied to the system.

5.4.3 Choice of Impact Tests Conditions

The main consideration when choosing the impact test conditions for a post-impact compression test is that delamination damage should be the major failure mode, since this is the type of damage which is known to lead to degradation in compression strength. Based on results from the literature (see section 1.2) it would appear that delamination damage is very likely to be created as the result of an impact event, whatever the chosen test conditions. Cantwell (1985) found that for flexible specimens damage initiates by tensile cracking on the lower surface, and is caused by bending induced tensile stresses. For inflexible specimens damage is initiated on the impacted surface by contact induced tensile stresses. In both cases delamination damage is initiated when the tensile cracks penetrate to a weak interfacial region. This means that there is quite a lot of scope when choosing the dimensions of the specimen support and the thickness of the material when defining the impact conditions for a PICS test.

Having said this the chosen impact conditions will have an effect on the absolute results of the PICS test. This is because the incident energy required to initiate damage and the final damage state (both the extent and through thickness distribution of damage) will be dependent upon specimen flexibility. Because residual compression strengths are plotted as a function of incident impact energy the curves would be expected to shift along the energy axis - the direction and amount of shift depending on the exact impact conditions used. This will be discussed further in Chapter 7.

In this work the choice of impact test conditions was limited by the fact that a miniaturised testing geometry was being used. A machine with a 20 mm diameter hemispherical tup and a 40 mm diameter support ring was already available. Initial tests confirmed that delamination damage was initiated at low incident impact energies for this testing geometry and it was therefore adopted. One slight modification was that a clamping plate was added. This was to ensure that specimens of different width sustained the same level

of impact damage when impacted at the same incident energy. The results obtained during the impact tests (for example measurements of force and absorbed energy) and measurements of the lateral extent of damage confirmed that in the main this objective was achieved.

The clamping plate was found to have a small effect on the energy absorbed at damage initiation. For the TCE-QI-16-55 material it was 0.80 J for the clamped condition and 1.01 J for the unclamped condition (see table 5.1). Although this is a small difference in absolute terms it is quite large when calculated as a percentage (20%). The reason that damage initiates at a higher energy in the unclamped specimen is that the specimen is slightly more flexible and can therefore absorb more energy in bending before failure is initiated. The indications are that the total amount of damage is also less for the unclamped specimen. This is supported to some extent by the fact that the lateral extent of damage is less for the unclamped specimen (fig 5.19). Differences in the through thickness distribution of damage were not investigated but are not expected to be large.

5.4.4 Damage Initiation

The load drop at F1 in figs 5.1 (a), (f) and (g) was found to be associated with the initiation of delamination damage. This is a useful result because reductions in residual compression strength would be expected once delamination damage is formed during the impact test.

This delamination damage is thought to have been initiated by bending induced shear stresses which are at a maximum at the neutral axis. The presence of isolated delaminations close to the neutral axis in many of the specimens shown in fig 5.25 supports this hypothesis. Boll et al (1986) reported that crack initiation appeared to result from shear stresses. Sjoblom et al (1988) also reported delamination as the first damage for a carbon epoxy material although reasons for this were not discussed. It is somewhat surprising that delamination damage was initiated first by bending induced shear stresses because the support ring diameter to thickness ratio varied between 10 and 20 (for 4 and 2 mm thick specimens respectively). For simply supported beam specimens a span-to-thickness ratio of 5 is specified (for the short beam shear test) to ensure that shear failure occurs first. Even allowing for the fact that there are differences between a simply supported beam specimen and a ring supported specimen this failure mode would not have been predicted. Because of this the other possible initiation mechanisms will be considered. As was explained in section 1.2, Cantwell (1985) suggests that delamination damage follows after the initiation of tensile cracks either on the impacted surface (due to

contact induced stresses) or on the back face (due to bending induced tensile stresses). These tensile cracks were not observed when the sectioned specimens were examined under the microscope. In addition the damage pattern was slightly different to that shown schematically by Cantwell. In figs 1.2 (a) and (b) the delamination damage is connected by shear cracks and a fracture path can be traced back to the initial tensile crack(s). In the schematic diagrams in fig 5.25 this is not the case, delamination damage can be seen in the material which is not connected back to either surface. The only other possibility is that the delaminations were initiated by internal stress waves. However for low velocity impact events this damage mechanism is not thought to operate (Sjoblom et al, 1988).

The variation of force and absorbed energy at damage initiation with thickness also provides some evidence to help in assessing the initiation mode. The variation of force at damage initiation with thickness is shown in fig 5.9 (a). A linear relationship between force and thickness appears to exist over the range of thicknesses tested. This would appear to support the theory that damage was initiated by bending induced shear stresses. A suitable equation could not be located for a circular plate but for a simply supported beam loaded at the mid-span:

$$F = (4 / 3) \tau w t \qquad \text{Eq 5.1}$$

where: F is the force at damage initiation, τ is the shear strength, w is the specimen width and t is the specimen thickness.

Hence there is a linear relationship between force and thickness, assuming that the shear strength is a constant. However the equation predicts that the curve should pass through the origin which is not the case in fig 5.9 (a). The data has been replotted in fig 5.28 and a curve fitted which does pass through the origin. The equation of the best fit curve is:

$$F = 0.5\, t^{1.9} \qquad \text{Eq 5.2}$$

with the coefficient of correlation, r = 0.998
The force may be considered to be proportional to t squared for convenience.

The equation relating force and maximum tensile stress for a simply supported beam loaded at the mid-span is:

$$F = (2 / 3) \sigma w t^2 / L \qquad \text{Eq 5.3}$$

where σ is the tensile bending strength and L is the support span.

The force is directly proportional to t^2 in both equations which would tend to support the theory that damage was initiated by bending induced tensile failure. In this case an equation is also available for a circular plate (Timoshenko, 1958):

$$F = t^2 \sigma / (1+ \upsilon) (0.485 \log_e (R / t) + 0.52) \quad \text{Eq 5.4}$$

where: R is the radius of the plate and υ is the Poissons ratio.

By assuming a value of $\upsilon = 0.3$, $\sigma = 1$ the value of F was calculated for R = 20 mm and t = 1, 2, 3 and 4 mm. The results are shown below:

t	F
1	0.390
2	1.880
3	4.807
4	10.322

A graph of F against t was plotted and a curve was fitted to this data. The equation of the curve is:

$$F = 0.38\ t^{2.3}$$

and the coefficient of correlation (r) = 0.999.

This gives, for the 20 mm radius support ring and for thicknesses of up to 4 mm, a predicted force which is proportional to thickness raised to the power of 2.3. For materials of the same thickness as the radius of the support ring, the predicted force will again be proportional to thickness squared (since $\log_e 1 = 0$). The difference in the predicted force for plate and beam specimens is therefore found to be quite small.

The trend of absorbed energy with thickness also supports the theory that damage was initiated by bending induced tensile failure. Again for a simply supported beam loaded at the mid-span (Dorey, 1987):

$$\text{Energy} = (1 / 18) \sigma^2 w t L / E \quad \text{for tensile failure} \quad \text{Eq 5.5}$$

and

$$\text{Energy} = (2 / 9) \tau^2 w L / E t \quad \text{for shear failure} \quad \text{Eq 5.6}$$

where: E is the Youngs Modulus

For tensile failure the energy absorbed in bending is proportional to t and for shear failure energy is proportional to 1 / t.

The amount of energy absorbed in bending can be estimated using equation 1.3 which is repeated below:

$$\text{Energy} = (1 / 2)\,(F^2 / K_p) + (2 / 5)\,(F^{5/3} / n'^{2/3})$$

The first term allows the energy absorbed in bending, and the second term the energy absorbed in contact deformation to be estimated, provided that the force at damage initiation is known. The calculations of the energy absorbed in bending for the three thicknesses are summarised in the table below:

Material	t (mm)	F1 (KN)	K_p (N/m)	Energy Absorbed in Bending $F1^2 / 2K_p$ (x 10^6) (J)
TCE-QI-16-55	2	1.82	2.6	0.64
TCE-QI-24-55	3	4.19	7.4	1.19
TCE-QI-32-55	4	6.75	17.3	1.32

The energy absorbed in bending is seen to be increasing, which would indicate that damage was initiated by bending induced tensile failure, since a reduction in the energy absorbed in bending would be expected if damage was initiated by shear. Having said this the energy absorbed in bending does not increase linearly with thickness.

Even though the energy absorbed in bending appears to be leveling off as the thickness increases, the total increases because the energy absorbed by contact deformations increases. This is shown in the table below:

Material	t (mm)	Energy Absorbed in Bending (J)	n' ($N/m^{3/2}$) (x 10^9)	Contact (2 / 5) $F1^{5/3} / n'^{2/3}$ (J)	Calculated Energy (J)	Measured Energy (J)
TCE-QI-16-55	2	0.64	0.63	0.15	0.79	0.80
TCE-QI-24-55	3	1.19	0.64	0.59	1.78	1.94
TCE-QI-32-55	4	1.32	0.61	1.34	2.66	3.14

As the thickness increases the calculated energy is lower than the measured energy. This is somewhat surprising since the values of Kp and n' were found experimentally. The reason for this discrepancy is not known.

Discussion concerning the damage initiation mechanism will be concluded here. Inspection of the damage in the material supports the theory that damage was initiated by bending induced shear stresses, while the trends in the measured force and absorbed energy at damage initiation tend to suggest that damage was initiated by bending induced tensile stresses. On balance the evidence for initiation by bending induced shear stresses appears to be slightly more convincing since it was obtained by direct observation of the damage state in the material, whereas the evidence for the initiation by tensile cracking was obtained by comparing the measured and expected results.

The effect of specimen width, lay-up and material type on the force and absorbed energy at damage initiation will now be discussed:

(a) Lay-up

The bending stiffness and the force and absorbed energy at damage initiation were very similar for the ±45 and 0/90 specimens. This was the expected result because, as was mentioned previously, the only difference between the two materials is the orientation of the fibres with respect to the edges of the specimen. Since the impact conditions are symmetric this was not expected to influence the behaviour significantly. The bending stiffness measured for the QI material was very similar to that measured for the ±45 and 0/90 materials. The alignment of the fibres in the plane of the specimen was not expected to alter the bending stiffness for a plate-like specimen (although significant differences would be expected for beam type specimens).

The only anomaly in the results was that both the bending stiffness and the force at damage initiation for the 45 mm wide QI specimens, were lower than was measured for the 55 and 75 mm wide specimens. In chapter 4 the ILSS of laminates 2, 3 and 4 (from which the 45 mm wide specimens were made, see table B7 in appendix B) was found to be lower in comparison to the rest of the QI material. The reason given for this was that some of the matrix material was bled off during processing leaving the material slightly 'dry'. This would explain both the lower force at damage initiation (due to the low ILSS) and the lower bending stiffness (the lack of resin reducing the ability for load transfer into all of the fibres). It is interesting to note that the absorbed energy at damage initiation for the 45 mm wide specimens was almost identical to that measured for the 55 and 75 mm wide specimens. The reason for this is seen when the energy absorbed in flexure is calculated:

Material Measured	F1 (KN)	K_p (N/m) (x 10^6)	n' ($N/m^{3/2}$) (x 10^9)	Flexure $F1^2 / 2K_p$ (J)	Contact (2 / 5) $F1^{5/3} / n'^{2/3}$ (J)	Calc'd Energy (J)	Energy (J)
TCE-QI-16-45	1.64	1.90	0.63	0.71	0.12	0.83	0.81
TCE-QI-16-55	1.82	2.60	0.63	0.64	0.15	0.79	0.80
TCE-QI-16-75	1.97	2.80	0.63	0.69	0.17	0.86	0.88

For the 45 mm wide specimens an almost identical amount of energy is absorbed in bending as for the 55 and 75 mm wide specimens, even though the force at damage initiation was lower. This is because the bending stiffness was also lower. The fact that the absorbed energies at damage initiation are so similar for the materials with different bending stiffnesses and ILSS's is thought to be coincidental. There is no evidence to suggest that the absorbed energy at damage initiation is a fundamental property for any particular set of impact conditions.

The force required to initiate damage in the QI material was approximately 2/3 of the value measured for the ±45 and 0/90 materials. Higher stresses must have been generated in the QI lay-up causing failure at lower applied forces. However the reason for this was not investigated. Once the failure forces were known it was possible to obtain a good estimate of the energy absorbed in flexural and contact deformations. These are shown in the table below:

Material Measured	F1 (KN)	K_p (N/m) (x 10^6)	n' ($N/m^{3/2}$) (x 10^9)	Flexure $F1^2 / 2K_p$ (J)	Contact (2/5)$F1^{5/3} / n'^{2/3}$ (J)	Calculated Energy (J)	Energy (J)
TCE-±45-16-55	2.66	2.6	0.75	1.36	0.25	1.61	1.63
TCE-0/90-16-55	2.74	2.7	0.75	1.39	0.26	1.65	1.71
TCE-QI-16-55	1.82	2.6	0.63	0.64	0.15	0.79	0.80

Because the stiffness and the value of n' is similar for each lay-up the lower force at damage initiation for the QI material means that less energy is absorbed.

Changes in the stacking sequence of the QI lay-up were not found to affect the plate stiffness or the force and absorbed energy at damage initiation. Again this is because the support and striker used for the impact test were symmetric. A change in stacking

sequence from [-45, 0, +45, 90] to [-45, 90, +45, 0] is equivalent to a 90 degree rotation in the plane of the specimen.

(b) Effect of Material

Only small differences in the force at damage initiation were found between the three epoxy based materials: the force required to initiate damage in the GRP material was the lowest at 1.54 KN, this was followed by the CE material at 1.66 KN and then the TCE material at 1.80 KN. In contrast much higher forces were required to cause failure in the APC material. This is attributed to the much higher mode II fracture toughness of the thermoplastic matrix material. Leach (1989) quotes a value of between 2.1 and 2.7 KJ/m^2 for APC-2 and 0.22 KJ/m^2 for a 'typical current carbon epoxy'.

Again once the forces required to initiate damage have been measured, the differences between the absorbed energies at damage initiation can be explained. The table below shows the calculated energies at damage initiation (from eq 1.3) for the four materials:

Material Measured	F1 (KN)	K_p (N/m) (x 10^6)	n' ($N/m^{3/2}$) (x 10^9)	Flexure $F1^2/2K_p$ (J)	Contact $(2/5)F1^{5/3} / n'^{2/3}$ (J)	Calculated Energy (J)	Energy (J)
TCE-QI-16-55	1.82	2.6	0.63	0.64	0.15	0.79	0.80
CE-QI-16-55	1.66	2.7	0.86	0.51	0.10	0.61	0.64
GRP-QI-16-55	1.54	1.3	0.71	0.91	0.10	1.01	1.05
APC-QI-16-55	3.45	2.9	0.74	2.05	0.39	2.44	2.54

The three carbon fibre reinforced materials all had similar stiffnesses and contact deformation behaviour (i.e. similar values of n'). Because of this the absorbed energy would be expected to increase as the force at damage initiation increased. For the CE, TCE and APC materials this is exactly what happens. The GRP material has the lowest damage initiation force but absorbs more energy than the CE and TCE materials. The reason for this is that the stiffness of the GRP material is much lower and therefore much more energy can be absorbed in flexure before damage is initiated.

5.4.5 Final Damage State

5.4.5.1 Introduction

In this work the final damage state after impact is of considerable interest because this determines the residual strength of the material. From the literature it is known that both the lateral extent and through thickness distribution of damage can effect the residual strength. The destructive and non-destructive techniques used to assess the damage after impact were chosen with this in mind. Unfortunately a simple and effective measure to describe the total amount of impact damage does not exist. The in-plane area of damage is often quoted because it is relatively simple to measure, directly for glass reinforced materials or with an ultrasonic C-scan for carbon fibre reinforced materials. The relevance of such measurements alone is questionable because the through thickness distribution of damage is not considered. Classification of the through thickness distribution of damage is more of a problem. Photographs or schematic diagrams are almost exclusively used to record and display the damage state. The approach taken in this work was to measure both the damage width and the through thickness distribution of damage, to give some indication of the total damage state of the material. In the next section the accuracy of these measurements will be assessed. After some general comments about the impact damage, the effect of specimen thickness and lay-up and material type on the damage state will be assessed. Finally the utility of the instrumented impact data for assessing the final damage state will be discussed.

5.4.5.2 Accuracy of Measurements

The accuracy of the ultrasonic C-scan was checked by scanning impact damaged GRP specimens. The maximum damage width measured from the C-scan was then compared to the direct measurements made with a steel engineer's rule. The GRP specimens were back-lit to make the damage more visible. The rule was divided into 0.5 mm divisions and the accuracy of the measurements is estimated to be ± 0.25 mm. The table below shows the results of the experiment:

Damage Width (mm)	
Ruler	C-Scan
16.5	16.4
19.0	19.7
24.0	23.8
36.5	36.1
39.0	39.3
42.0	42.6
41.5	41.0
43.5	43.4

From these results the accuracy of the ultrasonic C-scan is estimated to be ± 1 mm. This level of accuracy is consistent with the estimates of Preuss et al (1988).

5.4.5.3 General Observations Relating to the Damage State After Impact

For each material the general trend of damage width with incident impact energy was the same. Initially the specimens absorbed the energy in bending and the material remained un-damaged. At a certain incident energy damage was initiated and propagated. Further increases in the incident impact energy lead to increases in damage width until a maximum width of approximately 40 mm was reached. This corresponds to the diameter of the support ring used during the impact test. Damage cannot spread far outside the support ring because bending is inhibited. As was discussed earlie, bending induced shear stresses are thought to be responsible for the initiation and propagation of delamination damage. Once the damage has reached a maximum, the total amount of absorbed energy continues to increase (see for example fig 5.6 (a) and (b)), indicating that the total amount of damage is increasing. In particular the total area of delamination (i.e. the sum of the areas of delamination at each interface) is increasing. This is supported by the results shown in fig 5.25. Because the C-scan cannot differentiate between single and multiple

delaminations this is not evident when the in-plane area is used to assess the damage state. More sophisticated ultrasonic scanning machines have been developed which do give an indication of the through thickness distribution of damage (see for example Preuss et al, 1988). Although the total area of damage is seen to increase it is interesting to note that the total number of delaminated interfaces does not always increase with increasing impact energy (see fig 5.26 (c)). This can be seen for the TCE-0/90, QI-16 and QI-24 materials. This is not a result which would have been expected. Increasing the impact energy would not be expected to suppress delamination at an interface where delamination was previously found. One possible reason for this apparently anomalous result is that the full damage state was not revealed because the specimens were only sectioned through the impact centre in one direction. Other authors (for example Guynn et al, 1985) have reported "peanut" shaped delaminations, so the possibility remains that the damage did not appear because the section was taken through the node of the "peanut" shape. Sectioning at 90 degrees to the chosen direction (but still the through thickness) would possibly have revealed a different damage pattern.

It is also interesting to note that the number of 'major' delaminations (i.e. any delamination extending further than 5 mm from the impact centre) stayed reasonably constant as the incident impact energy was increased (see fig 5.26 (c)). Reference to figs 5.26 (a) and (b) shows that the positions of these delaminations also remains constant. This is of interest because it is these delaminations which would be expected to have the most influence on residual strength. Some patterns in the distribution of delamination can be seen in figs 5.26 (a) and (b). There are plies between which delamination appears to be inhibited. This is most noticeable in the TCE-QI-24 material where there are no delaminations in the 90, -45, 0, +45 sequence of plies in the top half of the laminate closest to the neutral axis. Other authors have reported patterns in the distribution of delamination damage through the thickness, particularly in thicker laminates (see for example Guynn et al, 1985). Further study of these patterns may help in advancing the understanding of the impact behaviour of laminated composites. Because of the limited number of specimens sectioned in this work it is difficult to arrive at any firm conclusions.

A further observation of interest is that the delaminations were never observed at the neutral axis even though this is the position where the interlaminar shear stresses are at a maximum. The reason for this is that the laminates were always symmetric and therefore the two plies at the centre of the laminate were oriented in the same direction. During processing the two plies fuse together, effectively forming a single ply, which is approximately twice as thick as the other plies in the laminate. This can be clearly seen in

the photograph shown in fig 5.24. Since there is no resin rich interlaminar region delamination does not occur at the neutral axis during impact loading.

5.4.5.4 Effect of Specimen Width

In general the impact damage was contained to approximately the area of the support ring. The exception was for the TCE-QI-16-45 material where damage spread to the edge of the specimen for impact energies above approximately 5 J. This is not surprising since the material used to manufacture the 45 mm wide specimens has been shown to be of slightly lower quality. This difference is not particularly evident when the damage widths are compared at low incident energies (see fig 5.18 (a)).

5.4.5.5 Effect of Thickness

For the reasons discussed previously, the energy required to initiate damage increased with thickness over the range of thicknesses studied. It can be seen in fig 5.21 that once initiated, damage width increases at a similar rate for the three different thicknesses. It would appear that the three curves are essentially the same shape, the curves being shifted to the right as thickness increases. As was discussed before, the damage width does not increase above approximately 40 mm.

An observation concerning the through thickness distribution of damage, which is of interest in relation to future analysis of residual strength tests, is that for each thickness 'major' delaminations were found in the interfaces closest to the neutral axis. Analysis by Donaldson (see section 1.5.4) suggests that deeper delaminations lead to larger reductions in strength (once a certain delamination length has been achieved) than shallow delaminations.

5.4.5.6 Effect of Lay-up

The effect of lay-up on the damage width was found to be small (fig 5.20 (a)). For the three different lay-ups the damage initiation energy and the shape of the curves were found to be similar. Stacking sequence (fig 5.20 (b)) did not appear to have any effect on the damage width curves. In addition the through thickness distribution did not appear to be affected by lay-up, although this is based on a limited number of observations.

5.4.5.7 Effect of Material

The damage width versus incident impact energy curves in fig 5.22 for the TCE, CE and GRP materials, are remarkably similar. This is because differences between the mechanical properties of the epoxy matrix materials are small. Since delamination damage is being propagated in the resin rich interlaminar regions, the type of fibre would not be expected to, and does not appear to significantly effect the result. It is interesting that the resistance to impact is so similar for the carbon and glass reinforced materials when most of the other mechanical properties are so different. Large improvements in performance are obtained when a thermoplastic matrix material is used. Damage was initiated at a higher energy, and once initiated the damage width was much less than for the epoxy based materials at the same incident impact energy. This is generally attributed to the higher interlaminar fracture toughness of the APC material. In addition it has been suggested that the APC can absorb energy in plastic deformation (see for example Morton et al, 1989) therefore leaving less energy free to propagate delamination damage.

It was noted previously that the scatter in the force required to initiate damage was higher for the APC material. It is also evident that the scatter in the data shown in fig 5.22 is also higher for the APC material. This can also be seen in the results of Bishop (1985) where delaminated area was plotted against incident impact energy. In general it appears that data collected for composites with thermoplastic matrix materials is more prone to scatter.

5.4.5.8 The use of Instrumented Impact Data to Assess the Total Amount of Damage

The total absorbed energy measured from the instrumented impact data is often used as a measure of the total amount of damage contained in the material. In a material such as carbon / epoxy where the failure is of a quite brittle nature there is probably a reasonable correlation between the total amount of damage and the total absorbed energy. Of course this does not reveal any information about the type, extent or distribution of damage. However the information can be of use. For example it was seen earlier that the lateral extent of damage did not extend beyond approximately 40 mm. However the total amount of absorbed energy continued to increase as the incident energy was increased, indicating that the total amount of damage was increasing.

In the case of more ductile materials, such as APC, where permanent plastic deformation results from impact, the total absorbed energy would not be expected to correlate very well with the total amount of damage. This is because the local plastic deformation may

not be defined as damage. Morton et al (1989) found that local permanent deformation (described as a 'dimple' in the material) did not significantly effect residual performance in post-impact tension and compression tests. If damage is defined as having occurred when residual properties are affected, then local plastic deformation would not be included and therefore measurements of the total absorbed energy would be misleading if used as a measure of the total amount of damage. Having said this there may be some circumstances where the total absorbed energy does prove to be useful. For example the total energy required to cause the striker to penetrate the specimen may be of interest in some circumstances.

Given that the total absorbed energy will almost certainly continue to be measured and reported, it is suggested that the results should be expressed as a fraction of the incident impact energy. The benefit of this is demonstrated by comparing the data shown in figs 5.6 (a) and (d). Differences between the behaviour of the materials is much more easily detected when the data is plotted in this way. Sjoblom et al (1988) used the same method and reported a correlation between sudden increases in the normalised energy and observed failure events, such as delamination or back-face damage. These events cannot be identified when the absolute absorbed energy is plotted against incident energy because the curves are smoother. The results presented in this chapter appear to support the observation made by Sjoblom in some cases. For example the abrupt change in slope of the curves shown in fig 5.13 (d) for the TCE, CE and GRP materials between 1 and 2 J, roughly coincide with the onset of delamination damage. This may be associated with the release of energy stored in elastic bending of the specimen, which is released when damage is initiated, the energy being used in damage propagation. For the APC material there does not appear to be a change in slope at the incident energy where delamination is known to have been initiated. This may be connected with the fact that the material can absorb energy in plastic deformation and therefore there is less stored elastic energy available for release. The suggestion is that sharp changes in the slope of the curves occur for each new damage initiation event. In the case of the TCE-QI-16 material (fig 5.3 (e)) the first change in slope is associated with delamination damage and the second with the onset of tensile failure on the back face of the specimen.

One other interesting observation is that the curves for the 0/90 and ±45 materials are different (fig 5.6 (d)). This was not the expected result, since measurements of other parameters (such as damage initiation force and energy and damage width) have been very similar. The reason for the difference in the curves is not known and was not investigated further since it was not directly related to the problem of post-impact compression testing.

Material	Force at Damage Initiation (KN)	Standard Deviation (KN)	Coefficient of Variation (%)	Absorbed Energy at Damage Initiation (J)	Standard Deviation (J)	Coefficient of Variation (%)	Number of Tests
TCE-±45-16-45	2.60	0.18	6.9	1.67	0.17	10.2	4
TCE-±45-16-55	2.66	0.11	4.1	1.63	0.13	8.0	5
TCE-±45-16-75	2.52	0.18	7.1	1.47	0.21	14.3	5
TCE-0/90-16-45	2.73	0.10	3.7	1.76	0.14	8.0	5
TCE-0/90-16-55	2.74	0.13	4.7	1.71	0.17	9.9	5
TCE-0/90-16-75	2.76	0.13	4.7	1.67	0.07	4.2	4
TCE-QI-16-45	1.64	0.08	4.9	0.81	0.15	18.5	6
TCE-QI-16-55-Clamped	1.82	0.15	8.2	0.80	0.10	12.5	20
TCE-QI-16-55-Unclamped	1.84	0.03	1.6	1.01	0.02	2.0	4
TCE-QI*-16-55	1.84	0.09	4.9	0.81	0.06	7.4	6
TCE-QI-16-75	1.97	0.15	0.8	0.88	0.12	13.6	5
TCE-QI-24-55	4.19	0.28	6.7	1.94	0.32	16.5	4
TCE-QI-32-55	6.75	0.25	3.7	3.14	0.24	7.6	4
CE-QI-16-55	1.66	0.05	3.0	0.64	0.07	10.9	7
GRP-QI-16-55	1.54	0.11	7.1	1.05	0.17	16.2	11
APC-QI-16-55	3.45	0.29	8.4	2.54	0.47	18.5	11

Table 5.1 Results of impact tests: forces and absorbed energies at damage initiation.

Material	P_i (KN)	K_p (N/m) ($x10^6$)	n' ($N/m^{3/2}$) ($x10^9$)	$d_t = P_i / K_p$ (mm)	$d_c = (P_i / n')^{2/3}$ (mm)	$d_t - d_c$ (mm)	Corrected K_p (N/m) ($x10^6$)
TCE-±45-16-45	2.60	2.04	0.75	1.27	0.23	1.04	2.5
TCE-±45-16-55	2.66	2.13	0.75	1.25	0.23	1.02	2.6
TCE-±45-16-75	2.52	2.08	0.75	1.21	0.22	0.99	2.5
TCE-0/90-16-45	2.73	2.15	0.75	1.27	0.24	1.03	2.7
TCE-0/90-16-55	2.74	2.16	0.75	1.27	0.24	1.03	2.7
TCE-0/90-16-75	2.76	2.21	0.75	1.25	0.24	1.01	2.7
TCE-QI-16-45	1.64	1.57	0.63	1.04	0.19	0.85	1.9
TCE-QI-16-55-Clamped	1.82	2.05	0.63	0.89	0.20	0.69	2.6
TCE-QI-16-55-Unclamped	1.84	1.57	0.63	1.17	0.20	0.97	1.9
TCE-QI*-16-55	1.84	2.05	0.63	0.90	0.20	0.70	2.6
TCE-QI-16-75	1.97	2.16	0.63	0.91	0.21	0.70	2.8
TCE-QI-24-55	4.19	4.53	0.64	0.92	0.35	0.57	7.4
TCE-QI-32-55	6.75	7.58	0.61	0.89	0.50	0.39	17.3
CE-QI-16-55	1.66	2.14	0.86	0.78	0.16	0.62	2.7
GRP-QI-16-55	1.54	1.17	0.71	1.32	0.17	1.15	1.3
APC-QI-16-55	3.45	2.33	1.74	1.48	0.28	1.20	2.9

Table 5.2 Calculated values of K_p, illustrating method for correcting values of K_p by using a deflection value equal to overall striker displacement minus indentation .

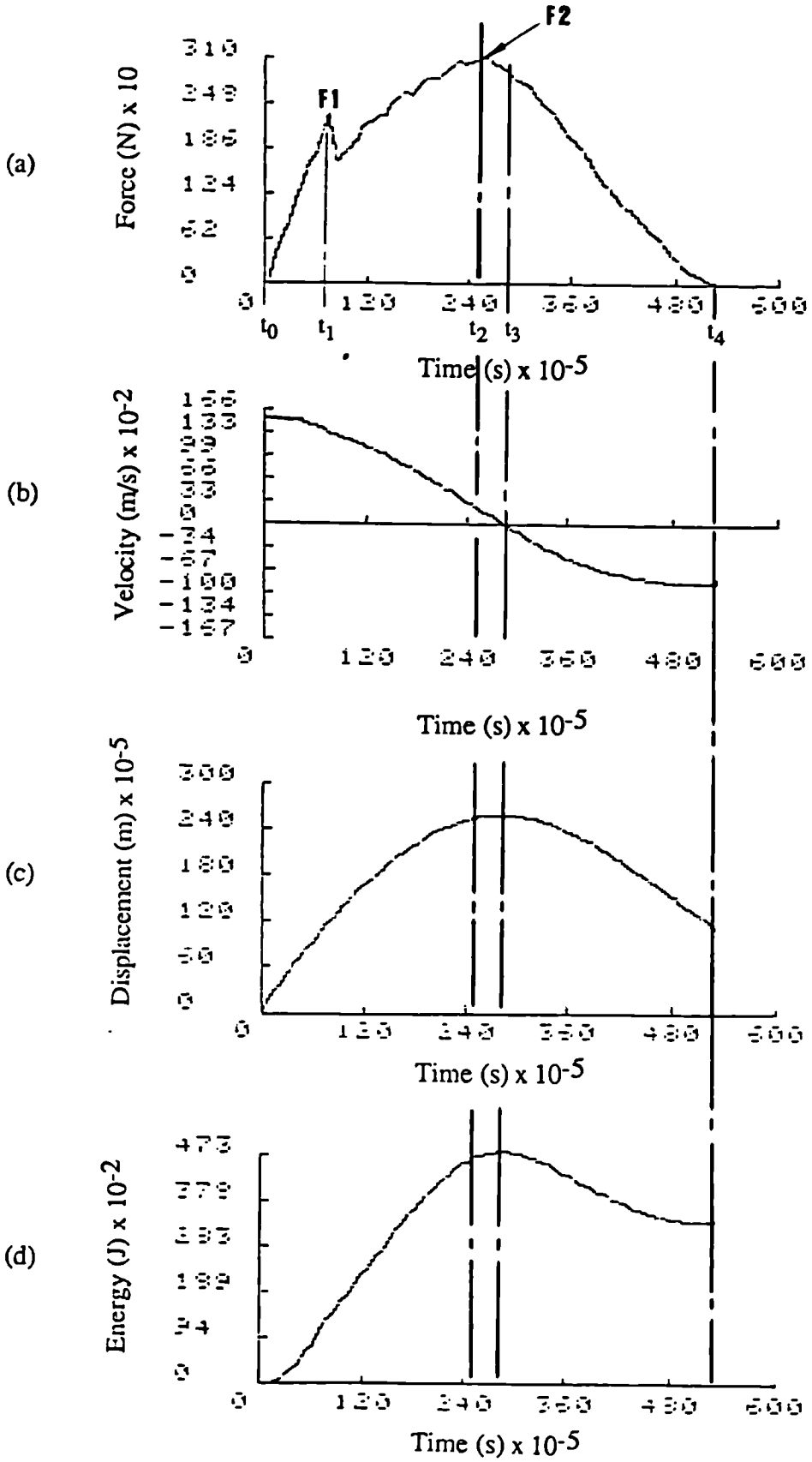

Fig 5.1 Instrumented impact data for TCE-0/90-16 material. (a) Force, (b) Velocity, (c) Displacement and (d) Absorbed Energy plotted as a function of time. Spec no 14/5, Incident impact energy 4.73 J.

(e)

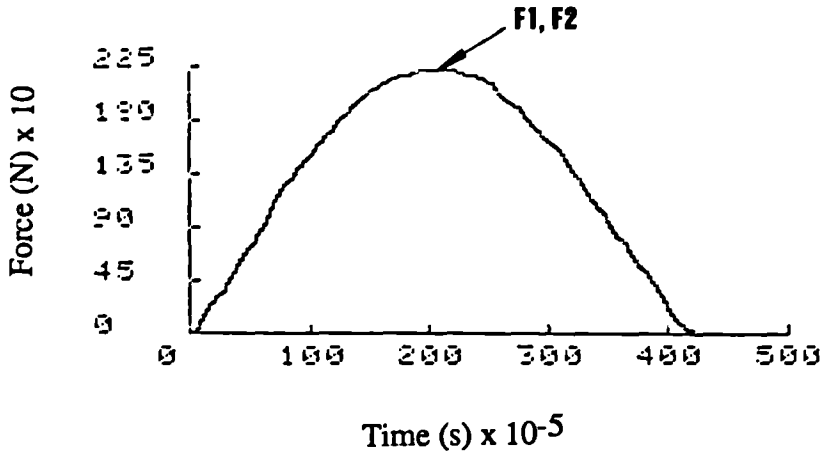

(f)

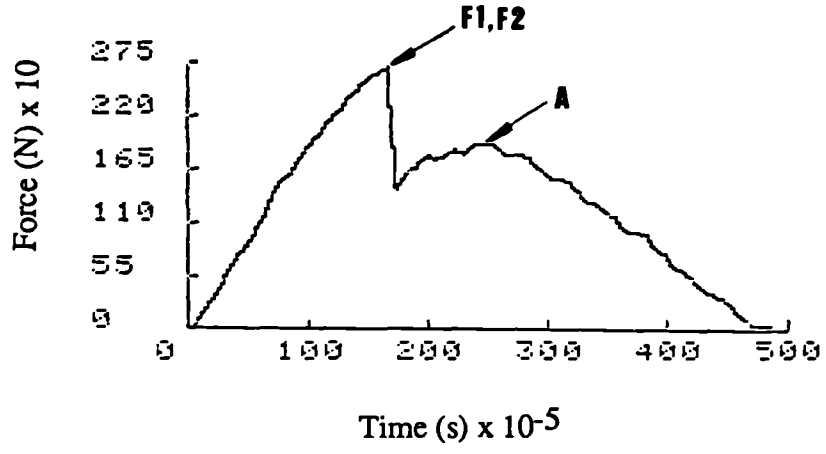

(g)

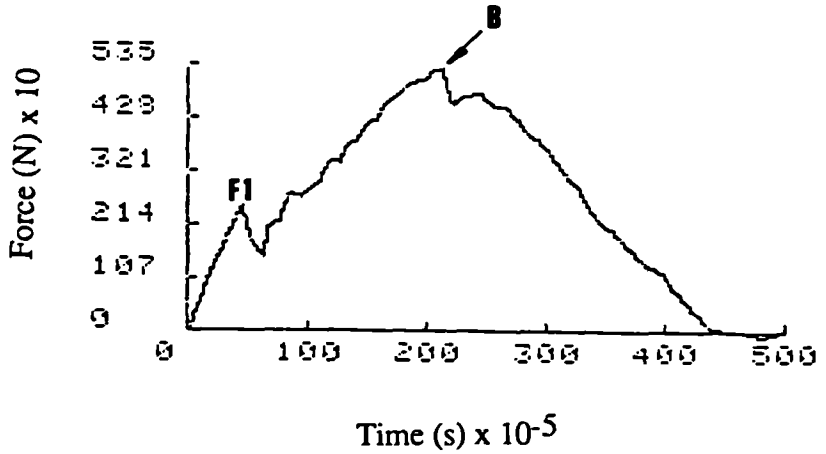

Fig 5.1 continued. Force versus time curves for:

(e) Spec 11/3, Incident Impact Energy 1.25 J.

(f) Spec 12/2, Incident Impact Energy 1.94 J.

(g) Spec 14/2, Incident Impact Energy 11.34 J.

Fig 5.2 (a) Impact force versus incident impact energy. Material, TCE-QI-16-55.

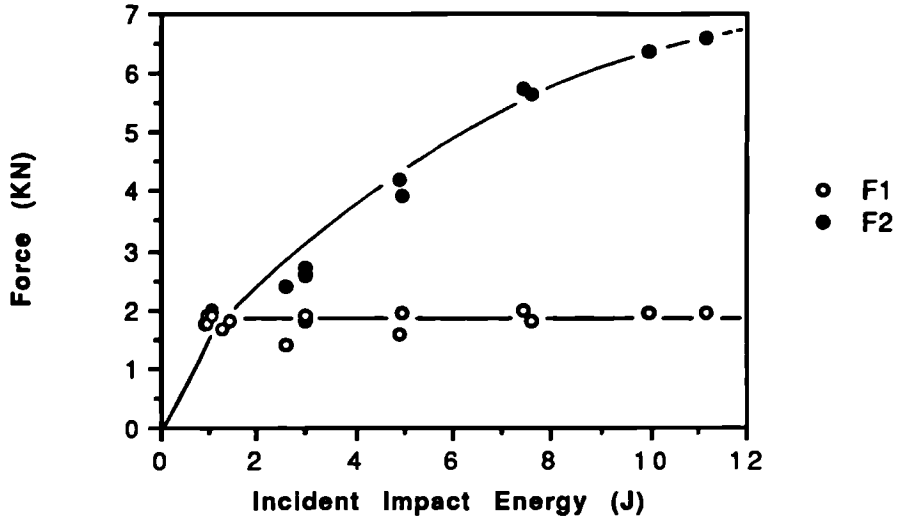

Fig 5.2 (b) Absorbed energy versus incident impact energy. Material, TCE-QI-16-55.

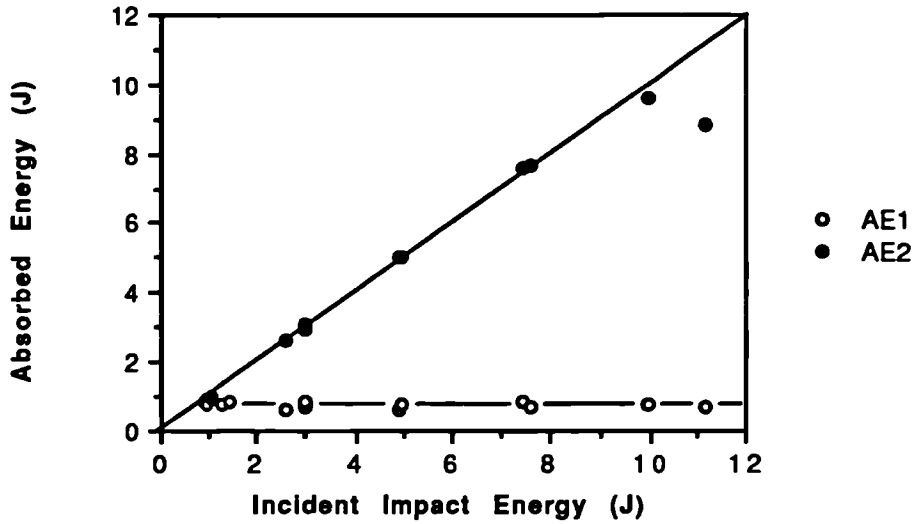

Fig 5.2 (c) Total absorbed energy versus incident impact energy. Material, TCE-QI-16-55.

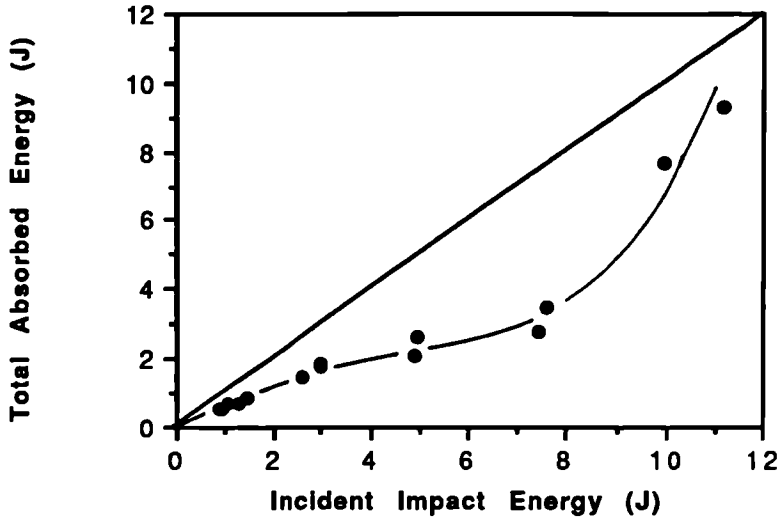

Fig 5.2 (d) Normalised total absorbed energy versus incident impact energy. Material, TCE-QI-16-55.

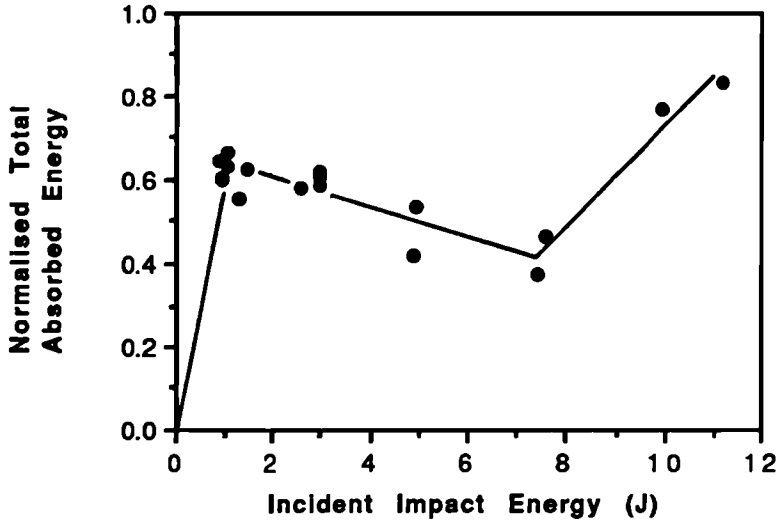

Fig 5.3 (a) Effect of specimen width on force F1. Material, TCE-QI-16.

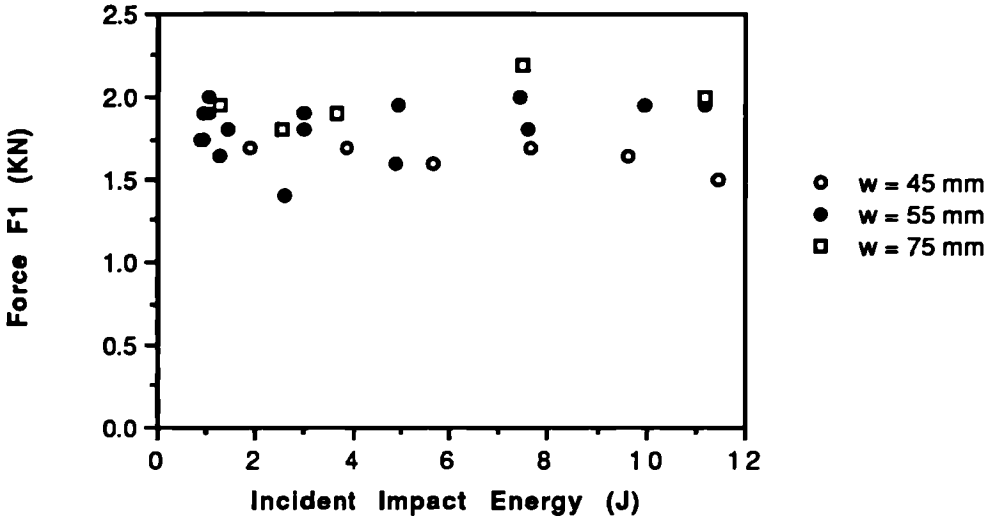

Fig 5.3 (b) Effect of specimen width on absorbed energy at F1. Material, TCE-QI-16.

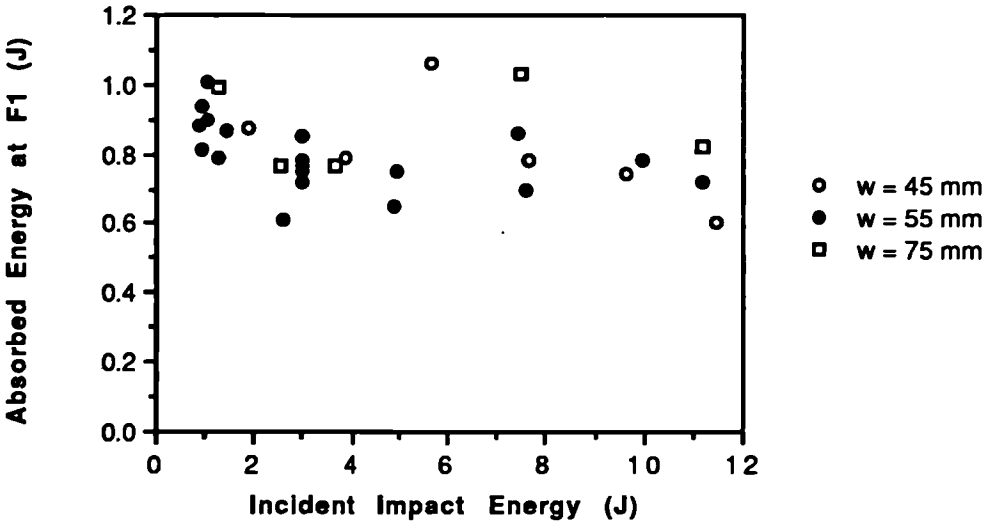

Fig 5.3 (c) Effect of specimen width on force F2. Material, TCE-QI-16.

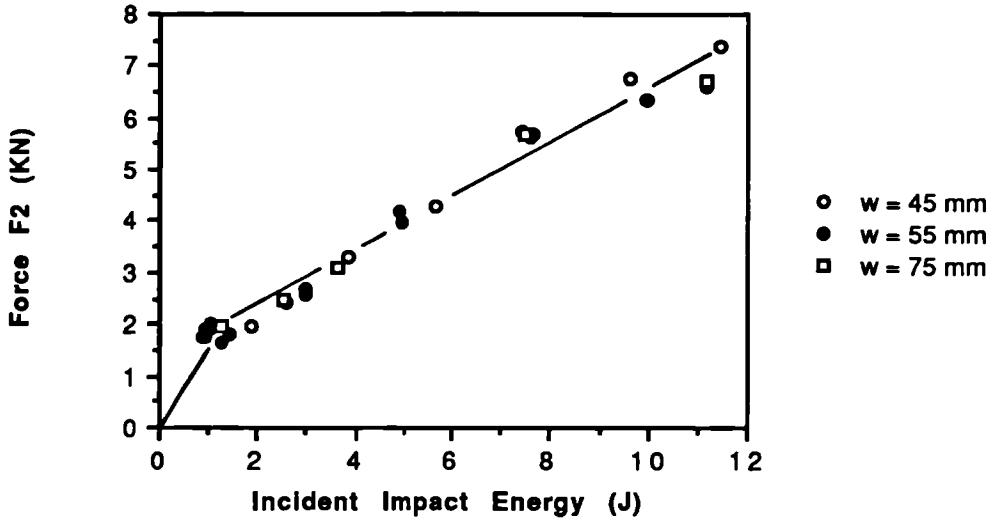

Fig 5.3 (d) Effect of specimen width on absorbed energy at F2. Material, TCE-QI-16.

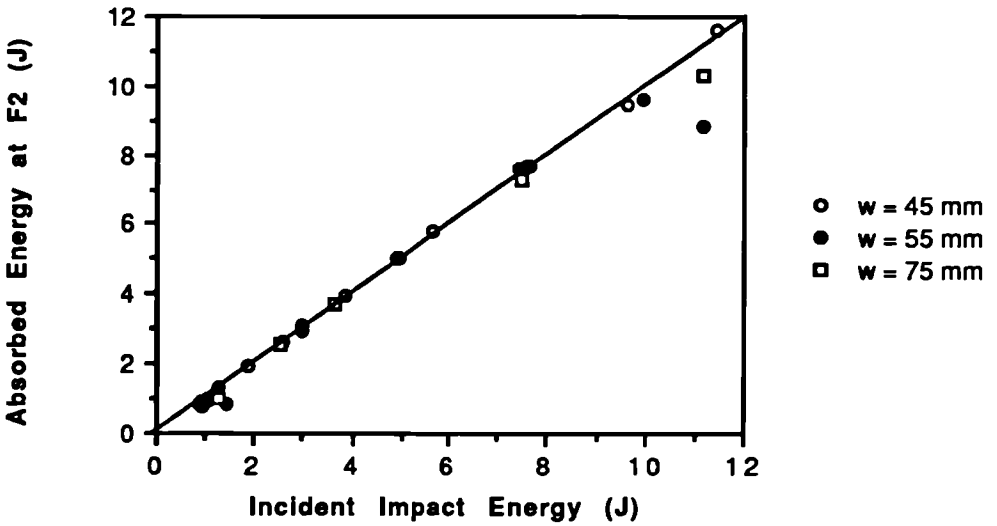

Fig 5.3 (e) Effect of specimen width on normalised total absorbed energy. Material, TCE-QI-16.

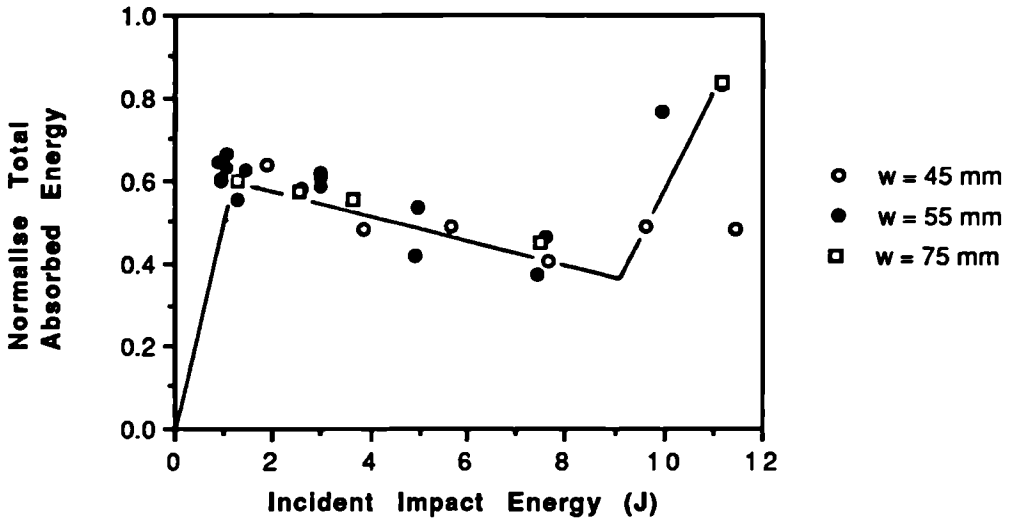

Fig 5.4 Comparison of absorbed energies at damage initiation for different specimen widths and lay-ups for TCE 16 ply material.

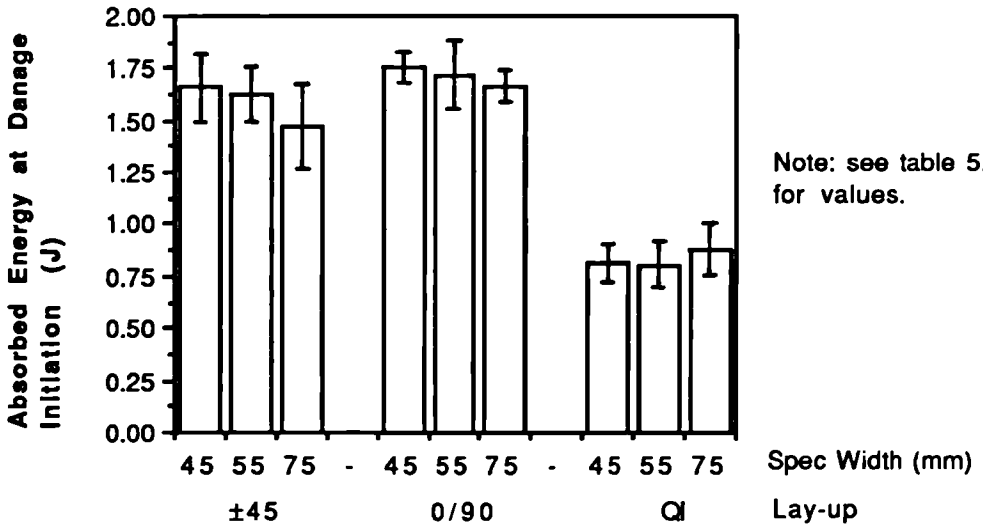

Fig 5.5 (a) Effect of clamping during impact on force F1. Material, TCE-QI-16-55.

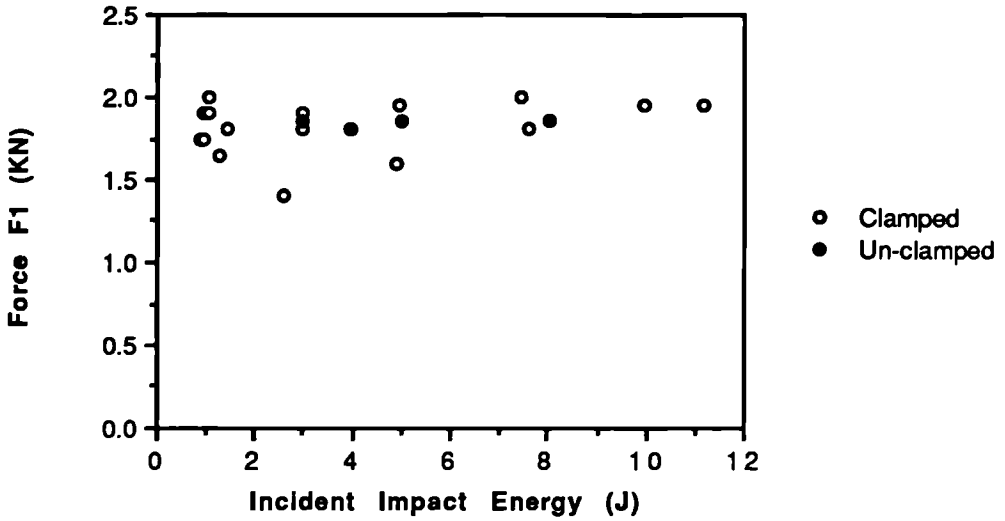

Fig 5.5 (b) Effect of clamping during impact on absorbed energy at force F1. Material, TCE-QI-16-55.

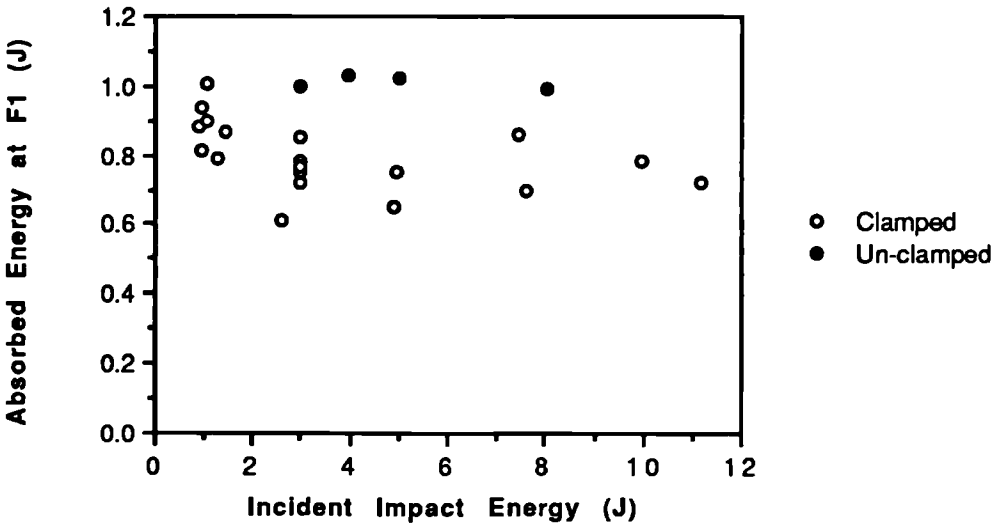

Fig 5.5 (c) Effect of clamping during impact on normalised total absorbed energy. Material, TCE-QI-16-55.

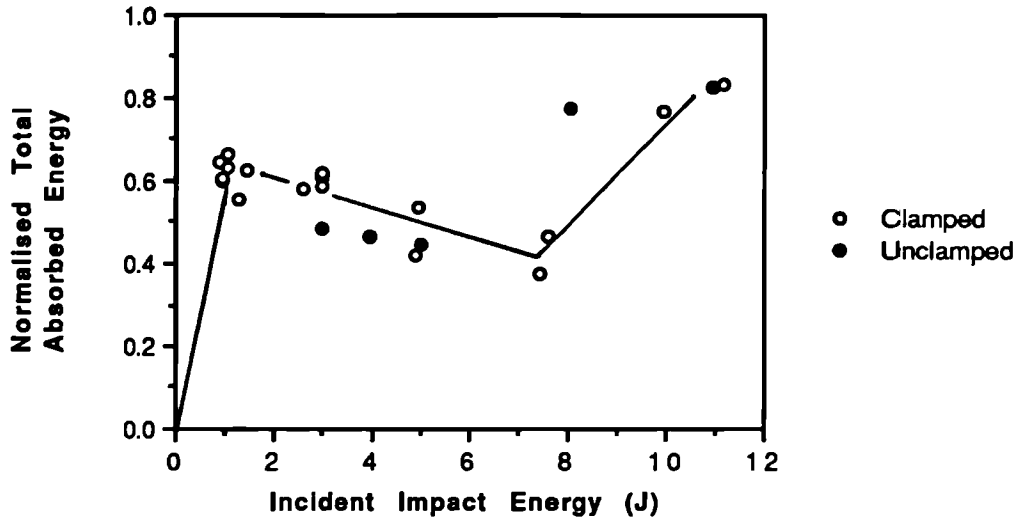

Fig 5.6 (a) Effect of layup on total absorbed energy. Material, TCE-QI, 0/90 and ±45-16-55.

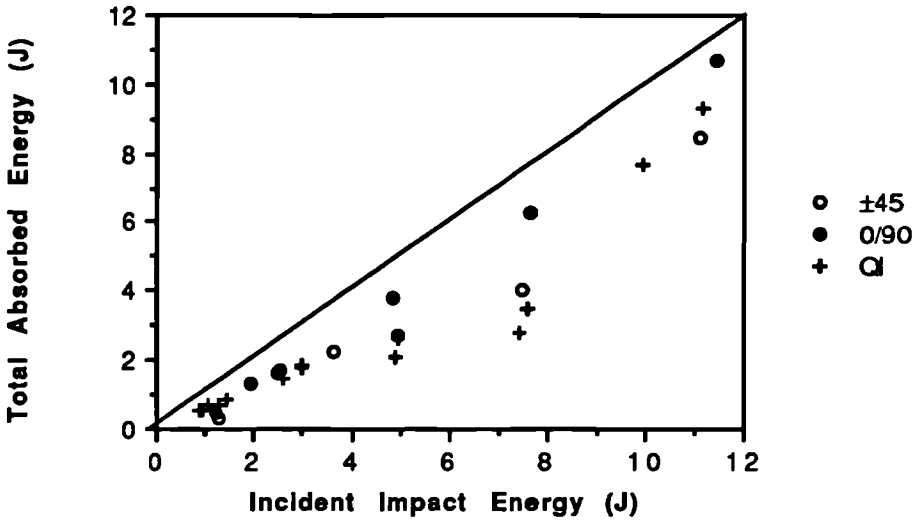

Fig 5.6 (b) Normalised total absorbed energy versus incident impact energy. Material, TCE-0/90-16-45, 55 and 75.

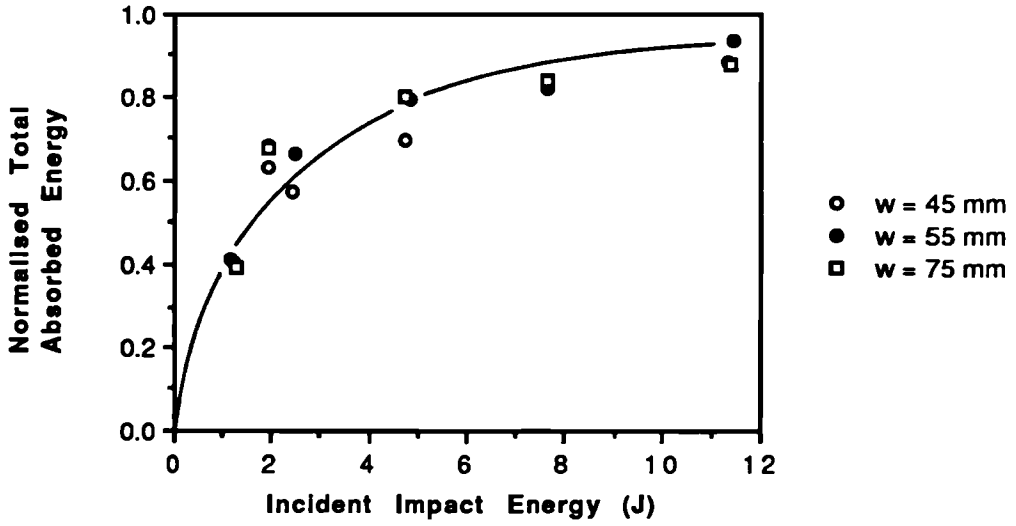

Fig 5.6 (c) Normalised total absorbed energy versus incident impact energy. Material, TCE-±45-16-45, 55 and 75.

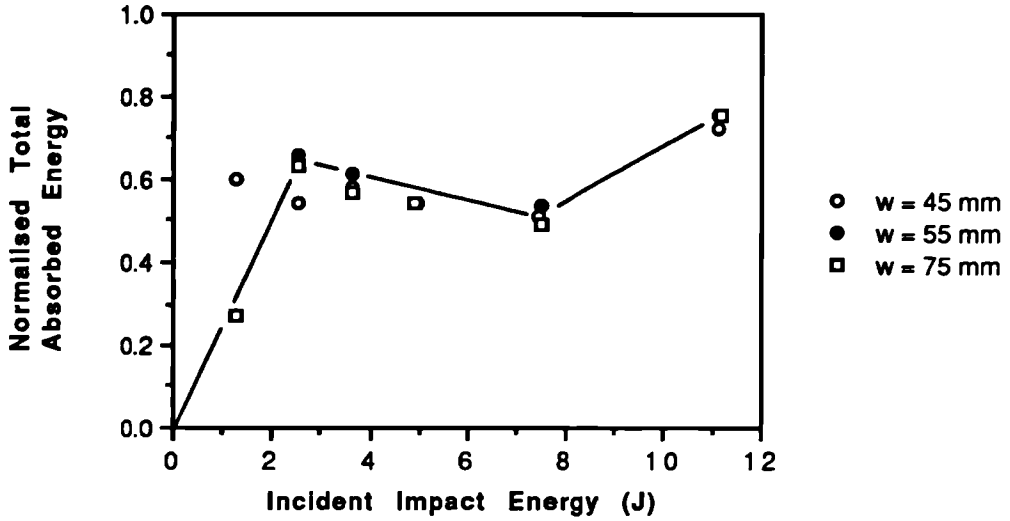

Fig 5.6 (d) Effect of layup on the normalised total absorbed energy. Material, TCE-QI, 0/90 and ±45-16-45, 55 and 75.

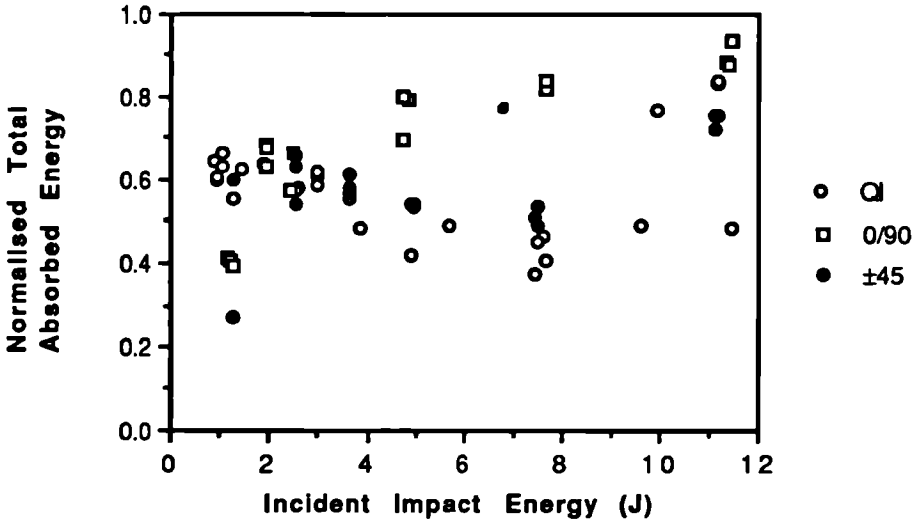

Fig 5.7 (a) Effect of fibre stacking sequence on force F1. Material, TCE-QI and QI*-16-55.

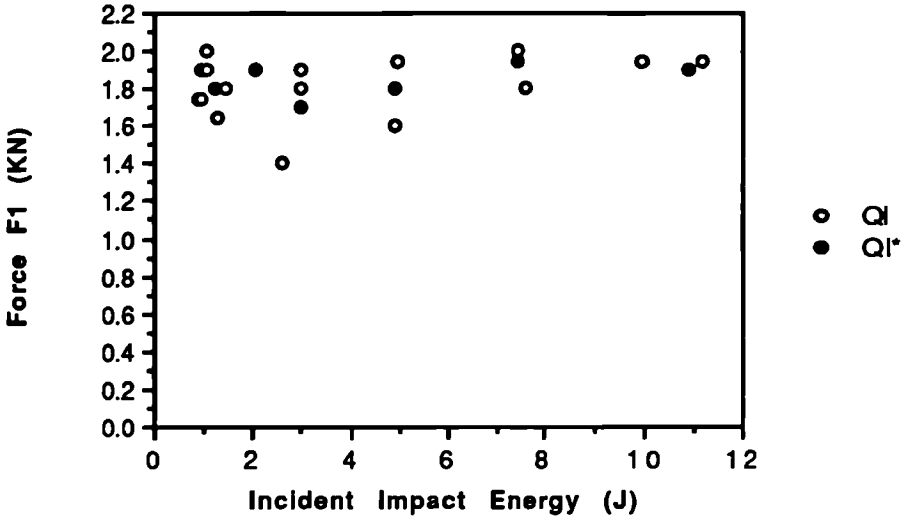

Fig 5.7 (b) Effect of fibre stacking sequence on absorbed energy at F1. Material, TCE-QI and QI*-16-55.

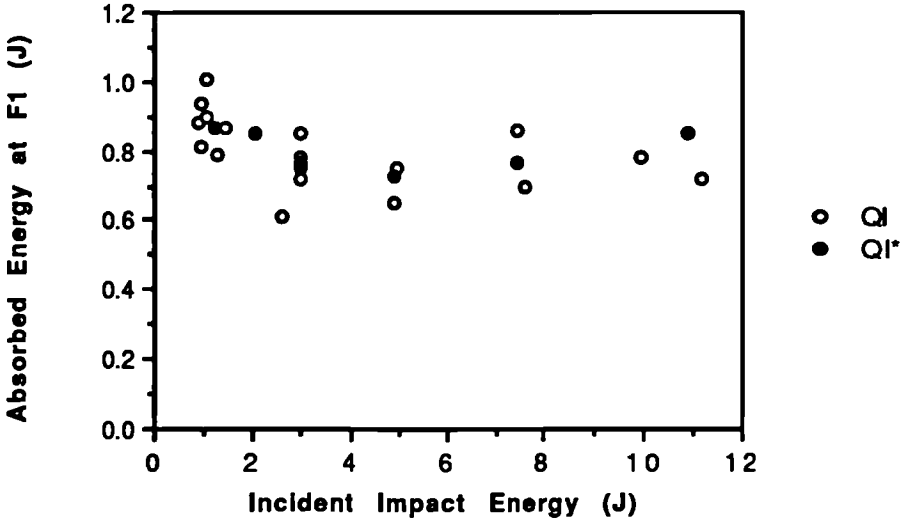

Fig 5.7 (c) Effect of fibre stacking sequence on normalised total absorbed energy. Material, TCE-QI and QI*-16-55.

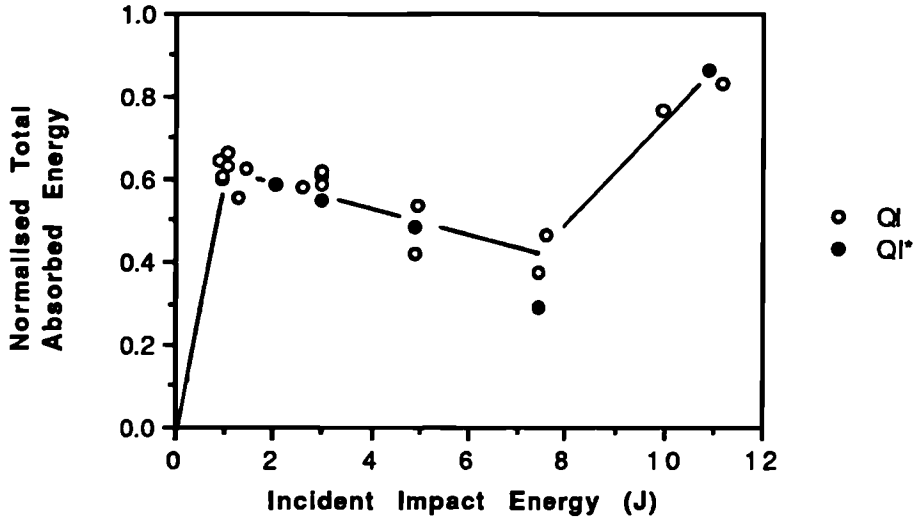

Fig 5.8 (a) Effect of material thickness on force F1 Material, TCE-QI-16, 24 and 32-55.

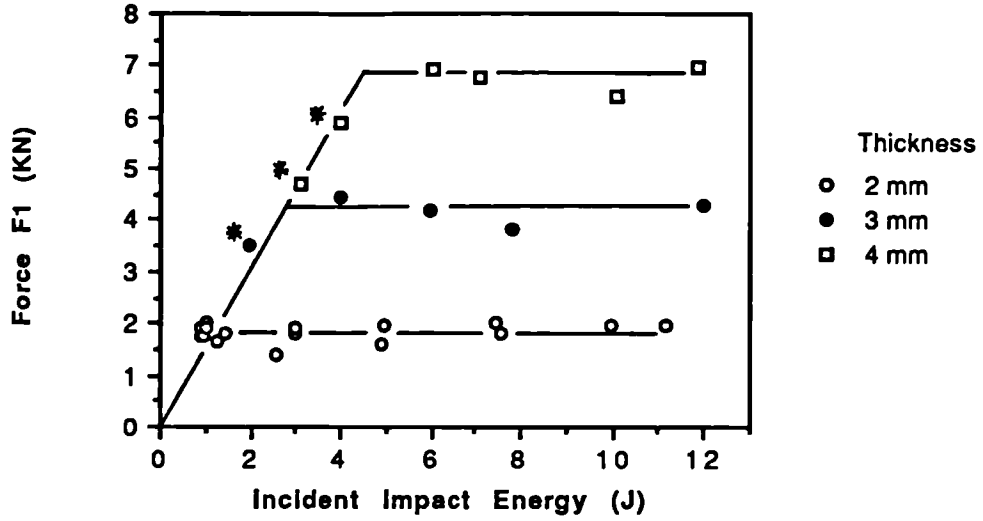

* Note: Damage not initiated.

Fig 5.8 (b) Effect of material thickness on absorbed energy at F1. Material, TCE-QI-16, 24 and 32-55.

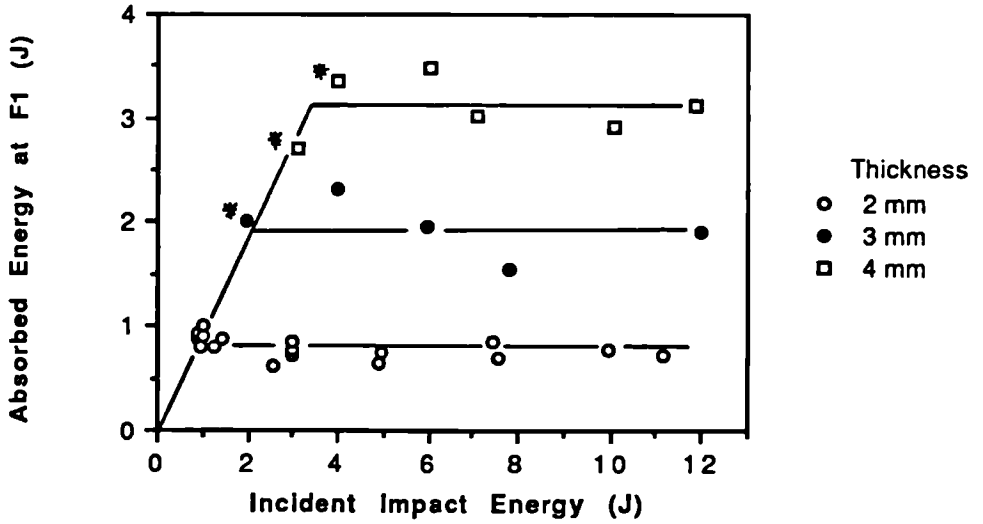

* Note: Damage not initiated.

Fig 5.9 (a) Effect of material thickness on the average force at damage initiation. Material, TCE-QI-16, 24 and 32-55.

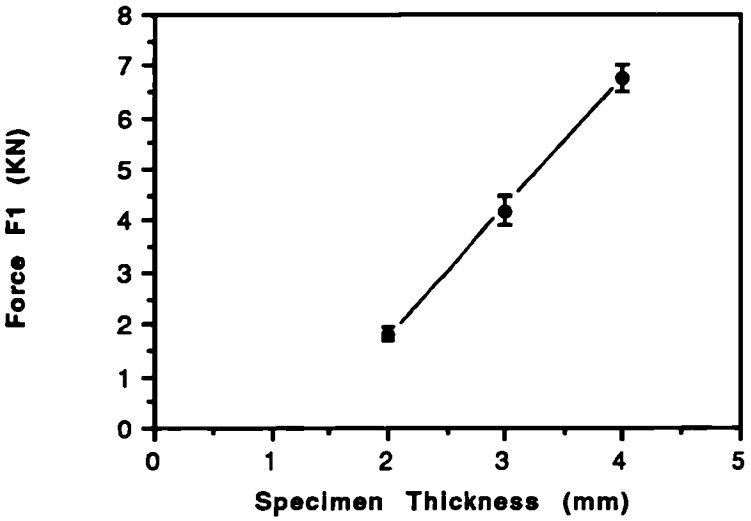

Fig 5.9 (b) Effect of material thickness on the average absorbed energy at damage initiation. Material, TCE-QI-16, 24 and 32-55.

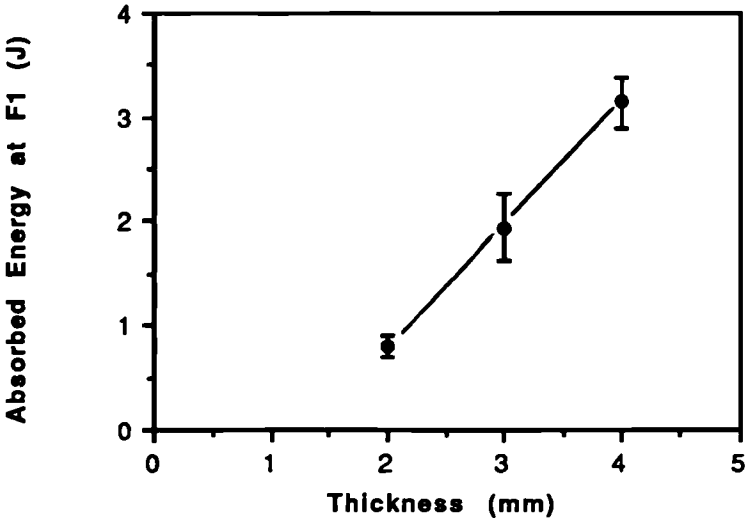

Fig 5.10 (a) Total absorbed energy versus incident impact energy. Material, TCE-QI-24-55.

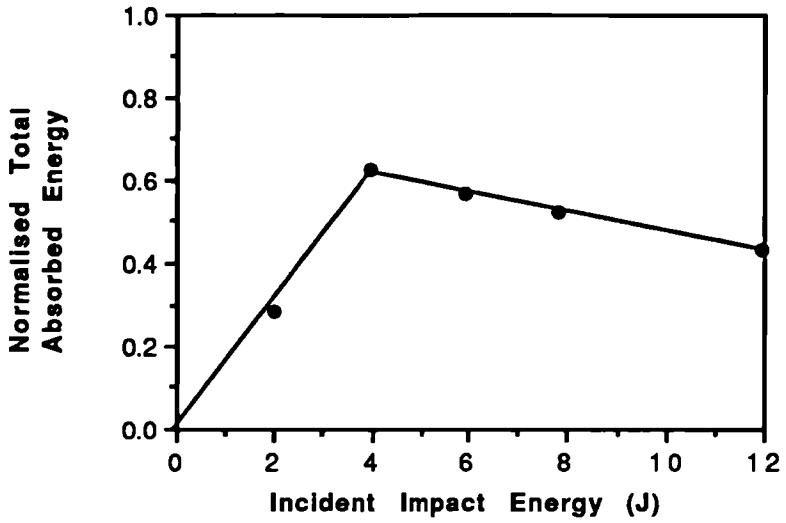

Fig 5.10 (b) Total absorbed energy versus incident impact energy. Material, TCE-QI-32-55.

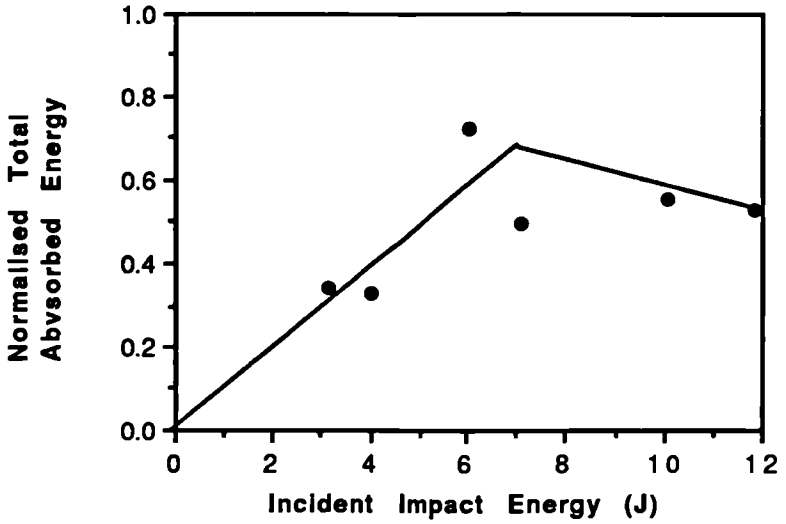

Fig 5.10 (c) Effect of thickness on the total absorbed energy. Material, TCE-QI- 16, 24 and 32-55.

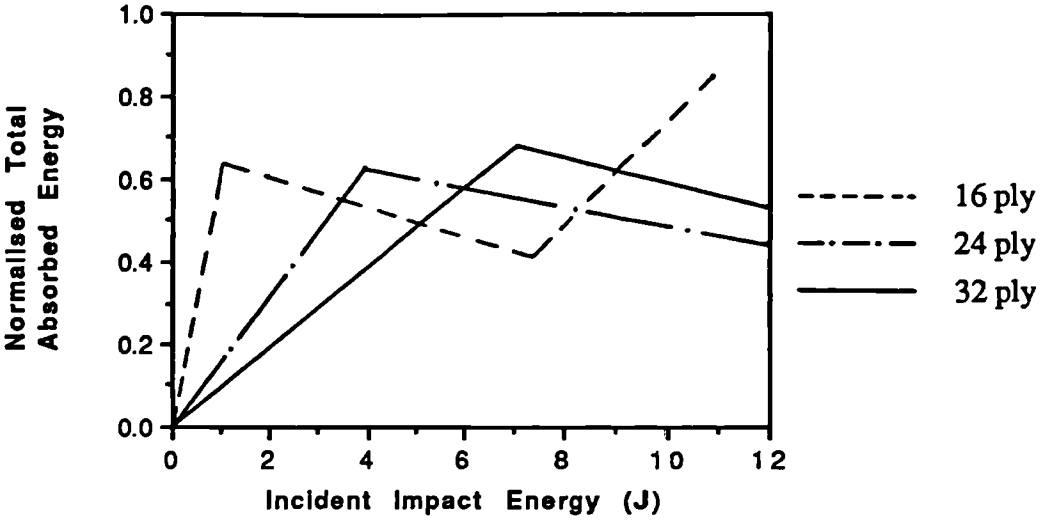

Fig 5.11 (a) Effect of material on force F1. Material, TCE, CE, GRP, APC-QI-16-55.

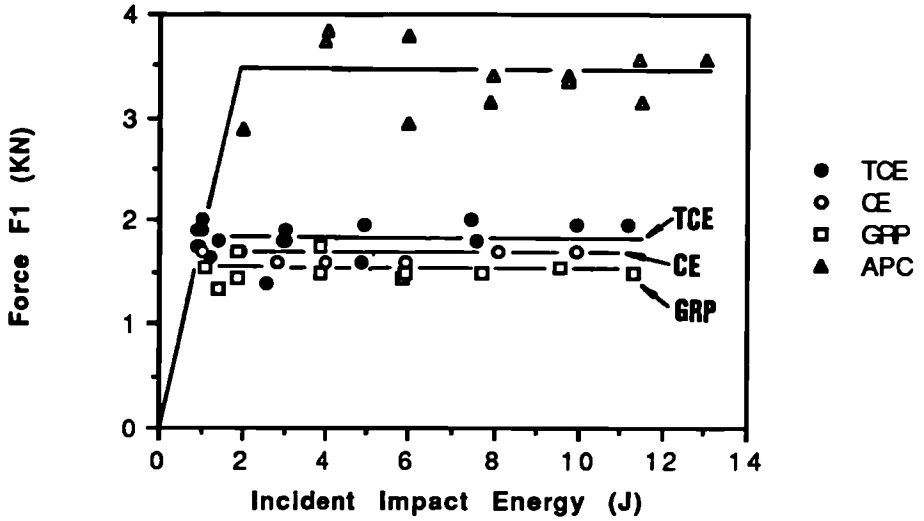

Fig 5.11 (b) Effect of material on the absorbed energy at F1. Material, TCE, CE, GRP, APC-QI-16-55.

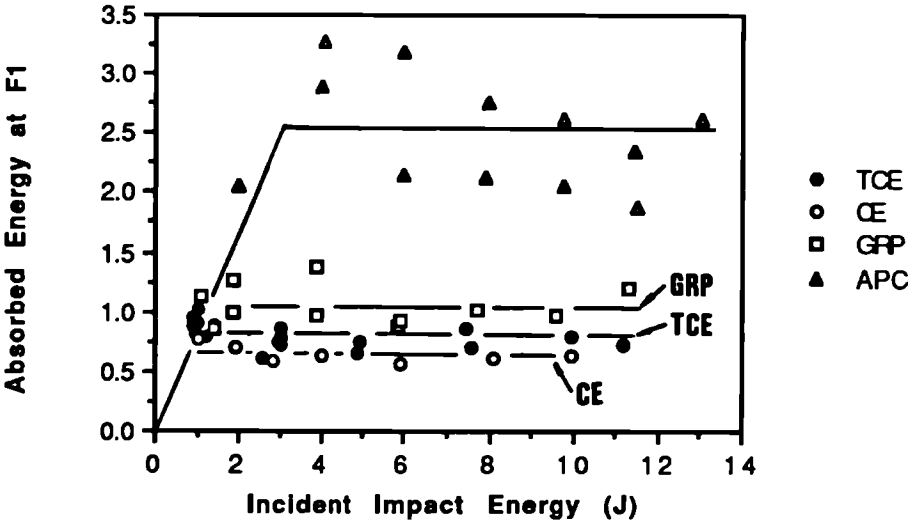

Fig 5.12 Effect of material on the average absorbed energies at F1.

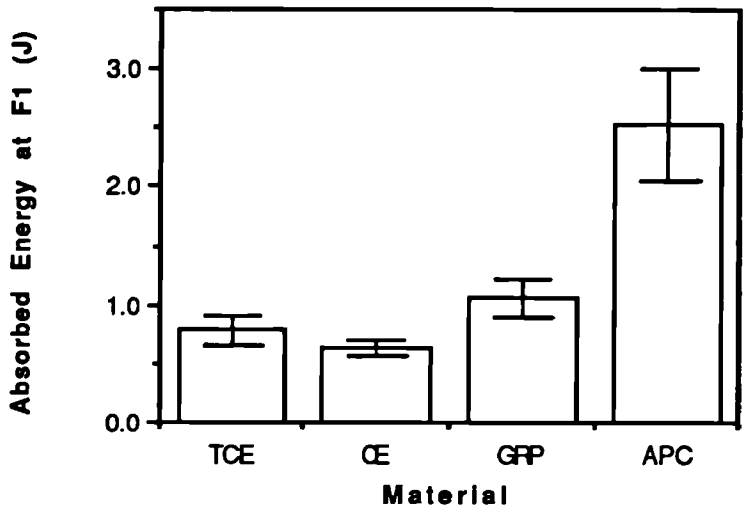

Fig 5.13 (a) Normalised total absorbed energy versus incident impact energy. Material, APC-QI-16-55.

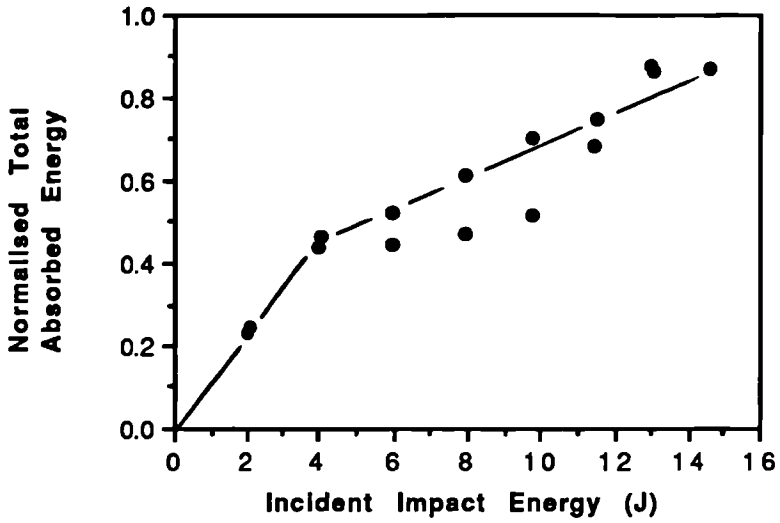

Fig 5.13 (b) Normalised total absorbed energy versus incident impact energy. Material CE-QI-16-55.

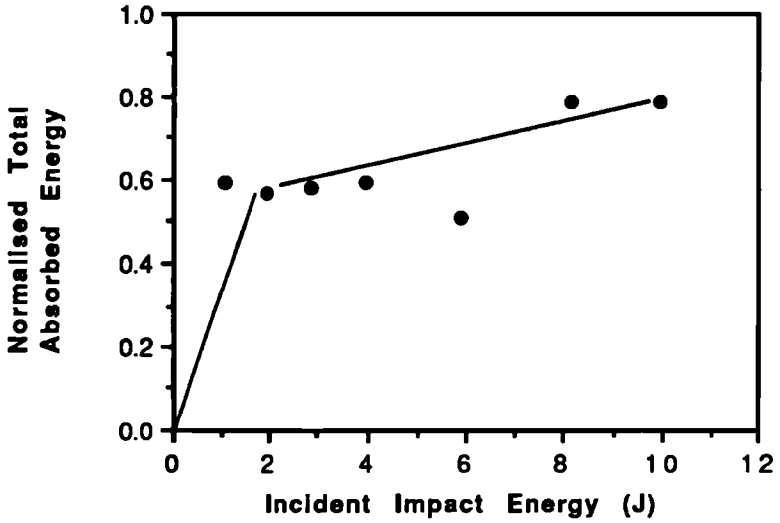

Fig 5.13 (c) Normalised total absorbed energy versus incident impact energy. Material GRP-QI-16-55.

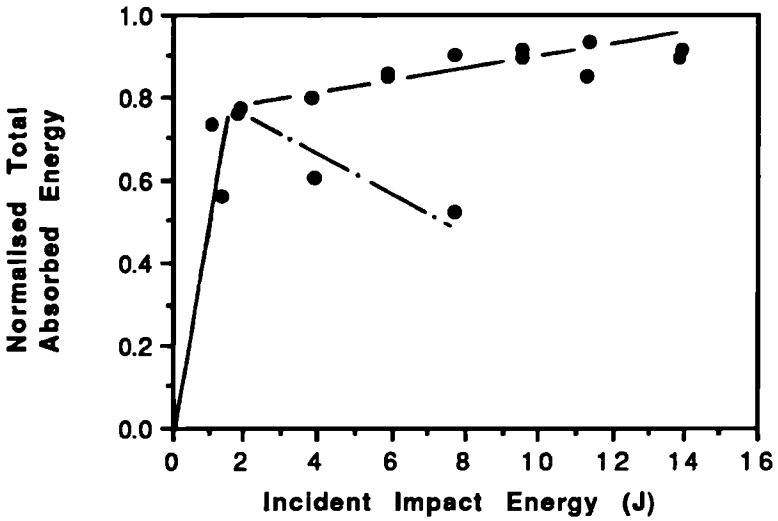

Fig 5.13 (d) Effect of material on normalised total absorbed energy. Material, TCE, CE, GRP, APC-QI-16-55.

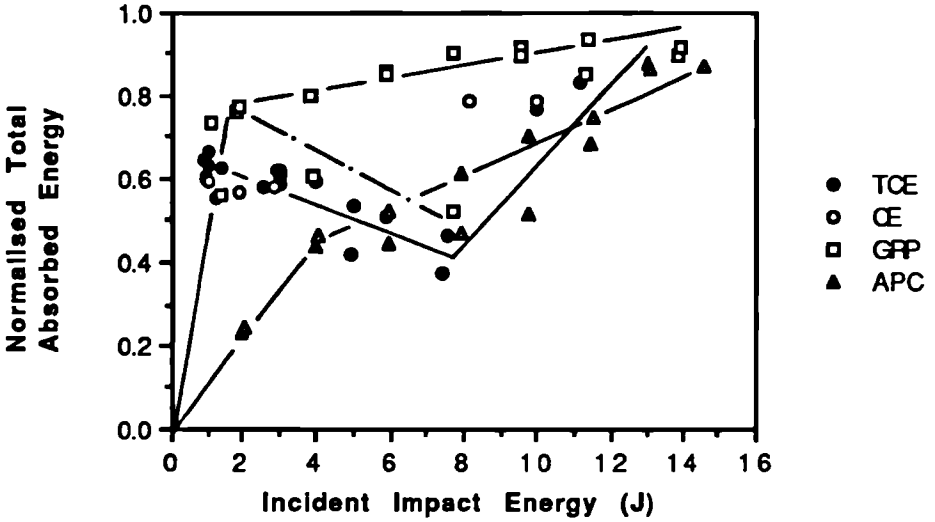

Fig 5.14 Results of ultrasonic C-scans showing damaged areas in GRP-0/90-16-55 specimens.

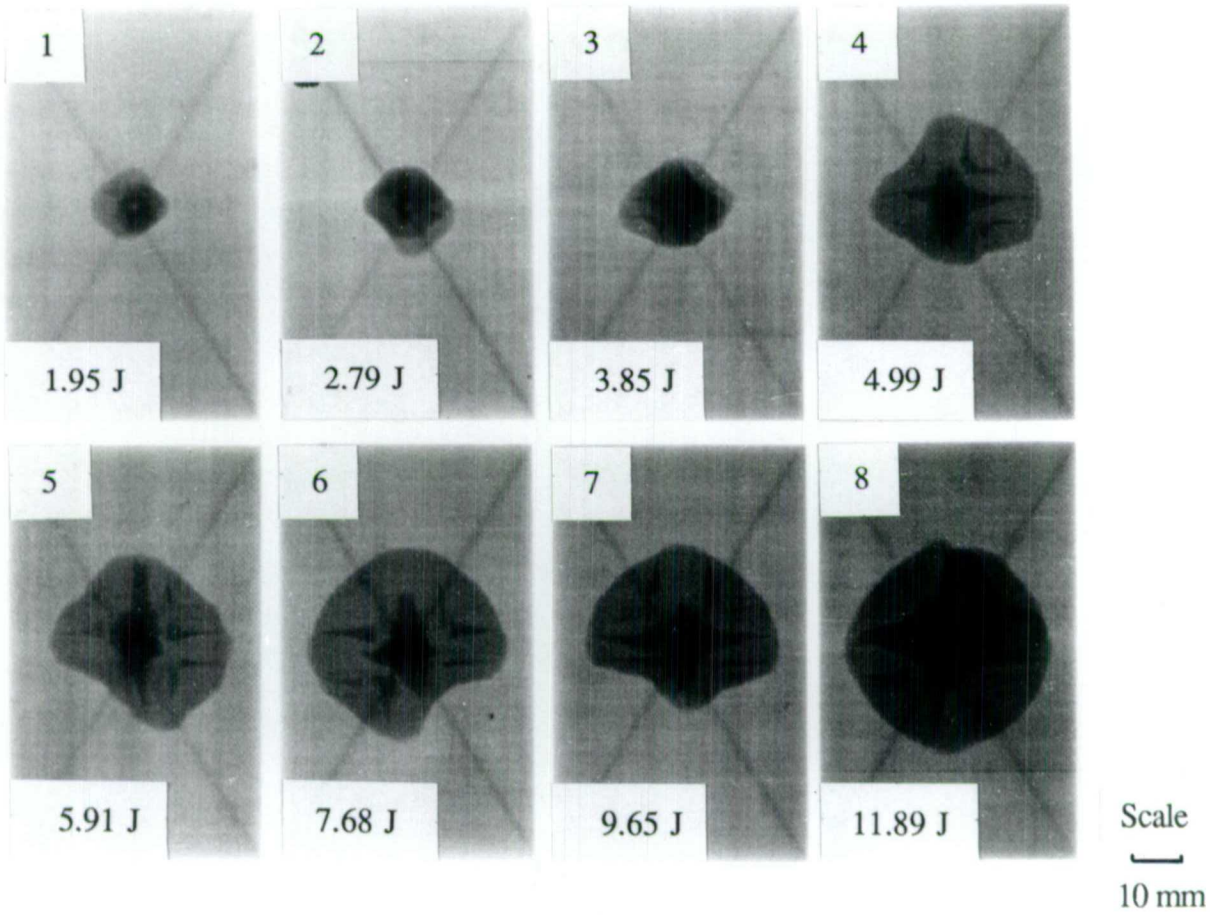

Fig 5.15 Photographs showing impact damage in GRP-QI-16-55 specimens.

Fig 5.16 (a) Damage area versus incident impact energy. Material, GRP-QI-16-55.

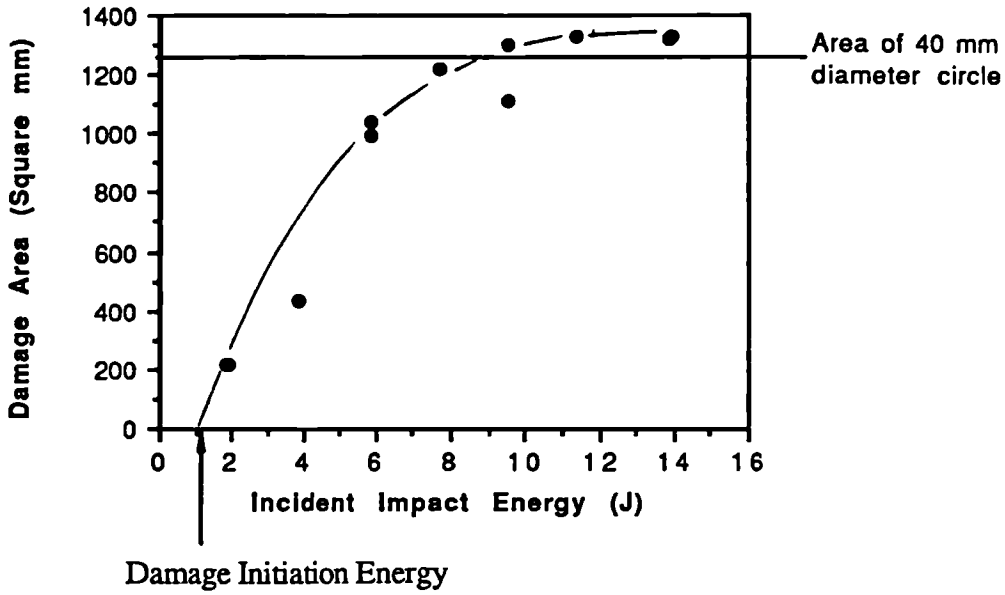

Fig 5.16 (b) Total absorbed energy versus incident impact energy. Material, GRP-QI-16-55.

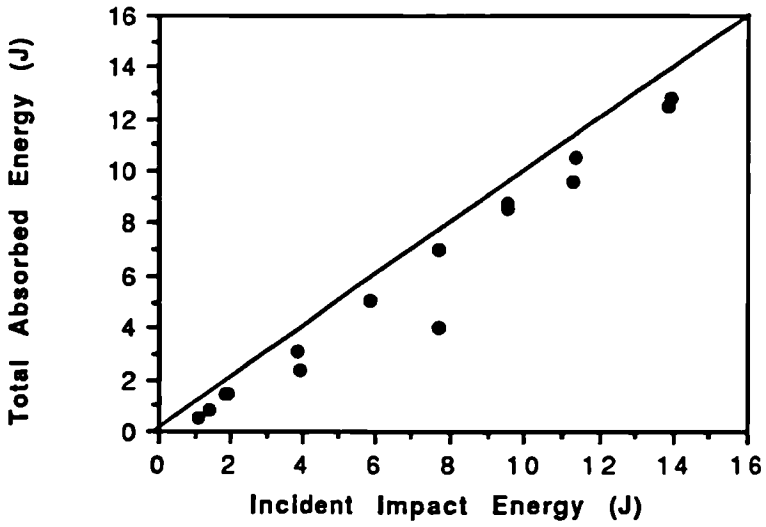

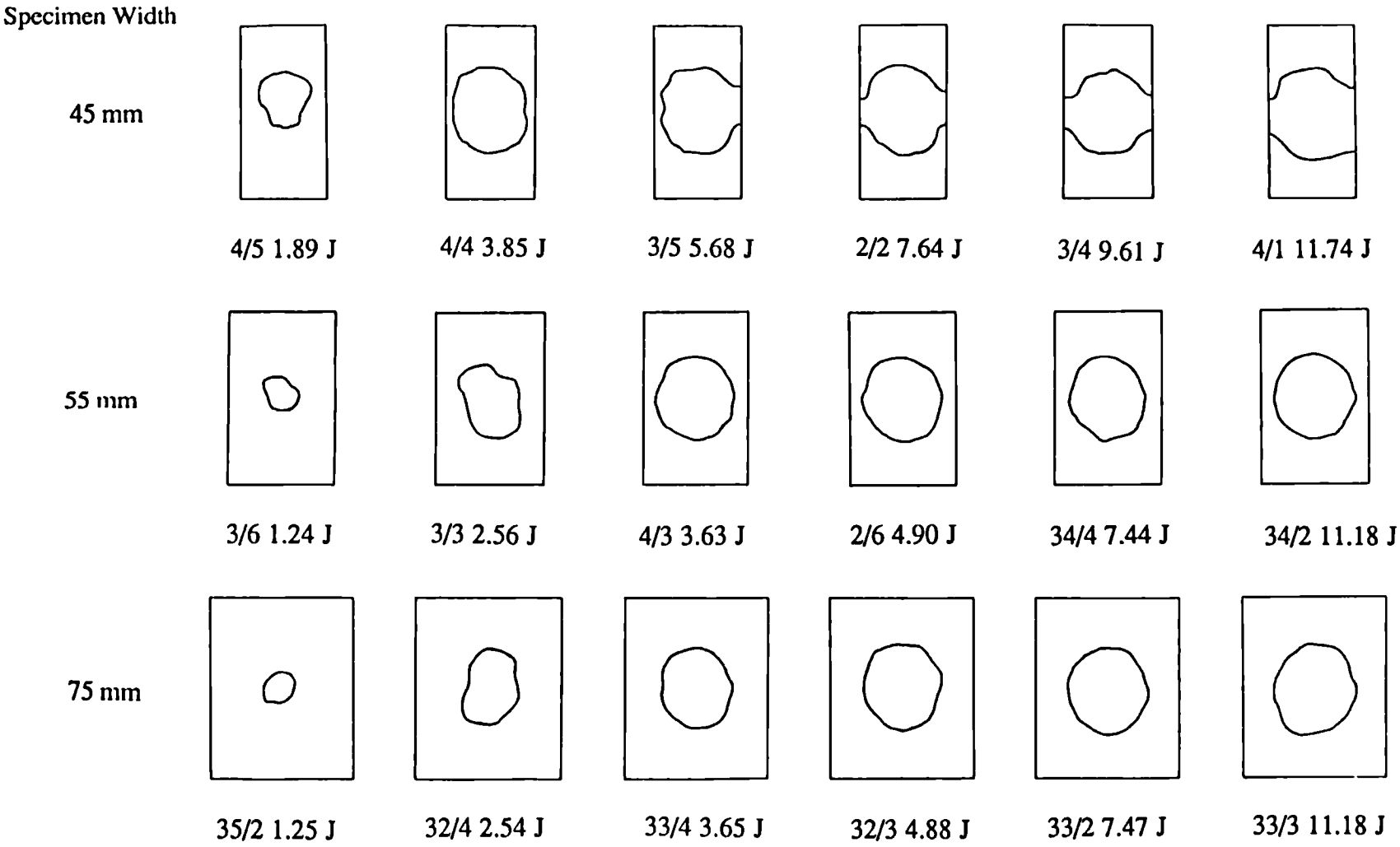

Note: Damaged areas were traced from ultrasonic C-scan prints (of the same size as those shown in fig 5.14) and reduced in size to fit this page.

Fig 5.17 Impact Damaged areas for TCE-QI-16 specimens of different widths.

Fig 5.18 (a) Effect of specimen width on damage width. Material, TCE-QI-16-45, 55 and 75.

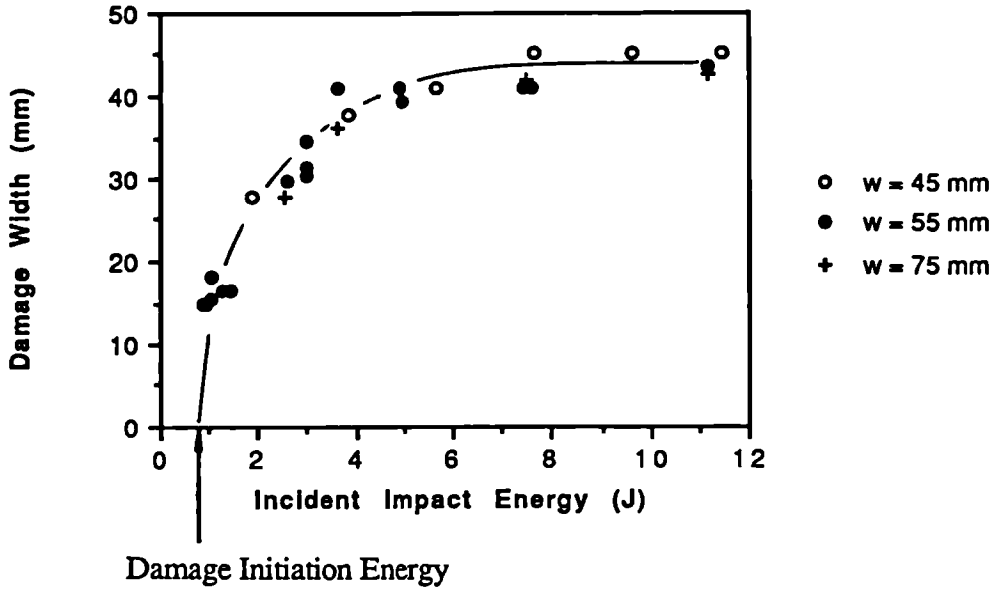

Fig 5.18 (b) Effect of specimen width on damage width. Material, TCE-0/90-16-45, 55 and 75.

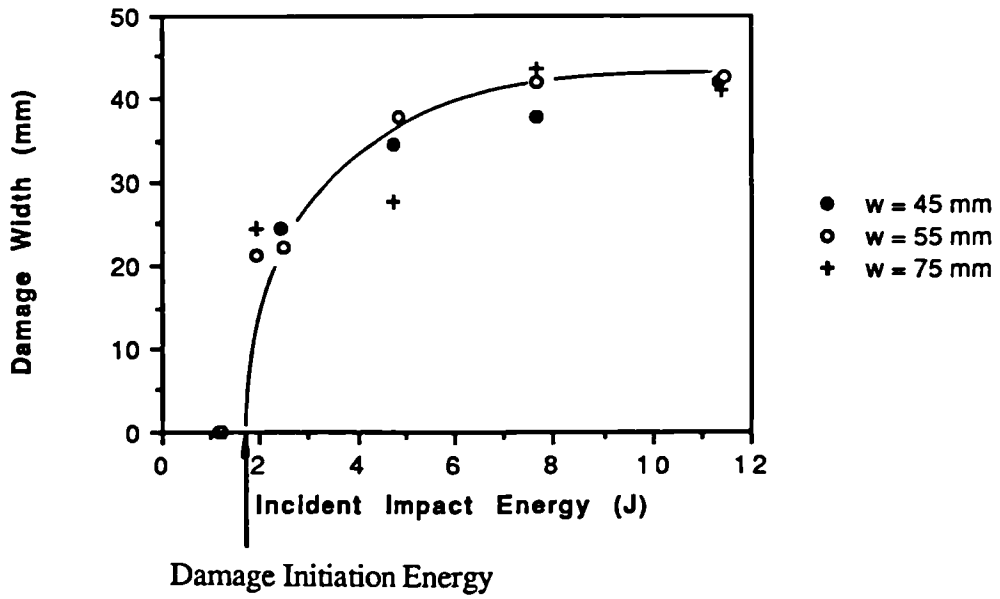

Fig 5.18 (c) Effect of specimen width on damage width. Material, TCE-±45-16-45, 55 and 75.

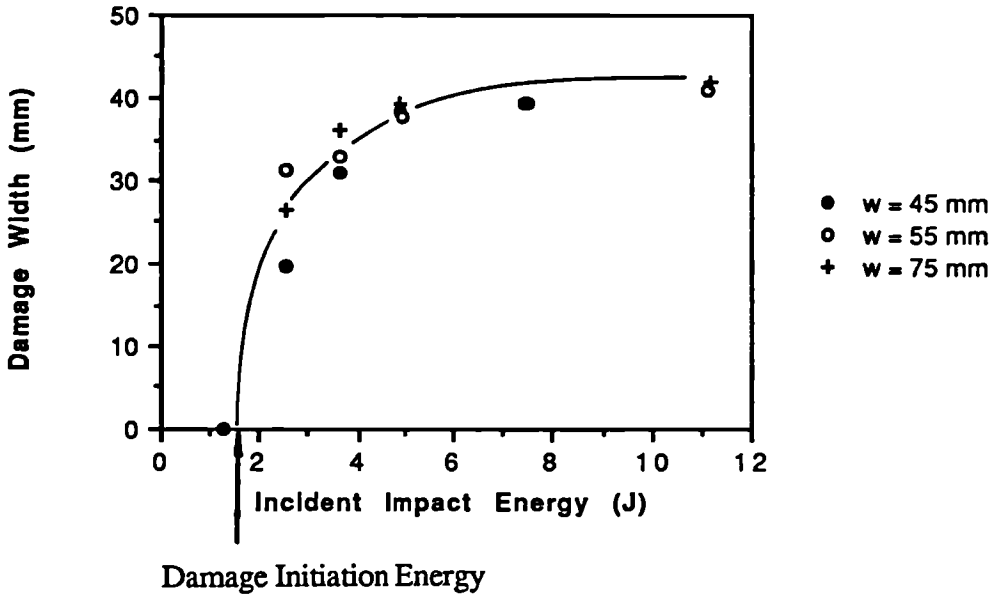

Fig 5.19 Effect of clamping during impact test on damage width. Material, TCE-QI-16-55.

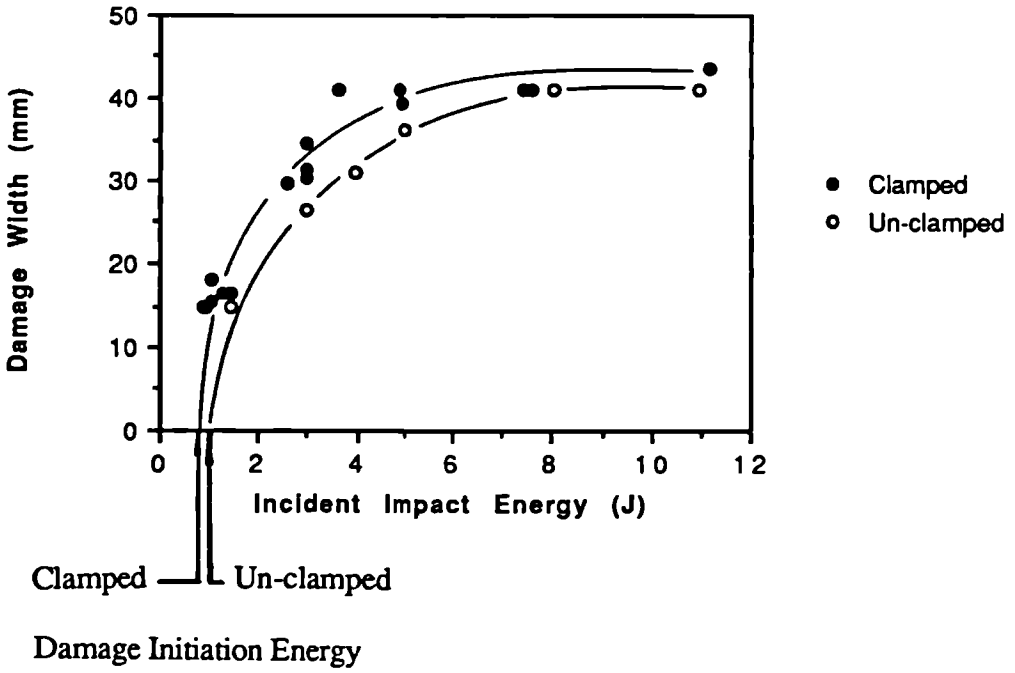

Fig 5.20 (a) Effect of lay-up on damage width. Material, TCE-QI, 0/90 and ±45-16-55.

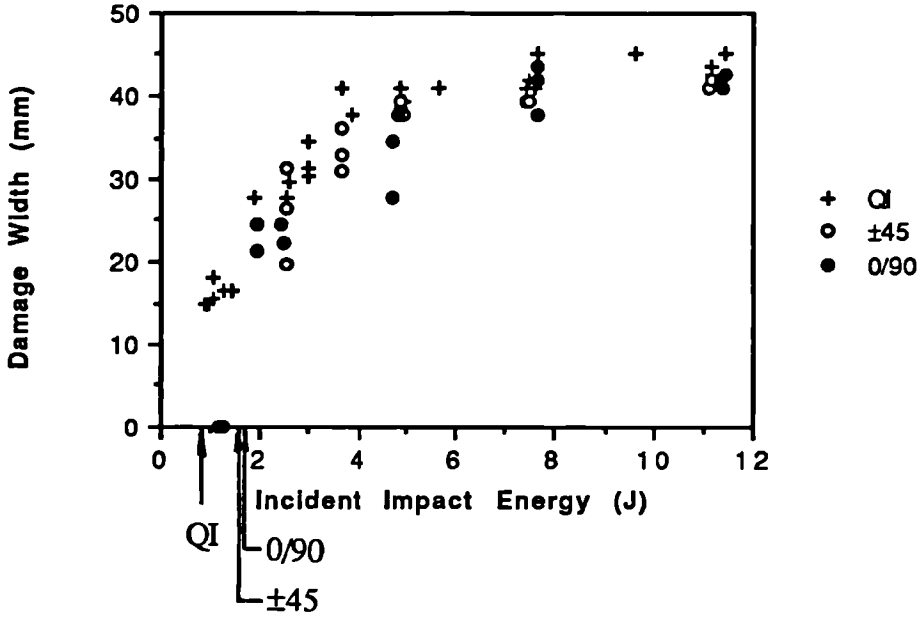

Damage Initiation Energy

Fig 5.20 (b) Effect of stacking sequence on damage width. Material, TCE-QI and QI*-16-55.

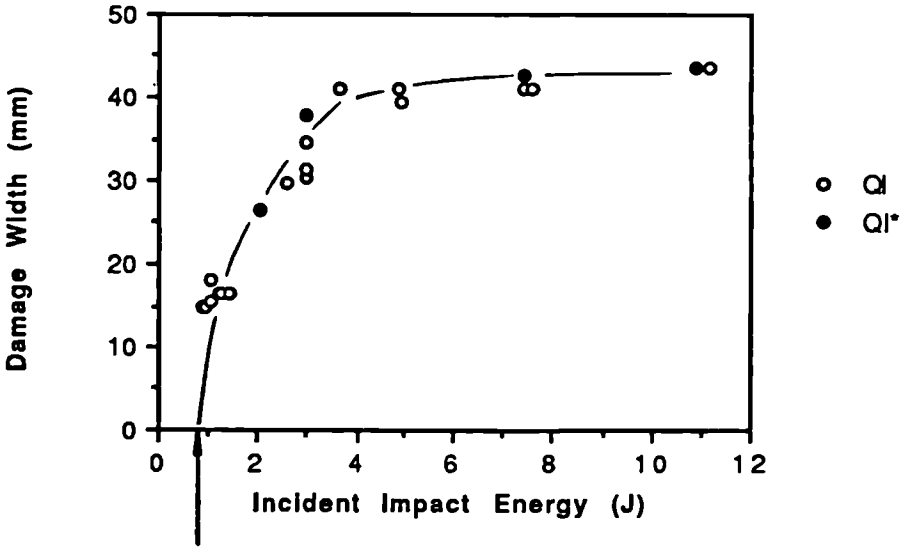

Damage Initiation Energy

Fig 5.21 Effect of material thickness on damage width. Material, TCE-QI-16, 24 and 32-55.

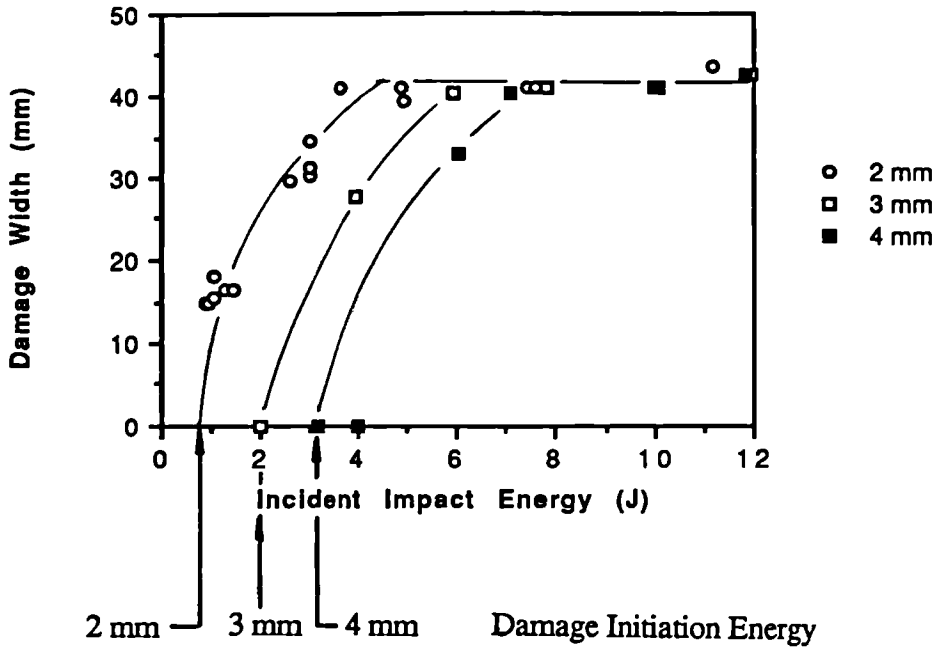

Fig 5.22 Effect of material on damage width. Material, TCE, CE, GRP, APC-QI-16-55.

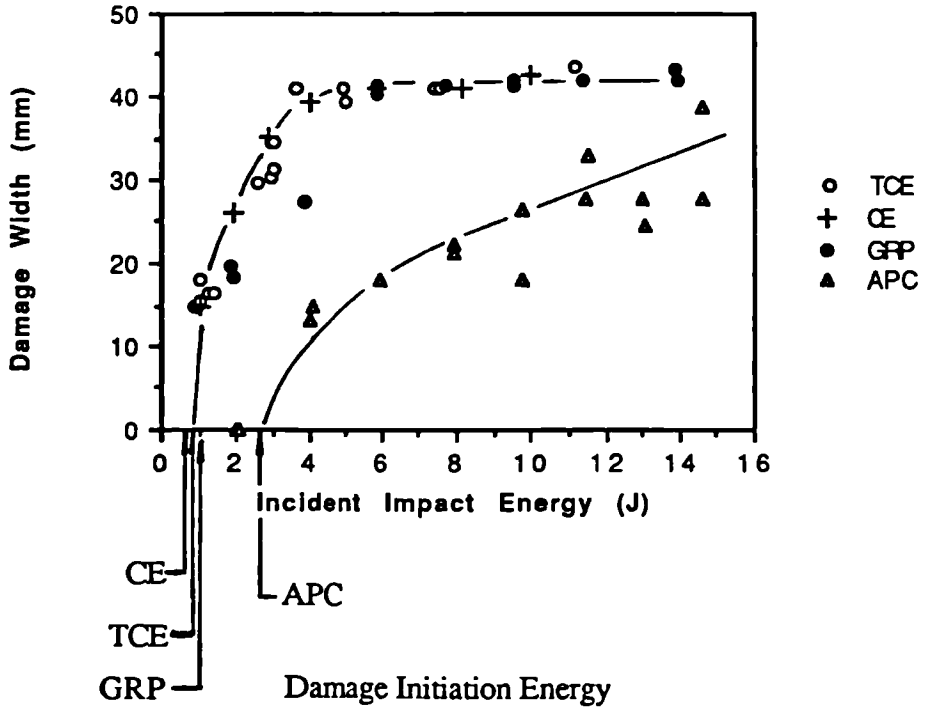

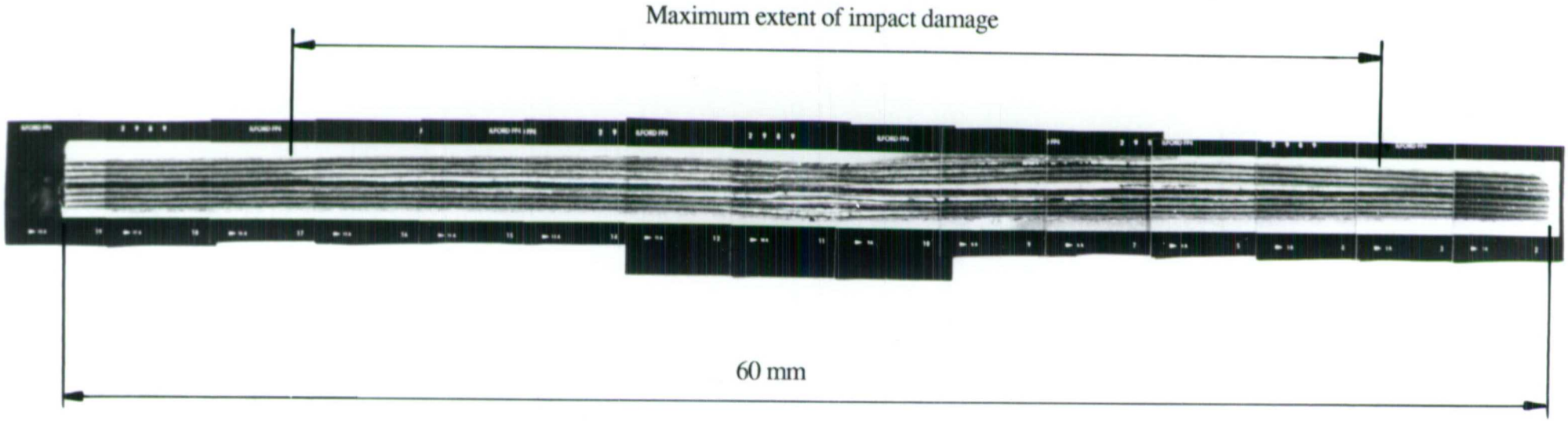

Spec No 49/7. Incident Impact Energy 11.89 J.

Fig 5.23 Montage of 35 mm contact prints showing general view of impact damage in a sectioned TCE-QI-16-55 specimen.

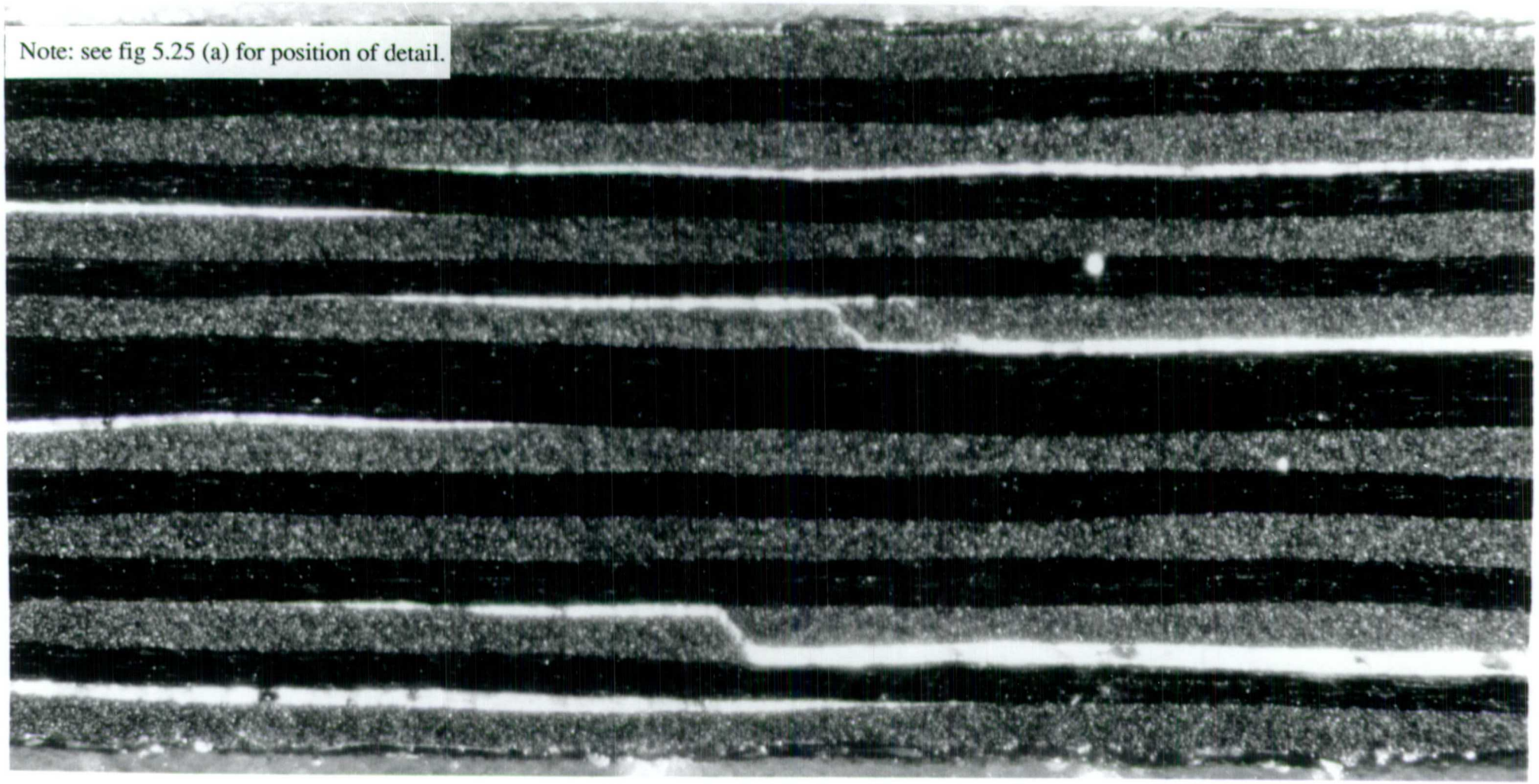

Scale

1 mm

Fig 5.24 Detail of impact damage in TCE-0/90-16 material. Spec No 49/3. Incident Impact Energy 1.78 J.

Fig 5.25 Schematic diagrams showing the through thickness distribution of damage in TCE specimens.

(a) TCE-0/90-16	Spec No 49/3	Incident Impact Energy 1.78 J
(b) TCE-0/90-16	Spec No 49/5	Incident Impact Energy 5.01 J
(c) TCE-0/90-16	Spec No 49/7	Incident Impact Energy 11.89 J

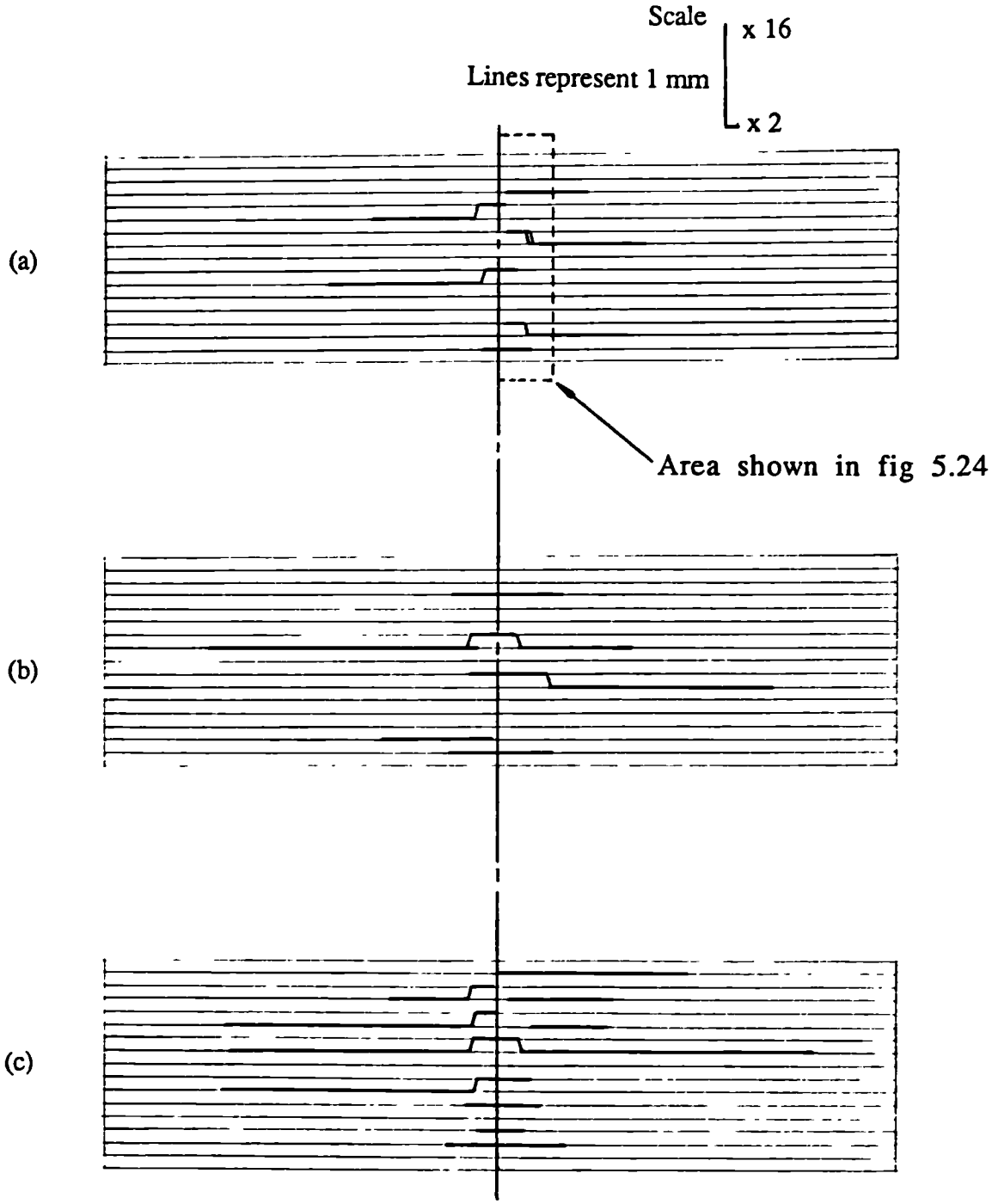

Fig 5.25 continued.

(d) TCE-QI-16	Spec No 48/2	Incident Impact Energy 1.50 J
(e) TCE-QI-16	Spec No 48/4	Incident Impact Energy 3.99 J
(f) TCE-QI-16	Spec No 48/7	Incident Impact Energy 10.01 J

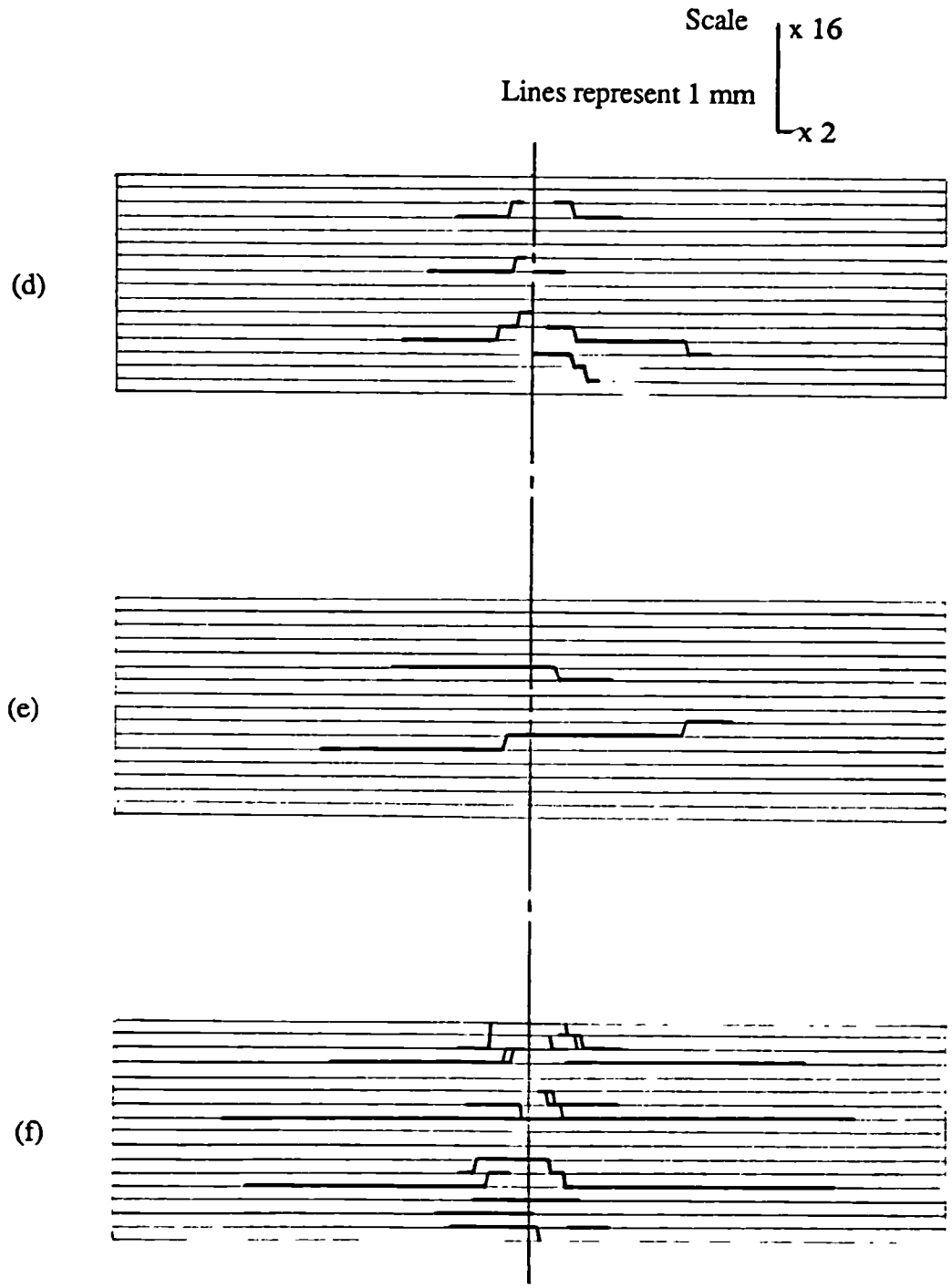

Fig 5.25 continued.

(g) TCE-QI-24	Spec No 50/6	Incident Impact Energy 2.98 J
(h) TCE-QI-24	Spec No 50/7	Incident Impact Energy 5.06 J
(i) TCE-QI-24	Spec No 50/9	Incident Impact Energy 11.96 J

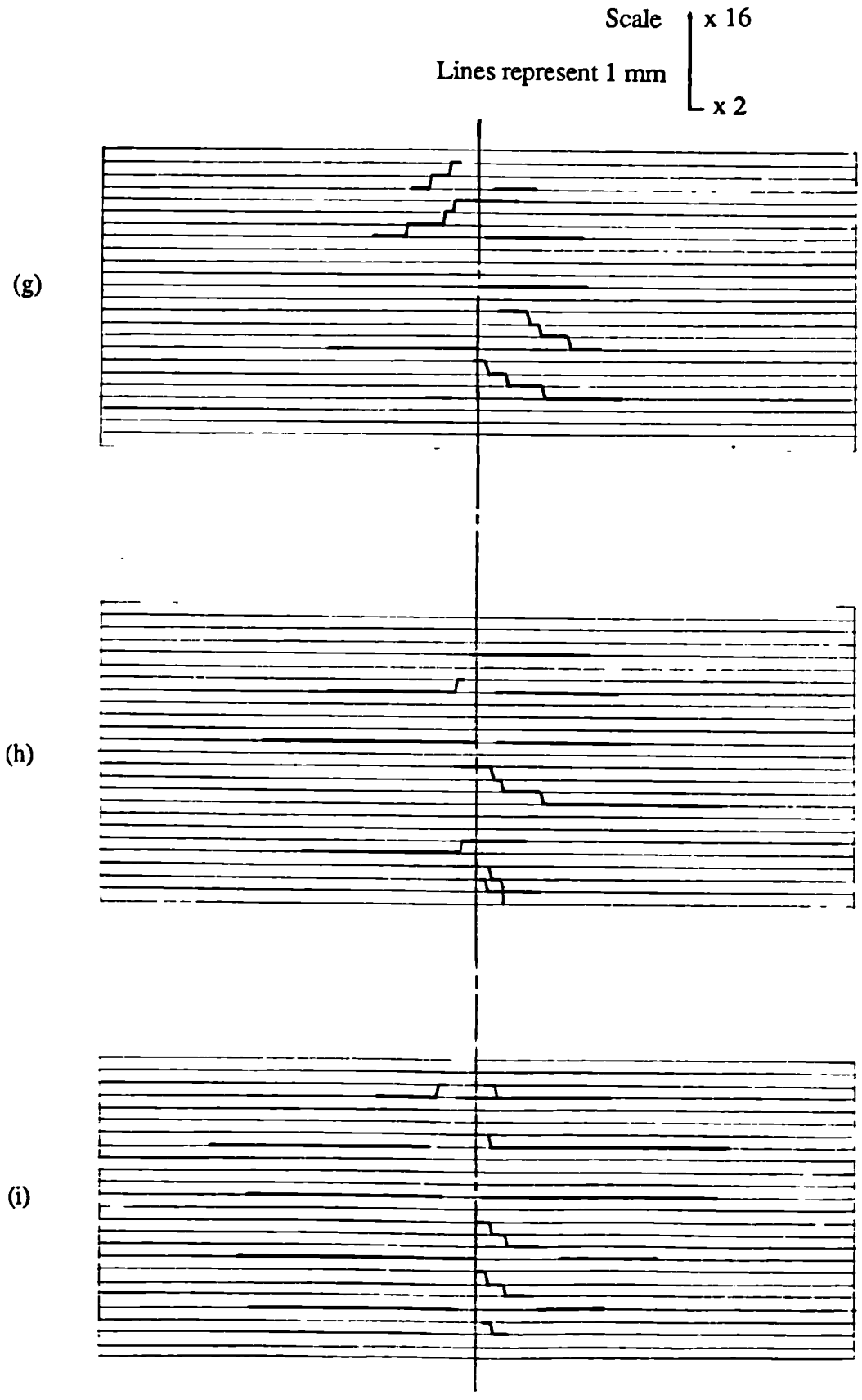

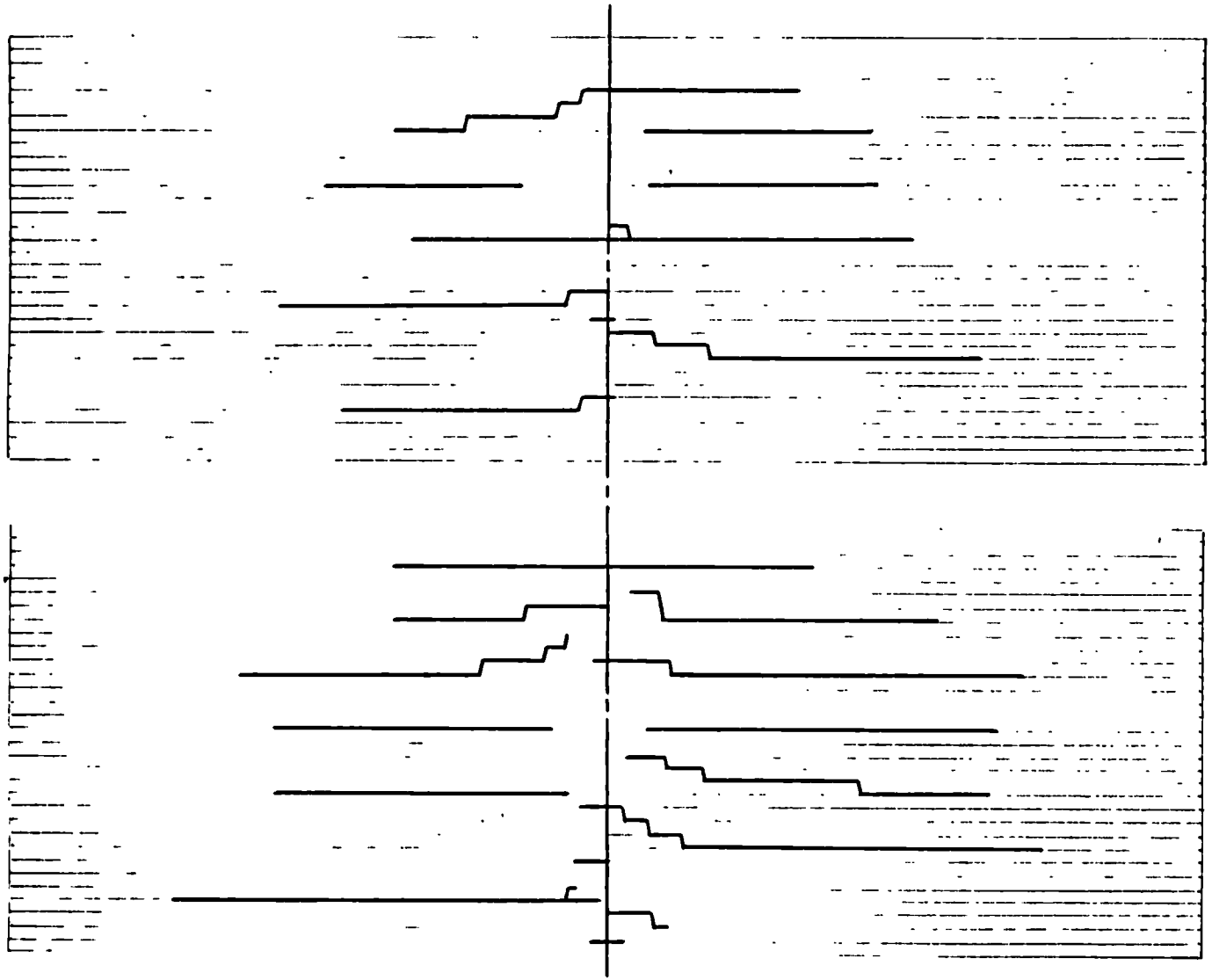

Fig 5.25 continued.

(j) TCE-QI-32 Spec No 51/7 Incident Impact Energy 5.97 J

(k) TCE-QI-32 Spec No 51/8 Incident Impact Energy 11.96 J

TCE-0/90-16

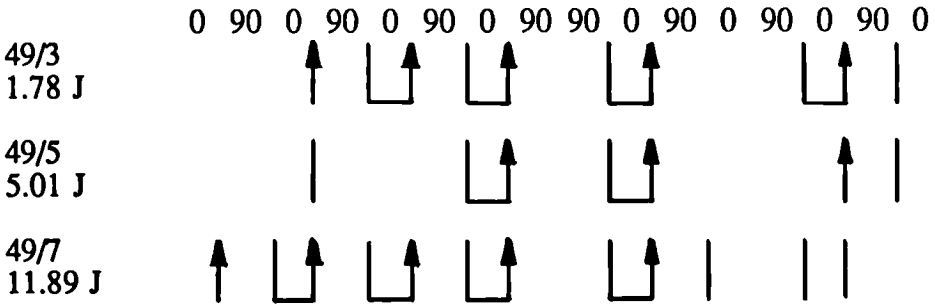

Notes:

1 Top ply (i.e. impacted surface) is shown on left hand side above.

2 Lines with arrow heads denote 'major' delaminations (i.e. than 5 mm from impact centre line) and lines without arrow heads denote 'minor' delaminations. Horizontal connecting lines indicate positions of matrix shear cracks.

Fig 5.26 (a) Positions of Delaminations for TCE-0/90-16 Material

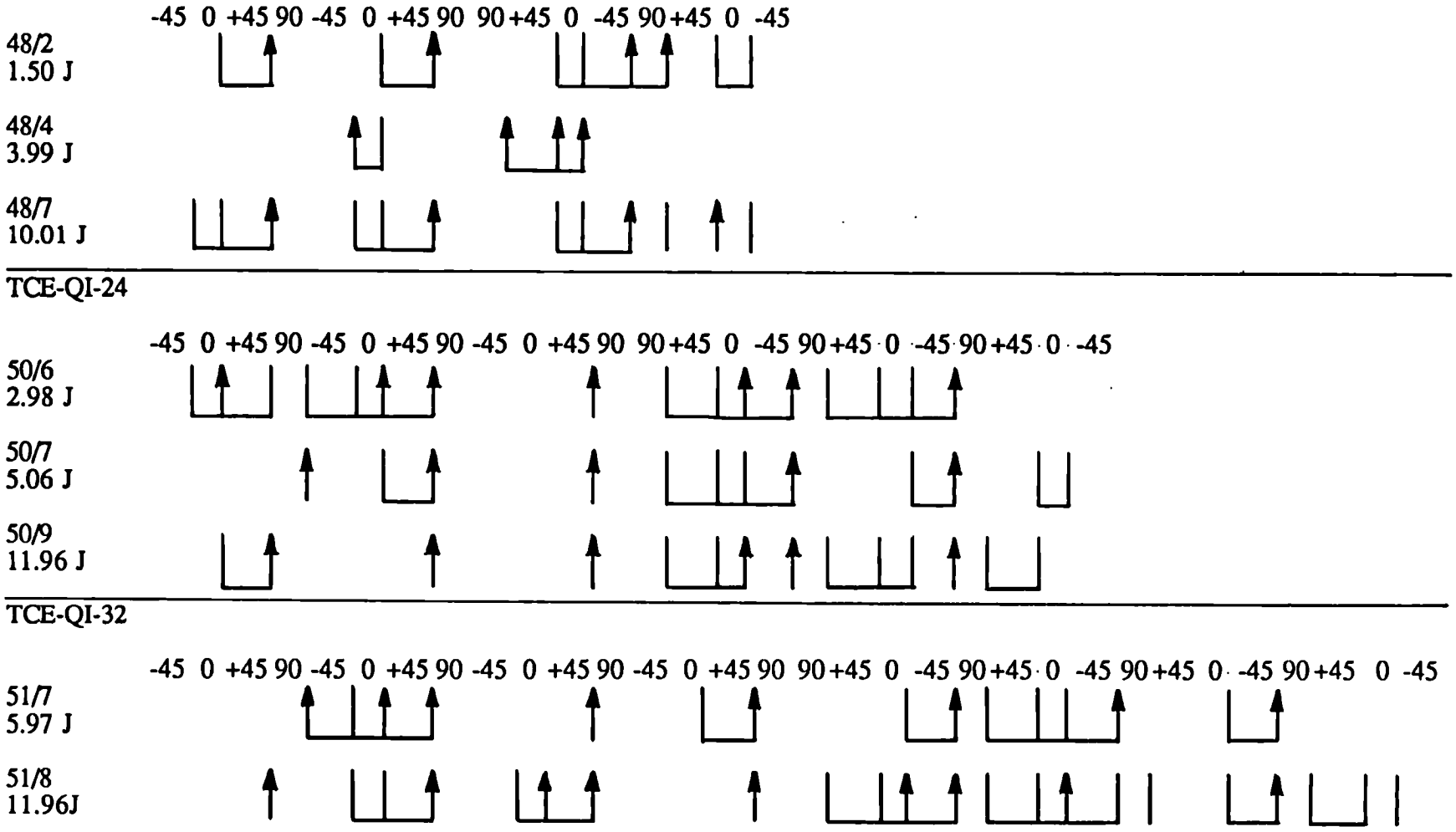

Fig 5.26 (b) Positions of Delaminations for TCE-QI Material

TCE-0/90-16

Specimen No	Impact Energy (J)	Number of 'Minor' Delaminations	Number of "Major' Delaminations	Total
49/3	1.78	5	5	10
49/5	5.01	4	3	7
49/7	11.89	7	5	12

TCE-QI-16

Specimen No	Impact Energy (J)	Number of 'Minor' Delaminations	Number of "Major' Delaminations	Total
48/2	1.50	6	4	10
48/4	3.99	1	4	5
48/7	10.01	8	4	12

TCE-QI-24

Specimen No	Impact Energy (J)	Number of 'Minor' Delaminations	Number of "Major' Delaminations	Total
50/6	2.98	9	7	16
50/7	5.06	7	5	12
50/9	11.96	8	6	14

TCE-QI-32

Specimen No	Impact Energy (J)	Number of 'Minor' Delaminations	Number of "Major' Delaminations	Total
51/7	5.97	7	8	15
51/8	11.96	13	9	22

Fig 5.26 (c) Numbers of delaminated interfaces in sectioned specimens

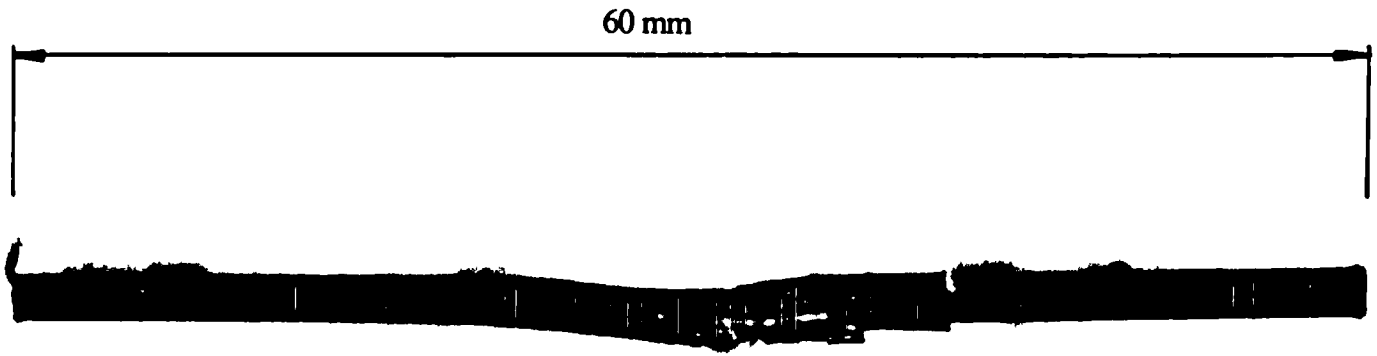

Fig 5.27 Photograph of sectioned APC-QI-16-55 specimen showing permanent plastic deformation after impact testing. Spec No 53/4. Incident Impact Energy 15.14 J.

Fig 5.28 Data from fig 5.9 (a) replotted.

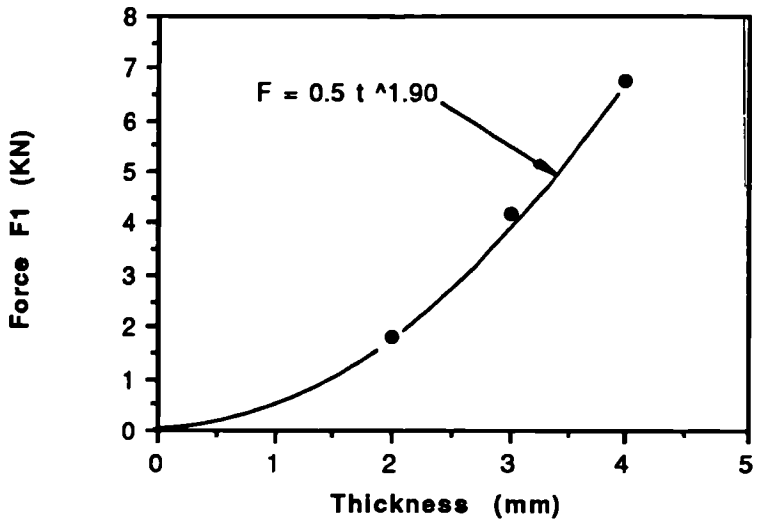

6 Compression Testing of Initially Undamaged Specimens

6.1 Introduction

In this chapter the results of compression tests on initially undamaged specimens will be presented and discussed. A limited number of tests were carried out to give some indication of the properties which could be expected for the test geometry for later comparison with the properties of impact damaged specimens.

6.2 Compression Strength and Modulus

6.2.1 Results

The force - time curves recorded during the tests were converted to stress - nominal strain curves using the method described in section 3.2.3.2. Typical examples are shown in fig 6.1(a) for the three tests on TCE-QI-16-55 and fig 6.1(b) for the tests on GRP-QI-16-55. Initial regions of slightly lower slope on the curves are caused by the specimen being 'bedded-in' to the ABG. A region of linear stress/strain response was followed by non-linear behaviour up to failure. The degree of non-linear behaviour observed depended on the material being tested. More non-linear behaviour was observed for the GRP material than the TCE material. Fig 6.1(c) shows the stress - strain curves for the two materials plotted on the same axes for comparison. The majority of failures were characterised by a sudden drop in load accompanied by a loud report. In a few cases a slightly more progressive failure was observed, subsidiary load peaks were evident on the stress - strain curves for this type of failure. The majority of the failures occurred in the region of the specimen which was not supported by the ABG; i.e. between the loading plate and the top of the side supports on the ABG itself (See fig 3.6). These compression failures were characterised by local crushing and evidence of shear deformation. Photographs of typical failures are shown in fig 6.2. A smaller number of failures occurred by end-crushing. C-scans revealed that extensive delamination was associated with this type of failure. A photograph of an end crushing failure is shown in fig 6.3. However no trend was apparent in the strength values for the two different types of failure and consequently the type of failure was not considered when calculating the average strength values.

The average compression moduli and strengths are given in table 6.1. Three tests were carried out for each of the materials listed. The average modulus and strength and nominal standard deviations are tabulated for each material tested. (The standard deviation quoted is nominal because a minimum of five results are usually considered to be required for an

accurate estimate of the standard deviation to be made, (note: no value of standard deviation has been quoted where there were less than three results). The modulus and strength values for each specimen can be found in appendix B. Where the results are available they are listed at the top of each table in the rows corresponding to an impact energy of zero joules. In the case of the ±45 specimens it is not possible to quote a failure stress because the gap between the anti-buckling guide (ABG) and the loading plate was closed before catastrophic failure occurred. In the case of the 32 ply TCE-QI material only one specimen failed, the load required to fail the other two specimens exceeded the capacity of the machine (100 KN).

6.2.2 Effect of Specimen Width and Lay-up

The effect of specimen width on the plate modulus was found to vary with lay-up. For the 0/90 material, increasing the specimen width led to a decrease in the measured plate modulus. Fig 6.4 shows that this decrease appears to be almost linear over the range of specimen widths tested. For the QI material, an initial increase in plate modulus is followed by a decrease as specimen width is increased. Little effect was observed for the ±45 orientation, the plate modulus remaining almost constant over the range of specimen widths investigated.

The 0/90 specimens had the highest plate moduli followed by the QI and ±45 lay-ups. This was the trend expected from laminate analysis. Fig 6.5 shows modulus plotted as a function of the proportion of ±45 fibres in the material. The measured moduli are much lower than those calculated using laminate theory (see Halpin (1984) for details of method). The data used in the calculations was taken from Ciba-Geigy (1988) and was obtained using the ASTM D-695 test method which gave values of 161 GPa for E_0, and 11.5 GPa for E_{90}. (Values of 5 GPa and 0.3 were assumed for the in-plane shear modulus and Poissons ratio respectively). The reason for the discrepancy between the measured and calculated moduli is that the specimens buckled during the tests performed for this work, whereas the data used in the calculations was obtained using a face supported specimen, designed to prevent buckling.

Fig 6.6 shows the effect of specimen width on compression strength. The trends are very similar to those already observed for the variation of plate modulus with specimen width. As was explained previously, a failure stress could not be measured for the ±45 specimens. Instead the stress at which a nominal strain of 3% was reached has been plotted in fig 6.6.

The difference between the strengths of the QI (360.4 MPa) and 0/90 (473.3 MPa) materials is quite large when compared for the 45 mm wide specimens. However the differences between the results for the 55 and 75 mm wide specimens are small in comparison with the scatter in the data. The error bars indicating ±1 standard deviation have been omitted from fig 6.6 for clarity, however the data can be found in table 6.1.

6.2.3 Effect of Thickness

A linear relation between specimen thickness and plate modulus was observed for the TCE-QI material. Fig 6.7 (a) shows that the plate modulus decreased with increasing thickness. At the same time the measured strengths showed a tendency to increase as thickness was increased. Fig 6.7 (b) shows a clear increase in strength between the 16 and 24 ply materials. After this the trend is less clear, one of the 32 ply specimens failed at a similar strength to the 16 ply material, while two more specimens exceed the capacity of the loadcell.

6.2.4 Effect of Material

The plate moduli and strengths measured for the four materials are shown in figs 6.8 (a) and (b) respectively. The properties of the carbon fibre reinforced materials were found to be very similar, in spite of the fact that a range of fibres and matrix materials were tested. The slight difference in the fibre stacking sequence of the CE material does not appear to have had a large effect. As would be expected, both the modulus and strength of the GRP material are substantially lower than the carbon fibre reinforced materials.

6.3 Buckling Behaviour

A limited number of tests were carried out to assess the effect of material type and lay-up on the buckling behaviour of the specimens. The experiments were designed to find the deformed profiles of the specimens and the amount of out of plane displacement. Details of the test method used are given in full in section 3.2.3.3.

6.3.1 Results for GRP-QI-16-55

A complete set of data was obtained for the three GRP specimens. Tests at low loads were performed to reveal the deformed shape of the specimens; the deflection at the position of maximum deflection was then measured up to failure for each specimen.

The profiles of the deformed specimens are shown in fig 6.9. As the load was increased each of the specimens were observed to buckle, adopting a roughly symmetrical two lobed profile in the vertical direction and a single buckle in the other direction. The load versus lateral deflection curves (at position no 2) for the three low load tests are shown fig 6.10. There are small differences in the exact behaviour of each specimen when compared on this scale. However when the load - deflection curves for position number 2 up to failure are plotted (fig 6.11) it is apparent that the three specimens are behaving in a very similar manner. The curves show that the specimens have buckled, however it is not possible to define a buckling load since instability buckling has not occurred. Instead a gradual increase in the lateral deflection was observed (the initial load increase with no measured lateral deflection probably being a reflection on the method used to measure the deflection rather than the actual behaviour).

In general a good degree of repeatability was observed for these tests. When the results of the tests at low loads are compared with the results of the tests to failure, almost identical load - lateral deflection curves were followed for two of the specimens (fig 6.12), however a slight difference between the two tests was apparent for specimen 25/2.

6.3.2 Effect of Lay-up

The effect of lay-up on the buckling behaviour was assessed by comparing the results for the 75 mm wide specimens. Fig 6.13 shows the deflected profiles, and fig 6.14 the load versus lateral deflection curves (for position 3) for the 0/90 and QI specimens tested. All of the specimens deformed in the same manner, however the deformed profiles are different than were observed for the 55 mm wide GRP specimens. This is thought to be a specimen geometry effect rather than a material effect. A clear (but small) difference is observed between the results for the 0/90 and QI specimens. It was reported above that the strengths of the 0/90 and QI specimens for 75 mm wide specimens were very similar, the results in fig 6.14 suggest that failure occurred at slightly larger deflections for the 0/90 material.

Tests to monitor the deflections of the ±45 specimens were also carried out. No out of plane deflections were observed, i.e. the specimen did not appear to buckle at the loads applied in these tests, which were curtailed when the loading plate fouled the ABG. Hence the results would lie on the force axis in fig 6.14, the maximum force being of the order of 20 KN. This is put into perspective when compared with the results for the QI and 0/90 lay-ups which have only just started to buckle at this load.

6.3.3 Effect of Material

Fig 6.15 shows the deformed shapes for the TCE-QI-16-55 material. (The results for the GRP-QI-16-55 material have already been plotted in fig 6.3.1). The deformed profiles are the same for each type of material, confirming the observation made previously that the change in deformed shape for the 75 mm wide TCE-QI-16-75 material was due to the change in specimen shape rather than a material effect. The load versus lateral deflection curves are shown in fig 6.16. All of the curves relate to position 2 on the specimen. As was found previously, for plate modulus and strength measurements the results are clearly divided into those for the carbon fibre reinforced materials and those for the glass fibre reinforced material. As would be expected the lower modulus GRP exhibits higher lateral deflections at lower loads than the higher modulus carbon reinforced materials. These limited results suggest that the particular type of carbon fibre and matrix material have little effect on the buckling behaviour of these materials. One of the curves for the TCE material (specimen number 4/2) is set slightly apart from the other curves for the carbon reinforced materials. This specimen failed at a stress of 344.2 MPa compared to 416.7, 443.6 and 443.4 MPa for the other carbon reinforced specimens shown on the graph.

6.4 Discussion

6.4.1 Introduction

The main reason for testing undamaged material was to provide a base - line strength against which the strength of impact damaged specimens could be compared. In addition a more limited investigation of the buckling behaviour of these undamaged specimens was undertaken. This data is of interest because when small or intermediate amounts of impact damage are present, the specimen may buckle in a global or mixed mode rather than locally in the area of the impact damage (see fig 1.7) during a post-impact compression test.

6.4.2 Buckling Behaviour

In Chapter 1 (section 1.3.2) it was stated that instability type buckling behaviour is not usually expected in practice because initial specimen curvature or eccentric load introduction means that lateral deflections occur as soon as load is applied. However some of the load versus lateral deflection curves indicate that instability type buckling did occur (see for example fig 6.12 (b)). It is apparent that the instability occurred at much lower

loads than those which would have been predicted, other workers have found that the predicted instability buckling load is only ever approached for initially imperfect specimens (see section 1.3.2). It is possible that out-of-plane deformations did occur in all cases as soon as load was applied but in some cases were too small to be measured by the method used, therefore giving the impression that instability buckling had occurred. In other cases (see for example fig 6.12 (a)) lateral deflections were apparent as soon as load was applied and instability buckling was not observed. In the long run it would appear that discussion about which mechanism was responsible for buckling is of little importance because it is evident from figure 6.11 that once the load and lateral deflection have increased (beyond approximately 1 mm in this case) the load - deflection curves follow very similar paths.

Large differences between the buckling behaviour of the carbon and glass fibre reinforced materials were observed (fig 6.16). The carbon fibre reinforced materials are more resistant to buckling and suffer smaller lateral deflections than the glass reinforced material. These differences occur simply because the modulus of the carbon fibres is much greater than that of the glass fibres. The type of matrix material does not appear to have much influence with the APC and TCE materials showing similar behaviour. This is presumably because the modulus of the matrix is small compared to the modulus of the fibres and therefore has only a small effect on the total stiffness of the material. It is interesting to note that, for all of the materials, the lateral deflections at failure are quite small. In fact they are of the same order of magnitude as the thickness of the specimens.

The effect of lay-up on the buckling behaviour varied considerably. The results are limited but indicate that there are only small differences between the behaviour of QI and 0/90 materials when the load versus lateral deflection behaviour is compared (fig 6.14). The situation was completely different for the ±45 specimens where no lateral deflections could be measured, even when nominal compressive strains of 3% had been reached. Leissa (1985 (b)) reports that analysis of the buckling behaviour of laminates with large numbers of alternating (±θ) plies reveals that the maximum buckling stress is obtained for $\theta = 45$ degrees. The buckling stress can be more than twice the value obtained for unidirectional materials (i.e. for $\theta = 0$ or 90 degrees). No explanation is offered by Leissa for this behaviour. The results presented in this chapter tend to confirm that the ±45 specimens were more resistant to buckling than the QI and 0/90 specimens. Having said this the loads were of the order of 20 KN (at a nominal strain of 3% when the tests were stopped) and at the same load the QI specimens had only just begun to show signs of lateral deflection (see fig 6.16). Inspection of the ±45 specimens suggests that the reason that they did not buckle is that the material was able to deform in the plane by a shearing

mechanism and the deflection was produced by this shearing rather than by the material buckling and deforming out of the loading plane.

One other observation of interest was that a change in buckling mode was evident (for both the QI and 0/90 lay-ups) when the specimen width was increased from 55 to 75 mm. The probable reason for this is that the narrower specimen obtains more support from the ABG than the wider specimen. Because of the extra support the specimen is more stable and a higher buckling mode is adopted. These differences in buckling mode could be important in the post-impact compression test, when specimens with intermediate amounts of impact damage are being tested. As has already been mentioned for intermediate amounts of impact damage the specimen can buckle in a mixed mode with both local and global buckling occurring. So for specimens of different widths, different modes of global buckling can occur which could affect the local stress field around the impact damage. In the case of a 55 mm wide specimen the impact damage would lie on a node and in the case of a 75 mm wide specimen on an anti-node. This information may be important when looking at the effect of specimen width on residual compression strength.

6.4.3 Strength Measurements

6.4.3.1 Failure Modes

For the materials tested two different failure modes were observed, both yielding similar strength values. In a small number of specimens end crushing failures were evident. It seems likely that this type of failure was initiated by stress concentrations caused by slightly uneven specimen ends. Instead of the load being introduced evenly across the full width of the specimen it became concentrated at slightly raised areas causing failure to occur. The problem is caused by using a slitting saw to cut the specimens. Because the saw is thin it can wander during the cutting operation. The problem could be overcome by improving the method used to manufacture the specimens. For example by milling or grinding the ends to ensure that they are flat. Because this problem occurred in only a very small number of cases when undamaged specimens were being tested (and not at all for the post-impact compression tests) the slitting saw was used to cut all of the specimens.

The majority of failures occurred in the unsupported region of the specimen, between the end of the side supports and the grips of the end loading plate. Failures in the same region were reported by Rhodes et al (1979). They suggest that strain concentrations develop in the unsupported region due to local deformations. This appears to be a reasonable explanation. However they also suggest that "the failures occurred at the onset of

buckling". Since the lateral displacements in the unsupported region were not monitored, no evidence can be offered to confirm or deny this observation. Having said this the results reported in this section clearly show that global specimen buckling occurred well before final failure and it would seem likely that the material in the unsupported section would also have buckled. Whether failure occurs at or after buckling in the unsupported region the problem could be overcome by supporting the specimen over its entire length by reducing the width of the end grips and extending them down so they fit inside the side supports. This method has been adopted by SACMA (Anon, 1988 (b)) for the ABG used for post-impact compression strength measurements. The type of failure which would now be produced is not known, but whatever the failure mode the results indicate that undamaged specimens of this size supported in ABG's of this type cannot be made to fail before global buckling has occurred.

In spite of the problems involved with measuring the strength of undamaged specimens supported in ABG's (specifically designed to prevent buckling at the loads required to cause failure in impact damaged specimens) it is preferable to retain the same size specimen and loading conditions if the results are to be of any use for later comparison with the results of post-impact compression tests. This is because the measured strength of undamaged material is dependent upon specimen geometry. This will be discussed in the following section.

6.4.3.2 Effect of Specimen Geometry

(a) Specimen Width

Port (1982) measured the compression strength of small plate like specimens (135 mm long and varying in width between 50 and 76 mm) supported by an ABG. Symmetric laminates with 24 plies (giving an approximate thickness of 3 mm) and a fibre lay-up of [0, ±45] were used. For specimens with 16.7% (or less) of 0 degree plies no effect of specimen width on strength was found. For laminates with more than 16.7% of 0 degree plies the strength was found to decrease with increasing specimen width over the range of widths tested. Port suggests that this variation may be due to non-uniform load input.

The results presented in this chapter appear to confirm the observations made by Port. Consider first the results for the ±45 specimens. For the reasons already discussed the ±45 specimens could not be failed and the stress at a nominal 3% strain has been plotted in fig 6.6 instead. Although the specimens did not fail it is suggested that the values obtained are probably quite good estimates of the strength under these loading conditions.

The stress - strain curves were very flat by the time the strain had reached 3% and further loading would probably not have increased the stress appreciably. Ciba-Geigy (Anon, 1988 (a)) quote a value of 232 MPa for the compression strength of a 24 ply ±45 laminate for this material which is between approximately 26 and 41 % larger than the values of stress at 3% strain plotted in fig 6.6. The results in fig 6.6 for the ±45 material appear to support the observation made by Port (1982) that for angle ply dominated lay-ups specimen width has little effect on strength.

Fig 6.6 shows that for 0/90 and QI materials specimen width does have a considerable effect on the measured strength. The trend for the 0/90 material is the same as that described by Port (1982). However the trend for the QI material is slightly different. The strength values measured for the 45 mm wide QI specimens are almost certainly low because of defective material rather than the trend being genuine. It was reported in Chapter 4 that the ILSS was noticeably lower for laminates 2, 3 and 4 from which the 45 mm wide specimens were made. In Chapter 5 the bending stiffness of this material was found to be lower. The results in fig 6.4 show that the plate modulus is lower than would be expected. It is speculated that the same trend in plate modulus and strength would be found for the QI lay-up as for the 0/90 lay-up if tests on the 45 mm were to be repeated, using material of the same quality as was used for the 55 and 75 mm wide specimens.

The results reported in this chapter appear to confirm those of Port (1982). However it seems unlikely that non-uniform load input would produce this trend in measured strength. If non-uniform load input were responsible why are the results for the 0/90 and QI materials affected while the ±45 material is unaffected? The suggestion is that width effects are related to the buckling behaviour of the specimens. There are two pieces of evidence which appear to support this suggestion. Firstly the ±45 specimens were not observed to buckle and it was found by Port (1982) and indicated in this work, that the measured strength does not vary with specimen width. Secondly the trends for the variation of plate modulus (fig 6.4) and strength (fig 6.6) are very similar for all three lay-ups. It is assumed that the variation in both plate modulus and strength are related to the buckling behaviour of the specimens. In Chapter 1 (see fig 1.4) the predicted trends in buckling behaviour with specimen width were presented. In the case of the 0/90 material there would appear to be a good correlation between the predicted buckling behaviour and the measured variation of modulus and strength.

(b) Specimen Thickness

Because of the limited capacity of the load-cell it was not possible to obtain a strength value for the 32 ply thick material. However it is speculated that the strength would continue to increase with increasing thickness. One unexpected trend was that the plate modulus fell as the material thickness was increased, indicating that the specimen becomes less stable as thickness is increased. This means that the strength appears to be increasing as the plate modulus is falling, which is different to the situation seen for variations in specimen width where plate modulus and strength followed the same trends.

6.4.3.3 Effect of Material

The absolute values of strength obtained appear to be slightly lower than would have been obtained if a test specifically designed to measure undamaged compression strength had been used. For example Ciba-Geigy quote a compression strength value of 657 MPa for the TCE material (Anon, 1988 (a)). The value was obtained using material with a $[\pm 45, 0, 90]_{3s}$ lay-up and the test recommended by CRAG (Curtis, 1988) for multi-angular laminates. The value measured in this work for the 24 ply material (lay-up $[-45, 0, +45, 90]_{3s}$ was 454.3 MPa obtained using the 55 mm wide specimen. The difference between the values measured using the two different methods is attributed to specimen geometry. As was discussed above the differences in measured strength are attributed to differences in the buckling behaviour of the specimens. The CRAG specimen is much narrower and therefore more stable.

Even though the absolute values of strength measured are low the test appears to produce reasonable comparative results. For example when the strengths of the carbon and glass fibre reinforced materials are compared the test shows that the CFRP materials are stronger than the GRP material which is the expected result. The value obtained for the GRP was 269.1 MPa and around 400 MPa for the CFRP materials (TCE = 401.5 MPa, CE = 398.1 MPa and APC = 414.7 MPa). The ratio of the strengths of the GRP to the CFRP materials lies between 0.68 (269.1 / 398.1) and 0.65 (269.1 / 414.7). This compares very well with the ratio of the strength of unidirectional materials. Ciba-Geigy (Anon, 1984) quote a value of 1200 MPa for the strength of a carbon / epoxy (Fibredux 913-XAS) at room temperature. For the same matrix material with 'E' glass fibres a value of 750 MPa is quoted. The ratio is 0.63 (750 / 1200) which is remarkably similar to the value obtained above.

The results show that when the GRP material failed it had suffered much higher lateral deflections than the CFRP materials (fig 6.16). This is explained by the fact that the glass fibres have a higher strain to failure than carbon fibres. Currently 'high strain' carbon fibres have a strain to failure typically of the order of 2% (maximum), whereas 'E' glass fibres fail at strains of 3%.

As was mentioned above the three CFRP materials were all found to have similar strengths. The similarity between the strengths of the TCE and CE materials was expected because they are quite similar materials. The fact that the APC was stronger than the epoxy matrix materials was slightly surprising. Some authors (see for example Curtis (1987) and Lee (1987)) have reported slightly lower values of compression strength for materials with thermoplastic matrices. The reason given for this is that the slightly lower shear stiffness of these materials reduces the ability of the material to support fibres against local buckling (Curtis, 1987). In this case the failure is thought to have been precipitated by global rather than local buckling and therefore the slightly lower shear stiffness did not affect the results.

6.4.4 Final Comments

The main aim of the work reported in this chapter was to provide base-line strength data for undamaged material. It has been clearly shown that the anti-buckling guide could not suppress global specimen buckling at the loads required to cause failure in previously undamaged specimens. Therefore the values of strength measured are lower than were quoted by Ciba-Geigy using a test specifically designed for the purpose. This and the fact that large variations in strength were observed for variations in specimen width and thickness underlines the importance of using the same testing geometry to gather data on undamaged and damaged material if meaningful comparisons are to be made.

Nb Plate moduli reported in this chapter may be somwhat low as they were calculated using cross head displacement without correcting for loading-train deflection

Material	Average Plate Modulus (GPa)	Standard Deviation (GPa)	Number of Tests	Average Strength (MPa)	Standard Deviation (MPa)	Coefficient of Variation (%)	Number of Tests
TCE-±45-16-45	10.2	0.3	3	See note 1 below	-		3
TCE-±45-16-55	9.6	-	2	See note 1 below	-		3
TCE-±45-16-75	10.7	0.8	3	See note 1 below	-		3
TCE-0/90-16-45	32.1	-	1	473.3	36.0	7.6	3
TCE-0/90-16-55	30.2	0.7	3	426.3	5.5	1.3	3
TCE-0/90-16-75	24.6	0.7	3	321.7	1.7	0.5	3
TCE-QI-16-45	24.0	1.2	3	360.4	38.2	10.6	3
TCE-QI-16-55	25.1	0.8	3	401.5	51.4	12.8	3
TCE-QI-16-75	22.0	0.4	3	307.8	19.1	6.2	3
TCE-QI-24-55	20.9	0.5	3	454.3	14.0	3.1	3
TCE-QI-32-55	18.3	0.4	3	See note 2 below	-	-	3
CE-QI-16-55	24.5	0.6	3	398.1	13.7	3.4	3
GRP-QI-16-55	16.3	0.3	3	269.1	8.6	3.2	3
APC-QI-16-55	23.1	0.3	3	414.7	41.1	9.9	3

Notes:
1) Failure stresses were not obtained for these specimens because the loading plate fouled the ABG before catastrophic failure occurred. The stresses at a nominal strain of 3% are listed in appendix C. Tables C1 to C3.

2) One specimen failed at 400.8 MPa. Capacity of load-cell was exceeded before the other two specimens failed (426.5 and 426.1 MPa)

Table 6.1 Average compression moduli and strengths for compression tests on previously undamaged material.

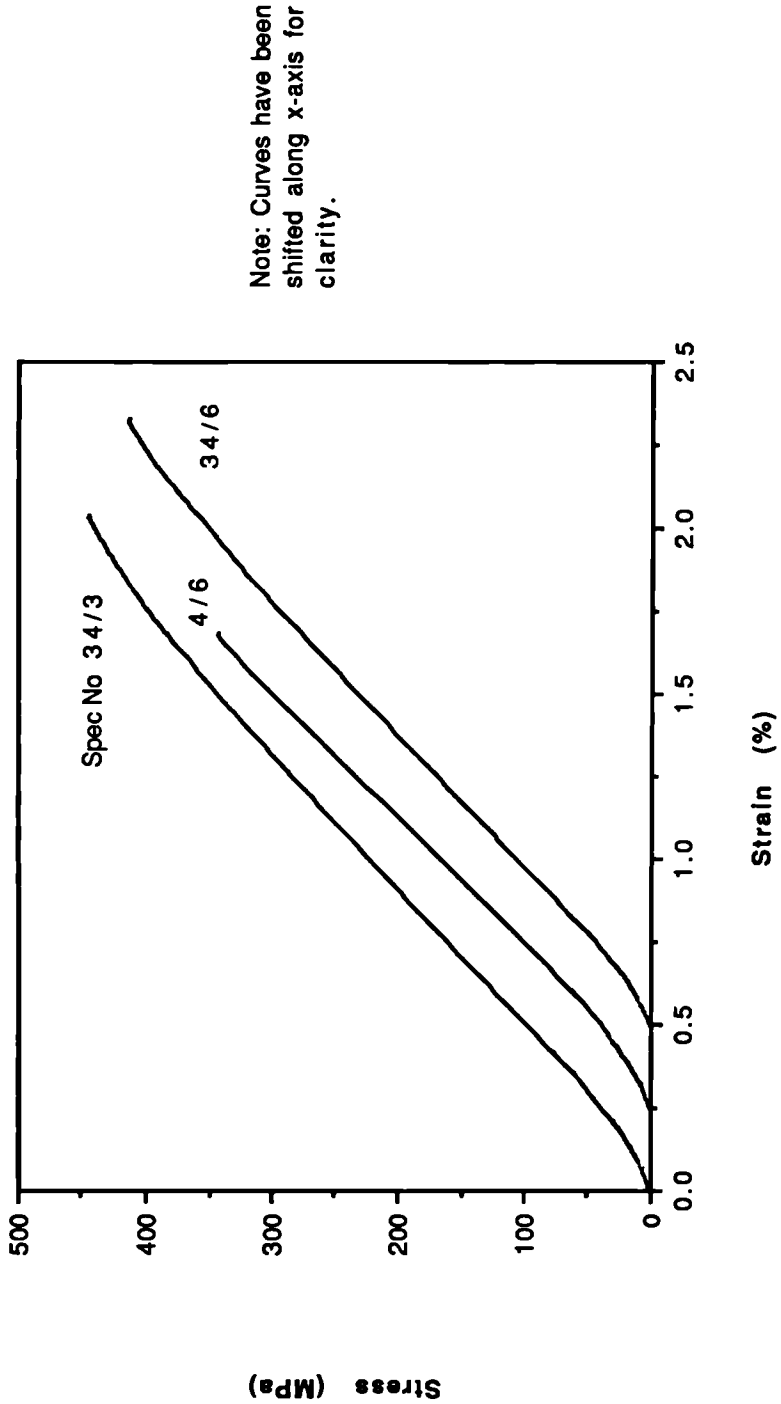

Fig 6.1 (a) Stress - Strain curves for compression tests on previously undamaged specimens. Material, TCE-QI-16-55

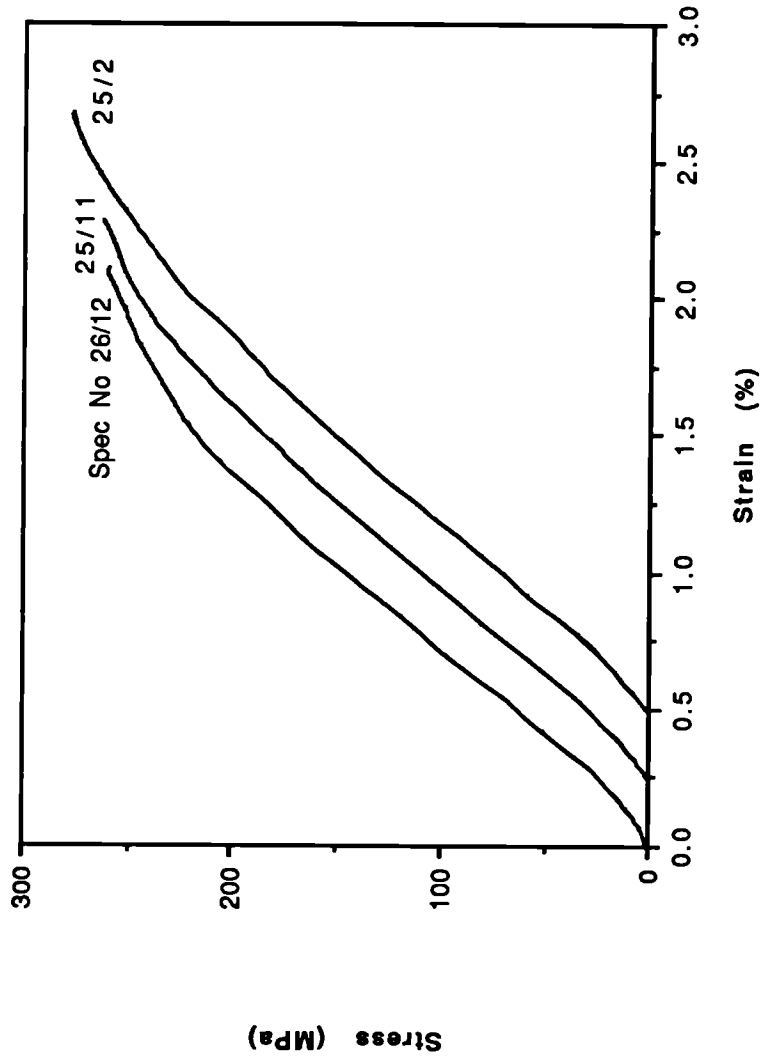

Fig 6.1 (b) Stress - Strain curves for compression tests on previously undamaged specimens. Material GRP-QI-16-55.

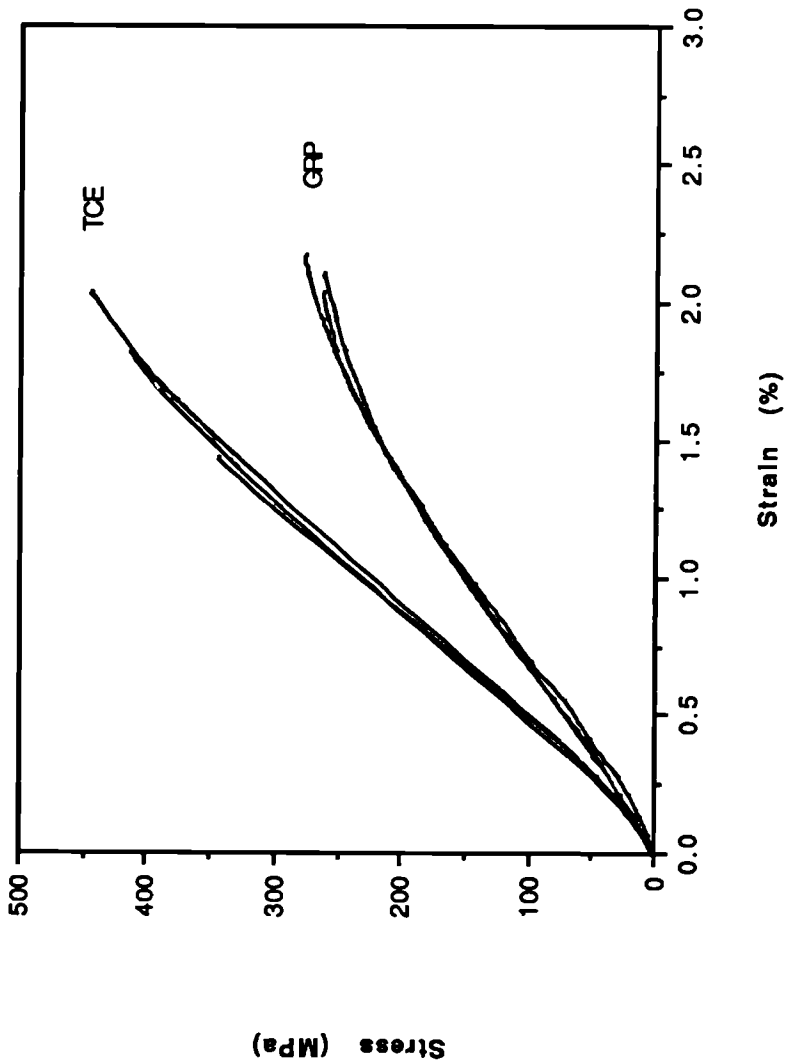

Fig 6.1 (c) Comparison of stress - strain curves for compression tests on undamaged TCE and GRP-QI-16-55 specimens.

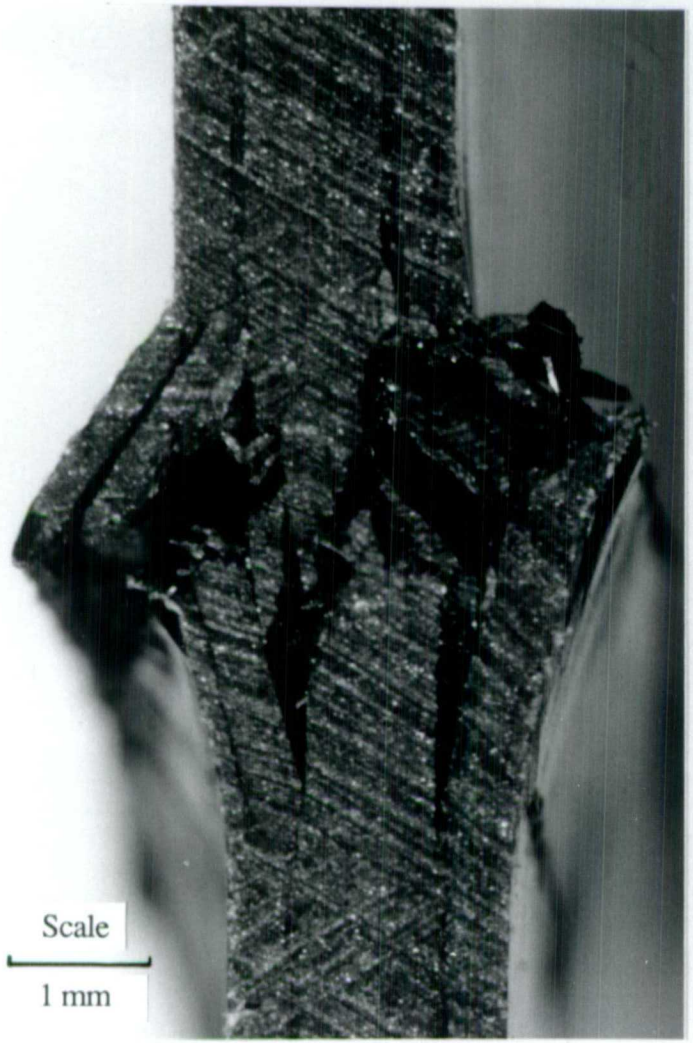

(a) Spec No 21/5. APC-QI-16-55.

(b) Spec No 22/5. APC-QI-16-55.

Fig 6.2 Typical compression failure in unsupported region of specimens.

Fig 6.3 Photograph of an end crushing failure. Spec No 39/2. TCE-QI-24-55.

Fig 6.4 Effect of specimen width on measured plate modulus. Material, TCE-QI, 0/90 and ±45-16-45, 55 and 75.

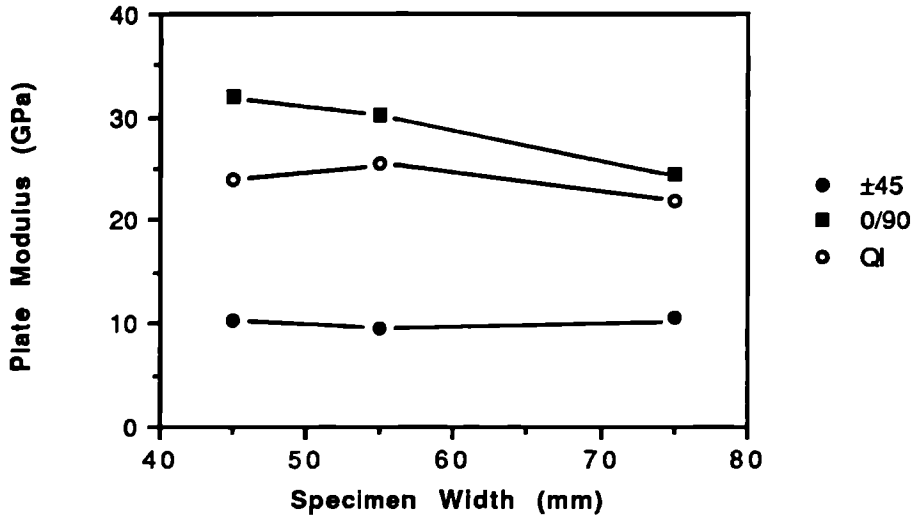

Fig 6.5 Calculated and measured moduli. Material, TCE-QI, 0/90 and ±45,16-45, 55 and 75.

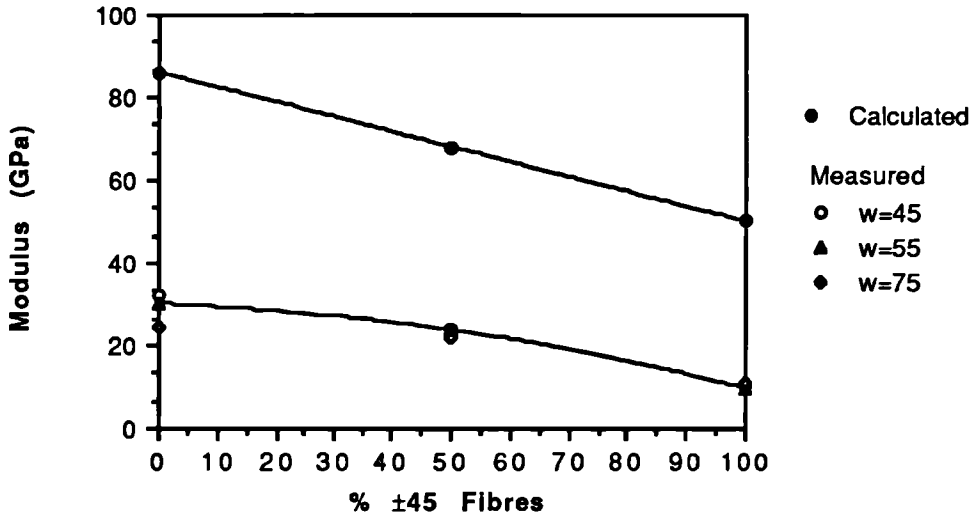

Fig 6.6 Effect of specimen width on compression strength. Material, TCE-QI-16-45, 55 and 75.

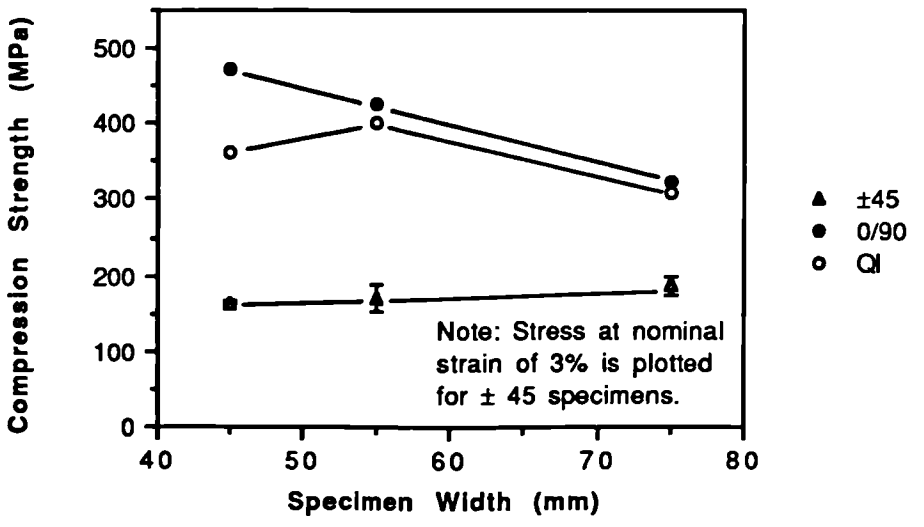

Fig 6.7 (a) Effect of specimen thickness on plate modulus. Material, TCE-QI-16,24 and 32.

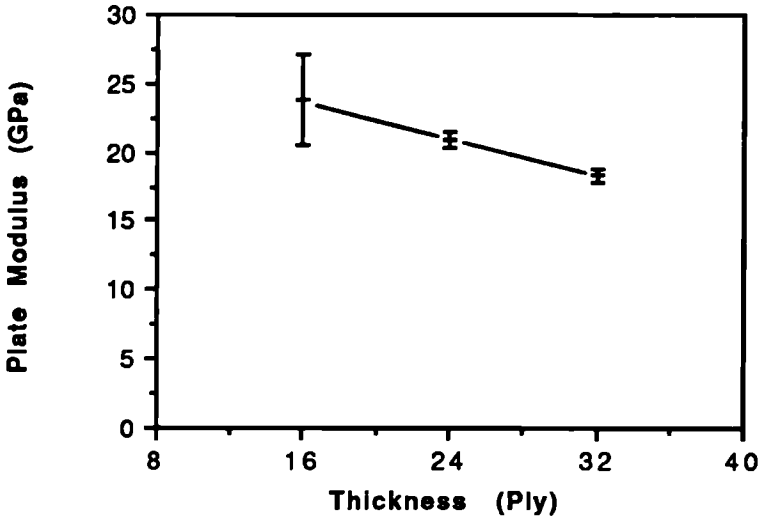

Fig 6.7 (b) Effect of specimen thickness on compression strength. Material, TCE-QI-16, 24 and 32-55

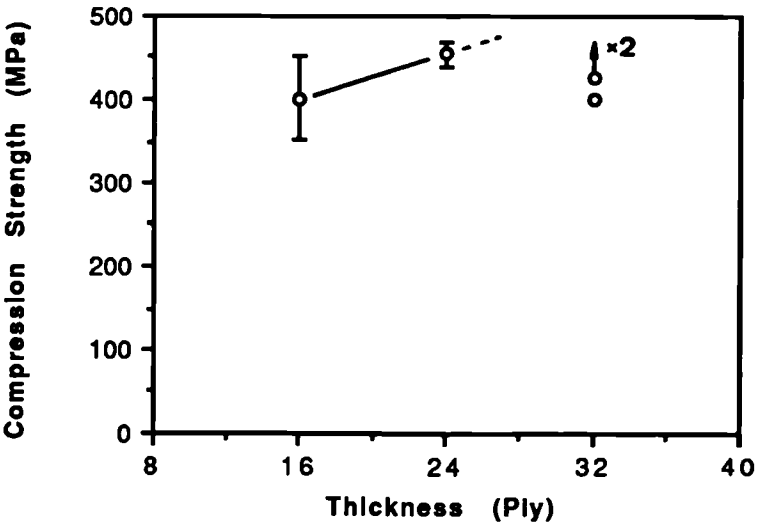

Fig 6.8 (a) Effect of material on plate modlus. Material, TCE, CE, APC, GRP-QI-16-55.

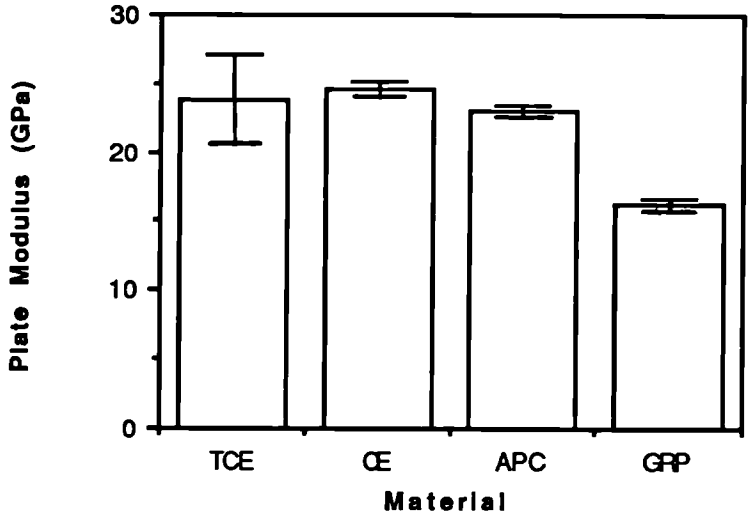

Note CE lay-up is QI*.

Fig 6.8 (b) Effect of material on compression strength. Material, TCE, CE, APC, GRP-QI-16-55.

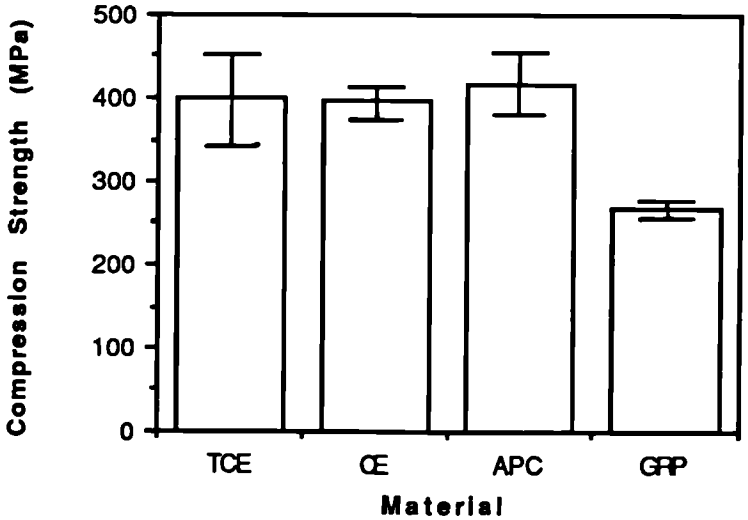

Note CE lay-up is QI*.

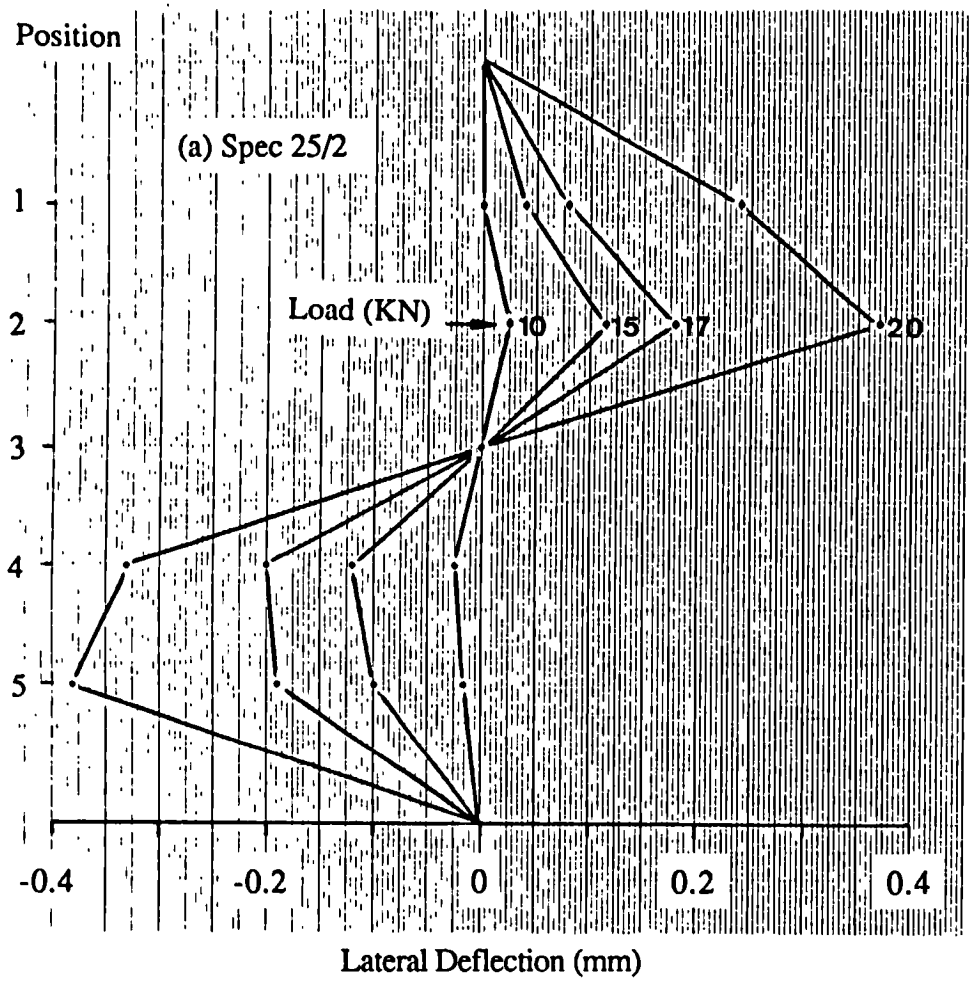

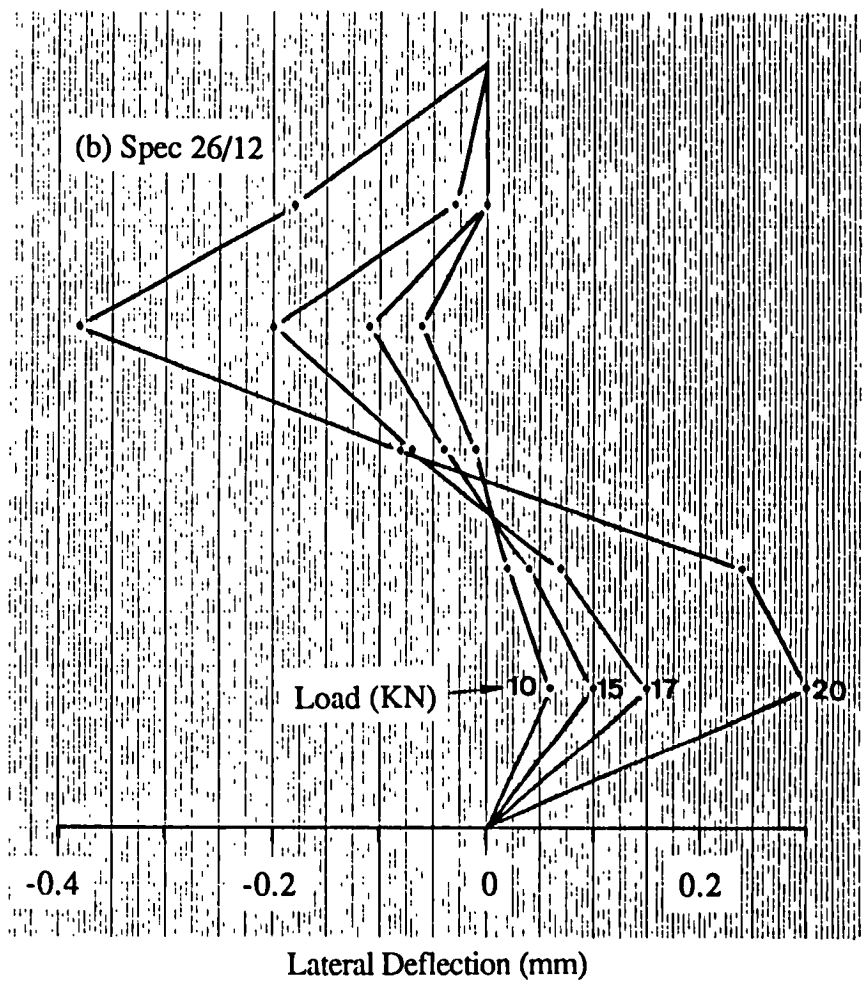

Fig 6.9 Deformed profiles of compression specimens for GRP-QI-16-55.

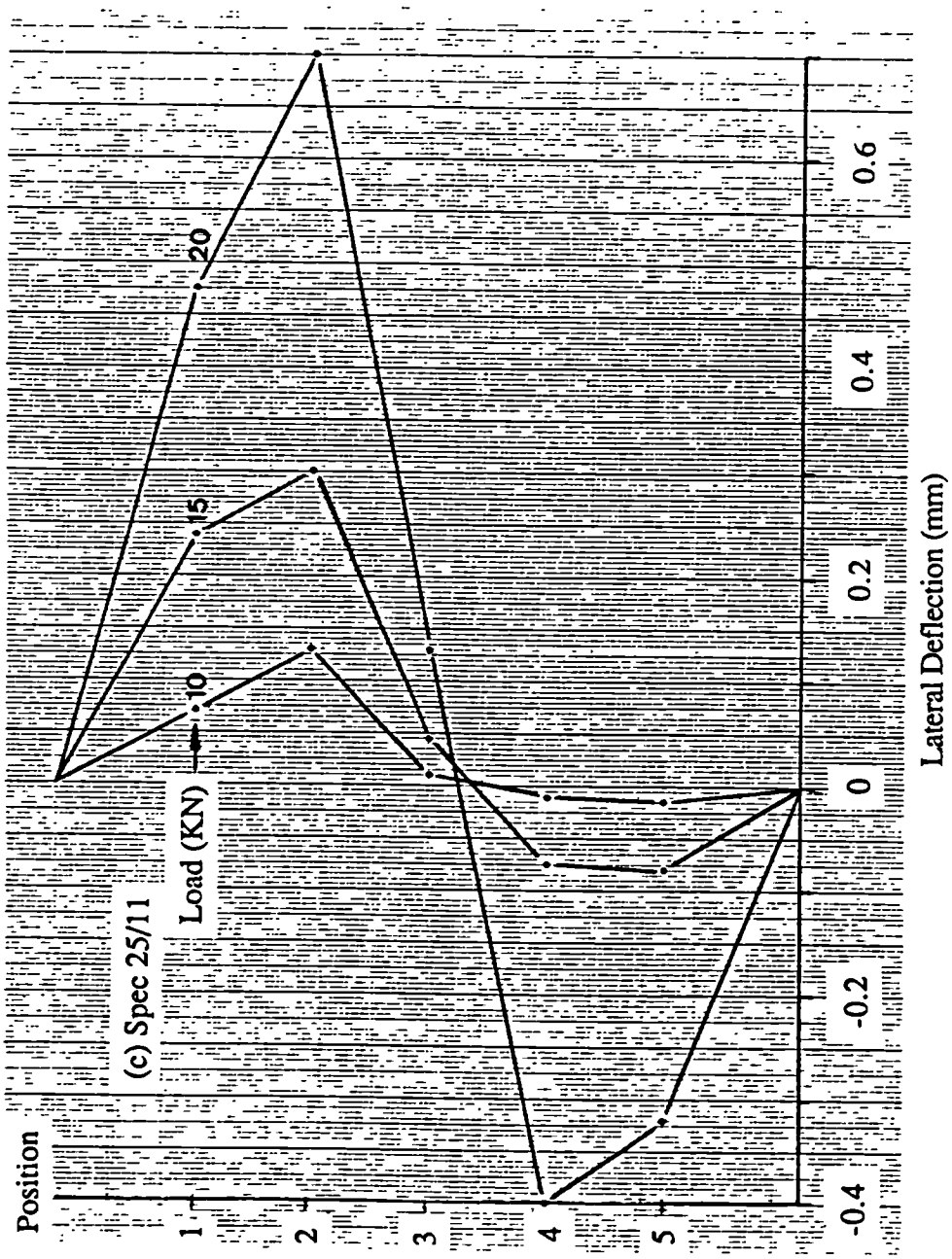

Fig 6.9 continued.

Fig 6.10 Load versus lateral deflection curves for tests at low loads. Material, GRP-QI-16-55.

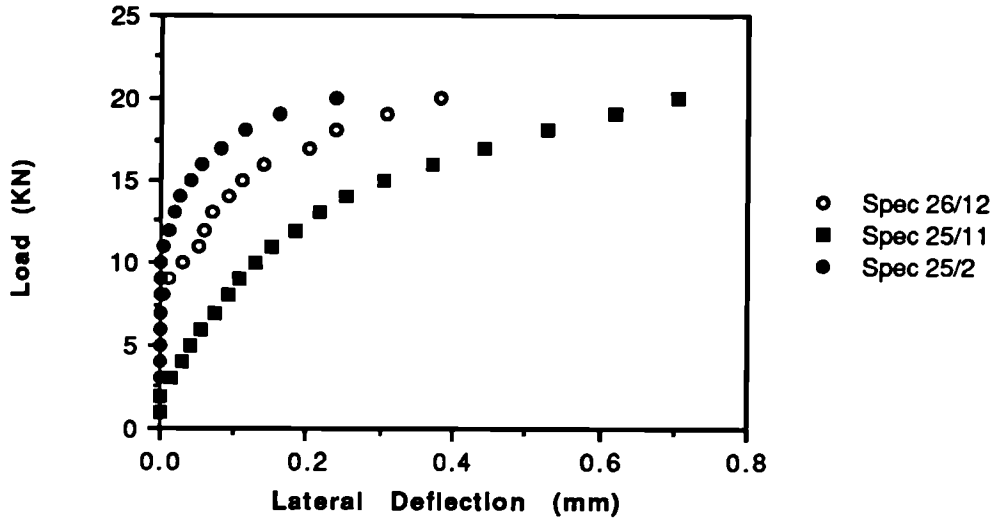

Fig 6.11 Load versus lateral deflection to failure. Material, GRP-QI-16-55.

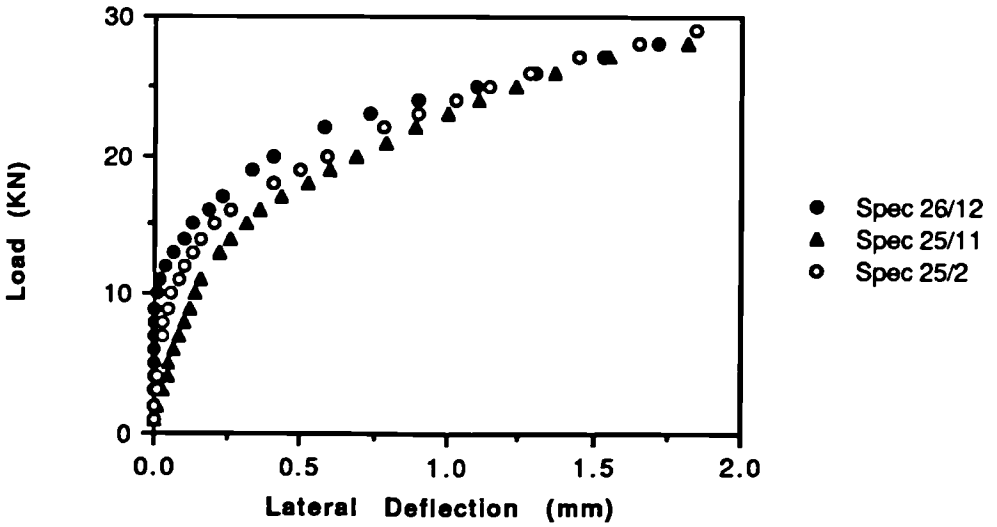

Fig 6.12 (a) Comparison of load versus deflection curves for 'low' and 'high' load tests on specimen 25/11. Material, GRP-QI-16-55.

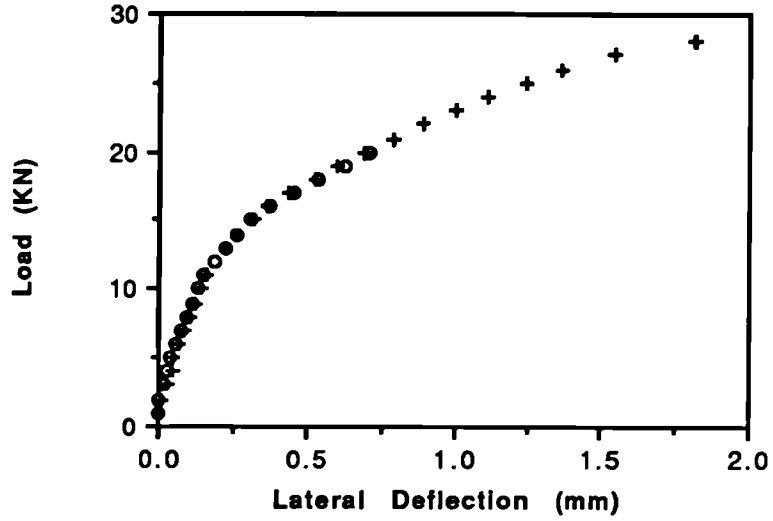

Fig 6.12 (b) Comparison of load versus deflection curves for 'low' and 'high' load tests on specimen 26/12. Material GRP-QI-16-55.

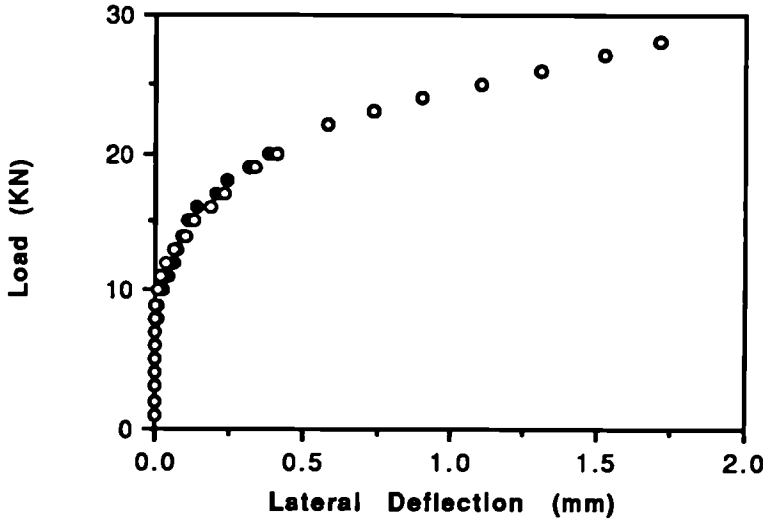

Fig 6.12 (c) Comparison of force versus deflection curves for 'low' and 'high' load tests on specimen 25/2. Material GRP-QI-16-55.

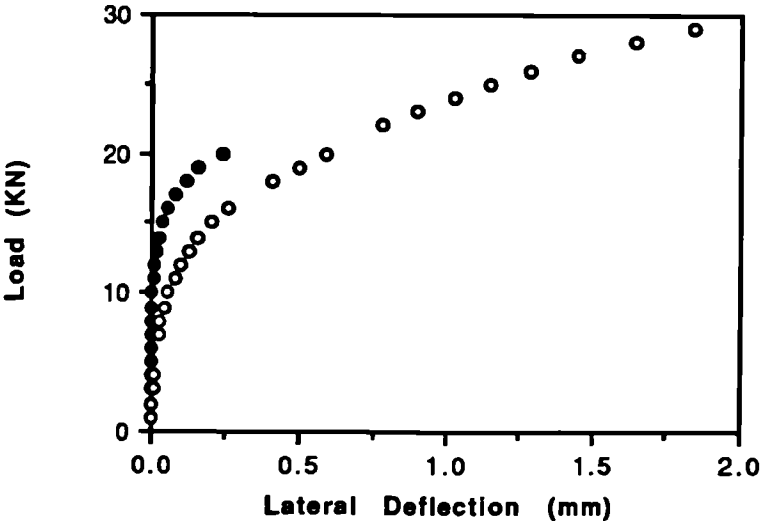

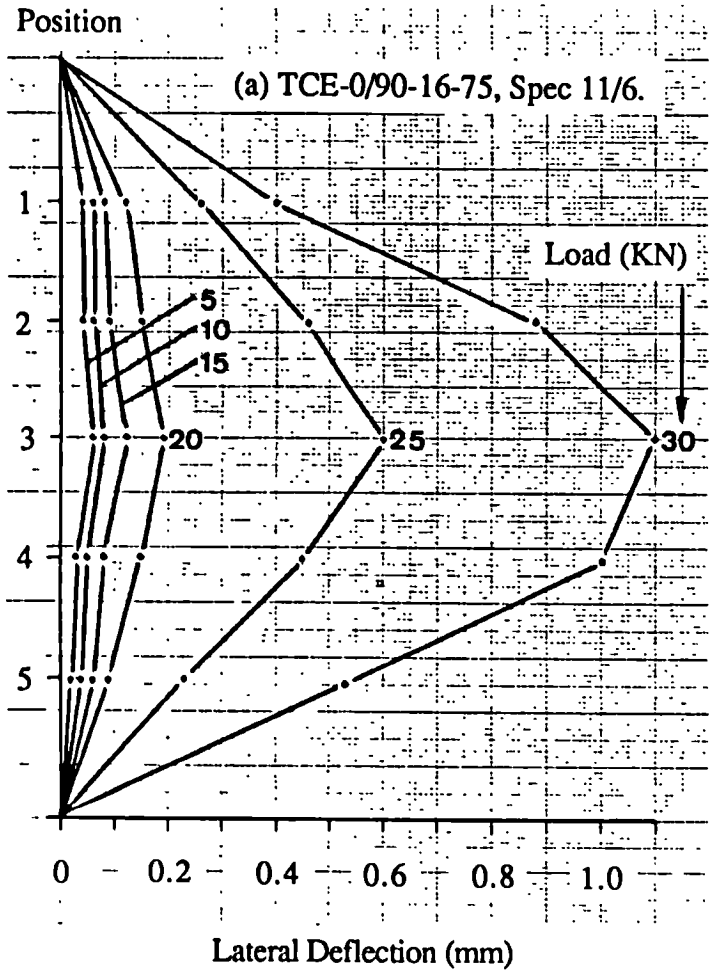

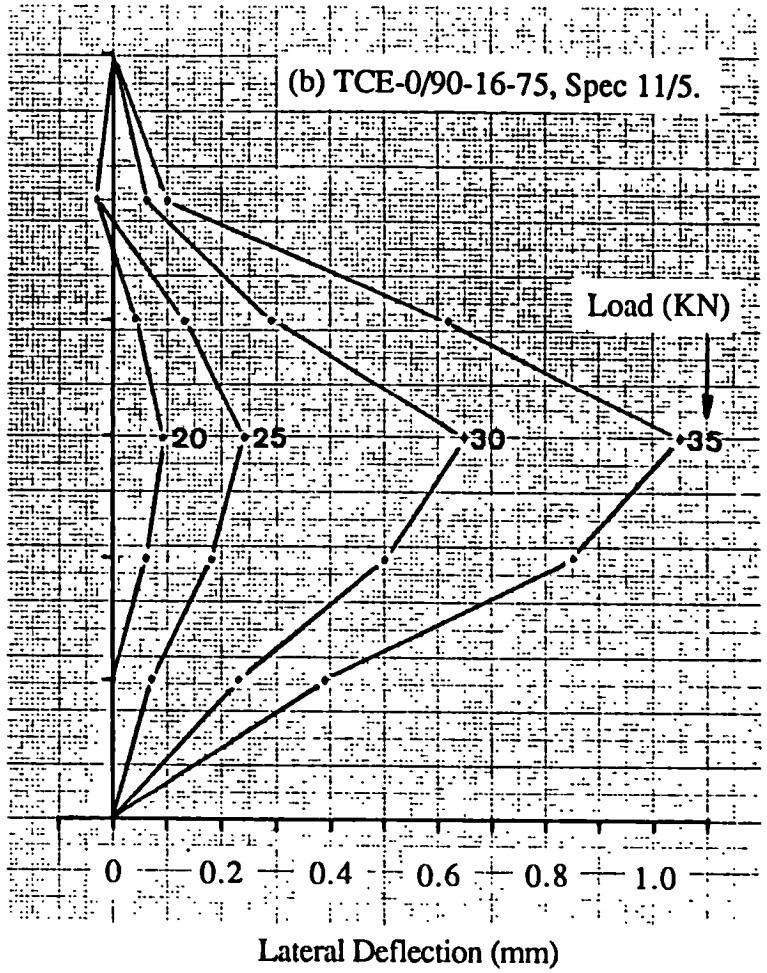

Fig 6.13 Deformed profiles of compression specimens.

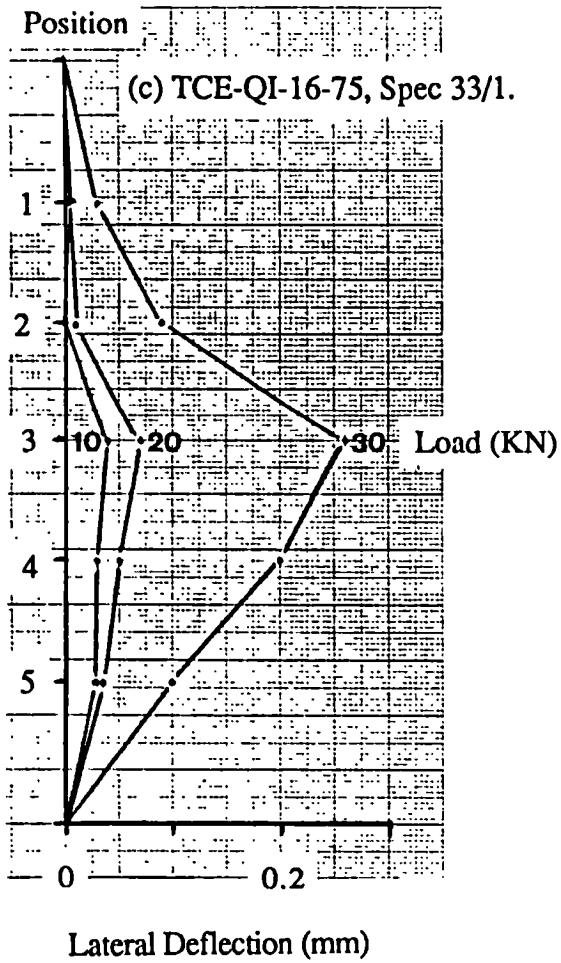

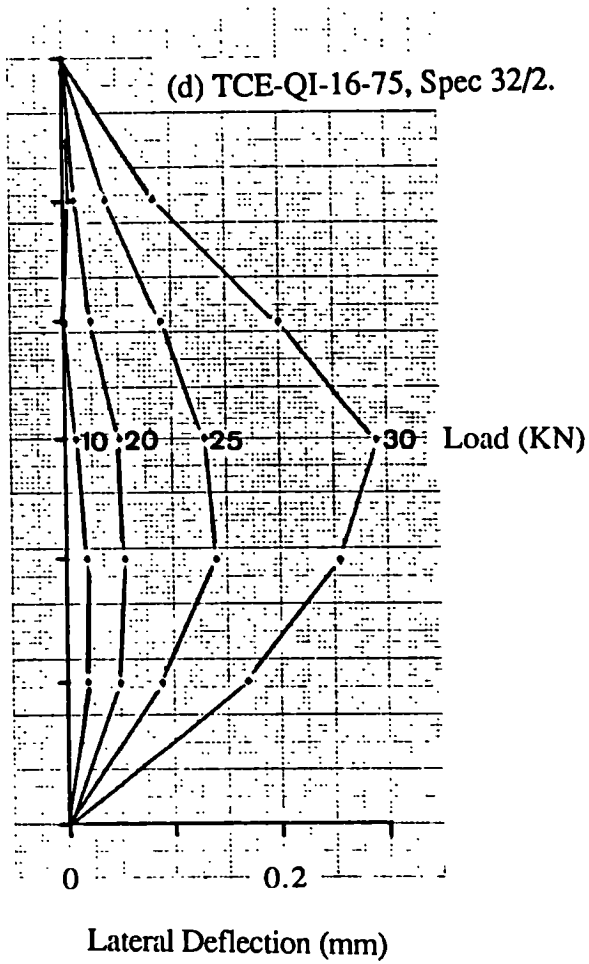

Fig 6.13 continued.

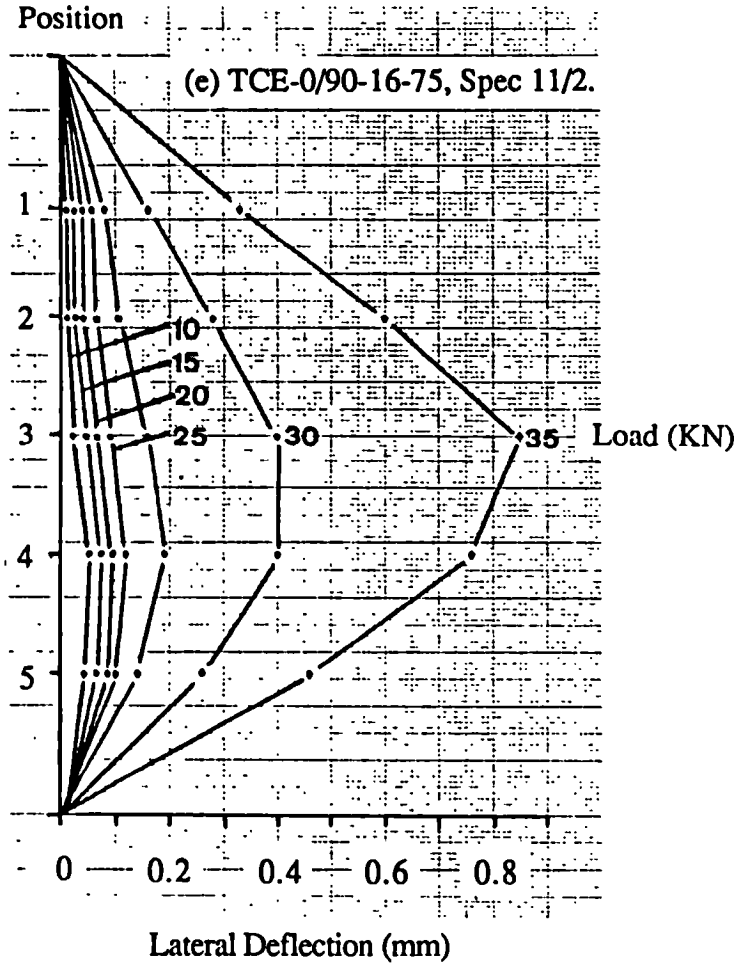

Fig 6.13 continued.

Fig 6.14 Effect of layup on load versus lateral deflection curves for 75 mm wide specimens. Material TCE-QI and 0/90-16-75.

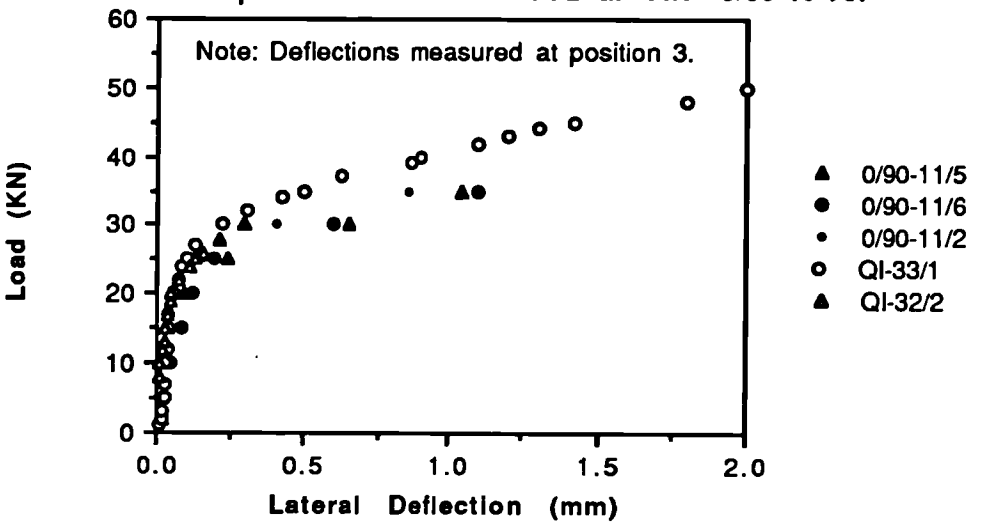

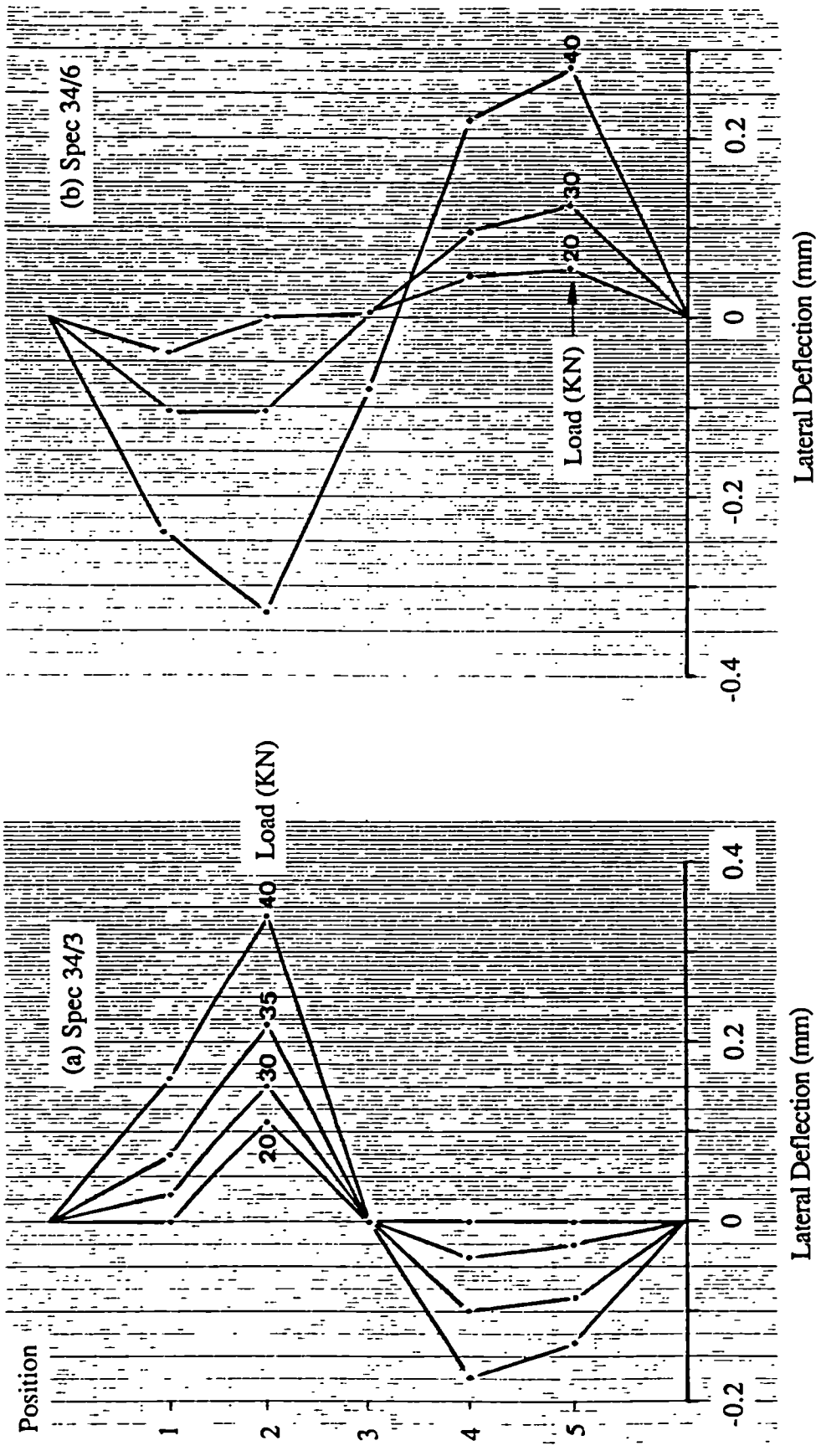

Fig 6.15 Deformed profiles of compression specimens for TCE-QI-16-55.

Fig 6.16 Effect of material on load versus lateral deflection curves. Materials, TCE, APC, GRP-QI-16-55.

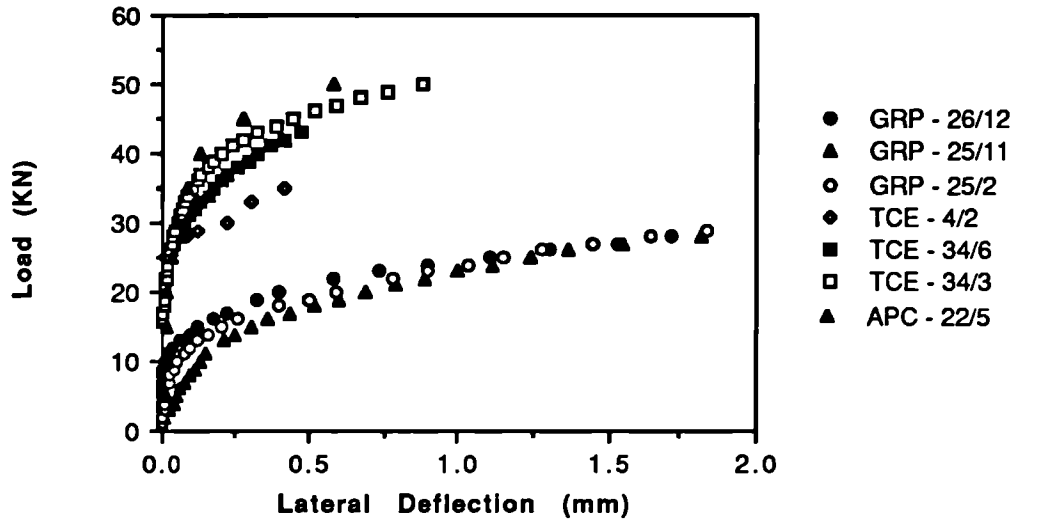

7 Post-Impact Compression Testing

7.1 Introduction

In this chapter all of the results of post-impact compression strength tests will be presented and discussed. Firstly the data for TCE-QI-16-55 will be used to show how the results have been presented. Results of tests on this material will also be used to assess the scatter in the data and to show the effect of clamping during the impact test and loading rate during the compression test on PICS. The results of experiments demonstrating the effect of specimen width, lay-up, thickness and material on PICS will then be shown.

7.2 Results

7.2.1 Results for TCE-QI-16-55

7.2.1.1 Post-Impact Compression Strength

PICS data is usually presented by plotting compression strength against incident impact energy. Fig 7.1 shows the results for the TCE-QI-16-55 material plotted in this way. Initially the compression strength remains constant, this is because low incident impact energies do not initiate damage. When damage has been initiated during the impact test an initial sharp fall in compression strength is observed, this is followed by a region of relatively constant strength. In this work an additional point has been plotted to indicate where the initial fall in compression strength would be expected. This point is plotted using the average strength value from compression tests on previously undamaged specimens (see table 6.1, chapter 6) and the average damage initiation energy calculated from the results of instrumented impact tests (see table 5.1, Chapter 5). The error bars correspond to ±1 standard deviation for each measurement. In a few cases a specimen which had been subjected to an impact test failed in a similar manner to the specimens which had not been impacted (i.e. in the unsupported region, close to the loading plate). This occurred either where no damage had been initiated by the impact test or where the amount of damage was small. These points are identified on the graphs and in appendix B. The compression failures were seen to occur in the region of the initial impact damage for all other specimens. During the compression test large out-of-plane deflections of the surface plies were observed. However this deformation was not permanent and the specimens were flat again after they were unloaded. In fact, in some cases the amount of external damage was so small that it was by no means obvious that the material had ever been tested. Most specimens displayed some external damage - a common feature is

shown in fig 7.2. The angled fracture line suggests that the specimen has failed in a shear mode. This is thought to have occurred after the maximum load had been reached and is therefore considered to be post-failure damage.

Fig 7.3 shows some typical stress - strain curves for compression tests on specimens impacted over a range of incident energies. As was found previously for tests on undamaged specimens the initial slope is lower than the linear section of the curve as the specimen is being "bedded-in". The results show that the stress - strain behaviour for specimens impacted at different incident energies is initially very similar. Fig 7.4 shows that a slight reduction in plate modulus (taken from the linear part of the stress - strain curves) occurs as the incident impact energy is increased. For this lay-up the amount of non-linear behaviour before final failure was small but the failures tended to be more progressive (indicated by audible cracking noises from specimens) than the failures for undamaged specimens. In some cases subsidiary load peaks coincided with audible indications of progressive failure (fig 7.3, specimens 42/5 and 34/2). The curves in fig 7.3 have been terminated at the point where final failure occurred. This was characterised by a sudden drop in load. Loading was continued to ensure that the maximum load had been reached but the results have not been plotted because they have no physical significance. The specimen was being crushed into the ABG. Ultrasonic C-scans performed after compression testing showed that the damage had spread laterally during the compression test with little evidence of growth in the loading direction (Note: this can be seen even more clearly in the photographs of GRP specimens shown in fig 7.5).

7.2.1.2 Assessment of Scatter in PICS Test Results

Each of the data points in fig 7.1 represents the result of a single test. Since the data was collected at different impact energies it is difficult to quantify the degree of scatter in the data. In order to do this five tests using material from four different laminates were carried out at an incident impact energy of 3 Joules.

The results of the individual PICS tests can be found in table B8 in appendix B. The average PICS at 3 J for the five specimens was 171.5 MPa and the standard deviation was 18.6 MPa. This gives a coefficient of variation of 10.9 % which is quite reasonable. However, it is apparent that one of the measured strengths is somewhat higher than the rest. A statistical test was carried out to assess whether the result is an outlier. The method given by Neal et al (1987) was used. For this data the maximum normed residual is 1.681. This is smaller than the critical value of 1.715 (for a sample size of 5 and α = 0.05) and therefore the value is not classified as an outlier by the test.

7.2.1.3 Specimen Dimensions

The nominal specimen dimensions were 89 mm x 55 mm for this series of tests. We are interested both in the tolerances to which the specimens have been manufactured and in the squareness of the specimens. Table 7.1 lists the dimensions (in inches) for the TCE-QI-16-55 specimens. The average specimen height was 88.87 mm with a maximum of +0.23 and a minimum of - 0.27 mm. The average width for the specimens was 54.76 mm with a maximum of + 0.23 and a minimum of - 0.41 mm.

The accuracy of the dimensions of individual specimens was better than this. Table 7.2 shows the dimensions and calculated angles at the corners of the specimens for all of the TCE-QI-16-55 specimens. The results for the specimens tested to assess the scatter in the data (section 7.2.1.2) are grouped together at the top of the table for ease of reference. If the specimen sides had been perfectly straight the sum of the four angles would be 360 degrees. The angles calculated for specimen (42/1) stand out from the rest. The dimension B is large in comparison with the other specimens and is thought to have been taken in error. If we discount the results for this specimen then the average angle for all of the other specimens is 89.84 degrees with a maximum angle of 90.09 degrees and a minimum angle of 89.53 degrees. (Average = 89.84 + 0.25 / -0.31 degrees). The fact that the majority of the calculated angles are below 90 degrees leads to the conclusion that the specimen edges were not perfectly straight. Fig 7.6 shows one specimen shape which allows the angles at the corners to all be less than 90 degrees.

7.2.1.4 Effect of Clamping During Impact Test

A few tests were performed to assess the effect of clamping during the impact test on PICS. The results are shown in fig 7.7. There is some indication that the PICS is marginally higher for the specimens which were not clamped during the impact test. It has already been reported that the difference in the incident energy required to initiate damage was very similar for the two test configurations (clamped 0.8 J and un-clamped 1.0 J). Since the undamaged strength remains the same, the point at which the strength should start to fall is almost the same for both cases. The strengths appear to be similar for incident impact energies above 5 J so the difference between the two test configurations is confined to the initial portion of the curve.

7.2.1.5 Effect of Loading Rate During Compression Testing

The majority of the compression tests were carried out using a loading rate of 0.3 mm/min. Four tests were carried out at a loading rate of 30 mm/min. Fig 7.8 shows that there was a slight effect due to loading rate, with specimens failing at higher stresses for the higher loading rate. This is not attributed to the rate dependence of the matrix material but is thought to be a structural effect; higher loads being generated as the specimen fails because the material does not have as much time to move aside as the specimen is crushed. However, the effect is quite small considering that the loading rates differ by two orders of magnitude.

7.2.2 Effect of Specimen Width

The effect of specimen width for the three different layups is shown in figs 7.9 (a) - (c). In comparison with the effect of specimen width on the compression strength of previously undamaged specimens, the effect on PICS is small. In the case of the QI material the results for the three specimen widths appear to lie on a single curve. The 'cut-off' point where the failure mode changes and the specimens fail in the unsupported region close to the loading plate occurs at a different point on the curve for each specimen width. Similar results are seen for the 0/90 material (fig 7.9 (b)). The apparent difference in behaviour for the 45 mm wide specimen is attributed to a lack of results between 3 and 4 J. The PICS strengths for the ±45 material were also very similar for the three specimen widths tested (fig 7.9 (c)).

7.2.3 Effect of Lay-up

Figures 7.9 (a) and (b) show that the trend of compression strength with impact energy is the same for the 0/90 and QI materials tested. The trend for the ±45 material (fig 7.9 (c)) appears to be slightly different. An almost linear reduction in strength is observed as the incident energy is increased. However no results are available for incident energies of less than 2 J. Specimens impacted at low energies could not be failed. Again the loading plate fouled on the anti-buckling guide before failure occurred.

The absolute strength values for the three layups are compared in fig 7.10 (a). To avoid confusion only the results for specimens which failed through the impact damage have been plotted. (The effect of lay-up on the strength of previously undamaged specimens has already been shown in section 6.2.2). The results for all three specimen widths have been plotted since it was shown in the previous section that specimen width did not affect

PICS dramatically. The 0/90 specimens are found to be strongest followed by the QI and ±45 materials, which have remarkably similar strengths between 2 and 12 Joules.

It is interesting to note that the in the case of the 0/90 and QI materials the apparent stress - strain behaviour was found to be mainly linear up to failure (although the plate moduli were different as expected). The observed stress - strain behaviour of the ±45 specimens was different, with slightly more non-linear behaviour occurring before failure (fig 7.10 (b)).

Fig 7.11 shows that stacking sequence has a small effect on PICS. The material with the zero degree plies in the middle (QI*) was found to have slightly higher PICS than the material with the 90 degree plies in the middle (QI).

7.2.4 Effect of Thickness

The effect of thickness on PICS is shown in fig 7.12. There appears to be a general tendency for the curves to be shifted upwards and to the right as the thickness increases. This shift to the right occurs because the incident energy required to initiate damage increases with specimen thickness, as was reported in chapter 5. There is less data to support the upwards shift because it was not possible to fail the undamaged 32 ply specimens. Again after an initial sharp fall the strength becomes relatively constant as the incident impact energy is increased. It is apparent that specimen thickness has the greatest effect on residual strength for low incident energies, the graph shows that at higher energies the strengths are very similar.

7.2.5 Effect of Material

In this section the results for the TCE material will be compared with the other three materials in turn.

7.2.5.1 Comparison of TCE and APC Materials

The results for tests on TCE-QI-16-55 and APC-QI-16-55 materials are shown in fig 7.13. As was shown in chapter 6 the undamaged strengths for the two materials are very similar, but the damage initiation energy for the APC material is higher than for the TCE material causing the curve to shift to the right before any loss in strength is observed. Once the strength does begin to fall, a clear difference between the behaviour of the two materials is apparent. For the TCE material, an initial rapid loss in strength is observed.

As the impact energy is increased further the strength remains relatively constant. In the case of the APC material a steady decrease in PICS is observed as the incident impact energy is increased.

The performance of the APC material is clearly superior to that of the TCE material when the results are compared in this way. However it is not possible to tell from fig 7.13 whether the superior performance of the APC is due to the resistance to the impact damage, resistance to the propagation of the damage during the compression test or a combination of both. It was noted in section 7.2.1.1 above that damage was observed to propagate laterally during the compression part of the test. On this basis the damage width after impact has been chosen as the parameter suitable for quantifying the degree of impact damage. Fig 7.14 shows compression strength for the two materials plotted as a function of damage width. (Note: the average strengths of specimens with damage widths of zero have been re-calculated to include those specimens which were subjected to impact but failed in the unsupported region of the specimen close to the loading plate). Although the scatter in the data appears to be high there is a clear indication of a link between compression strength and damage width. Furthermore differences between the two materials are much reduced, the indication being that the APC performs only marginally better than the TCE during the compression test.

The diagonal line in fig 7.14 represents the strength reduction which would be expected if the loss in strength were simply due to a decrease in the cross sectional area of the specimen able to carry load (the net section strength reduction line (NSRL)). (Note: the line will be approximately the same for each material since they have almost the same undamaged strengths). The triangular area formed by the axes and the line may be regarded as a notch sensitive zone while the area above the line represents a notch insensitive zone. For the TCE material the points lie very closely to the NSRL for damage widths up to 35 mm. For larger damage widths the points are lying above the line indicating that the strength does not reduce to zero once the damage has spread all the way across the specimen. This is expected since the material on either side of the delamination(s) can still support load. The points for APC lie almost exclusively above the NSRL indicating that the material is notch insensitive in this loading mode for this type of damage.

In order to investigate the significance of the scatter in the results a statistical analysis of the data was performed. This analysis was based on the assumption both that the strength and damage width data are normally distributed.

Initially a least squares method was used to obtain a regression line of compression strength on damage width. The equations of the straight lines and the correlation coefficients are shown below:

Material	Equation of Regression Line	Correlation Coefficient (r)
TCE	CS = 387.39 - 6.1896 DW	- 0.96
APC	CS = 426.26 - 6.1624 DW	- 0.92

where: CS is the compression strength (MPa) and DW is the damage width (mm).

Note that the slopes of the two lines are very similar. Both of the materials have a high coefficient of correlation, r (negative because the slope is negative). By definition | r | must lie between 0 and 1. If | r | = 0 then there is no correlation between the two variables. If | r | = 1 then there is a functional relationship (Bajpai et al, 1982). A statistical test can be used to check that the high value of the correlation coefficient did not occur by chance. This test is used to examine whether the correlation coefficient is significantly different from zero (Chatfield, 1978). If :

$$\left| \frac{\sqrt{(n-2)}}{\sqrt{(1-r^2)}} \right| \geq t_{\alpha/2,\, n-1}$$

then the correlation coefficient is significantly different from zero at the α level of significance (n is the number of data points and $t_{\alpha/2,\, n-1}$ is the appropriate value from the students t distribution).

For a = 0.05 the critical value of | r | is 0.444 for TCE and 0.456 for APC (table 6 in Bajpai, 1982). In both cases the critical values of | r | are exceeded, showing that the correlation between compression strength and damage width is significant at the 5 % level.

In addition the 95 % confidence and prediction intervals have been calculated for these fitted lines. (The equations used to calculate these intervals can be found in appendix C). The intervals are shown in figs 7.15 and 7.16 for TCE and APC respectively. For TCE the standard deviation S y/x = 28.45 and for APC S y/x = 33.96. Fig 7.17 shows the 95 % prediction intervals for the two materials plotted together. This appears to confirm the tentative conclusion, drawn from fig 7.14, that the APC performs only slightly better than the TCE during the compression test.

A notional value for the undamaged strength may be obtained from the point where the regression curves in fig 7.14 cross the strength axis. This gives values for the strength which are very similar to the average values calculated from the tests on undamaged specimens (i.e. mean value for APC, 421.8 MPa, value from regression line 426.3 MPa, mean for TCE, 392.4 MPa, value from regression line 387.4 MPa). When the strengths obtained from the regression lines are compared the APC is found to be 10 % stronger than the TCE material. To allow for this the results can be normalised by dividing by the undamaged strengths found from the regression lines. The 95 % prediction intervals normalised in this way are shown in fig 7.18. When the results are compared in this way the difference between the materials is very small.

7.2.5.2 Comparison of TCE and CE Materials

The results of tests on TCE and CE materials are shown in fig 7.19. (Note that the tests were carried out on the QI* lay-up, $[-45,90,45,0]_{4S}$). The two materials appear to behave in an almost identical manner when the PICS is plotted as a function of incident impact energy. Similar results for the two materials were observed when damage width was plotted as a function of incident impact energy (see fig 5.22). Consequently the graph of PICS versus damage width should show the materials behaving in a similar manner. Fig 7.20 shows that this is the case. Again there appears to be more scatter in the data when the two materials are compared in this way. However no statistical analysis has been undertaken because of the limited number of data points and the absence of an undamaged strength value for the TCE material..

7.2.5.3 Comparison of TCE and GRP Materials

The TCE material was found to be much stronger than the GRP material when the strengths of undamaged specimens were compared. However, when the absolute strengths of impact damaged specimen are compared, the two materials perform in an almost identical manner (fig 7.21). When the results are normalised with respect to the undamaged strength (fig 7.22) the GRP is found to be retain a greater proportion of it initial strength than the TCE and is judged to be the superior of the two materials when compared on this basis.

Fig 7.23 shows the compression strength of the GRP material plotted as a function of damage width. Again a statistical analysis has been performed to calculate the 95 % confidence and prediction intervals. The equation of the regression line was found to be:

CS = 259.81 - 2.5894 DW and the correlation coefficient, r = 0.98

where: CS is the compression strength (MPa) and DW is the damage width (mm).

Again there is a reasonably convincing correlation between compression strength and damage width. The scatter in the data is less than was found for the APC and TCE materials, the standard deviation S y/x being 10.33 MPa and consequently the 95 % confidence and prediction intervals are smaller than those calculated for the TCE and APC materials. The data for the GRP and TCE materials is compared in fig 7.24. Again the performance of the GRP is seen to be superior when the normalised data is compared in this way. For completeness the 95% prediction intervals for the two materials are shown in fig 7.25.

It was found that the amount of non-linear behaviour during the tests was much greater for the GRP material (fig 7.26) than was found for the TCE material (fig 7.3).

7.3 Discussion

7.3.1 Introduction

The results of the post-impact compression tests will be discussed in the following sections. The discussion has been divided into four parts:

7.3.2 Accuracy of Results
7.3.3 Effect of Specimen Geometry
7.3.4 Effect of Material
7.3.5 Utility of the Post-Impact Compression Test
7.3.6 Assessment of Miniaturised Post-Impact Compression Test

7.3.2 Accuracy of Results

For the TCE-QI-16-55 material a coefficient of variation (Cv) of 10.9% was obtained from the five tests at a nominal incident impact energy of 3 J. As was stated earlier, Cv's of this order are reasonable for this type of material based on the results of other types of test (for example tensile tests or interlaminar shear strength tests). However no published data has been found to support this statement for the PICS test.

The scatter in the data was also assessed when the residual strength was plotted as a function of damage width. A linear relationship was assumed and justified by values of the correlation coefficient (r) close to unity. Calculation of the 95% confidence and prediction intervals showed that the data scatter was high for both the APC and TCE materials. It is interesting to note that the 95% intervals were very similar for these two materials indicating a similar amount of data scatter for each. It was noted previously that thermoplastic materials are generally prone to larger amount of scatter in the data. Another observation is that the scatter in the data for the GRP material is noticeably smaller than for the APC and TCE materials. This may be connected with the accuracy of the measurement of damage width. For the C-scan the accuracy was estimated to be ±1 mm and for the direct measurements on the GRP specimens ±0.25 mm. Reductions in the data scatter of one variable would lead to reductions in the size of the confidence and prediction intervals.

In common with all test methods the accuracy of the specimen itself will have an effect on the measured parameter, in this case compression strength. When the end loading method is used it is important to cut the specimen so that it has square corners, this is to ensure

that pure axial loading is achieved. In addition the orientation of the specimen edges with respect to the fibres needs to be defined since the measured strength (at least of undamaged specimens) will vary with the in-plane loading direction. The problem is that the effect of any deviation from squareness or edge alignment is not known. The answer has been to specify very close tolerances for the manufacture of specimens. Take for example the SACMA testing specification for compression after impact properties (Anon, 1988). The drawing of the specimen is reproduced in fig 7.28; geometrical tolerances have been used to define the squareness of the specimen and the orientation of the specimen edges with respect to the fibres. The problem is that the specimen is impossible to manufacture because the tolerances are too tight. For example the left hand edge of the specimen must be parallel to the zero degree fibres within 0.0095 degrees but the general orientation of the fibres is known only within approximately ± 0.5 degrees. Another example is that the top edge must be perpendicular to the right hand edge within 0.01 degrees. In order for this (and the other tolerances relating to the squareness of the specimen) to be achieved the specimen would need to be roughly machined and then ground. However as soon as the specimen is rough machined the orientation of the fibres is lost. In any case manufacture of the specimens in this way would probably be prohibitively expensive. Informal contacts with industry have indicated that the geometrical tolerancing is generally ignored and the specimens are manufactured using slitting wheels, which defeats the object of having a standard test method. In fact the results reported in this chapter indicate that the measured strengths are not significantly affected by small deviations from squareness. The average angle at the corners was found to be 89.84 +0.25 / - 0.31 degrees (average over 19 specimens) and the coefficient of variation was 10.9 % for the average strength for 5 specimens. More work is required to assess the effect of deviations from squareness and also fibre alignment on the results of residual strength tests so that sensible tolerances can be specified in future standard methods.

7.3.3 Effect of Specimen Geometry

One of the main objectives of this work was to assess the effect of specimen geometry on the results of the post-impact compression strength tests. The effect of specimen width and thickness were investigated and will be discussed in this section. This will be followed by discussion on the effect of clamping the specimen during the impact test and compression loading rate on the PICS results.

7.3.3.1 Specimen Width

As was discussed in chapter 6 the undamaged strength of ±45 specimens does not appear to be affected by specimen width. The results given in fig 7.9 (c) show that this also appears to be the case for the PICS tests. In the case of the 0/90 and QI materials the undamaged strength was affected by specimen width. Reductions in compression strength were attributed to reductions in the resistance to buckling as specimen width is increased. In common with the ±45 material the PICS results for the 0/90 and QI materials did not appear to affected by specimen width over the range of widths tested (see fig 7.9 (a) and (b)). For the QI material it is interesting to notice that the residual strengths of the 45 mm wide specimens are the same as for the 55 and 75 mm wide specimens. This is in spite of the earlier observations that the stiffness and interlaminar shear strength for the material used to make the 45 mm wide specimens were lower than for the materials used to manufacture the 55 and 75 mm wide specimens. Another important observation is that the low undamaged compression strength for the 45 mm wide specimens does not appear to affect the residual strength results. Based on the results of modelling Ilcewicz et al (1989) suggest that in order to achieve high absolute values of residual strength the initial (undamaged) strength should be maximised. The results reported here suggest otherwise, some other results which, also suggest that initial compression strength is not important as may have been expected, will be discussed later.

Some testing specifications (for example CRAG (Curtis, 1988) do not permit impact damage to extend to the edges of the specimen for the test to be valid. The CRAG specification does not allow the impact damage width to exceed 40 mm (leaving nominally 5 mm of undamaged material on each side). The reasoning behind this is that free edge stresses could cause the damage to grow from the edges inwards which is not the desired situation. Having said this, the residual strength of the 45 mm wide specimens did not appear to be affected by the fact that the impact damage extended to the edges.

The fact that specimen width did not affect the measured residual strength indicates that the growth of damage during the compression test and final failure of the material is controlled by local rather than global specimen response. This is supported by the graphs showing compression strength plotted as a function of damage width (see for example fig 7.14). The results indicate that the materials tested are notch insensitive for impact induced damage under the compression loading conditions used. These materials have been found to be notch sensitive under other testing conditions. For example Dorey (1989) notes that under tensile loading, multidirectional materials are usually notch sensitive. The difference between the tests is that in the case of the open hole test the load is only being supported

by the material to either side of the hole and stress concentrations cause the material to fail at a lower applied stress. The results reported in this chapter were obtained from specimens which were not penetrated during the impact test. For this reason some of the load was supported by the material in the damaged area reducing the stress concentration effect.

It was noted in chapter 6 that the there was a change in buckling mode for undamaged material as the specimen width was increased from 55 to 75 mm. For small amounts of damage the global specimen response would be expected to dominate. This may be expected to lead to different stress distributions being set up in the damaged area because in one case the damage is at a node and in the other it is at an anti-node. In fact the residual strength of the 55 and 75 mm wide specimens does not appear to be affected lending more support to the argument that local rather than global specimen behaviour dominates the failure process.

The indications that the width of the specimen does not affect the measured residual strength are further supported when the results of tests on the TCE-QI-24 and 32-55 specimens are compared with data taken from the literature (Ilcewicz et al, 1989) for two carbon / epoxy systems tested using the Boeing test (Anon, 1982). The test conditions used in this work and for the Boeing test are compared in the table below:

Test	Material: thickness / lay-up	Impact: tup / suppt conditions	Specimen Size	Compression Loading Rate
Boeing	4 to 5 mm $(-45, 0, +45, 90)_S$	Tup - ϕ15.75 mm Mass 4.6 to 6.8 Kg Support - 127 x 76 mm (Clamped at four points)	h =152 mm w = 102 mm	0.5 mm/min
This Work	2, 3 and 4 mm $(-45, 0, +45, 90)_S$	Tup - ϕ20 mm Mass - 3.96 Kg Support - ϕ40 mm (Clamped)	h = 89 mm w = 55 mm	0.3 mm/min

Comparison of the test conditions shows that the layups are the same and based on the the results reported in this chapter (which will be discussed later) the loading rates are similar enough not to affect the comparison. The situation is slightly confused because the nominal ply thickness of the materials is different. Details are shown in the table below:

Material	Nominal Ply Thickness	No of Ply	Nominal Material Thickness
IM7/8551-7 and IM6/3501-6	0.188 mm	24	4.51 mm
TCE-QI-24-55	0.125 mm	24	3.00 mm
TCE-QI-32-55	0.125 mm	32	4.00 mm

Because of this the results for both the TCE-QI-24 and 32 materials will be compared with the results of Ilcewicz et al.

Because the impact conditions are so different a direct comparison of the results on a graph of compression strength versus incident impact energy would be meaningless (in any case the results were not plotted in this way by Ilcewicz et al). This is because different amounts of damage would be sustained by the material for impact events of the same incident energy. The difference in the size and shape of the support conditions is mainly responsible for this. More energy can be absorbed in bending for the larger support. The Boeing test data would be expected to be further to the right on a residual strength versus incident impact energy curve. Differences in the diameter and mass of the impacter would be expected to have a minor effect on the results in comparison. The problem can be overcome by comparing the results of the two tests on a graph showing compression strength plotted as a function of damage width. The effect of the impact geometry on the result is no longer important because the extent of damage is being measured after the impact test.

The results of Ilcewicz et al are compared in figs 7.27 (a) and (b) for the TCE-QI-32 and TCE-QI-24 materials respectively. Although based on a limited number of results there is evidence that for materials of similar thickness, the height and width of the specimen do not affect the results. In comparing the results two assumptions have been made. The first is that the carbon / epoxy materials all have the same (or at least very similar) impact and compression properties. Based on the results of Ilcewicz et al and the results reported in this chapter. The second is that the ABG used for this work was not a scaled down version of the Boeing ABG. The end loading methods used are essentially the same. However in the Boeing test the ABG is designed so that lateral expansion of the material cannot occur whereas the ABG used in this work does allow lateral expansion of the

material. The other difference in the design of the ABG's is that in the Boeing test the edges of the specimens are supported by knife edges whereas in this work flat faced side supports were used. In the absence of evidence to suggest otherwise the effect of these differences has been assumed to be small.

This observation that the height and width of the specimen does not affect the results is supported further by the results of combined compression and impact tests reported by Rhodes et al (1979) and Avva (1983). Rhodes et al suggested that specimen width, and Avva that specimen height does not affect the results.

7.3.3.2 Specimen Thickness

In chapter 5 it was reported that the incident energy required to initiate damage increased linearly with specimen thickness over the range of thicknesses investigated. The consequence of this is that the curves on the PICS versus incident impact energy graph are shifted to the right as the thickness increases (see fig 7.12). In chapter 6 an increase in the undamaged compression strength was indicated. This causes the curves in fig 7.12 to shift upwards. For each thickness, a rapid drop in residual strength coincides with a rapid increase in damage width (compare figs 5.21 and 7.12). It would be possible to have predicted these trends given the results of the impact and undamaged compression tests. A more surprising observation is that the residual strengths appear to be converging as the incident impact energy is increased. The simple explanation for this is that for incident impact energies of above 8 J the damage width is 40 mm for all three thicknesses. However the through thickness distribution would also be expected to influence the result. The theory is that the lateral extent and distribution of delamination damage is the same for all three thicknesses. In other words the material is broken down into a series of sublaminates of nominally equal thickness in the damaged region. The different number of sub-laminates in specimens of different thickness being accounted for by quoting a stress rather than a force at failure. There is evidence in chapter 5 to support this theory. Consider the specimens 48/7, 50/9 and 51/8 shown in fig 5.26 (b). The incident impact energies are similar and in the region where the PICS are the same for the three different thicknesses. As a first indication it is interesting to calculate the number of major delaminations as a fraction of the total number of plies in the laminate. The results are shown in the table below:

Spec No	Incident Impact Energy (J)	No of Plies (A)	No of Major Delaminations (B)	B/A
48/7	10.01	16	4	0.25
50/9	11.96	24	6	0.25
51/8	11.96	32	9	0.28

The results show that the average sub-laminate thickness is essentially the same for the three thicknesses of material. The actual distribution of delaminations is perhaps of more interest. The table below shows the number of undamaged interfaces between major delaminations for the three specimens considered:

48/7 2, 3, 4, 1
50/9 2, 3, 3, 3, 3, 3
51/8 2, 3, 2, 3, 3, 2, 4, 3

(Note that the first and last numbers are the number of interfaces between the final delamination and the surface of the material).

It can now be seen that the delaminations are distributed quite evenly through the thickness providing some experimental evidence to support the theory.

The similarity of the strengths for the different thickness materials at higher incident impact energies may therefore simply be caused by the extent of damage being limited by the support conditions during the impact test. Further work with larger specimens is required to investigate this further.

7.3.3.3 Effect of Clamping During Impact

In chapter 5 it was found that the lateral extent of damage was slightly less (at any given incident impact energy up to approximately 8 J) for the specimens which were not clamped during the impact test (fig 5.19). Based on these results these specimens were expected to have a higher PICS up to approximately 8 J. Reference to fig 7.7 shows that this is the case. After 8 J where the damage width is approximately 40 mm for both impact conditions the residual strengths were expected to be similar and the results indicate that this is the case.

7.3.3.4 Effect of Loading Rate

A slight change in residual compression strength was found when the compression loading rate was increased from 0.3 to 30 mm/min (fig 7.8).The apparent improvement in residual strength for the high loading rate is not attributed to inherent rate sensitivity of the composite originating from the matrix material. It is thought to be a structural effect, higher loads being generated at higher loading rates simply because the material does not have as much time to move aside as it is crushed. This result is helpful in terms of test design because at least one testing variable can be eliminated. The possibility remains that materials with thermoplastic matrices could exhibit some rate dependence caused by the inherent properties of the matrix. However this was not investigated.

7.3.4 Effect of Material

7.3.4.1 Fibre Lay-up

In chapter 6 it was found that the undamaged strength of the 0/90 and QI materials were essentially the same. Based on the results reported here and elsewhere the general trend is for the strength to decrease as specimen width is increased. Although it was not possible to measure the strength of the ±45 specimens the indications were that the strength would have been much lower than for the 0/90 and QI materials. This has been established by other workers using different compression test methods.

The results presented in this chapter showed that the residual compression strengths were not affected by specimen width. The residual strengths for all three lay-ups (for all three specimen widths in each case) have been plotted in fig 7.10 (a). The results show that a high undamaged strength does not necessarily lead to a high residual strength. The undamaged strength of the QI material is the same as the 0/90 but the residual strength of the 0/90 material is consistently higher. In contrast the initial strength of the QI material is higher than for the ±45 material yet the residual strengths are very similar. This supports the suggestion made earlier that a high undamaged compression strength does not necessarily lead to improvements in residual strength.

There is clear effect due to fibre lay-up which is thought to be caused by the buckling behaviour in the damaged region of the specimen. Consider first the differences between the residual strengths of the 0/90 and QI materials. The modulus of the QI material is lower than the 0/90 material in the direction of loading. This would be expected to reduce the load required to cause local buckling and hence precipitate failure at a lower load. At

first sight this explanation would not appear to apply to the results for the ±45 and QI materials since the modulus of the ±45 material is lower than that of the QI material. In fact this trend can be explained when it is remembered that the buckling load (for a plate specimen) is maximised for a ±45 fibre lay-up (see Leissa, 1985 (b)). The suggested reason for this is that the material shears in the plane rather than buckling out of the plane. The above explanation is incomplete because it does not account for the influence of laminate asymmetry (resulting from an uneven distribution of delamination damage in the material) which Jones et al (1984) consider to be an important factor affecting residual compression strength because out-of-plane deflections are automatically generated when in-plane loads are applied. Some modelling work would be required to resolve the situation. It is worth mentioning at this point, the indications are that models concentrating on local buckling behaviour may be superior to those which adopt a fracture mechanics type approach when attempting to predict the residual strength of a damaged laminate. The model due to Whitcomb used by Donaldson (1987) predicts a higher residual strength for a thermoplastic matrix material compared to an epoxy matrix material based on the higher mode II fracture toughness of the thermoplastic. The results presented here and by Ilcewicz et al (1989) strongly suggest that material toughness (both mode I and mode II) have little effect on compression strength for a given damage state. The model developed by Ilcewicz et al appears to be superior to that of Whitcomb for the reason that it models the buckling behaviour and does not include fracture toughness as a variable.

Minor changes in the lay-up of the material were also found to affect the residual strength. Comparison of the data for the QI and QI* materials shows that although the lateral extent of impact damage was the same the residual strength of the QI* material was slightly higher than that for the QI material (fig 7.11). Again this is attributed to differences in the local buckling behaviour of the two materials. The through thickness position of individual plies appears to affect the local stability. Again modelling is required in order to investigate this further.

Changes in stacking sequence were also found to affect the post-impact compression strength by Morton et al (1989). The strength of $(\pm 45, 0)_S$ laminates with two different stacking sequences was studied. Marginally higher residual compression strengths were measured for the material with the 45 degree fibres on the surface. The reason given for this improvement was that the load bearing (zero degree) fibres are protected from damage during the impact event.

Another observation of interest is that a small recovery in strength was found for the 0/90 material as the incident impact energy was increased from approximately 5 to 8 J (see fig

7.9 (b)). This behaviour appears to be genuine since it occurred for all three specimen widths and the specimens were cut from different laminates. Reference to fig 5.18 (b) shows that the damage width is still increasing between 5 and 8 J so a decrease in residual strength would be expected. This behaviour may be linked with the through thickness distribution of the impact damage. If the through thickness distribution of impact damage became more symmetric as the energy was increased then local instability may occur at a higher load thus increasing the final failure load. The problem with this theory is that neither the QI or ±45 materials show the same behaviour. Further study of the reasons for this behaviour may be justified as part of a more general investigation into the failure mechanisms as a whole.

7.3.4.2 Effect of Material

(a) Effect of Matrix Type

The results of PICS tests have traditionally been compared by plotting compression strength as a function of incident impact energy. The results presented in this chapter show that when compared on this basis the TCE and CE materials behave in a very similar manner (fig 7.19) and that the APC material is superior to the TCE material (fig 7.13) and by implication also to the CE material. What is not clear from this type of graph whether the superior performance of the APC is due to its resistance to damage during the impact test or resistance to the propagation and final failure during the residual strength test. Some insight into the relative importance of the impact and compression properties can be obtained by plotting damage width after impact as a function of incident impact energy (fig 5.22) and compression strength as a function of damage width (fig 7.14). It now clear that the APC material is more resistant to the initiation and propagation of impact damage than the TCE material. It is suggested that the higher mode II fracture toughness of the APC and its ability to absorb energy in plastic deformation during the impact event are responsible for this. It is evident from fig 7.14 (or 7.18) that the APC and TCE materials perform in a similar manner during the compression test. It would appear that quite large differences in the properties of the matrix material do not affect the post-impact compression performance.

Based on these results it is true to say that APC is more resistant to damage than the TCE material. However it is not true to say that it is more damage tolerant because for the same initial amount of damage, the residual compression strengths are the same. Following on from this the results indicate that the best way to improve the post-impact behaviour is to maximise the resistance of the material to impact damage. In particular a high value of

mode II fracture toughness is desirable because this decreases the size and density of delamination. Having said this there is probably a limit to the improvements which can be made by adopting this approach. For example Sun et al (1988) found that interleafing with tough material between the plies led to an improvement in resistance to delamination. This would be expected to lead to improvements in residual compression strength. However, because delamination is being suppressed the energy has to be absorbed by other mechanisms and the authors noted that tensile cracks penetrated more deeply into the material. The presence of these tensile cracks could result in more severe reductions in post-impact tensile strength. In addition the fibre volume fraction is reduced when interleafs are incorporated; this would be expected to lead to reductions in stiffness, possibly affecting the stability of the impact damaged zone. If the residual compression strength of a particular fibre / matrix combination, with and without interleafs, were to be compared by plotting residual compression strength as a function of damage width then larger reductions in strength may be expected for the interleafed material.

Recent developments have led to improved PICS for epoxy based materials. For example Cyanamid have produced a material (Cycom ®) with a residual compression strength of 342 MPa which is higher than the value of 338 MPa for APC-2 at an incident impact energy of 1500 in-lbs/in (Anon, 1991).

(b) Effect of Fibre Type

The performance of materials reinforced with glass and carbon fibres was assessed using the GRP and TCE materials. Based on the results discussed previously the differences between the two epoxy matrix materials are assumed to be small for the purposes of this comparison. In chapter 5 the damage width versus incident energy curves for the two materials were found to be very similar. In chapter 6 it was found that the undamaged strength of the TCE material was approximately 1.5 times that of the GRP material when measured using the anti-buckling guide to support the specimen. Fig 7.21 shows that the absolute residual strengths of the two materials are almost identical. These results appear to support the suggestion made previously (see section 7.3.4.1) that maximising the initial strength of the material does not necessarily lead to higher residual compression strength. In this case the two materials have very similar resistance to the initiation and propagation of impact damage but the smaller reduction in compression strength of the GRP material indicates that it is more damage tolerant. This is in agreement with the generally accepted view that glass fibre reinforced materials are more damage tolerant than carbon fibre reinforced materials. However a generally accepted reason for the better damage tolerance of glass reinforced materials does not appear to exist. Assuming that the damage tolerance

is linked to the properties of the fibres the most obvious differences between the glass and carbon fibres is that the glass fibres have a lower modulus and higher strain to failure. Assuming that final failure occurs when the fibres in the damaged region collapse it could be argued that although local buckling of the damage occurs at a lower load for the glass reinforced material (because of the lower modulus of the fibres) but larger out of plane deformations can occur because of the higher strain to failure of the fibres. The results show that the absolute residual strength values are almost identical for the GRP and TCE materials, and it would appear that the opposing effects of fibre modulus and strain to failure have almost exactly cancelled out for these two materials. The fact that two different combinations of modulus and strain to failure should produce such similar strengths almost appears to be too much of a coincidence. Further testing with more fibre/matrix combinations is deemed necessary before any firm conclusions can be drawn.

7.3.5 Utility of the Post-Impact Compression Test

Sjoblom et al (1989) pointed out that post-impact compression tests carried out at a single incident impact energy does not reveal the true performance of the material and suggest that tests should always be carried out over a range of incident impact energies. The results reported in this chapter support the suggestion. Take for example the comparison of the results for the TCE and APC materials (fig 7.13). If the arbitrarily chosen impact energy had been 12 J then the two materials would have been judged to perform in a very similar manner. When compared over the full range of energies it is clear that the APC is superior to the TCE in PICS tests. In fact comparison of the strengths at 12 J is not valid because the lateral extent of impact damage in the TCE material has been constrained to a maximum of 40 mm by the support conditions and therefore the strength became almost constant after 5 J. However this would not have been revealed if the test had been carried out at a single incident energy.

If the PICS test is to be successfully used as a means of developing and selecting materials it is suggested that the approach used in this chapter to analyse the data should be adopted. This means assessing both the resistance of the material to impact damage (specifically delamination damage) by plotting a damage dimension (maximum lateral damage width has been suggested) as a function of incident impact energy and damage tolerance by plotting residual compression strength as a function of damage width. In addition the residual strength can be plotted as a function of incident impact energy to give an overall comparison of the material performance. By analysing the results in this way the superior performance of a material can be traced to either superior resistance to impact damage or superior damage tolerance.

Note that the use of instrumented impact testing for the PICS test has not been suggested. The energy required to initiate damage is the only parameter which was really useful in understanding the post-impact compression behaviour. If the total absorbed energy was a reliable measure of the total amount of damage this may also have been of use. However for the reasons given in chapter 5 this was not possible.

One problem is that the suggested approach could be more expensive because an extra stage has been incorporated (namely that of measuring the damage width after impact). However the total number of specimens required need not be increased, for example the five specimens required to be tested at one incident energy for the Boeing test could be spread over a range of incident impact energies. In addition smaller / thinner specimens could be used resulting in a cost saving on raw material and processing, machining and the capital cost of high capacity testing machines. Having made these proposals there is a strong probability that they would not be adopted in any standard in the near future. The SACMA test is currently being assessed with a view to adopting it as the ASTM standard for compression after impact testing. This is very similar to the Boeing test method and as was pointed out by Sjoblom et al (1989) there is already a large amount of data available against which new materials can be compared.

A second problem is that of data presentation. Computer data bases are being used increasingly to store information about materials and assist with materials selection. The single strength value generated by the Boeing test is ideal for this purpose. Presentation of data in the form of several graphs causes a problem for these automated systems.

7.3.6 Assessment of the Miniaturised Post-Impact Compression Test

The results presented in this chapter strongly suggest that much smaller specimens than those typically being used at the present time can be used successfully to test for post-impact compression strength. The main reservation is that the lateral extent of damage is constrained by the dimensions of the support during the impact test or for very small specimens the edges of the specimen (for example the simply supported beam specimens used by Ishai et al, 1990). The problem is that the compression strength remains almost constant as the incident energy is increased and does not reflect the true behaviour of the material under those particular testing conditions. The problem can be overcome to some extent when residual compression strength is plotted as a function of damage width. The results presented in this chapter suggest that a linear relationship between compression strength and specimen width exists. However theory suggests, and other experimental

results have confirmed, that residual strength tends to an asymptotic value as damage size is increased (Jones et al, 1984). This trend is also suggested in the results of Ilcewicz et al (1989) which are shown in fig 7.28. The lack of results for damage widths above 40 mm for the test used in this work mean that this trend is not shown.

Specimen Number	Specimen Width (in)			Specimen Height (in)		
	W1	W2	W3	L1	L2	L3
34/3	2.154	2.156	2.153	3.500	3.500	3.498
4/6	2.158	2.164	2.161	3.508	3.503	3.506
34/6	2.154	2.155	2.154	3.500	3.503	3.500
54/1	2.153	2.154	2.155	3.497	3.489	3.491
54/5	2.157	2.154	2.155	3.495	3.497	3.498
41/6	2.155	2.155	2.155	3.492	3.498	3.499
41/2	2.140	2.144	2.148	3.498	3.499	3.497
47/1	2.164	2.156	2.159	3.502	3.495	3.492
42/1	2.151	2.155	2.154	3.490	3.490	3.497
3/6	2.162	2.160	2.164	3.502	3.504	3.502
3/3	2.165	2.165	2.162	3.501	3.504	3.503
47/3	2.164	2.165	2.162	3.501	3.502	3.500
41/4	2.155	2.160	2.146	3.499	3.498	3.498
54/3	2.157	2.158	2.156	3.497	3.496	3.496
42/5	2.154	2.154	2.154	3.497	3.497	3.497
42/4	2.152	2.150	2.148	3.497	3.498	3.497
4/3	2.163	2.164	2.155	3.505	3.504	3.504
2/6	2.165	2.152	2.159	3.501	3.502	3.500
34/4	2.152	2.154	2.153	3.500	3.500	3.500
34/2	2.153	2.155	2.158	3.498	3.500	3.500

Average 2.156 in = 54.76 mm
Max 2.165 in = 54.99 mm
Min 2.140 in = 54.35 mm

Average 3.499 in = 88.87 mm
Max 3.508 in = 89.10 mm
Min 3.489 = 88.6 mm

Average $54.76^{+0.23}_{-0.41}$ mm

Average $88.87^{+0.23}_{-0.27}$ mm

Table 7.1 Dimensions of TCE-QI-16-55 compression specimens.

	Specimen Dimensions						Calculated Angles				Total
Specimen Number	W1 (in)	W3 (in)	L1 (in)	L3 (in)	A (in)	B (in)	a	b	c	d	a+b+c+d
47/3	2.164	2.162	3.501	3.500	4.109	4.112	89.88	89.81	89.82	89.94	359.45
41/4	2.155	2.146	3.499	3.498	4.100	4.103	89.80	89.73	89.85	89.97	359.35
54/3	2.157	2.156	3.497	3.496	4.105	4.104	89.84	89.91	89.90	89.88	359.53
42/5	2.154	2.154	3.497	3.497	4.104	4.102	89.84	89.90	89.90	89.84	359.48
42/4	2.152	2.148	3.497	3.497	4.101	4.103	89.90	89.84	89.91	89.97	359.62
34/3	2.154	2.153	3.500	3.498	4.101	4.107	89.92	89.78	89.74	89.98	359.42
4/6	2.158	2.161	3.505	3.504	4.118	4.105	89.66	90.09	90.01	89.63	359.39
34/6	2.154	2.154	3.50	3.50	4.105	4.104	89.82	89.85	89.85	89.82	359.34
54/1	2.153	2.155	3.501	3.501	4.104	4.096	89.56	89.81	89.78	89.53	358.68
54/5	2.157	2.155	3.495	3.498	4.104	4.105	89.94	89.83	89.94	89.89	359.60
41/6	2.155	2.155	3.492	3.499	4.095	4.105	90.05	89.55	89.74	89.86	359.20
41/2	2.140	2.148	3.498	3.497	4.101	4.095	89.82	90.04	89.88	89.72	359.46
47/1	2.164	2.159	3.502	3.492	4.111	4.105	89.64	90.09	89.91	89.98	359.62
42/1	2.151	2.154	3.490	3.497	4.095	4.150	91.60	89.67	89.86	91.36	362.49
3/6	2.162	2.164	3.502	3.502	4.109	4.111	89.86	89.79	89.76	89.82	359.23
3/3	2.165	2.162	3.501	3.503	4.108	4.104	89.62	89.69	89.79	89.61	358.71
4/3	2.163	2.155	3.505	3.504	4.113	4.108	89.67	89.85	89.95	89.82	359.29
2/6	2.165	2.159	3.501	3.500	4.118	4.102	89.55	90.08	89.96	89.68	359.27
34/4	2.152	2.153	3.500	3.500	4.103	4.107	89.95	89.82	89.94	89.93	359.64
34/2	2.153	2.158	3.498	3.500	4.109	4.102	89.83	89.99	89.97	89.69	359.48

Note: See fig 3.4 for key to dimensions

Table 7.2 Dimensions and calculated angles of TCE-QI-16-55 compression specimens

Fig 7.1 Compression strength versus incident impact energy for TCE-QI-16-55.

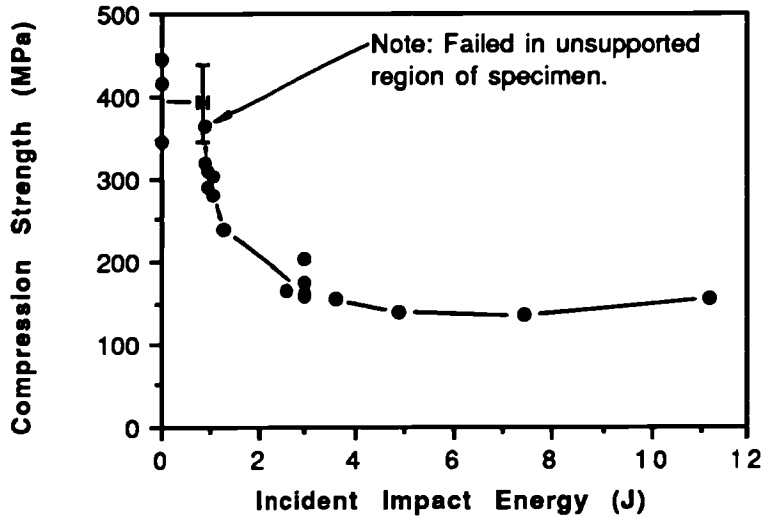

Fig 7.2 Shear type failure at edge of specimen after impact and compression testing. Spec No 41/2. Incident Impact Energy 0.96 J. TCE-QI-16-55.

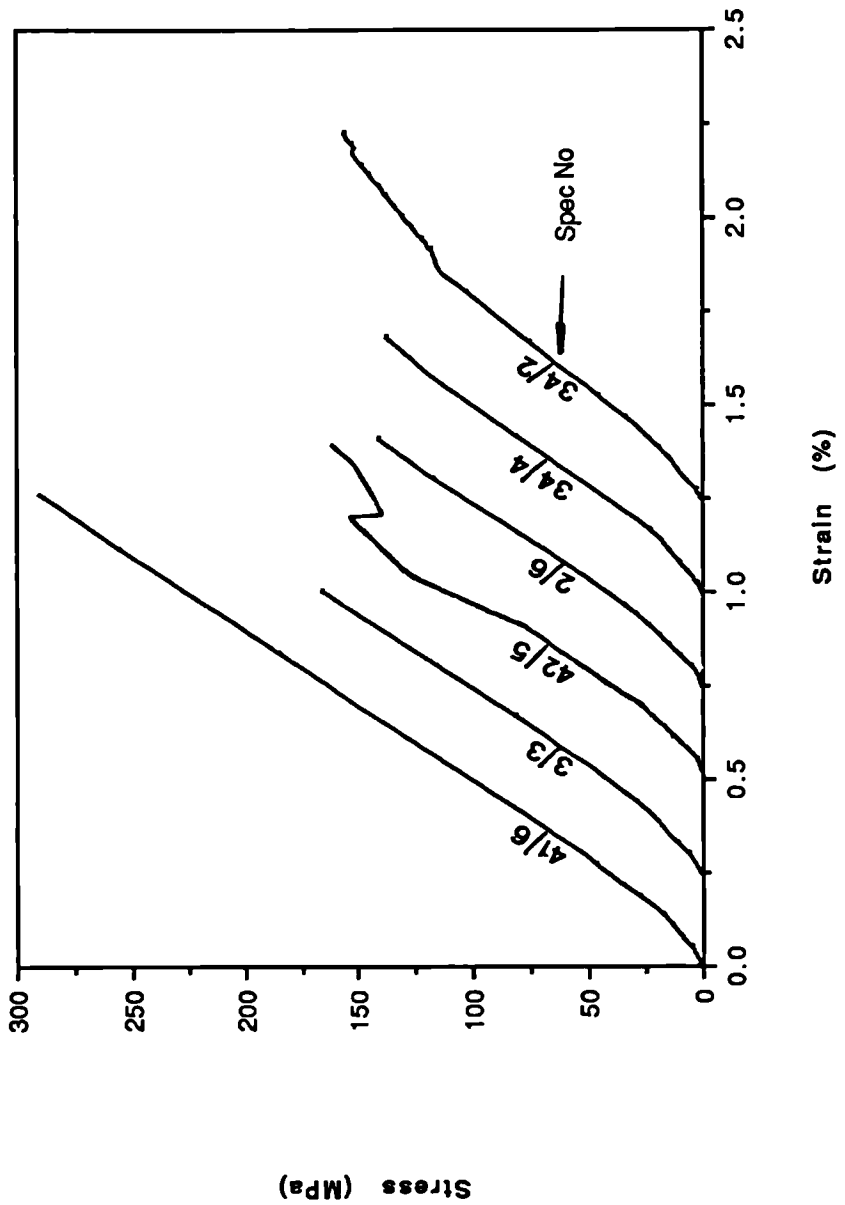

Fig 7.3 Typical stress - strain curves for PICS tests on TCE-QI-16-55 material.

Fig 7.4 Plate modulus versus incident impact energy for TCE-QI-16-55.

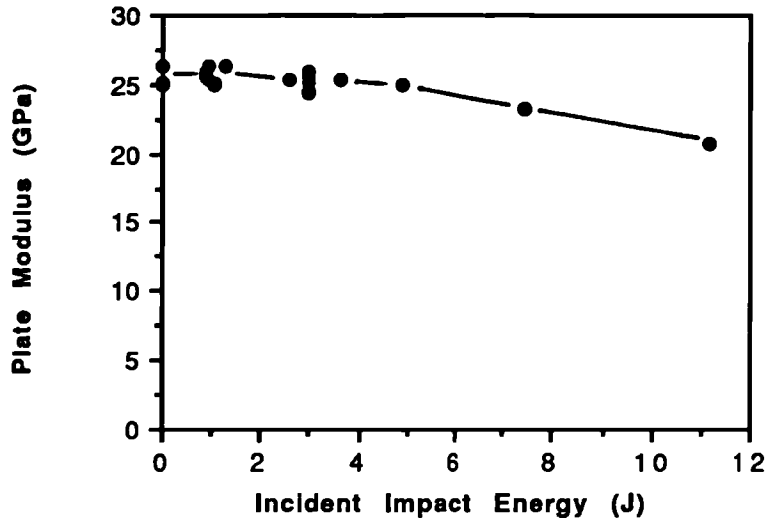

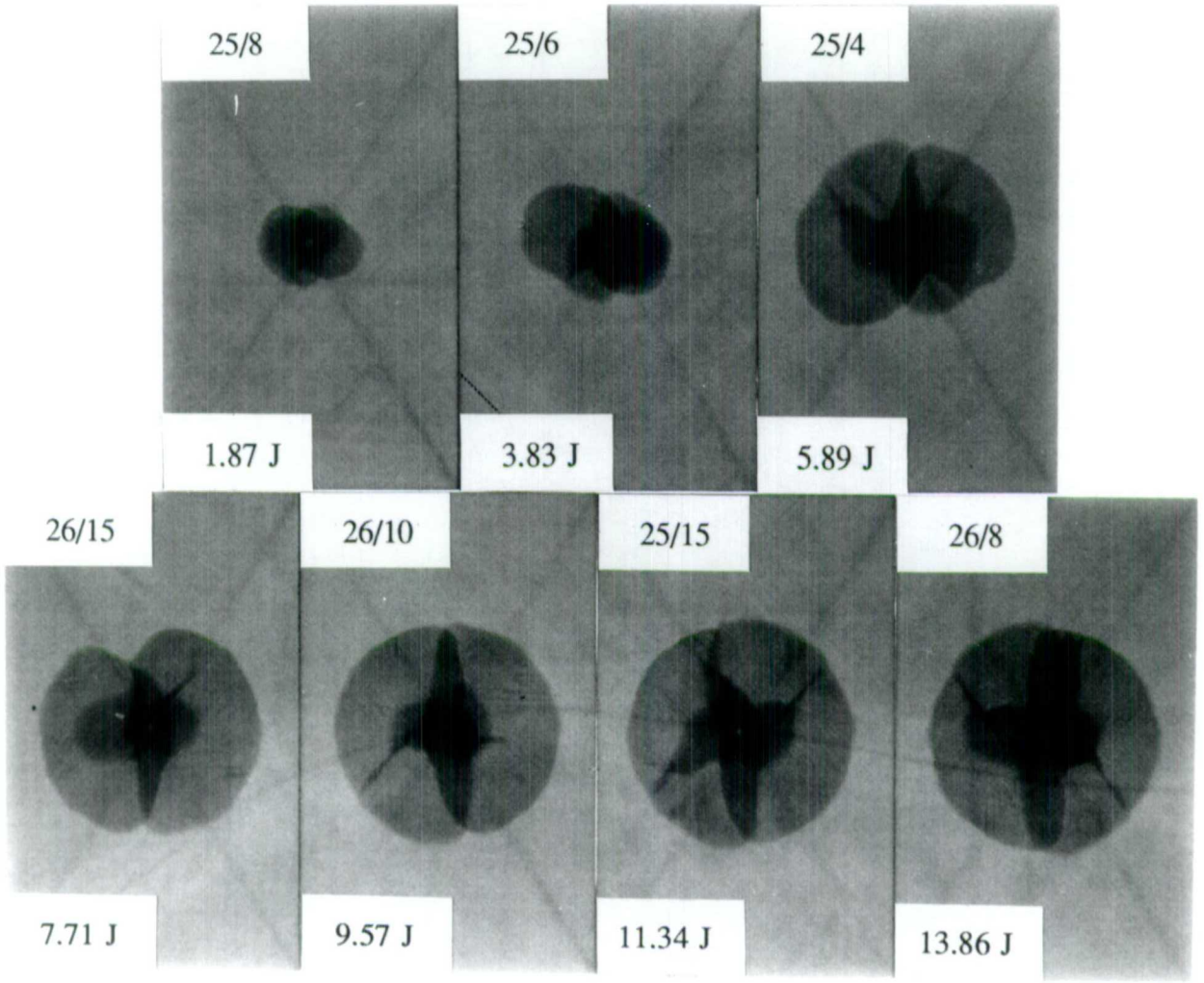

Fig 7.5 (a) Photographs showing impact damage in GRP-QI-16-55 specimens.

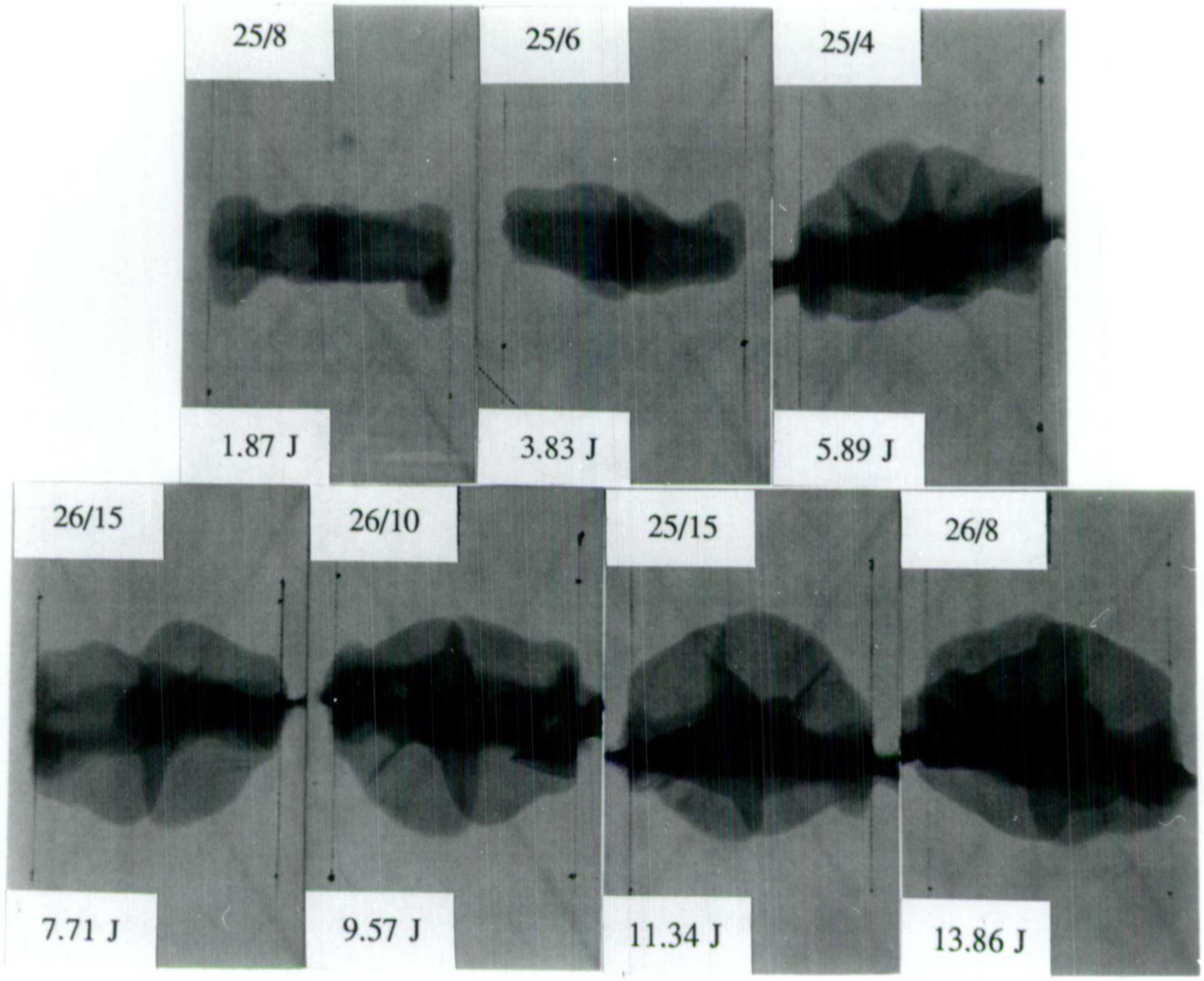

Fig 7.5 (b) Photographs showing damage state after compression testing of the specimens shown in fig 7.5 (a).

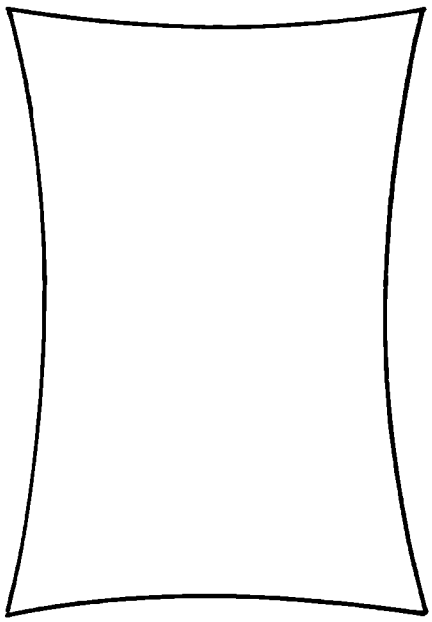

Fig 7.6 Drawing to show an example of a specimen where all of the angles at the corners are less than 90 degrees.

Fig 7.7 Effect of clamping during impact on compression strength. Material TCE-QI-16-55.

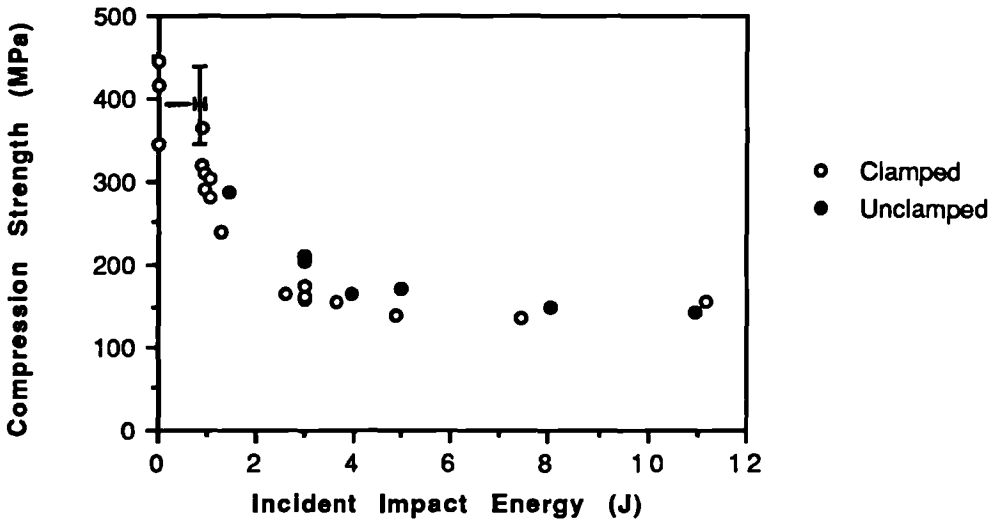

Fig 7.8 Effect of loading rate on compression strength. Material, TCE-QI-16-55.

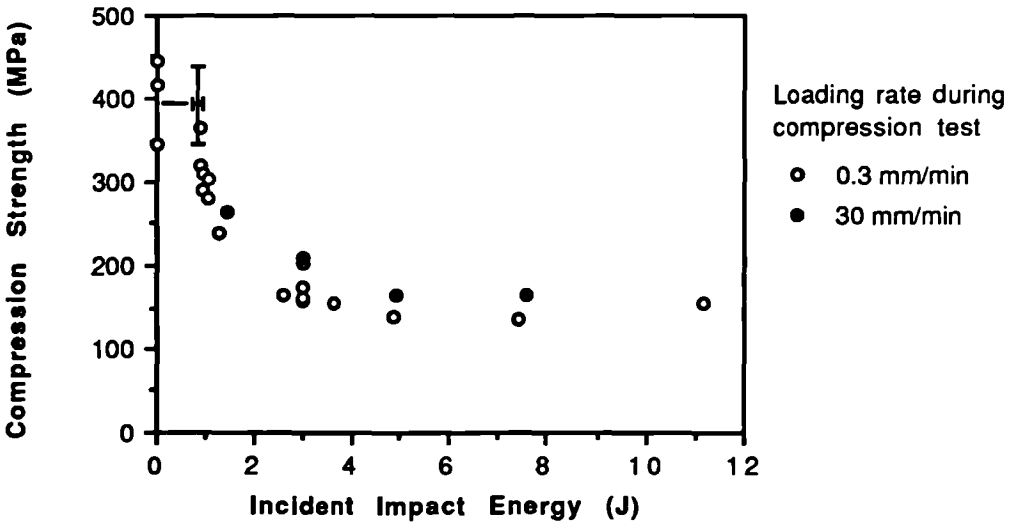

Fig 7.9 (a) Effect of specimen width on compression strength. Material, TCE-QI-16-45, 55 and 75.

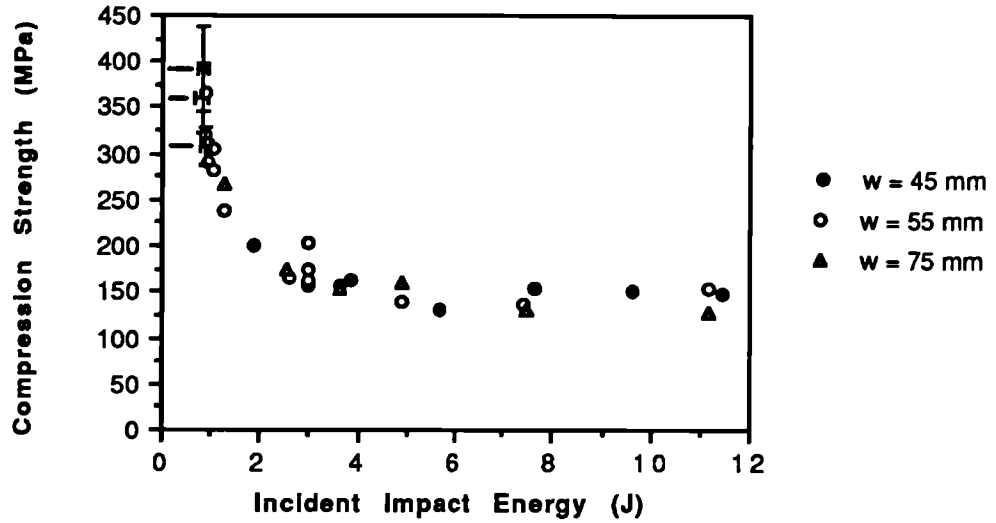

Fig 7.9 (b) Effect of specimen width on compression strength. Material, TCE-0/90-16-45,55 and 75.

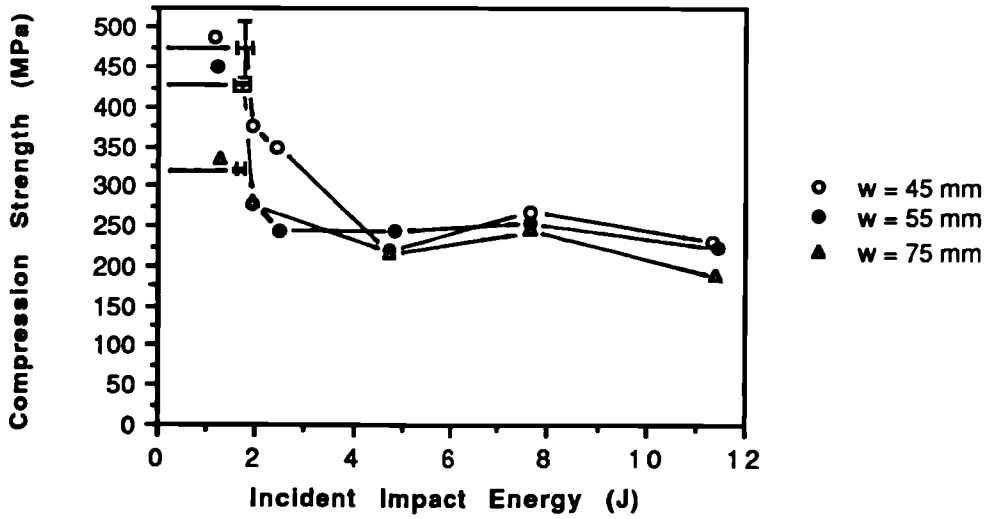

Fig 7.9 (c) Effect of specimen width on compression strength Material, TCE-±45-16-45, 55 and 75.

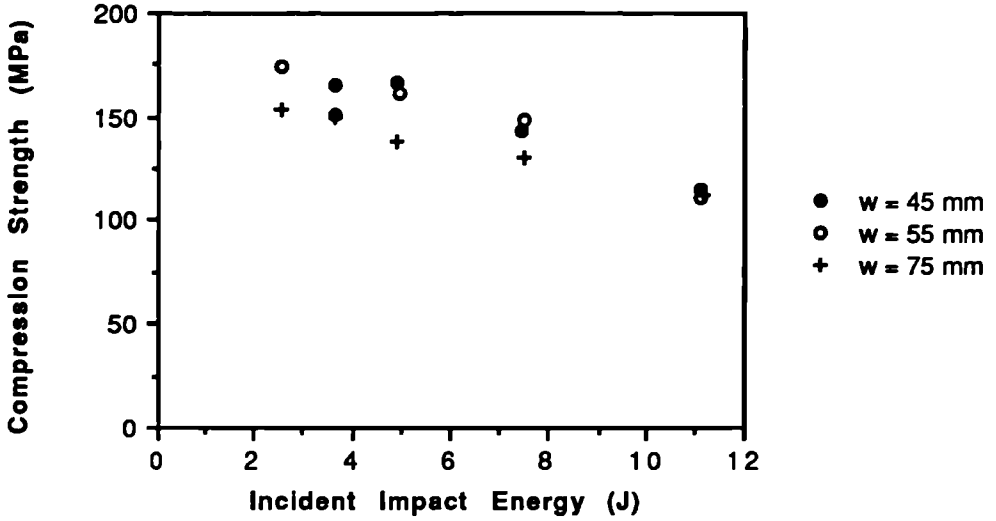

Fig 7.10 (a) Effect of layup on PICS for TCE-0/90, QI and ±45-16-45,55 and 75 materials.

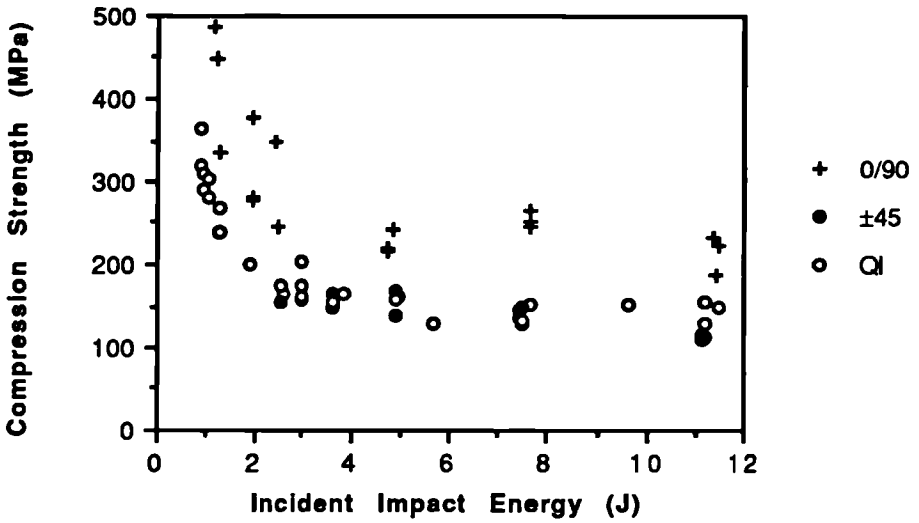

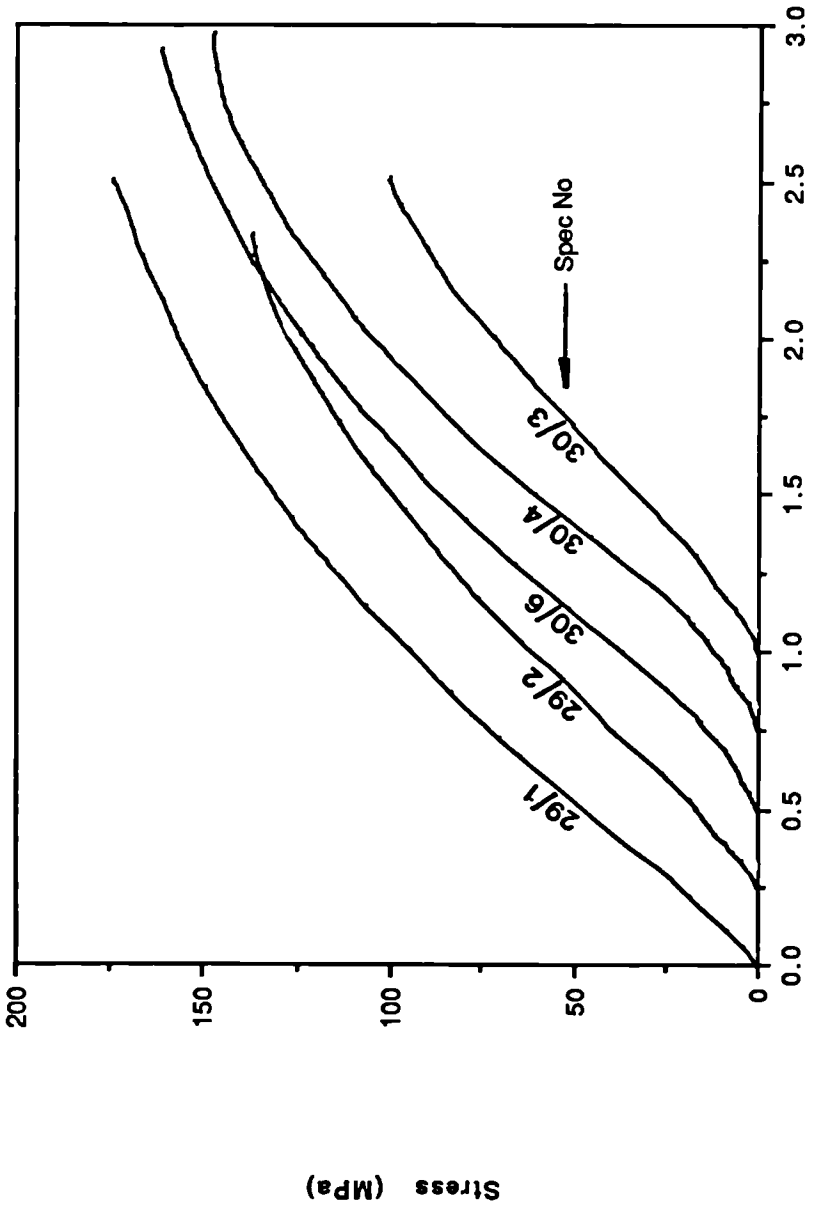

Fig 7.10 (b) Stress - strain curves for PICS tests on TCE-±45-16-55 material.

Fig 7.11 Effect of stacking sequence on PICS for TCE-QI and QI*-16 materials.

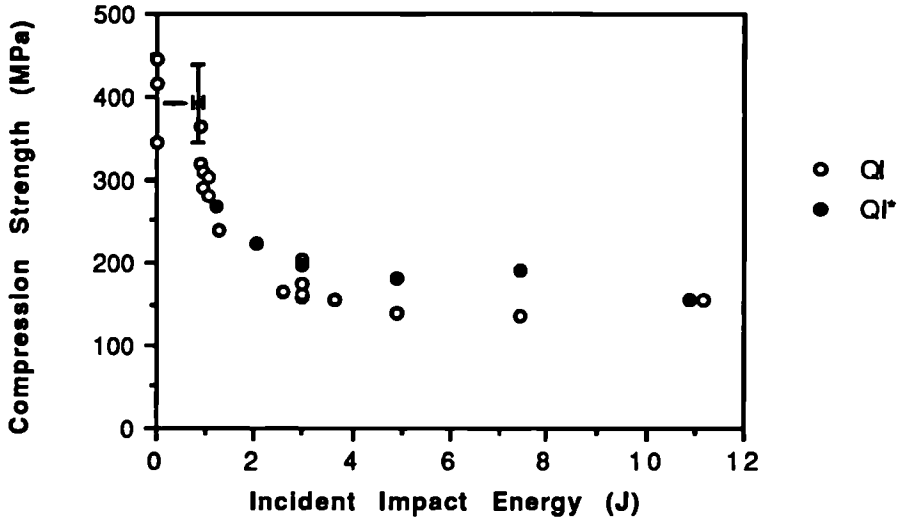

Fig 7.12 Effect of specimen thickness on compression strength for TCE-QI-16, 24 and 32-55 material.

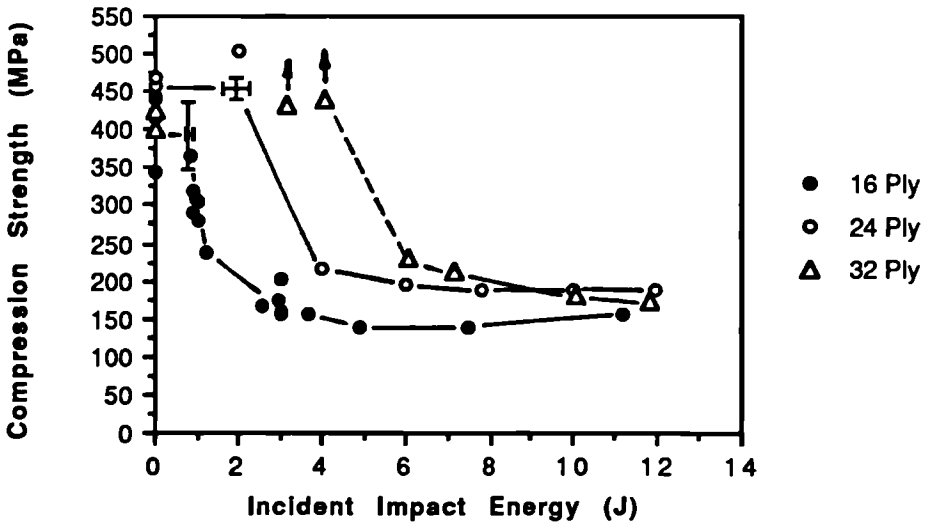

Fig 7.13 Compression strength versus incident impact energy for TCE and APC-QI-16-55 materials.

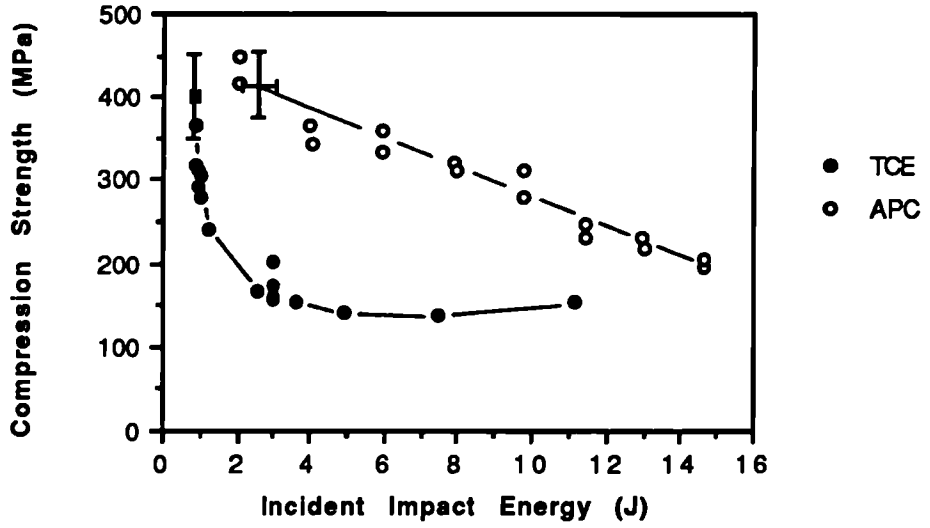

Fig 7.14 Compression strength versus damage width for TCE and APC-QI-16-55 material.

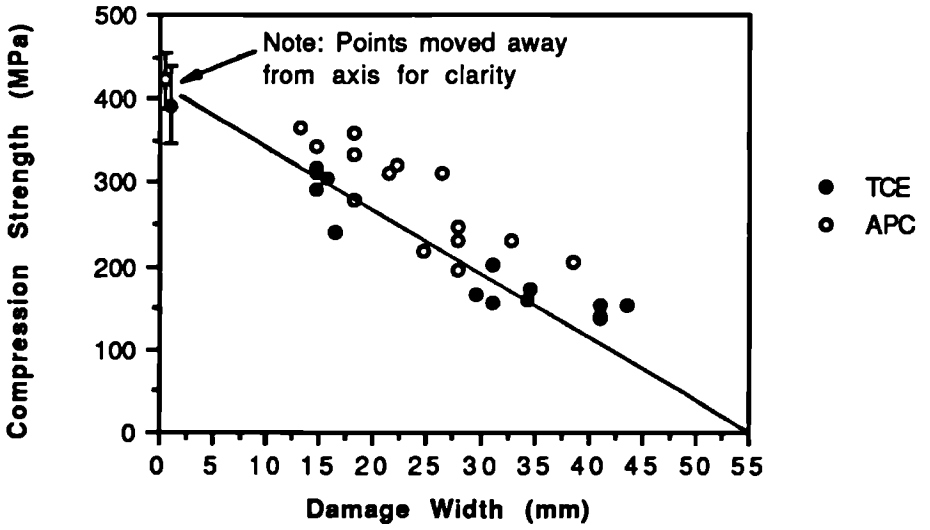

Fig 7.15 Compression strength plotted as a function of damage width with 95% confidence and prediction intervals. Material, TCE-QI-16-55.

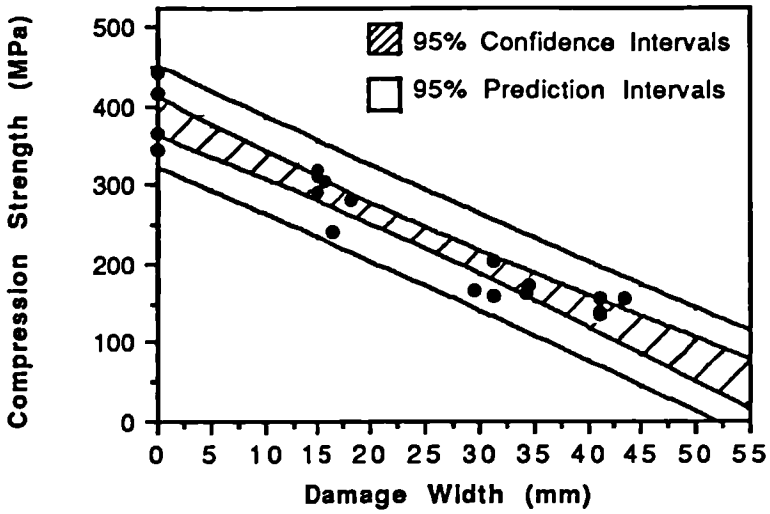

Fig 7.16 Compression strength plotted as a funtion of damage width with 95% confidence and predition intervals. Material, APC-QI-16-55.

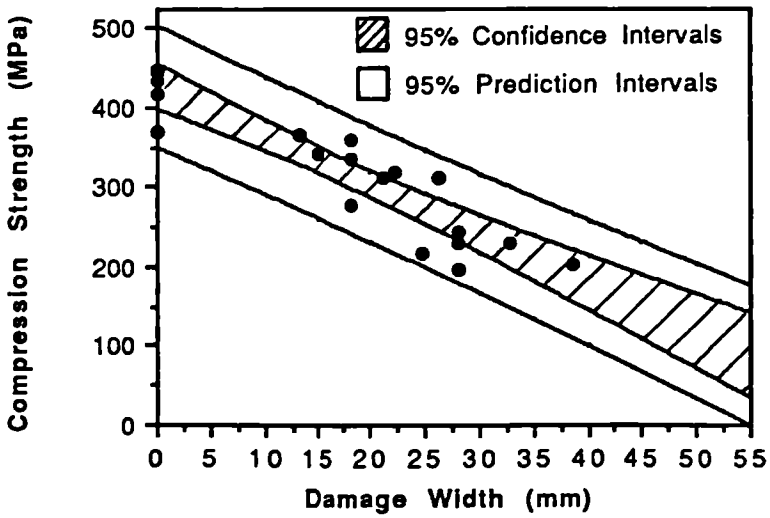

Fig 7.17 Compression strength versus damage width. Comparison of 95% prediction intervals for TCE and APC-QI-16-55.

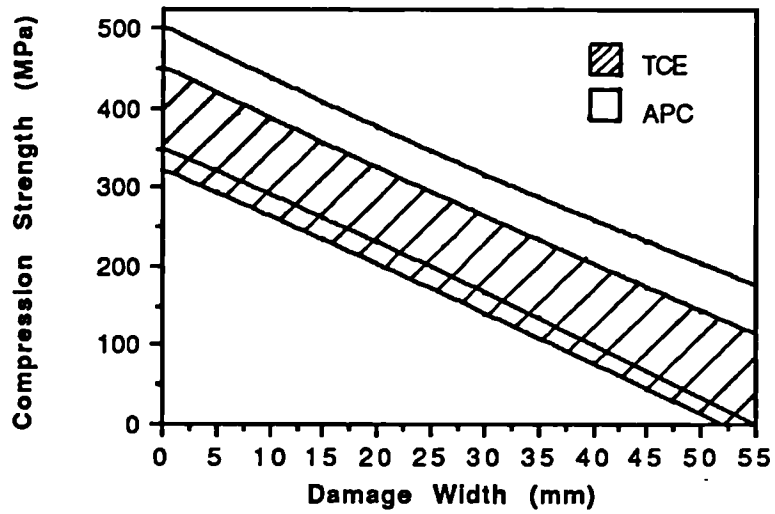

Fig 7.18 Normalised compression strength versus damage width. Comparison of 95% prediction intervals for TCE and APC-QI-16-55.

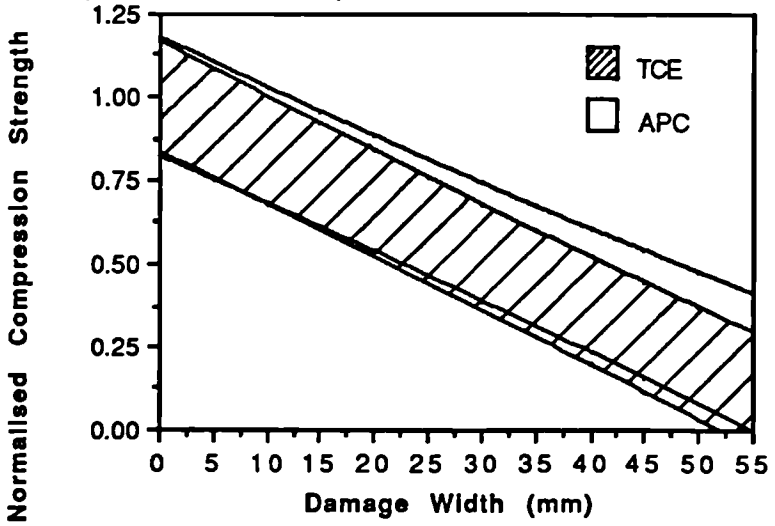

Fig 7.19 Compression strength versus incident impact energy for TCE and CE-QI*-16-55 materials.

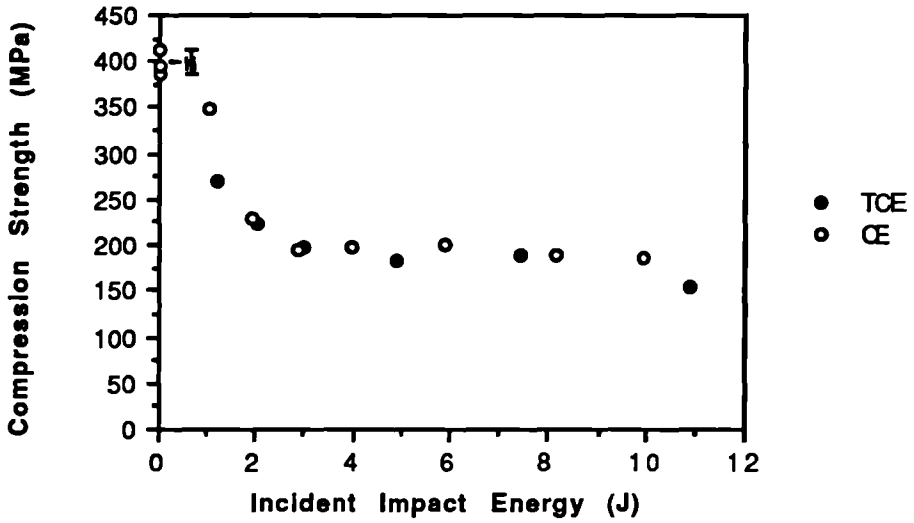

Fig 7.20 Compression strength versus damage width for TCE and CE-QI*-16-55 materials.

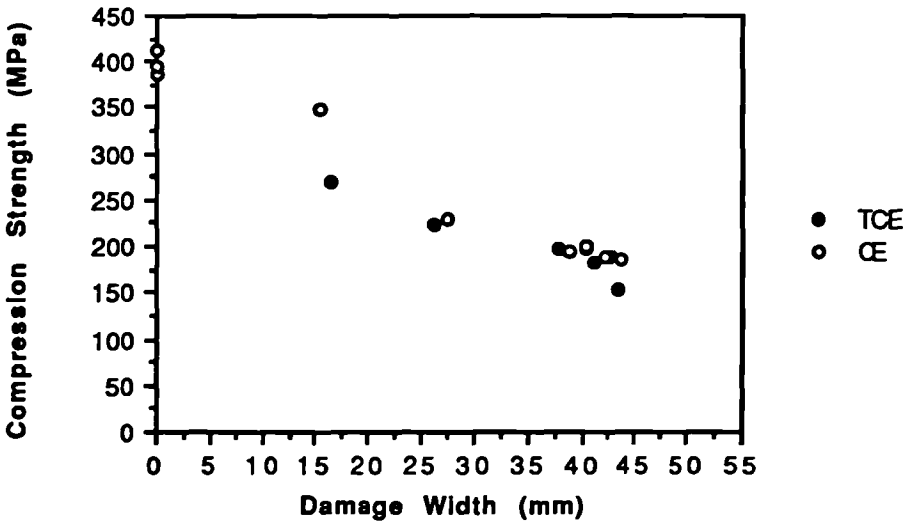

Fig 7.21 Compression strength versus incident impact energy for TCE and GRP-QI-16-55 materials.

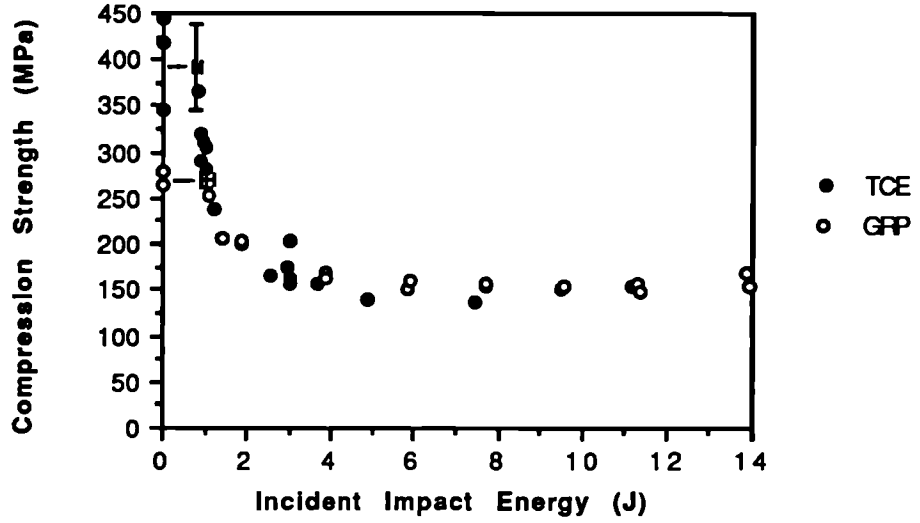

Fig 7.22 Normalised compression strength versus incident impact energy for TCE and GRP-QI-16-55 materials.

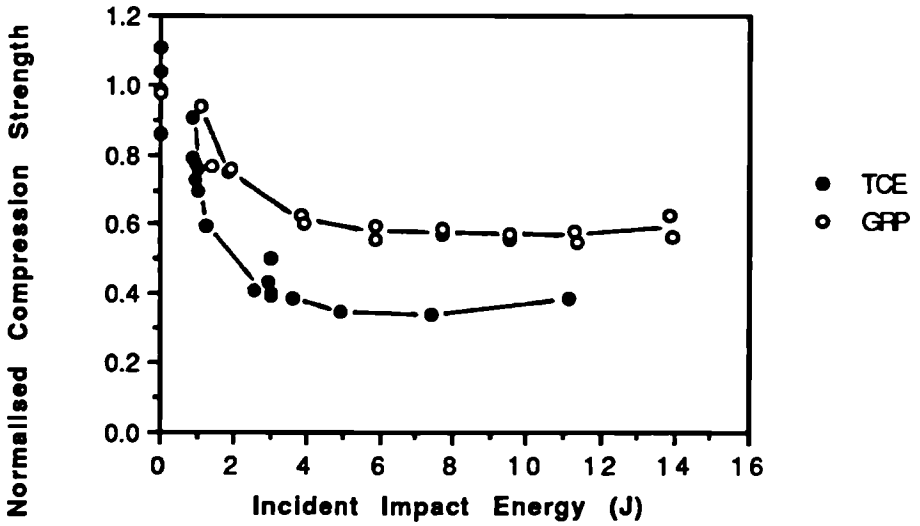

Fig 7.23 Compression strength versus damage width with 95% confidence and prediction intervals for GRP-QI-16-55 material.

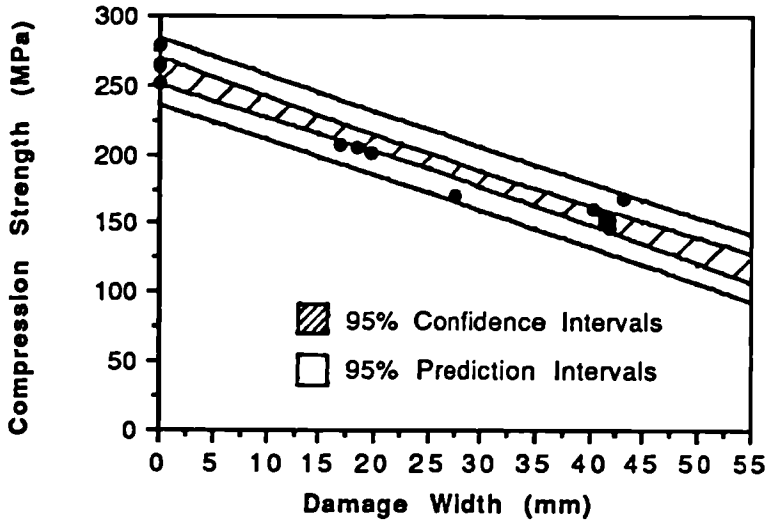

Fig 7.24 Normalised compression strength versus damage width for TCE and GRP-QI-16-55 materials.

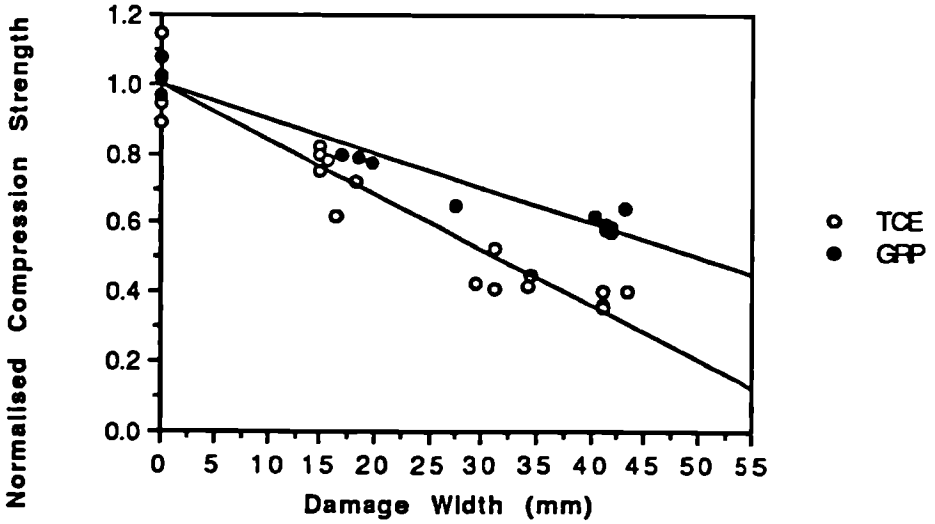

Fig 7.25 Normalised compression strength versus damage width. Comparison of 95% prediction intervals for TCE and GRP-QI-16-55.

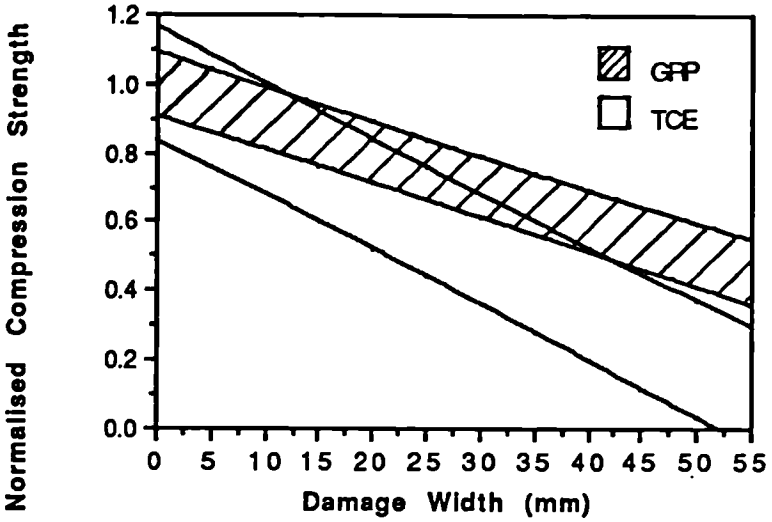

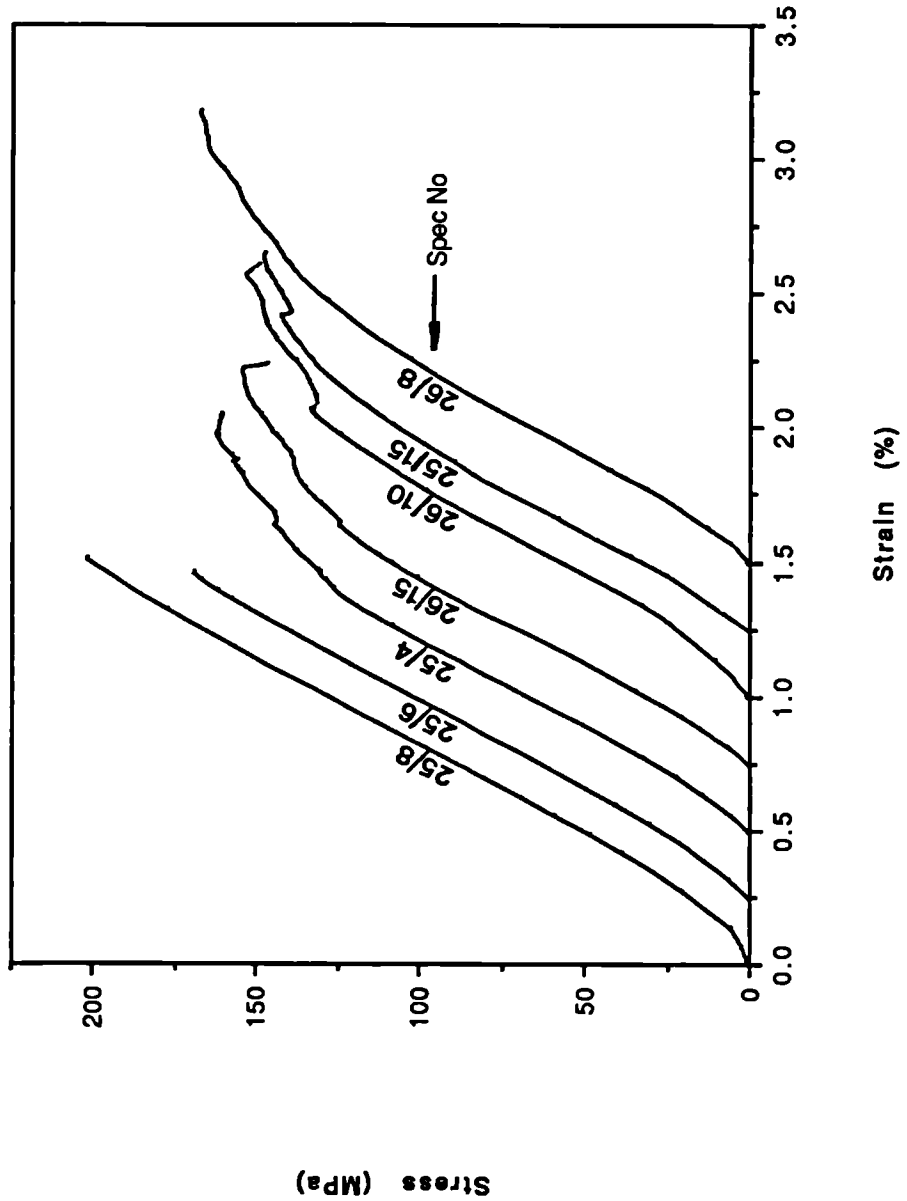

Fig 7.26 Stress - Strain graphs for residual compression tests on GRP-QI-16-55 material.

Fig 7.27 (a) Comparison of data for TCE-QI-32-55 and results from Ilcewicz et al (1989).

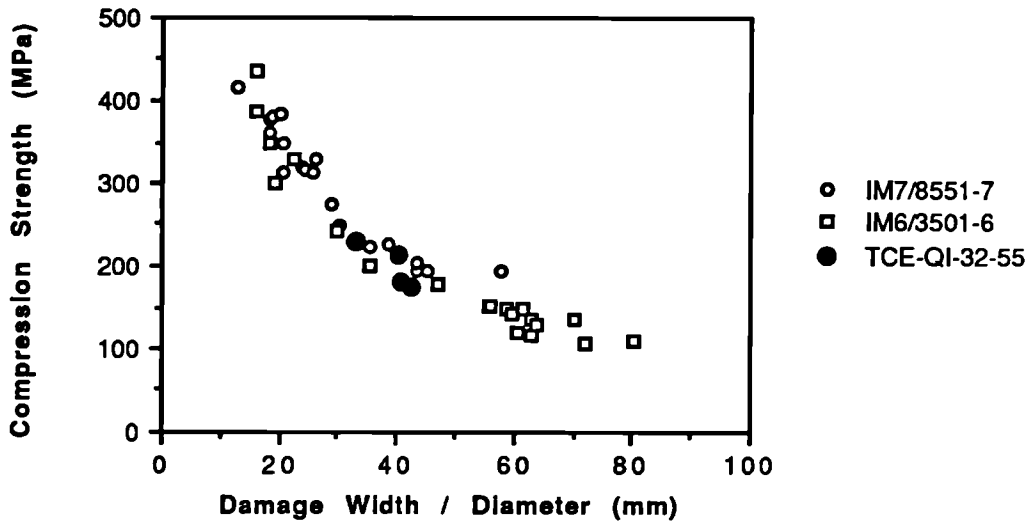

Fig 7.27 (b) Comparison of data for TCE-QI-24-55 and results from Ilcewicz et al (1989).

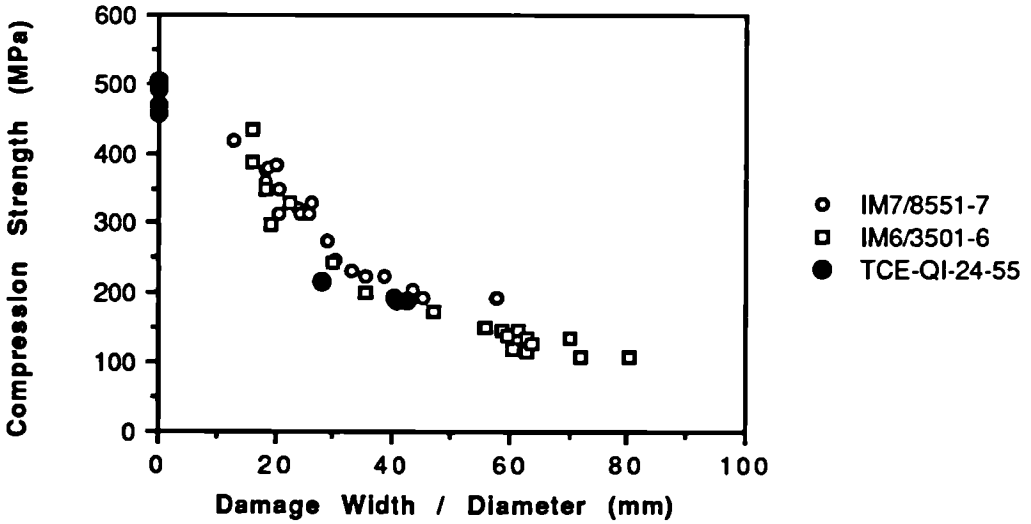

8 Concluding Discussion

8.1 Introduction

The object of this chapter is to discuss the post-impact compression test in more general terms in the light of the results presented in chapters 5, 6 and 7.

8.2 Impact

None of the current specifications for the PICS test require the impact part of the test to be instrumented. In this work an instrumented tup was used to measure force, enabling information about the velocity, displacement and absorbed energy during the test to be derived. The most useful information obtained was related to the initiation of damage. The force peak F1 (see fig 5.1 (a)) was found to be associated with the initiation of delamination damage. Following from this it was possible to estimate the incident energy required to initiate damage. This information is useful in terms of the PICS test because reductions in compression strength will only occur once this impact energy has been exceeded. Of the other parameters measured the total absorbed energy was potentially the most useful because of the widely held belief that a correlation between the total absorbed energy and the total amount of damage exists. In practice this correlation does not appear to be very reliable because materials with thermoplastic matrices can absorb energy in plastic deformation. This plastic deformation is not thought to contribute to the loss in residual strength, and therefore would not necessarily be classified as damage. In addition the total absorbed energy does not reveal any information about the extent of damage, and this has been shown to be important in determining the residual compression strength. The conclusion drawn from this work is that instrumented impact testing does not contribute very much to the understanding of the PICS test as a whole, and would not merit inclusion in any standard test method. Having said this the instrumented impact test will continue to be useful for research purposes.

One of the consequences of using a small compression test specimen is that there is only a limited area in which impact damage an be created during the impact part of the test. In this case a 40 mm diameter ring was used. The advantage of having a small support is that delamination damage is initiated at low incident impact energies with little evidence of other damage , which is ideal for the PICS test. An apparent disadvantage is that the maximum extent of in-plane damage is limited. The consequence of this is that a sudden cut-off in the curve occurs when compression strength is plotted as a function of incident impact energy, and the 'true' material response is not revealed. In fact this should not be a

problem provided the incident impact energies are chosen so that the damage width is 40 mm at the maximum incident energy used. This would allow a fair comparison of different materials. The point at which the impact damage first reached its maximum extent could be identified approximately by reference to the graph of residual strength versus incident impact energy. However, direct measurement of the extent of damage would be preferable, and given that the necessary equipment is available, is simple to measure. The problem is that the ultrasonic scanning equipment required is expensive and therefore would probably not be available on a wide enough basis to make this a compulsory part of any standard test, although it could be included as an option.

In the above discussion it has been taken as read that testing will be performed over a range of incident impact energies. In the SACMA test (Anon, 1988) a single, arbitrary impact energy of 1500 in-lbs/in is specified. The danger of this is that two materials may appear to have the same residual strength when in fact one material has superior properties to the other. This would have been the case if the TCE and APC materials had been compared at an incident impact energy of 14 J (see fig 7.13).

8.3 Compression Testing of Previously Undamaged Specimens

A measure of the undamaged strength is very useful because it provides a base-line strength against which the residual strength values can be compared. Having said this the anti-buckling guides used for the residual strength tests are not really suitable for measuring the undamaged strength. In this work failure occurred either in the unsupported region of the specimen or by end crushing. The end crushing failure will always be a problem for this type of loading arrangement and the only way to overcome the problem would be to use an end tabbed and shear loading arrangement. Improvements to the design of the ABG may help to stabilise the specimen. For example the ABG used for the SACMA test (Anon, 1988) provides support along the whole length of the specimen (the clamps on the end loading plates are narrow enough to fit between the brackets). However, even with this arrangement it is still likely that failure would occur close to the end of the specimen because of stress concentrations in this region. Compression strength is generally acknowledged to be highly dependent upon the geometry of the test method used, and this was confirmed in this work with compression strength generally decreasing as specimen width was increased. For this reason it is considered better to measure the strength using the ABG rather than to use some other method which may produce a higher value, but which would bear no relation to the strengths measured for the damaged specimens.

8.4 Post-Impact Compression Testing

In complete contrast to the tests on previously undamaged material the residual strengths were not significantly affected by variations in specimen width. In fact comparison of the results with those of Ilcewicz et al (1989) indicated strongly that the absolute dimensions of the specimen do not affect the results when the strengths are compared for the same extent of impact damage. The reason for this is that local rather than global specimen response controls the failure process. It is generally accepted that the PICS test is highly geometry dependent and this is reasonable. However, much of this geometry dependence originates from the impact part of the test rather than the compression test. This does not mean that the compression test is not affected by geometry. The type of ABG used is very important. The design of the ABG used in this work and that used by Ilcewicz et al (1989) were very similar and so comparison of the results to assess the effect of specimen size was valid. If the designs of the ABG's had been different then the comparison would not have been valid. This was demonstrated in the results of Davies et al (1990) who compared results from the Boeing test with those of their own miniaturised specimen. Their own test specimen was stabilised by bonding pieces of perspex to each face of the specimen. Different trends were found for the two test methods, leading the authors to conclude that the miniaturised test was not valid. The results reported in this thesis have demonstrated that the miniaturised test can work and it would appear that the reason for the difference in their results was that the face supported specimen local buckling was suppressed whereas the material was free to deform out of plane when tested in the Boeing ABG.

Based on the results reported in this thesis the following procedure would be recommended for future post-impact compression testing:

The simple impact test, already in general use for this test, should be retained. A free falling spherical impactor dropped down a guide tube, with the provision for achieving different incident impact energies would be adequate. After impact the lateral extent of damage should be measured. This would enable an assessment of the resistance of the material to the initiation and propagation of impact damage to be made. This should than be followed by a compression test, the compression strength results being plotted as a function of both damage width and incident impact energy. The former allows the damage tolerance of the material to be assessed, while the latter gives an indication of the overall performance, of the material.

If the currently available test specifications were to be used for this work it would be prohibitively expensive. The results presented in this thesis strongly suggest that the cost could be reduced by using a miniaturised test specimen. However, the cost would still be high since there are other factors to consider apart from the cost of the material and fabrication of the specimens, for example the labour cost.

An alternative suggestion is that materials could be selected simply on the basis of their resistance to the formation of impact damage. The results in chapter 7 showed that this was the most important factor in determining the residual compression strength for materials with a particular type of fibre. Of course this would not give any information about the damage tolerance of the material and for this reason the full test would still need to be used for materials development purposes.

9 Conclusions

The conclusions drawn below are valid for the particular testing conditions, ranges of specimen width and thickness, and material type and lay-up used to gather the experimental data.

9.1 Compression Testing of Previously Undamaged Specimens

Based on a limited amount of testing it was found that:

(a) The measured strength of previously undamaged material is highly dependent upon specimen geometry:

- Strength was found to decrease as specimen width was increased.
- Strength was found to increase as specimen thickness was increased.

(b) Two failure modes were observed; end crushing and failure in the unsupported region of the specimen. End crushing will always be a problem with the loading method used in this work. The failures in the unsupported region are related to buckling. Redesign of the ABG (using the method employed in the SACMA test) so that support is provided along the whole length of the specimen, may improve the situation.

(c) The measured strengths were lower than would have been measured if a test method designed for measurement of 'pure' compression strength had been used. However, the relative difference between the strengths of the carbon and glass materials measured in this work were reasonable.

(d) Measurement of the undamaged strength provides a useful baseline against which the post-impact compression strengths can be compared.

9.2 Post-Impact Compression Testing

(a) Specimen Geometry

-The PICS test results were found to be insensitive to specimen width. Comparison with results from the literature indicates that the results are insensitive to both specimen height and width. This appears to justify the use of a miniaturised test.

(b) Lay-up

-The 0/90 material was found to have the highest residual compression strength. Surprisingly, the residual strengths of the QI and ±45 materials were almost identical.

-Stacking sequence was found to have a small, but noticeable, effect on residual compression strength.

(c) To obtain the most information from the test it is recommended that:

-Testing should be performed over a range of incident impact energies.

-The resistance to impact damage should be assessed by plotting damage width as a function of incident impact energy.

-Damage tolerance should be assessed by plotting residual compression strength as a function of damage width.

- An overall comparison of different materials can be made by plotting a graph of residual strength against incident impact energy.

9.3 Materials

(a) Impact

- For the glass and carbon fibre reinforced materials with thermosetting matrices (epoxy) the resistance to the initiation and propagation of impact damage was found to be very similar. The carbon reinforced thermoplastic was considerably more resistant to the initiation and propagation of impact damage.

- For the TCE material the energy required to initiate damage increased linearly as specimen thickness was increased.

- Fibre lay-up did not have a significant effect on the energy required to initiate, or the final extent of damage for the TCE material.

(b) Post-Impact Compression Strength

- The carbon/thermoplastic material (APC) was found to retain higher residual compression strength than the carbon/epoxy materials.

- The superior strength of the APC is attributed to its ability to resist the initiation and propagation of impact damage. Because the two types of material had very similar residual strength for a particular amount of impact damage, the damage tolerance of the two materials is judged to be very similar.

Suggestions for Further Work

In Chapter 2 it was noted that there are a large number of testing variables related to the compression part of the post-impact compression test. A natural progression of the work reported in this thesis would be to investigate the effect of some of these variables. For example investigation into the effect of anti-buckling guide design and the method of load introduction would provide useful information, both for the development of a standard test method and a better understanding of the test in general.

In addition a study of the effect of impact test variables on the results of post-impact compression strength tests would also be of interest. It is known that the impact test conditions effect the extent and through thickness distribution of damage. Following on from the work reported here it is suggested that by plotting residual compression strength as a function of a damage parameter (damage width for example) the effect of impact test variables on the subsequent behaviour of the material could be assessed. Variables such as the size and shape of the support conditions and the size and profile of the impacter would be of interest. In addition the effect of using different mass / velocity combinations to deliver impacts of the same incident energy would be of interest.

From the work reported in this thesis here are strong indications that the use of a 'miniaturised' test to compare the post-impact compression behaviour of different materials. In order to confirm this it is suggested that direct comparison of several different test methods should be undertaken using a range of materials. The main aim of this work would be to increase confidence in the validity of a miniaturised test with the ultimate aim of it being adopted as a standard test.

Apart from investigations into the test method itself work aimed at understanding and improving the materials themselves is required. There is currently a lot of work being performed with the aim of improving the resistance to impact damage. The minimisation of damage from the impact event will help to improve the residual strength after an impact of a given energy. Work is required to gain a better understanding of the residual strength test itself so that the material properties which control the failure can be identified, and steps taken to improve them. At the same time other material properties, such as residual tensile strength after impact, need to be monitored to ensure that the improvements in one property do not lead to serious degradation in another.

Some studies of the effect of impact damage on the strength of real structures has already been undertaken, however, there is a need for more work. An understanding of the effect of impact damage on structures is important if procedures are to be formulated which allow designs to be optimised. In addition the utility of data collected using small test specimens needs to be assessed for its potential use as design data.

Composite materials often operate at elevated temperatures in both military and commercial aircraft applications, however, the effect of testing at elevated temperatures on the impact and post-impact performance does not appear to have received much attention and is another area which could be explored.

Some work has already been done to measure the performance of composite materials when a compression loaded test specimen is impacted. It has been suggested that the combined test defines a lower bound for the compression after impact strength. Further investigation into the performance of composite materials under the combined loading condition is required.

Acknowledgements

I would like to thank my supervisor, Dr P.J. Hogg, for his comments, suggestions and encouragement, freely offered during the course of this work.

Thanks also to Dr S. Turner for his occasional advice, which is greatly appreciated.

Thanks also to all the members of the lecturing staff, technicians and fellow students in the Materials Department who helped at one time or another with this work, and to Mr D. Bacon, of Media Services who printed the photographs for inclusion in this thesis.

I am indebted to the Department of Aeronautics at Imperial College of Science, Technology and Medicine for allowing me to use their Ultrasonic C-scanning machine. Particular thanks to Mr E. Godwin for his advice concerning the operation of the machine and the interpretation of the results.

Thanks to Ciba-Geigy (Duxford) and ICI (Wilton) who provided the materials for this work and to the SERC who provided the maintenance grant.

I am deeply grateful to Miss S. Grant and Mr E. Prichard for doing such a magnificent job of proof reading the text.

Finally, I would like to thank my parents for their unfailing support and encouragement.

References

Anderson, B.W.

The impact of carbon fibre composites on a military aircraft establishment. J. Phys. D: Appl. Phys. **20** (1987). pp 311 - 314.

Anglin, J.M.

Aircraft Applications. In Engineered Materials Handbook Vol 1. Composites. ASM International, 1988. pp 801 - 809

Anon

Advanced Composite Compression Tests. Boeing Specification Support Standard 7260 (1982).

Anon

Ciba-Geigy. Fibredux 913. Information Sheet No. FTA.46d. (1983).

Anon

Ciba-Geigy. Fibredux 914. Information Sheet No. FTA.49e. (1984).

Anon

NASA Aircraft Industry Standard Specification for Graphite Fibre Toughened Thermoset Resin Composite Material. NASA-RP-1142. (1985 (a)).

Anon

Standard test method for compressive properties of rigid plastics. ASTM D695-85 (1985 (b)).

Anon

Standard test method for compressive properties of unidirectional or crossply fiber-resin composites. ASTM D3410-87 (1987).

Anon

Ciba-Geigy. Fibredux 924. Information Sheet No. FTA.159b. (1988 (a)).

Anon

SACMA recommended test method for compression after impact properties of oriented fibre - resin composites. Recommended Method SRM 2-88 (1988 (b)).

Anon

Advanced Composites Bulletin. Elsevier Science Publishers, England. February, 1991.

Akoi, R. and Stellbrink, K.

The influence of defects on the behaviour of composites. AGARD Conference Proceedings No 355 (1980). pp 12-1 - 12-25.

Aldstadt, V., Heckmann, W., Tesch, H., Weber, T.H. and Recker, H.G.

From fundamental fracture mechanics investigations to highly damage tolerant prepreg systems. In Proc. 11th SAMPE European Chapter Conference, Basel, Switzerland. May 1990. pp 267 - 280.

Avva, V.S.

Buckling behaviour of laminated composites subjected to low - velocity impact. In Compression testing of homogeneous materials and composites, ASTM STP 808. American Society for Testing and Materials, 1983, pp 140 - 154.

Bajpai, A.C., Callus, I.M. and Fairley, J.A.

Statistical Methods for Engineers and Scientists. John Wiley and Sons, 1982

Baker, A.A., Jones, R. and Callinan, R.J.

Damage tolerance of graphite / epoxy composites. Composite Structures **4** (1985) pp 15 - 44.

Barker, A.J. and Balasundaram, V.

Compression testing of carbon fibre - reinforced plastics exposed to humid environments. Composites **18**, 1987. pp 217 - 226.

Bishop, S.M. and Dorey, G.

The effect of damage on the tensile and compressive performance of carbon fibre laminates. AGARD Conference Proceedings No 355 (1983). pp 10-1 - 10-10.

Bishop, S.M.

The mechanical performance and impact behaviour of carbon-fibre reinforced PEEK. Composite Structures **3** (1985) pp 295 - 318.

Boll, D.J., Bascom, W.D., Weidner, J.C. and Murri, W.J.

A microscopy study of impact damage of epoxy-matrix carbon-fibre composites. Journal of Materials Science **21** (1986) pp 2667 - 2677.

Bowles, K.J.

The correlation of low-velocity impact resistance of graphite-fibre-reinforced composites with matrix properties. In Composite Materials: Testing and Design (Eighth Conference), ASTM STP 972. American Society for Testing and Materials, Philadelphia, 1988, pp. 124 - 142.

Bradshaw, F.J., Dorey, G. and Sidey, G.R.

Impact resistance of carbon fibre reinforced plastic. Royal Aircraft Establishment, Technical Report 72240 (1972).

Brandt, J. and Warnecke, J.

Influence of material parameters on the impact performance of carbon-fibre-reinforced polymers. In High Tech - the way into the nineties. Eds: Brunsch. K, Golden, H.D. and Herkert, C.M. Elsevier Science Publishers B.V. Amsterdam, 1986. pp 251 - 260.

Brandt, J., Preller, T. and Drechsler, K.

Manufacturing and mechanical properties of 3-D fibre reinforced composites. Materials and processing - move into the 90's. Proc. of the eighth SAMPE (European Chapter) International Conference. Ed: Benson, S., Trewin, E. and Turner, R.M. Elsevier Science Publishers B.V., Amsterdam, 1989. pp 63 - 73.

Brunelle E.J. and Oyibo, G.A.

Generic buckling curves for specially orthotropic rectangular plates. AIAA Journal **21**(1983). pp 1150 - 1156.

Brush, D.O. and Almroth, B.O.

Buckling of Bars, Plates and Shells. MGraw-Hill, 1975.

Bucknall, C.B.

Approaches to toughness enhancement. In Advanced Composites. Ed: Partridge, I.K. Elsevier Applied Science Publishers, 1989. pp 145 - 161.

Buskell, N., Davies, G.A.O. and Stevens, K.A.

Postbuckling failure of composite panels. Composite Structures **3** (1985). pp 291 - 314.

Cantwell, W.J.and Morton, J.

Detection of impact damage in CFRP laminates. Composite Structures **3** (1985) pp 241 - 257.

Cantwell, W.J, Curtis, P.T. and Morton, J.

An assessment of the impact performance of CFRP reinforced with high strain carbon fibres. Composites Science and Technology **25** (1986) pp 133 - 148.

Cantwell, W.J.

The influence of target geometry on the high velocity impact response of CFRP. Composite Structures **10** (1988) pp 247 - 265

Cantwell, W.J.and Morton, J. 1989(a)

Comparison of low and high velocity response of CFRP. Composites **20** (1989) pp 545 - 551.

Cantwell, W.J.and Morton, J. 1989(b)

Geometrical effects in the low velocity impact response of CFRP. Composite Structures **12** (1989) pp 39 - 59.

Chatfield, C.

Statistics for Technology. Chapman and Hall, London, 1978.

Cheresh, M.C. and McMichael, S.

Instrumented impact test data interpretation. In Instrumented Impact Testing of Plastics and Composite Materials. ASTM STP 936. American Society for testing and Materials, 1987. pp 9 - 23.

Clark, R.K. and Lisagor, W.B.

Compression testing of graphite / epoxy composite materials. In Test methods and design allowables for fibrous composite materials. ASTM STP 734. American Society for Testing and Materials, 1981, pp. 34 - 53.

Curtis, P.T.

An investigation of the mechanical properties of improved carbon fibre composite materials. Journal of Composite Materials **21** (1987). pp 1118 - 1145.

Curtis, P.T.

CRAG test methods for the measurement of the engineering properties of fibre reinforced plastics. Royal Aircraft Establishment, Technical Report 88012 (1988).

Curtis, P.T.

Composite materials selection for damage tolerance. Royal Aircraft Establishment, Technical Report 89053 (1989).

Daniel, I.M. and Wooh, S.C.

Deformation and damage of composite plates under impact loading. Proc. of International Symposium on Composite Materials and Structures Beijing, China, 1986. Eds: T.T. Loo and C.T. Sun. Technomic Publishing Co, 1986.

Davies, C.K.L., Turner, S. and Williamson, K.H.

Flexed plate testing of carbon fibre reinforced polymer composites. Composites **16** (1985). pp 279 - 285.

Davies, M. and Moore, D.R.

Laboratory - scale screening of mechanical properties of resins and composites: relevance to composites for aerospace applications. Composites Science and Technology **40** (1990) pp 131 - 146.

Dexter, H.B.

Composite components on commercial aircraft. AGARD Conference Proceedings No 288 (1980). pp 19-1 - 19-22.

Donaldson, S.L.

The effect of interlaminar fracture properties on the delamination buckling of composite laminates. Composites Science and Technology **28** (1987) pp 33 - 44.

Dorey, G.

Fracture of composites and damage tolerance. AGARD Conference Proceedings No 124 (1982). pp 6-1 - 6-12.

Dorey, G., Bishop, S.M. and Curtis, P.T.

On the impact performance of carbon fibre laminates with epoxy and PEEK matrices. Composite Science and Technology **23** (1985) pp 221 - 237.

Dorey, G.

Impact and crashworthiness of composite structures. In Structural impact and crashworthiness. Volume 1. Ed: G.A.O Davies. Elsevier Applied Science Publishers, London, 1984.

Dorey, G.

Impact damage in composites - development, consequences and prevention. In Proc. ICCM VI and ECCM II, London 1987, Elsevier Applied Science Publishers, London 1987. pp 155 - 192

Dost, E.F., Ilcewicz, B. and Gosse, J.H.

Sublaminate stability based modelling of impact damaged composite laminates. In Proc. American Society for Composites, 3rd Technical Conference, September 1988. pp 354 - 363.

Ewins, P.D. and Ham, A.C.

The nature of compressive failure in unidirectional carbon fibre reinforced plastics. Royal Aircraft Establishment, Technical Report 73057 (1973).

Freeman, S.M.

Characterisation of lamina and interlaminar damage in graphite / epoxy composites by the deply technique. In Composite Materials: Testing and Design (Sixth Conference), ASTM STP 787. American Society for Testing and Materials, Philadelphia, 1982, pp. 50 - 62.

Galiotis, C.

Private Communication. (1990)

Ghaseminejhad, M.N. and Parvizi-Majidi, A.

Impact behaviour and damage tolerance of woven carbon - fibre reinforced composites. Composites **21** (1990). pp 155 - 167.

Gibson, A.G., Mines, R.A.W. and Worrall, C.M.

The impact and static behaviour of twin-skinned GRP laminates under three point bending. Fibre Reinforced Composites, 3rd International Conference. The Plastics and Rubber Institute. 1988. pp 20.1 - 20.9.

Greenhalgh, E.S.

On defect growth and failure in carbon fibre composite structures. Royal Aircraft Establishment, Technical Report 89045 (1989).

Greszczuk 1982

Damage in composite materials due to low velocity impact. Ch 3 in Impact Dynamics. Eds: J.A. Zukas, T. Nicholas, H.F. Swift, L.B. Greszczuk and D.R. Curran. John Wiley and Sons, 1982.

Griffin, C.E.

Damage tolerance of toughened resin composites. In Toughened Composites, ASTM STP 937. American Society for Testing and Materials, Philadelphia, 1987, pp. 23 - 33.

Guynn, E.G. and O'Brien, T.K.

The influence of lay-up and thickness on composite impact damage and compression strength. American Institute of Aeronautics and Astronautics, 1985. Paper No 85-0646.

Hart-Smith, L.J.

The story of the design and development of the first lear fan all-composite aircraft. Paper presented at International Conference on Design in Composite Materials, 7 - 8 March, 1989. IMechE, London.

Hirschbuehler, K.R.

An improved 270 ^{o}F performance interleaf system having extremely high impact resistance. SAMPE Quarterly **17** (1985) pp 46 - 49.

Hogg, P.J. and Turner, S.

The mechanical testing of long - fibre composites: Harmonisation and standardisation in the UK. Department of Materials, Queen Mary College, 1988.

Hoskin, B.C. and Baker, A.A.

Damage tolerance of fibre composite laminates. Ch 10 in: Composite materials for aircraft structures. Eds: Hoskin, B.C. and Baker, A.A. AIAA Education Series, New York, 1986.

Hull, D.

An Introduction to Composite Materials. Cambridge University Press (1981).

Ilcewicz, L.B., Dost, E.F. and Coggeshall, L.

A model for compression after impact strength evaluation. 21st International SAMPE Technical Conference (1989). pp 130 - 140.

Ireland, D.R.

Procedures and problems associated with reliable control of the instrumented impact test. ASTM STP 563. American Society for Testing and Materials, 1973. pp 3 -29.

Ishai, O. and Shragai, A.

Effect of impact loading on damage and residual compressive strength of CFRP laminated beams. Composite Structures **14** (1990) pp 319 - 337.

Jones, R., Baker, A.A. and Callinan, R.J.

Residual strength of impact - damaged composites. Technical Note. Composite Structures **2** (1984) pp 371 - 372.

Judd, N.C.W and Wright, W.W.

Voids and their effect on the mechanical properties of composites - an appraisal. SAMPE Journal. Jan/Feb (1978). pp 10 -14.

Kakarala, S. and Roche, J.L.

Experimental comparison of several impact test methods. In Instrumented impact testing of plastics and composite materials. ASTM STP 936. American Society for Testing and Materials, Philadelphia, 1987, pp. 144 -162.

Kardomateas, G.A. and Schmueser, D.W.

Buckling and postbuckling delaminated composites under compressive loads including transverse shear effects. AIAA Journal **26** (1988) pp 337 - 343.

Kutlu, Z. and Chang, F.K.

Compression strength of laminated composites containing multiple delaminations. Proc. American Society for Composites, 3 rd Technical Conference, September 1990.

Leach, D.C.

Continuous fibre reinforced thermoplastic matrix composites. In Advanced Composites. Ed: Partridge, I.K. Elsevier Applied Science Publishers, 1989. pp 43 - 109.

Lee, R.F., Scott, P.C., Gaudert, W.H., Ubbink, W.H. and Poon, C.

Mechanical testing of toughened resin composite materials. Composites **19** (1988) pp 300 - 310.

Lee, R.J.

Compression strength of aligned carbon fibre - reinforced thermoplastic laminates. Composites **18** (1987). pp 35 - 39.

Leonard, L.

Compression test results - a tough nut to crack. Advanced Composites Vol 4 No 4 (1989), pp 57 - 63.

Leissa, A.W.

Buckling of laminated composite plate and shell panels. Flight Dynamics Laboratory, Wright Patterson Air Force Base, Dayton, Ohio. Report No AFWAL-TR-85-3069 (1985 (a)).

Leissa, A.W.

An overview of composite plate buckling. Composite Structures 4 (1985 (b)). pp 1.1 - 1.29.

Manders, P.W. and Harris, W.C.

A parametric study of composite performance in compression - after - impact testing. SAMPE Journal **22** (1986) pp 47 - 50.

Masters, J.E.

Correlation of impact and delamination resistance in interleafed laminates. In Proc. ICCM VI and ECCM II, London 1987, Elsevier Applied Science Publishers, London 1987 (a).

Masters, J.E.

Characterisation of impact damage development in graphite / epoxy laminates. in Fractography of Modern Engineering Materials: Composites and Metals. ASTM STP 948. American Society for Testing and Materials. 1987 (b). pp 238 - 258.

Matondang, T.H. and Schutz, D.

The influence of anti-buckling guides on the compression - fatigue behaviour of carbon - fibre reinforced plastic laminates. Composites **15** (1984). pp 217 - 221.

McMullen, P.

Fibre / resin composites for aircraft primary structures: a short history, 1936 - 1984. Composites **15** (1984) pp 222 - 230.

Morton, J. and Godwin, E.W.

Impact response of tough carbon fibre composites. Composite Structures **13** (1989) pp 1 -19.

Mousley, R.F.

In-plane compression of damaged laminates. In Structural Impact and Crashworthiness Vol 2. Ed: J. Morton. Elsevier Applied Science Publishers 1984. pp 494 - 509.

Neal, D. and Vangel, M.

Statistical Analysis of Mechanical Properties. In Engineered Materials Handbook Vol 1. Composites. ASM International, 1988. pp 302 - 307.

Odagri, N., Muraki, T. and Tobukuro, K.

Toughness improved high performance Torayca prepreg T800H / 3900 series. 33rd International SAMPE Symposium 1986. pp 272 - 283.

Partridge, I.K.

High temperature thermosetting resin matrix resins. In Advanced Composites. Ed: Partridge, I.K. Elsevier Applied Science Publishers, 1989. pp 7 - 41.

Pavier, M.J. and Chester, W.T.

Compression failure of carbon fibre - reinforced coupons containing central delaminations. Composites **21** (1990). pp 23 - 31.

Port, K.F.

The compressive strength of carbon fibre reinforced plastics. Royal Aircraft Establishment, Technical Report 82083 (1982).

Preuss, T.E. and Clark, B.

Use of time-of-flight-C-scanning for assessment of impact damage in composites. Composites **19** (1988) pp 145 - 148.

Purslow, D.

Fractography of fibre - reinforced thermoplastics, Part 3. Tensile, compressive and flexural failures. Composites **19** (1988). pp 358 - 366.

Recker, H.G., Allspach, T., Altstadt, V., Folda, T., Heckmann, W., Ittermann, P., Linden, G., Tesch, H. and Weber, T.

Damage tolerant carbon fibre epoxy composites for aerospace applications. Materials and processing - move into the 90's. Proc. of the eighth SAMPE (European Chapter) International Conference. Ed: Benson, S., Trewin, E. and Turner, R.M. Elsevier Science Publishers B.V., Amsterdam, 1989. pp 63 - 73.

Recker, H.G., Aldstadt, V., Eberle, W., Folda, T., Gerth, D., Heckmann, W., Ittermann, P., Tesch, H. and Weber, T.

Toughened thermosets for damage tolerant carbon fibre reinforced composites. SAMPE Journal **26** (1990). pp 73 - 78.

Reed, P.R. and Turner, S.

Flexed plate impact, part 7. Low energy and excess energy impacts on carbon fibre-reinforced polymer composites. Composites **19** (1988) pp 193 - 203.

Reed, P.R.

Developments in instrumented impact testing of plastics and composites. Progress in Rubber and Plastics Technology 5 (1989) pp 157 - 172.

Rhodes, M.D., Williams, J.G. and Starnes, J.H. Jr.

Low - velocity impact damage in graphite fiber reinforced epoxy laminates. In Proc 34th Annual Technical Conference of the Reinforced Plastics / Composites Institute. The Society of the Plastics Industry Inc. (1979). Section 20-D pp 1 - 10.

Ryder, J.T. and Black, E.D.

Compression testing of large gauge length composite coupons. ASTM STP 617. American Society for Testing and Materials, Philadelphia, 1977, pp. 170 - 189.

Sokal, R.R.

Biometry. W.H. Freeman and Company. San Fransisco. 1969.

Sharples, T.

Applications of carbon fibre composites to military aircraft structures. Aeronautical Journal. July 1990. pp 177 - 182.

Sjoblom, P.O., Hartness, J.T. and Cordell, T.M.

On low-velocity impact testing of composite materials. Journal of Composite Materials 22 (1988) pp 30 - 52.

Sjoblom, P.O. and Hwang, B.

Compression after impact: the $5,000 data point. 34th International SAMPE Symposium, Reno, May 8 - 11 (1989). pp 1411 - 1421.

Soulezelle, B.

Low velocity impacts on carbon resin composites. Influence of experimental conditions. In Looking ahead for materials and processes. Proc. of the eighth SAMPE (European Chapter) International Conference. Eds: de Bossu, J.; Briens, G. and Lissac, P. Elsevier Science Publishers B.V., Amsterdam, 1987. pp 331 - 343.

Stone, D.E.W. and Clarke, B.

Non-destructive evaluation of composite structures - an overview. In Proc. ICCM VI and ECCM II, London 1987, Elsevier Applied Science Publishers, London 1987.

Stuart, M. and Altstadt, V.

Carbon fibre surface treatment and effect on composite damage tolerance performance. 21st International SAMPE Technical Conference (1989). pp 264 - 274.

Stubbington, C.A.

Materials trends in military airframes. Metals and Materials. July (1988). pp 424 - 431.

Sun, C.T. and Rechak, S.

Effect of adhesive layers on impact damage in composite laminates. ASTM STP 972. American Society for Testing and Materials, Philadelphia, 1988, pp. 97 - 123.

Takeda, N., Sierakowski, R.L. and Malvern, L.E.

Microscopic observations of cross sections of impacted composite laminates. Composites Technology Review **4** (1982). pp 40 - 44.

Timoshenko, S.

Theory of Elastic Stability. McGraw Hill. 1936.

Timoshenko, S.

Strength of Materials. Part II, Advanced. Van Nostrand Reinhold Company, 1958.

Verpoest, I., Marien, J, and Wevers.

Is absorbed energy a test independent parameter for damage and residual strength after impact ? Composites Evaluation Ed: J. Herriot. Proc 2nd International Conf. on Testing, Evaluation and Quality Control of Composites, 1987. pp 69 - 77.

Wedgewood, A.R., Su, K.B. and Narin, J.A.

Toughness properties and service performance of high temperature thermoplastics and their composites. SAMPE Journal Jan / Feb 1988. pp 41 - 45.

Whitney, J.M., Daniel, I.M. and Pipes, R.B.

Experimental Mechanics of fibre reinforced composite materials. Society for experimental mechanics. Monograph No 4, 1982.

Williams, J.G.

Fracture Mechanics of Composites Failure. Proceedings of the Institute of Mechanical Engineers. Part C, Journal of Mechanical Engineering Science. Vol 204, No 4C, 1990. pp 209 - 218.

Woolstencroft, D.H., Curtis, A.R. and Haresceugh. R.I.

A comparison of test techniques used for the evaluation of the unidirectional strength of carbon fibre-reinforced plastic. Composites **12** (1981) pp 275 - 280.

Wu, H.Y. and Springer, G.S.

Measurements of matrix cracking and delamination caused by impact on composite plates. Journal of Composite Materials **22** (1988). pp 518 - 532.

Appendix A
Results of ILSS Tests

Note: Standard deviations and coefficients of variation are shown in brackets when less than five results are available.

Table A1

TCE-±45-16

Laminate No	ILSS (MPa)	Average (MPa)	Standard Deviation (MPa)	Coefficient of Variation
7	58.9 58.5 57.5 62.5 54.8 60.2 53.9 55.4	57.7	2.9	5.0%
9	58.6 53.8 57.1 58.2 57.7	57.1	1.9	3.3%
20	53.5 58.2 49.2 51.3 54.2	53.3	3.4	6.4%
27	51.5 59.5 52.3 49.3 50.0	52.5	4.1	7.8%
28	40.4 60.3 54.8 53.8 53.0	52.5	7.3	13.9%
29	56.5 52.5 45.4 60.3 45.5	52.0	6.6	12.7%
30	58.3 48.9 55.7 48.9 56.1	53.6	4.4	8.2%
31	58.6 49.7 53.6 62.3 53.1	55.5	5.0	9.0%
46	53.4 50.4 50.4 51.4 46.9	50.5	2.4	4.8%

Table A2

TCE-0/90-16

Laminate No	ILSS (MPa)	Average (MPa)	Standard Deviation (MPa)	Coefficient of Variation
1	53.5 54.1 57.3 59.2 47.6 53.5 49.9 50.2 51.2 52.7 41.7	51.9	4.7	9.1%
6	95.8 95.9 97.3 98.4 95.6	96.6	1.2	1.2%
11	94.8 96.1 98.7 95.1 101.3	97.2	2.8	2.9%
12	97.0 91.7 98.6 93.6 90.7	94.3	3.4	3.6%
13	88.9 104.4 87.7 79.0 88.7	89.7	9.2	10.3%
14	98.7 102.2 86.2 94.4 94.6	95.2	6.0	6.3%
15	97.1 96.8 94.2 93.1 89.7	94.2	3.0	3.2%
49	93.0 97.4 94.7 98.2 95.5	95.8	2.1	2.2%

Table A3

TCE-QI-16

Laminate No	ILSS (MPa)	Average (MPa)	Standard Deviation (MPa)	Coefficient of Variation
2	66.2 72.7 80.5 55.0	68.6	(10.8)	(15.7%)
3	74.6 67.6 67.1	69.8	(4.2)	(6.0%)
4	75.2 75.3 71.7 60.2	70.6	(7.1)	(10.1%)
32	74.6 83.9 89.5 82.9 81.7	82.5	5.3	6.4%
33	81.0 83.5 91.3 87.9 73.7	83.5	6.8	8.1%
34	75.6 75.1 83.4 86.2 70.7	78.2	6.4	8.2%
35	71.9 78.8 69.7 70.0 71.6	72.4	3.7	5.1%
41	77.3 84.4 80.1 84.2 83.7	81.9	3.1	3.8%
42	84.4 77.9 84.4 82.6 84.2	82.7	2.8	3.4%
47	82.7 77.3 79.4 81.0 75.9	79.3	2.7	3.4%
48	77.3 77.2 81.4 88.2 87.5	82.3	5.3	6.4%

Table continued on next page

Table A3 continued

TCE-QI-16

Laminate No	ILSS (MPa)	Average (MPa)	Standard Deviation (MPa)	Coefficient of Variation
54	90.3 83.9 77.9 83.6 78.7	82.9	5.0	6.0%

Table A4

TCE-QI-24

Laminate No	ILSS (MPa)	Average (MPa)	Standard Deviation (MPa)	Coefficient of Variation
39	87.1 80.5 81.1 83.1 82.2	82.8	2.6	3.1%
40	73.0 76.6 80.1 80.7 80.6	78.2	3.4	4.3%
50	83.3 85.5 84.3 78.3 81.5	82.6	2.8	3.4%

Table A5

TCE-QI-32

Laminate No	ILSS (MPa)	Average (MPa)	Standard Deviation (MPa)	Coefficient of Variation
37	83.8 84.4 84.1 81.8 88.7	84.6	2.5	3.0%
38	79.3 81.0 80.6 87.6 85.9	82.9	3.6	4.3%
51	86.9 81.6 88.7 84.9 78.0	84.0	4.3	5.1%

Table A6

TCE-0-16 (See notes below for details of post-cure)

Laminate No	ILSS (MPa)	Average (MPa)	Standard Deviation (MPa)	Coefficient of Variation
17A	103.8 101.3 104.0 107.3 102.0	103.7	2.3	2.2%
17B	108.0 112.9 102.6 100.6 102.0	105.2	5.1	4.8%
18A	100.3 110.9 103.9 111.9 102.4	105.9	5.2	4.9%
18B	105.3 113.7 106.2 109.6 105.0	108.0	3.7	3.4%
18C	103.1 98.0 104.7 109.4 100.3	103.1	4.4	4.3%
19C	103.6 106.3 110.6 110.1	107.7	(3.3)	(3.1%)
36A	106.5 107.6 101.8 104.8 106.3	105.4	2.2	2.1%

Note: A = No post-cure
B = Post-cure 180 °C for 2 hours
C = Post-cure 210 °C for 4 hours

Table A7

CE-QI-16

Laminate No	ILSS (MPa)	Average (MPa)	Standard Deviation (MPa)	Coefficient of Variation
52	72.2 61.0 62.3 68.8 67.6	66.4	4.7	7.1%

Table A8

APC-QI-16

Laminate No	ILSS (MPa)	Average (MPa)	Standard Deviation (MPa)	Coefficient of Variation
21	82.6 85.9 84.1 82.3 84.3	83.8	1.5	1.8%
22	93.0 92.0 89.9 90.5 81.4	89.4	4.6	5.1%
53	97.2 88.9 94.0 87.3 88.4	91.2	4.2	4.6%

Appendix B
Results of Impact Tests

Table B1

TCE-±45-16-45

Specimen Number	Incident Impact Energy (J)	F1 (KN)	AE1 (J)	D1 (mm)	F2 (KN)	AE2 (J)	D2 (mm)	TAE (J)	Damage Width (mm)
31/1	1.25	1.95	0.99	1.00	1.95	0.99	1.00	0.75	0
31/4	2.52	2.35	1.50	1.28	2.35	2.55	1.75	1.36	19.7
31/5	3.65	2.75	1.91	1.35	2.75	3.61	2.08	2.13	31.1
7/2	4.88	-	-	-	-	-	-	-	38.5
7/4	7.44	2.60	1.62	1.24	4.50	7.56	3.17	3.79	39.4
7/1	11.12	2.70	1.66	1.25	6.05	10.84	3.74	8.04	41.0

Table B2

TCE-±45-16-55

Specimen Number	Incident Impact Energy (J)	F1 (KN)	AE1 (J)	D1 (mm)	F2 (KN)	AE2 (J)	D2 (mm)	TAE (J)	Damage Width (mm)
29/6	1.25	2.15	1.15	1.02	2.15	1.15	1.02	0.34	0
29/1	2.55	2.60	1.71	1.26	2.60	1.71	1.26	1.68	31.2
29/2	3.65	2.50	1.45	1.19	2.75	3.70	2.16	2.24	32.8
30/6	4.93	2.80	1.78	1.31	3.40	4.92	2.51	2.68	37.8
30/4	7.47	2.70	1.62	1.24	4.60	7.18	3.11	4.00	39.4
30/3	11.12	2.70	1.57	1.24	5.80	10.28	3.71	8.42	41.0

Table B3

TCE-±45-16-75

Specimen Number	Incident Impact Energy (J)	F1 (KN)	AE1 (J)	D1 (mm)	F2 (KN)	AE2 (J)	D2 (mm)	TAE (J)	Damage Width (mm)
27/4	1.25	2.20	1.29	1.13	2.20	1.29	1.13	0.34	0
28/4	2.51	2.80	1.80	1.34	2.80	1.80	1.34	1.58	26.3
28/3	3.61	2.50	1.45	1.21	2.80	3.70	2.22	2.06	36.1
20/3	4.88	2.50	1.43	1.16	3.50	4.89	2.51	2.65	39.4
20/2	7.47	2.30	1.22	1.13	4.95	7.57	3.20	3.64	39.4
27/1	11.18	2.50	1.45	1.22	6.00	11.02	3.82	8.44	41.9

Table B4

TCE-0/90-16-45

Specimen Number	Incident Impact Energy (J)	F1 (KN)	AE1 (J)	D1 (mm)	F2 (KN)	AE2 (J)	D2 (mm)	TAE (J)	Damage Width (mm)
6/5	1.13	2.00	1.18	1.07	2.00	1.18	1.07	0.47	0
15/3	1.93	2.70	1.77	1.23	2.70	1.77	1.23	1.22	21.3
15/2	2.43	2.70	1.86	1.33	2.70	1.86	1.33	1.39	24.6
14/1	4.72	2.60	1.58	1.21	3.10	4.69	2.43	3.30	34.5
15/5	7.65	2.85	1.92	1.38	4.05	7.63	3.23	6.29	37.8
14/2	11.34	2.80	1.68	1.21	5.35	10.34	3.68	10.04	41.8

TableB5

TCE-0/90-16-55

Specimen Number	Incident Impact Energy (J)	F1 (KN)	AE1 (J)	D1 (mm)	F2 (KN)	AE2 (J)	D2 (mm)	TAE (J)	Damage Width (mm)
14/4	1.19	2.20	1.24	1.03	2.20	1.24	1.03	0.48	0
11/4	1.94	2.65	1.69	1.30	2.65	1.69	1.30	1.33	21.3
6/4	2.47	2.80	1.95	1.36	2.80	1.95	1.36	1.64	22.2
15/4	4.82	2.85	1.76	1.26	3.10	4.50	2.35	3.81	37.8
11/1	7.65	2.85	1.70	1.25	4.25	7.33	3.11	6.27	41.9
6/2	11.44	2.55	1.47	1.19	5.20	9.87	3.64	10.70	42.7

TableB6

TCE-0/90-16-75

Specimen Number	Incident Impact Energy (J)	F1 (KN)	AE1 (J)	D1 (mm)	F2 (KN)	AE2 (J)	D2 (mm)	TAE (J)	Damage Width (mm)
11/3	1.25	2.25	1.29	1.09	2.25	1.29	1.09	0.49	0
12/2	1.94	2.75	1.73	1.26	2.75	1.73	1.26	1.32	24.6
13/5	4.74	2.60	1.58	1.27	3.25	4.69	2.45	3.80	27.9
12/3	7.65	2.80	1.64	1.23	4.15	7.41	3.08	6.42	43.5
12/5	11.39	2.90	1.73	1.24	5.50	10.68	3.66	9.98	41.0

Table B7

TCE-QI-16-45

Specimen Number	Incident Impact Energy (J)	F1 (KN)	AE1 (J)	D1 (mm)	F2 (KN)	AE2 (J)	D2 (mm)	TAE (J)	Damage Width (mm)
4/5	1.89	1.70	0.88	1.06	1.95	1.94	1.68	1.21	27.9
4/4	3.85	1.70	0.79	0.96	3.30	3.95	2.43	1.87	37.8
3/5	5.68	1.60	1.06	1.09	4.30	5.79	2.82	2.80	41.0
2/2	7.64	1.70	0.78	0.92	5.70	7.70	3.09	3.10	45.0
3/4	9.61	1.65	0.75	0.94	6.75	9.47	3.48	4.69	45.0
4/1	11.44	1.50	0.61	1.53	7.40	11.62	4.43	5.55	45.0

Table B8

TCE-QI-16-55-Clamped

Specimen Number	Incident Impact Energy (J)	F1 (KN)	AE1 (J)	D1 (mm)	F2 (KN)	AE2 (J)	D2 (mm)	TAE (J)	Damage Width (mm)
54/1	0.86	1.75	0.80	0.86	1.75	0.80	0.86	0.54	14.8
54/5	0.87	1.75	0.88	0.97	1.75	0.88	0.97	0.56	14.8
41/6	0.92	1.90	0.94	0.93	1.90	0.94	0.93	0.55	14.8
41/2	0.96	1.75	0.81	0.89	1.75	0.81	0.89	0.58	14.8
47/1	1.04	2.00	1.01	0.99	2.00	1.01	0.99	0.69	18.1
42/1	1.04	1.90	0.90	0.98	1.90	0.90	0.98	0.66	15.6
3/6	1.24	1.65	0.79	0.99	1.65	1.29	1.30	0.69	16.4
54/2	1.41	1.80	0.87	1.00	1.80	0.87	1.00	0.88	16.4
3/3	2.56	1.40	0.61	0.89	2.40	2.61	1.98	1.49	29.6
41/5	2.95	-	-	-	-	-	-	-	30.4
47/3	2.96	1.80	0.75	0.88	2.60	3.02	2.03	1.84	34.5
54/3	2.99	1.90	0.78	0.86	2.57	2.94	1.95	1.81	31.2
41/4	2.99	1.80	0.72	0.80	2.60	3.05	2.01	1.84	34.4
42/5	3.00	1.90	0.77	0.83	2.60	3.07	1.99	1.85	34.4
42/4	3.00	1.90	0.85	0.88	2.70	3.04	1.95	1.77	31.2
4/3	3.63	-	-	-	-	-	-	-	41.0
2/6	4.90	1.60	0.65	0.91	4.20	5.00	2.63	2.07	41.0
47/2	4.96	1.95	0.75	0.86	3.95	5.03	2.55	2.67	39.4
34/4	7.44	2.00	0.86	0.93	5.75	7.55	3.03	2.77	41.0
42/6	7.58	1.80	0.70	0.79	5.65	7.70	2.98	3.51	41.0
42/3	9.96	1.95	0.78	0.85	6.35	9.62	3.29	7.63	-
34/2	11.18	1.95	0.72	0.82	6.60	8.85	3.19	9.27	43.5

Table B9

TCE-QI-16-55-Un-clamped

Specimen Number	Incident Impact Energy (J)	F1 (KN)	AE1 (J)	D1 (mm)	F2 (KN)	AE2 (J)	D2 (mm)	TAE (J)	Damage Width (mm)
54/4	1.41	-	-	-	-	-	-	-	14.8
54/6	2.98	1.85	1.00	1.14	2.75	3.06	2.13	1.45	26.3
41/3	3.98	1.80	1.03	1.21	3.40	4.07	2.50	1.86	31.1
41/1	4.99	1.85	1.02	1.16	4.10	5.08	2.67	2.23	36.1
47/4	8.02	1.85	0.99	1.16	5.75	7.56	3.15	6.22	41.0
42/2	10.96	-	-	-	6.35	9.03	3.56	9.03	41.0

Table B10

TCE-QI*-16-55

Specimen Number	Incident Impact Energy (J)	F1 (KN)	AE1 (J)	D1 (mm)	F2 (KN)	AE2 (J)	D2 (mm)	TAE (J)	Damage Width (mm)
55/1	1.20	1.80	0.87	0.98	1.80	0.87	0.98	-	16.4
55/2	2.02	1.90	0.85	0.87	2.20	2.06	1.55	1.19	26.3
55/3	2.98	1.70	0.76	0.92	2.70	3.05	2.02	1.64	37.8
55/4	4.90	1.80	0.73	0.86	4.10	4.89	2.56	2.37	41.0
55/5	7.41	1.95	0.77	0.83	6.00	7.52	2.93	2.13	42.7
55/6	10.92	1.90	0.85	0.96	6.65	9.20	3.34	9.41	43.5

* Note - Layup : $[-45,90,+45,0]_{2s}$

Table B11

TCE-QI-16-75

Specimen Number	Incident Impact Energy (J)	F1 (KN)	AE1 (J)	D1 (mm)	F2 (KN)	AE2 (J)	D2 (mm)	TAE (J)	Damage Width (mm)
35/2	1.25	1.95	0.99	0.98	1.95	0.99	0.98	0.75	16.4
32/4	2.54	1.80	0.77	0.85	2.50	2.57	1.76	1.46	27.9
33/4	3.65	1.90	0.77	0.89	3.10	3.73	2.21	2.02	36.1
32/3	4.88	-	-	-	-	-	-	-	41.0
33/2	7.47	2.20	1.03	0.95	5.70	7.26	2.89	3.36	41.8
33/3	11.18	2.00	0.82	0.89	6.70	10.29	3.39	9.39	42.7

Table B12

TCE-QI-24-55

Specimen Number	Incident Impact Energy (J)	F1 (KN)	AE1 (J)	D1 (mm)	F2 (KN)	AE2 (J)	D2 (mm)	TAE (J)	Damage Width (mm)
39/6	1.98	3.50	2.02	1.00	3.50	2.02	1.00	0.56	0
39/4	3.98	4.45	2.33	1.04	4.45	2.33	1.04	2.48	27.9
40/4	5.97	4.20	1.96	0.90	4.60	6.04	2.15	3.39	40.2
39/1	7.80	3.80	1.54	0.82	5.60	7.89	2.57	4.06	41.0
40/3	10.00	-	-	-	-	-	-	-	41.0
40/2	11.96	4.30	1.92	0.95	8.05	12.07	2.94	5.15	42.7

Table B13

TCE-QI-32-55

Specimen Number	Incident Impact Energy (J)	F1 (KN)	AE1 (J)	D1 (mm)	F2 (KN)	AE2 (J)	D2 (mm)	TAE (J)	Damage Width (mm)
37/3	3.12	4.70	2.70	0.96	4.70	2.70	0.96	1.07	0
38/5	4.02	5.90	3.36	0.98	5.90	3.36	0.98	1.31	0
37/2	6.04	6.90	3.48	0.96	6.90	3.48	0.96	4.36	32.8
38/2	7.11	6.75	3.02	0.85	6.75	3.02	0.85	3.55	40.2
38/3	10.10	6.40	2.92	0.84	7.00	10.17	2.38	5.59	41.0
37/1	11.84	6.95	3.13	0.92	8.00	11.90	2.61	6.27	42.7

Table B14

CE-QI-16-55

Specimen Number	Incident Impact Energy (J)	F1 (KN)	AE1 (J)	D1 (mm)	F2 (KN)	AE2 (J)	D2 (mm)	TAE (J)	Damage Width (mm)
52/2	1.05	1.70	0.77	0.88	1.70	0.77	0.88	0.62	14.8
52/6	1.91	1.70	0.70	0.83	2.15	1.94	1.55	1.09	26.2
52/3	2.85	1.60	0.58	0.77	2.60	2.92	1.99	1.66	35.3
52/8	3.96	1.60	0.64	0.78	3.30	3.94	2.27	2.35	39.4
52/4	5.89	1.60	0.57	0.69	4.70	5.87	2.73	2.99	41.0
52/9	8.12	1.70	0.60	0.75	5.15	7.73	3.06	6.38	41.0
52/11	9.96	1.70	0.63	0.74	6.25	9.17	3.00	7.83	42.7

Table B15

GRP-QI-16-55

Specimen Number	Incident Impact Energy (J)	F1 (KN)	AE1 (J)	D1 (mm)	F2 (KN)	AE2 (J)	D2 (mm)	TAE (J)	Damage Width (mm)
26/5	1.09	1.55	1.14	1.35	1.55	1.14	1.35	0.80	-
26/4	1.43	1.35	0.86	1.23	1.55	1.50	1.67	0.80	-
25/8	1.87	1.45	1.00	1.30	1.75	1.92	1.87	1.42	19.8
25/9	1.89	1.70	1.26	1.45	1.75	1.93	1.85	1.46	18.4
25/6	3.83	1.75	1.38	1.55	2.60	3.80	2.65	3.06	27.4
25/1	3.86	1.50	0.98	1.28	2.75	3.97	2.69	2.33	-
25/5	5.87	1.45	0.89	1.18	3.35	5.72	3.19	5.05	41.4
25/4	5.89	1.50	0.92	1.22	3.35	5.84	3.22	5.03	40.3
26/15	7.71	-	-	-	3.95	7.30	3.65	6.98	41.4
26/1	7.71	1.50	1.01	1.25	4.75	7.85	3.64	4.05	-
26/13	9.52	-	-	-	4.50	9.03	4.03	8.74	41.4
26/10	9.57	1.55	0.96	1.27	4.60	9.19	4.01	8.61	42.0
26/2	11.28	1.50	1.20	1.50	4.75	11.01	4.80	9.61	-
25/15	11.34	-	-	-	5.05	10.78	4.36	10.58	41.9
26/8	13.86	-	-	-	6.20	12.88	4.52	12.44	43.1
26/7	13.93	-	-	-	6.10	12.96	4.59	12.80	42.0

Table B16

APC-QI-16-55

Specimen Number	Incident Impact Energy (J)	F1 (KN)	AE1 (J)	D1 (mm)	F2 (KN)	AE2 (J)	D2 (mm)	TAE (J)	Damage Width (mm)
21/8	2.01	2.90	2.06	1.35	2.90	2.06	1.35	0.47	0
22/1	2.02	2.90	2.05	1.39	2.90	2.05	1.39	0.49	0
22/6	3.99	3.75	2.90	1.58	3.95	4.06	1.83	1.74	13.1
22/7	4.02	3.85	3.28	1.68	3.90	4.03	1.89	1.86	14.8
21/7	5.97	3.80	3.19	1.74	4.45	6.01	2.51	2.67	18.1
21/6	5.97	2.95	2.14	1.31	4.35	5.84	2.31	3.12	18.1
21/2	7.90	3.15	2.12	1.38	5.40	8.01	2.75	3.70	22.2
22/3	7.96	3.40	2.76	1.63	5.15	8.05	2.93	4.89	21.3
22/2	9.74	3.40	2.62	1.56	4.95	7.83	2.84	6.83	18.1
21/4	9.78	3.35	2.05	1.27	6.20	9.49	2.97	5.06	26.3
21/3	11.44	3.55	2.35	1.42	5.60	8.00	2.77	7.85	27.9
22/8	11.50	3.15	1.87	1.21	6.00	9.84	2.97	8.60	32.8
53/3	12.96	-	-	-	5.30	7.00	2.61	11.40	27.9
53/1	13.03	3.55	2.63	1.54	4.95	7.65	2.77	11.23	24.6
53/6	14.62	-	-	-	5.75	7.55	2.53	12.76	38.6
53/5	14.62	-	-	-	-	-	-	-	27.9

Appendix C
Results of Post-Impact Compression Tests

Table C1

TCE-±45-16-45

Specimen Number	Incident Impact Energy (J)	Average Specimen Width (mm)	Average Specimen Thickness (mm)	Failure Stress (MPa)	Damage Width (mm)	Plate Modulus (GPa)
9/2	0	44.86	2.05	165.0*	0	10.5
9/1	0	44.82	2.05	165.1*	0	9.9
9/4	0	44.81	2.04	163.0*	0	10.3
31/1	1.25	44.30	2.04	183.7*	0	9.8
31/4	2.52	44.67	2.07	174.1*	19.7	8.9
31/5	3.65	44.72	2.06	165.5	31.1	8.8
7/2	4.88	44.60	2.03	166.2	38.5	10.5
7/4	7.44	44.72	2.06	143.8	39.4	9.3
7/1	11.12	44.64	2.08	114.8	41.0	9.4

* Note: Stress at 3 % strain - specimens did not fail.

Table C2

TCE-±45-16-55

Specimen Number	Incident Impact Energy (J)	Average Specimen Width (mm)	Average Specimen Thickness (mm)	Failure Stress (MPa)	Damage Width (mm)	Plate Modulus (GPa)
9/6	0	54.80	2.07	158.5*	0	9.5
29/5	0	55.25	2.05	183.8*	0	9.6
29/6	1.25	55.23	2.05	185.5*	0	8.9
29/1	2.55	54.53	2.05	174.4	31.2	10.8
29/2	3.65	54.54	2.05	151.1	32.8	10.1
30/6	4.93	54.54	2.06	160.9	37.8	10.3
30/4	7.47	54.42	2.07	147.8	39.4	11.1
30/3	11.12	54.53	2.05	110.5	41.0	8.9

* Note: Stress at 3 % strain - specimens did not fail.

Table C3

TCE-±45-16-75

Specimen Number	Incident Impact Energy (J)	Average Specimen Width (mm)	Average Specimen Thickness (mm)	Failure Stress (MPa)	Damage Width (mm)	Plate Modulus (GPa)
27/3	0	74.96	2.04	185.4*	0	10.4
28/1	0	74.95	2.04	186.7*	0	11.6
20/1	0	75.02	2.05	187.3*	0	10.0
27/4	1.25	74.97	2.07	175.8*	0	9.4
28/4	2.51	74.96	2.05	153.6	26.3	8.7
28/3	3.61	74.80	2.05	149.2	36.1	10.0
20/3	4.88	74.76	2.06	137.7	39.4	10.2
20/2	7.47	74.94	2.04	130.1	39.4	10.5
27/1	11.18	75.07	2.05	112.1	41.9	9.5

* Note: Stress at 3 % strain - specimens did not fail.

Table C4

TCE-0/90-16-45

Specimen Number	Incident Impact Energy (J)	Average Specimen Width (mm)	Average Specimen Thickness (mm)	Failure Stress (MPa)	Damage Width (mm)	Plate Modulus (GPa)
14/3	0	44.62	2.05	511.5*	0	32.1
15/6	0	44.59	2.09	468.4	0	-
15/1	0	44.64	2.05	439.9	0	-
6/5	1.13	44.92	2.09	488.7	0	31.5
15/3	1.93	44.62	2.09	377.3	21.3	31.8
15/2	2.43	44.59	2.06	349.5	24.6	31.4
14/1	4.72	44.59	2.07	219.2	34.5	30.9
15/5	7.65	44.56	2.09	266.1	37.8	30.8
14/2	11.34	44.69	2.09	231.5	41.8	28.5

* Note: End crushing failure.

Table C5

TCE-0/90-16-55

Specimen Number	Incident Impact Energy (J)	Average Specimen Width (mm)	Average Specimen Thickness (mm)	Failure Stress (MPa)	Damage Width (mm)	Plate Modulus (GPa)
12/1	0	54.68	2.07	427.3	0	30.9
12/4	0	54.63	2.08	431.3	0	30.1
13/4	0	54.26	2.11	420.4	0	29.6
14/4	1.19	54.63	2.06	449.7	0	29.1
11/4	1.94	54.51	2.07	279.0	21.3	28.8
6/4	2.47	54.99	2.12	243.6	22.2	26.2
15/4	4.82	54.64	2.07	242.6	37.8	28.4
11/1	7.65	54.63	2.06	252.8	41.9	29.1
6/2	11.44	55.03	2.08	223.1	42.7	-

Table C6

TCE-0/90-16-75

Specimen Number	Incident Impact Energy (J)	Average Specimen Width (mm)	Average Specimen Thickness (mm)	Failure Stress (MPa)	Damage Width (mm)	Plate Modulus (GPa)
11/5	0	74.79	2.09	322.6	0	23.8
11/6	0	74.77	2.09	319.7	0	25.0
11/2	0	74.78	2.09	322.7	0	25.0
11/3	1.25	74.79	2.09	334.1	0	25.2
12/2	1.94	74.75	2.10	279.8	24.6	23.7
13/5	4.74	74.76	2.11	215.2	27.9	25.4
12/3	7.65	74.80	2.07	246.0	43.5	22.7
12/5	11.39	74.85	2.08	188.2	41.0	20.9

Table C7

TCE-QI-16-45

Specimen Number	Incident Impact Energy (J)	Average Specimen Width (mm)	Average Specimen Thickness (mm)	Failure Stress (MPa)	Damage Width (mm)	Plate Modulus (GPa)
4/2	0	44.83	1.95	323.6*	0	23.1
2/4	0	44.65	1.86	399.8	0	23.5
3/1	0	43.95	1.82	357.7*	0	25.3
4/5	1.89	44.82	1.98	201.1	27.9	25.7
4/4	3.85	44.82	1.87	163.7	37.8	26.8
3/5	5.68	44.88	2.05	129.5	41.0	23.1
2/2	7.64	44.85	2.01	153.0	45.0	23.1
3/4	9.61	44.84	1.94	151.1	45.0	23.3
4/1	11.44	44.82	1.90	147.6	45.0	22.6

* Note: End crushing failure.

Table C8

TCE-QI-16-55-Clamped

Specimen Number	Incident Impact Energy (J)	Average Specimen Width (mm)	Average Specimen Thickness (mm)	Failure Stress (MPa)	Damage Width (mm)	Plate Modulus (GPa)
34/3	0	54.71	2.09	443.6	0	24.9
4/6	0	54.89	1.91	344.2 See Note 3	0	26.4
34/6	0	54.72	2.06	416.7	0	25.1
54/1	0.86	54.71	2.06	365.2	See Note 1	25.9
54/5	0.87	54.75	2.05	318.3	14.8	25.6
41/6	0.92	54.74	2.10	291.4	14.8	26.3
41/2	0.96	54.46	2.06	310.0	14.8	25.3
47/1	1.04	54.86	2.11	280.4	18.1	25.1
42/1	1.04	54.69	2.04	303.8	15.6	24.9
3/6	1.24	54.91	1.90	239.4	16.4	26.3
3/3	2.56	54.96	1.91	165.9	29.6	25.3
47/3*	2.96	54.96	2.07	174.4	34.5	24.4
41/4*	2.99	54.70	2.05	161.1	34.4	25.1
54/3*	2.99	54.79	2.07	157.8	31.2	25.5
42/5*	3.00	54.71	2.06	161.3	34.4	24.5
42/4*	3.00	54.61	2.05	202.8	31.2	25.9
4/3	3.63	54.88	1.86	155.4	41.0	25.3
2/6	4.90	54.83	1.92	139.7	41.0	25.0
34/4	7.44	54.69	2.07	137.0	41.0	23.2
34/2	11.18	54.75	2.10	155.1	43.5	20.7

Notes:

1 A damage width of 14.8 mm was measured for this specimen after impact. Because the specimen did not fail through the impact damage when tested in compression the damage width was taken as zero in the statistical analysis.

2 The results from five specimens marked with an asterix were used to calculate the average compression strength for an incident impact energy of 3 J.

3 Note: End crushing failure.

Table C9

TCE-QI-16-55-Un-Clamped

Specimen Number	Incident Impact Energy (J)	Average Specimen Width (mm)	Average Specimen Thickness (mm)	Failure Stress (MPa)	Damage Width (mm)	Plate Modulus (GPa)
54/4	1.41	54.78	2.05	288.7	14.8	25.2
54/6	2.98	54.75	2.07	210.0	26.3	25.7
41/3	3.98	54.77	2.08	165.6	31.1	24.0
41/1	4.99	54.71	2.02	169.4	36.1	25.8
47/4	8.02	54.97	2.04	146.8	41.0	23.4
42/2	10.96	54.74	2.04	141.1	41.0	24.2

Table C10

TCE-QI*-16-55

Specimen Number	Incident Impact Energy (J)	Average Specimen Width (mm)	Average Specimen Thickness (mm)	Failure Stress (MPa)	Damage Width (mm)	Plate Modulus (GPa)
55/1	1.20	55.00	2.06	269.3	16.4	24.7
55/2	2.02	55.10	2.09	222.4	26.3	24.7
55/3	2.98	55.12	2.07	197.8	37.8	23.3
55/4	4.90	55.07	2.07	181.7	41.0	24.1
55/5	7.41	55.11	2.09	189.3	42.7	23.4
55/6	10.92	55.11	2.07	154.4	43.5	22.2

Table C11

TCE-QI-16-55-Loading rate = 30 mm/min

Specimen Number	Incident Impact Energy (J)	Average Specimen Width (mm)	Average Specimen Thickness (mm)	Failure Stress (MPa)	Damage Width (mm)	Plate Modulus (GPa)
54/2	1.41	54.74	2.03	263.1	16.4	17.9
41/5	2.95	54.63	2.08	209.2	30.4	13.4
47/2	4.96	54.91	2.08	165.3	39.4	13.4
42/6	7.58	54.74	2.08	165.3	41.0	14.8

Table C12

TCE-QI-16-75

Specimen Number	Incident Impact Energy (J)	Average Specimen Width (mm)	Average Specimen Thickness (mm)	Failure Stress (MPa)	Damage Width (mm)	Plate Modulus (GPa)
32/2	0	74.75	2.08	302.2	0	22.2
33/1	0	74.87	2.07	329.1	0	21.5
35/3	0	74.97	2.07	292.2	0	22.3
35/2	1.25	74.92	2.07	267.0	16.4	21.1
32/4	2.54	74.95	2.08	174.9	27.9	22.5
33/4	3.65	74.96	2.07	153.4	36.1	21.7
32/3	4.88	74.93	2.05	158.6	41.0	20.1
33/2	7.47	74.92	2.08	130.9	41.8	19.5
33/3	11.18	74.90	2.06	128.6	42.7	19.0

Table C13

TCE-QI-24-55

Specimen Number	Incident Impact Energy (J)	Average Specimen Width (mm)	Average Specimen Thickness (mm)	Failure Stress (MPa)	Damage Width (mm)	Plate Modulus (GPa)
40/1	0	54.71	3.04	456.5	0	20.9
39/2	0	54.83	3.07	467.0*1	0	21.3
40/6	0	54.79	3.11	439.3	0	20.4
39/6	1.98	54.88	3.11	505.0*2	0	21.1
39/4	3.98	54.93	3.07	216.9	27.9	20.7
40/4	5.97	54.45	3.08	194.6	40.2	19.7
39/1	7.80	54.85	3.03	188.0	41.0	20.8
40/3	10.00	54.75	3.12	188.2	41.0	19.3
40/2	11.96	54.58	3.09	188.0	42.7	19.6

*1 Note: End crushing failure.

*2 Note: Failed in unsupported region of specimen.

Table C14

TCE-QI-32-55

Specimen Number	Incident Impact Energy (J)	Average Specimen Width (mm)	Average Specimen Thickness (mm)	Failure Stress (MPa)	Damage Width (mm)	Plate Modulus (GPa)
37/5	0	54.92	4.09	426.5*	0	18.4
37/6	0	54.97	4.09	426.1*	0	18.6
38/4	0	54.83	4.13	400.8	0	17.9
37/3	3.12	54.93	4.15	434.3*	0	17.7
38/5	4.02	54.91	4.11	438.7*	0	18.2
37/2	6.04	54.92	4.16	230.2	32.8	18.0
38/2	7.11	54.89	4.12	212.6	40.2	17.5
38/3	10.10	54.79	4.10	180.9	41.0	17.5
37/1	11.84	54.65	4.17	175.2	42.7	17.5

Note: Stresses marked with an asterix are not failure stresses, the machine capacity was exceeded before failure occurred.

Table C15

CE-QI-16-55

Specimen Number	Incident Impact Energy (J)	Average Specimen Width (mm)	Average Specimen Thickness (mm)	Failure Stress (MPa)	Damage Width (mm)	Plate Modulus (GPa)
52/5	0	54.75	2.09	386.4	0	23.9
52/1	0	54.69	2.05	394.7	0	24.6
52/12	0	54.75	2.02	413.1	0	25.0
52/2	1.05	54.75	2.05	347.5	14.8	24.0
52/6	1.91	54.74	2.04	230.2	26.2	24.3
52/3	2.85	54.75	2.01	195.6	35.3	24.8
52/8	3.96	54.75	2.10	197.8	39.4	23.3
52/4	5.89	54.69	2.10	200.3	41.0	22.8
52/9	8.12	54.76	2.03	189.7	41.0	21.5
52/11	9.96	54.74	2.10	184.4	42.7	20.5

Table C16

GRP-QI-16-55

Specimen Number	Incident Impact Energy (J)	Average Specimen Width (mm)	Average Specimen Thickness (mm)	Failure Stress (MPa)	Damage Width (mm)	Plate Modulus (GPa)
26/12	0	54.82	1.95	263.3	0	16.4
25/2	0	54.87	1.95	279.0	0	16.0
25/11	0	54.91	1.96	265.1	0	16.6
26/5	1.09	54.91	1.97	252.4	See note 1	16.2
26/4	1.43	54.89	2.00	206.6	17	15.8
25/8	1.87	54.81	1.98	201.7	19.8	15.6
25/9	1.89	54.69	2.00	204.4	18.4	15.9
25/6	3.83	54.86	2.00	169.5	27.4	15.4
25/1	3.86	54.90	1.96	162.4	-	15.7
25/5	5.87	54.90	1.98	150.2	41.4	15.9
25/4	5.89	54.87	1.97	160.8	40.3	15.6
26/15	7.71	54.91	1.91	154.2	41.4	15.8
26/1	7.71	54.74	1.97	157.4	-	15.6
26/13	9.52	54.87	1.88	150.2	41.4	15.5
26/10	9.57	54.87	1.96	153.8	42.0	15.7
26/2	11.28	54.62	1.99	156.8	-	15.4
25/15	11.34	54.85	1.91	148.0	41.9	15.8
26/8	13.86	54.89	2.02	167.8	43.1	15.0
26/7	13.93	54.90	2.03	152.6	42.0	15.2

Note: 1 A damage width of 9 mm was measured for this specimen after impact. Because the specimen did not fail through the impact damage when tested in compression the damage width was taken as zero in the statistical analysis.

Table C17

APC-QI-16-55

Specimen Number	Incident Impact Energy (J)	Average Specimen Width (mm)	Average Specimen Thickness (mm)	Failure Stress (MPa)	Damage Width (mm)	Plate Modulus (GPa)
22/5	0	54.62	2.14	443.4	0	22.7
21/5	0	54.68	1.87	367.6	0	23.3
53/4	0	54.82	2.13	433.0	0	23.2
21/8	2.01	54.70	2.06	447.7	0	24.8
22/1	2.02	54.65	1.99	417.2	0	23.6
22/6	3.99	54.72	2.15	364.6	13.1	23.0
22/7	4.02	54.69	2.16	342.1	14.8	22.8
21/7	5.97	54.75	1.98	334.6	18.1	25.3
21/6	5.97	54.75	1.91	358.6	18.1	24.8
21/2	7.90	54.73	2.09	319.4	22.2	23.4
22/3	7.96	54.66	2.00	312.3	21.3	24.5
22/2	9.74	54.79	2.00	279.2	18.1	24.5
21/4	9.78	54.76	2.22	311.1	26.3	23.0
21/3	11.44	54.76	2.15	245.3	27.9	22.6
22/8	11.50	54.74	2.18	231.1	32.8	22.5
53/3	12.96	54.92	2.02	230.0	27.9	23.7
53/1	13.03	54.93	2.00	217.9	24.6	23.9
53/5	14.62	54.94	2.05	196.0	27.9	21.3
53/6	14.62	54.95	2.15	203.8	38.6	22.2

Appendix D

Statistical Analysis used for ILSS Results

The Kruskal-Wallis Test

The equations in this appendix were taken from Sokal et al (1969).

The Kruskal-Wallis test looks for differences of location in ranked data grouped in a single classification. It is not concerned with absolute values. The technique can be used on any set of data of this type, however if the data is normally distributed the one way analysis of variance test is the more efficient statistical test. The method is best described by example. Two sets of fictitious strength data will be analysed to demonstrate the technique.

Data Set 1

	Laminate Number		
Test No	1	2	3
1	91	92	93
2	96	95	94
3	97	98	99
4	102	101	100
5	103	104	104

Data Set 2

	Laminate Number		
Test No	1	2	3
1	91	96	101
2	92	97	102
3	93	98	103
4	94	99	104
5	95	100	105

In the first set of data the strength values have been arranged so that they are evenly distributed between the three laminates. In the second set of data similar strengths have been grouped together for the three laminates. The null hypothesis is that there are no differences in the location of data taken from the three laminates in each example. The data has been distributed so that the null hypothesis will be accepted in the case of data set 1 and rejected in the case of data set 2. The Kruskal-Wallis test will now be applied to demonstrate the technique.

Analysis for Data Set 1

a is the number of groups of data (in this case 3)

n_i is the number of items in group i (in this case the sample sizes are equal and $n_i = n = 5$) (Note: the technique is still applicable when there are different numbers of items in different groups).

The first step is to rank the data from smallest to largest, treating all of the data as a single group. Where ties occur the average value is calculated:

Value	Rank	R	
91	1	1	
92	2	2	
93	3	3	
94	4	4	
95	5	5	
96	6	6	
97	7	7	
98	8	8	
99	9	9	
100	10	10	
101	11	11	
102	12	12	
103	13	13	
104	14	14)	(14 +15) / 2 = 14.5
104	15	14)	

The data table is now reconstituted but the values of ILSS are replaced by the ranking values (R):

	Laminate Number		
Test No	1	2	3
1	1	2	3
2	6	5	4
3	7	8	9
4	12	11	10
5	13	14.5	14.5
$(\sum R)_i^{n_i}$	39	40.5	40.5

The statistic H is now calculated from the following formula:

$$H = \left\{ \frac{12}{\sum^{a} n_i \left(\sum^{a} n_i + 1\right)} \quad \frac{\sum^{a} \left(\sum^{n_i} R\right)_i^2}{n_i} \right\} - \quad 3\left(\sum^{a} n_i + 1\right)$$

where the numbers 12 and 3 are constants.

In this example $H = \frac{12}{15(15+1)}\left\{\frac{39^2}{5} + \frac{40.5^2}{5} + \frac{40.5^2}{5}\right\} - 3\times(15+1)$

$= 0.015$

A correction factor D is than calculated to account for tied results:

$$D = 1 - \frac{\sum^{m} T_j}{\left(\sum^{a} n_i - 1\right)\sum^{a} n_i\left(\sum^{a} n_i + 1\right)}$$

where T_j is a function of the number of t_j variates tied in the j^{th} group:

$$T_j = (t_j)^3 - t_j$$

The table below gives values of T_j for t_j from 2 to 10

t_j	2	3	4	5	6	7	8	9	10
T_j	6	24	60	120	210	336	504	720	990

In this example there is only one tie (therefore $t_j = 2$) and:

$$D = 1 - \frac{6}{(15-1)\,15\,(15+1)} = 0.9982$$

The adjusted value of H is calculated from $H/D = \frac{0.015}{0.9982} = 0.015$

The value of H is now compared with the appropriate value of $\chi^2_{\alpha,\,(a-1)}$ which is found from statistical tables. A value of α of 0.05 is universally used. If H is less than $\chi^2_{0.05,\,(a-1)}$ the null hypothesis is accepted. In this case $\chi^2_{0.05,\,(2)} = 5.99$. Since H is much smaller than 5.99 the null hypothesis is accepted at the 5% confidence level. The test has shown that the individual strength values are distributed evenly throughout the population as a whole and it is reasonable to conclude that the material taken from the three laminates was of similar quality.

For the second data set H = 12.5 and as before $\chi^2_{0.05,\,(2)} = 5.99$. Since H is greater than 5.99 the null hypothesis is rejected. In this case the test has shown that the individual

strength values are not evenly distributed throughout the population as a whole. In this case it would be fair to conclude that a genuine difference existed between the strength of material taken from the three laminates.

Appendix E

Equations used to calculate confidence and predicion intervals

The following equations were used to calculate the confidence and prediction intervals:

(a) Confidence Interval

The 100 (1- α) per cent confidence interval for $a_0 + a_1 x$ is given by:

$$\hat{a}_0 + \hat{a}_1 x_0 \pm t_{\alpha/2,n-2} \times S_{y/x} \sqrt{\frac{1}{n} + \frac{(x_0 - \bar{x})^2}{\sum_{i=1}^{n} (x_i - \bar{x})^2}}$$

(b) Prediction Interval

There is a probability 1 - α that a future observation on y , at the point x_0, will lie between:

$$\hat{a}_0 + \hat{a}_1 x_0 \pm t_{\alpha/2,n-2} \times S_{y/x} \sqrt{1 + \frac{1}{n} + \frac{(x_0 - \bar{x})^2}{\sum_{i=1}^{n} (x_i - \bar{x})^2}}$$

where:

y = compression strength and x = damage width

a_0 and a_1 are constants in the equation of the true regression line: $y = a_0 + a_1 x$

$\hat{a}_0$ and $\hat{a}_1$ are constants in the equation of the estimated regression line: $y = \hat{a}_0 + \hat{a}_1 x$

n is the total number of observations

$t_{\frac{\alpha}{2},n-2}$ is the interval between the chosen percentage points of the students t distribution for n-2 degrees of freedom (for $\alpha = 0.05$ the 95 % intervals are calculated)

$S_{y/x}$ is the residual standard deviation and is estimated from:

$$S^2_{y/x} = \left(\sum_{i=1}^{n} (y_i^2 - \hat{a}_0) \sum_{i=1}^{n} (y_i - \hat{a}_1) \sum_{i=1}^{n} (x_i y_i) \right) \Big/ n-2$$

$\bar{x}$ is the mean of the x values.

These equations were taken from chapter eight of Chatfield (1978) where more details of the method can be found.